THE UNIVERSITY OF
WARWICK

University of Warwick institutional repository: http://go.warwick.ac.uk/wrap

A Thesis Submitted for the Degree of PhD at the University of Warwick

http://go.warwick.ac.uk/wrap/74261

This thesis is made available online and is protected by original copyright.

Please scroll down to view the document itself.

Please refer to the repository record for this item for information to help you to cite it. Our policy information is available from the repository home page.

The synthesis and characterisation of pH responsive polymers, understanding their self-assembly and their development as ashless detergents.

Daniel B. Wright

Submitted for the degree of Doctor of Philosophy

Department of Chemistry

April 2015

Contents

Declaration

This thesis is submitted to the University of Warwick in support of my application for the degree of Doctor of Philosophy. It has been composed by the author and not been submitted in any previous application for any degree. The work presented unless otherwise stated was carried out by the author between October 2011 and April 2015.

Acknowledgments

First and foremost I must give my sincere thanks to my supervisor Prof. Rachel O'Reilly for giving me the opportunity to work in her group, her relentless enthusiasm and drive has been an unmatched influence throughout this PhD. I am very grateful to all her constant support and guidance which was invaluable to me. I must thank the EPSRC for funding and the Department of Chemistry for providing equipment or help whenever needed.

A huge thank you goes to all the members of the O'Reilly group during the years of my study, especially the members of "Bay Awesome". Thank you for all the help and great times daily I have encountered both in and out of the lab whilst pushing each other towards better science; it has been an honour to work with you all. In particular I would like to recognise Dr Joseph Patterson, who very kindly guided me in the early stages of my study and continues to provide interesting scientific discussions, thank you.

Outside of the University of Warwick I would like to extend a huge thank you to both Dr Olivier Colombani and Prof. Christophe Chassenieux, from Université du Maine. I must thank you both for teaching me in depth laser light scattering, for all your guidance on polymer self-assembly, and for always taking the time to discuss these two extensively further with me in such a humble manner.

I would like to thank BP for also funding this project and the members of the Marine team at the BP Technology centre in Pangbourne for all the help in guidance and providing me with another outlook on the chemistry herein.

Moving further afield from Warwick I'd like to thank my very close friends for their endless unwavering support and encouragement throughout my PhD. Last and by no means least I would like to thank my family, particularly my parents, for all your help and support.

List of publications

- A Comparative Study of the Stimuli-Responsive Properties of DMAEA and DMAEMA containing polymers, Cotanda, P.; Wright, D. B.; Tyler, M.; O'Reilly, R. K. *J. Polym. Sci. Part A: Polym. Chem.* 2013, 51, 3333.

- Tuning the aggregation behaviour of pH responsive micelles by copolymerization, Wright, D. B.; Patterson, J. P.; Pitto-Barry, A.; Cotanda, P.; Chassenieux, C.; Colombani, O.; O'Reilly, R. K. *Polym. Chem.* 2015, 6, 2761. (**Chapter 4**)

- The copolymer blending method: A new approach for targeted assembly, Wright, D. B.; Patterson, J. P.; Pitto-Barry, A.; Lu, A.; Kirby, N.; Gianneschi, N. C.; Chassenieux, C.; Colombani, O.; O'Reilly, R. K. *Submitted* 2015. (**Chapter 5**)

- Lubricating composition comprising an ashless TBN booster, Wright, D. B.; O'Reilly, R. K; Chahine, S. *Patent Submitted 2015*. (**Chapters 2** and **3**)

Abbreviations

α – Degree of ionisation

β -Correction factor for seigert relation

ϕ - Partition coefficient

γ - Surface tension

%wt – Weight percent

A – Amplitude

A_2 – Second virial coefficient

$A(\tau)$ – Distribution of relaxation times

AIBN – 2,2′-Azobis(2-methylpropionitrile)

AM – Acrylamide

AN – Acrylonitrile

ASTM - American Society for Testing and Materials

BCP – Block copolymer

br –Broad peak in ^{1}H NMR spectrum

C – Concentration

CAC – Critical aggregation concentration

CMC – Critical micelle concentration

CMDT - Cyanomethyl dodecyl trithiocarbonate

CPDB - 2-Cyanoprop-2-yl dithiobenzoate

CPP – Critical packing parameter

Cryo – Cryogenic

CTA – Chain transfer agent

D – Diffusion coefficient

d – Deuterium labelled

D_{app} – Apparent diffusion coefficient

DEAEMA – 2-(diethylamino)ethyl methacrylate

DLS – Dynamic light scattering

$Đ$ – Molar mass dispersity (Mw/Mn)

DMA – Dimethyl acrylamide

DMAEMA – 2-(dimethylamino)ethyl methacrylate

DMAP – 4-dimethylaminopyridine

DMF – Dimethylformamide

DMSO – Dimethyl sulfoxide

$d\eta/dC$ – Refractive index increment

DP – Number average degree of polymerisation

DRI – Differential refractive index

DSC - Differential scanning calorimetry

E – Energy barrier for molecular exchange

EDCI - 1-Ethyl-3-(3-dimethylaminopropyl)carbodiimide

EHA – 2 – ethylhexyl acrylate

eq. – Equivalents

eqn. – Equation

EtOAc – Ethyl acetate

exp -exponential

f_A– A block volume fraction or mol fraction in monomer feed or free energy

g – Aggregation number

$g_1(q,t)$ – Electric field autocorrelation function

$g_2(q,t)$ – Intensity autocorrelation function

h – Proton labelled

h - Hours

I – Radical initiator

IBA – Isobornyl acrylate

$I(x)$ – Intensity as a function of x

J –NMR coupling constant

K – Constant for the contrast function is small angle scattering

kDa - Kilodaltons (g mol^{-1})

k’ – Rate constant for pseudo first order reactions

$k_{add,\text{-}add,addP,\text{-}addP,\beta,\text{-}\beta}$ – Rate constants in the RAFT equilibria

k_D – Dynamic second virial coefficient

$k_{,i,p,t,}$– Rate constant for initiator decomposition, initiation, propagation, chain transfer and termination respectively in a radical polymerisation

$k_{f,r,}$ – Rate constant for the forward reaction, reverse reaction

λ – Wavelength

L – Lamellar morphology

LCST - Lower critical solubility temperature

LLS – Laser light scattering

M – Monomer

M –Molar mass

m –Multiplet peak in ^{1}H NMR spectrum

MA – Methyl acrylate

m/z – Mass to charge ratio

MEMA- 2-*N*-morpholinoethyl methacrylate

MeOH – Methanol

MeONa – Sodium methoxide

MMA – Methyl methacrylate

M_n – Number average molecular weight

MW – Molecular weight

M_w –Weight average molecular weight

MWCO – Molecular weight cut-off

n – Refractive index

N_A - Avogadro's number

N_{agg} – Aggregation number

N_b – Degree of polymerisation of polymer block b

NMR – Nuclear magnetic resonance

NRET – Non-radiative energy transfer

NVP - *N*-vinyl-pyrrolidone

PAA – Poly(acrylic acid)

PB – Poly(butadiene)

PDMAEMA- Poly(2-(dimethylamino)ethyl methacrylate)

PDEAEMA - Poly(2-(diethylamino)ethyl methacrylate)

PEMA - 4-N-pyridine ethyl methacrylate

PEO – Poly(ethylene oxide)

PEP – Poly(ethylene - *alt* - propylene)

pK_a – Acid dissociation constant

pK_b – Base dissociation constant

pK_w – Water dissociation constant

PLMA – Poly(lauryl methacrylate)

PMANa – Poly(sodium methacrylate)

PMEMA – Poly(2-*N*-Morpholinoethyl methacrylate)

P*n*BuA – Poly(*n*-butyl acrylate)

PPEMA – Poly(4-*N*-pyridine ethyl methacrylate)

PPO – Poly(propylene oxide)

PPS – Poly(propylene sulfide)

P(q) – Particle form factor

PS – Poly(styrene)

P4VP – Poly(4-vinyl pyridine)

P_n – Polymer with DP = n

P_n• – Polymeric radical with DP = n

q - Scattering vector

ρ – Bulk density

R – Radius

r_x – reactivity ration of polymer x

RDRP – Reversible-deactivation radical polymerisation

ref. – Reference

REPES – Regularized Positive Exponential Sum

R_g –Radius of gyration

R_h – Hydrodynamic radius

RI – Refractive index

R_p – Rate of polymerisation

R_θ – Rayleigh ratio

RT – Room temperature

S – Sphere morphology

SANS – Small angle neutron scattering

SEC – Size exclusion chromatography

SLS – Static light scattering

S(q) – Structure form factor

τ – relaxation time

θ –Angle

T – Temperature

t – Time

t – Binomial triplet in ^{1}H NMR spectrum

TBN – Total base number

TEA – Triethylamine

TEM –Transmission electron microscopy

T_g – Glass transition temperature

THF – Tetrahydrofuran

TMS – tetramethylsilane NMR standard

TR-SANS – Time resolved small angle neutron scattering

UV - Ultraviolet

V or v – Volume

Vac - *N*-vinylcarbazole

χ_{AB} – Flory-Huggins interaction parameter between polymer block A and B

Z_i – Number of electrons for species *i*

Thesis Summary

Chapter 1 is an introduction to the hierarchy in block copolymer self-assembly from a bottom up approach. To begin with, the control at each hierarchical level is introduced and the influences are reviewed. This chapter is concluded by reviewing some techniques to understand self-assembled block copolymers and the applications from bottom up self-assembly of block copolymers is presented.

Chapter 2 reports the synthesis of a range of amine homopolymers and copolymers by RAFT polymerisation. These amino polymers are then explored further as lubricant additives and their solution self-assembly in non-polar media is explored.

Chapter 3 investigates the performance of the amino polymers from Chapter 2 as ashless detergents in lubricant formulations using a range of industrial testing methods.

Chapter 4 reports the synthesis and self-assembly of a range of pH responsive P(DMAEMA-*co*-DEAEMA)-*b*-PDMAEMA diblock copolymers, where the composition of the P(DMAEMA-*co*-DEAEMA) block was varied by copolymerisation, in aqueous solution studied by a range of scattering methods and microscopy.

Chapter 5 reports the initial copolymer blending method protocol, here two P(DMAEMA-*co*-DEAEMA)-*b*-PDMAEMA diblock copolymers with varying P(DMAEMA-*co*-DEAEMA) block compositions are blended together. The structures formed on the nanoscale are analysed and further compared to the structures formed by a pure P(DMAEMA-*co*-DEAEMA)-*b*-PDMAEMA diblock copolymer with the same composition as the blend.

Chapter 6 reports on the extension of the copolymer blending method protocol, here a range of neutral polymers and different self-assembly pathways are explored and the structures formed are analysed by detailed light scattering techniques and cryo-TEM.

1. Bottom-up approaches in polymer nanotechnology.

Synthetic polymers embody an extensive subject matter, across a large spectrum of length scales, from sub nanometre, by changes in the chemistry of the monomer, up to much larger macroscale lengths.[1] This great spectrum of research interest is a consequence of the comprehensive fundamental questions associated with the wide range of polymer applications and functions in both bulk and solution.

Block copolymers are an interesting class of polymer where two or more polymer blocks, differing in chemistry, are covalently linked. Consequently, unique advantages in both applications and functions in polymer science are apparent as it is now possible to produce materials that possess functionality and behaviour of two or more different polymers in the same material. Despite a wide range of applications and functions, diblock copolymers can also produce behaviours which are not inherent to the chemistry of the monomer; however, the behaviour is a result of the nanoscale organisation of the polymers into defined structures. These defined structures arise from the phase separation that diblock copolymers can exhibit, the covalent bond between the two blocks prevents macrophase separation but nanoscale self-organisation can indeed occur. In both bulk materials and when the polymers are dispersed in solution they can self-assemble into organised structures, leading to a new range of behaviours and a new subcategory of polymer understanding, polymer self-assembly.

This remarkably interesting subcategory of polymer self-assembly can be divided even further as the polymers, as mentioned can self- assemble in the bulk and in solution (Figure 1.1). By varying the polymers throughout the range of accessible sub-micron length scales in a bottom up approach much larger organised hierarchical structures can be controlled, paving the way for a fascinating array of characteristics and behaviours which can be exploited to solve a variety of industrial problems (Figure 1.1). Nevertheless it should be appreciated that for polymers to be successful in the desired application, for example lubricant additives

(solution assembly) or polymer solar panels (bulk assembly), that control at each hierarchical level must be achieved. This control is especially true on the larger length scales, 10 nm-1 μm, be it from control over morphology or control of the dynamics at equilibrium (Figure 1.1).

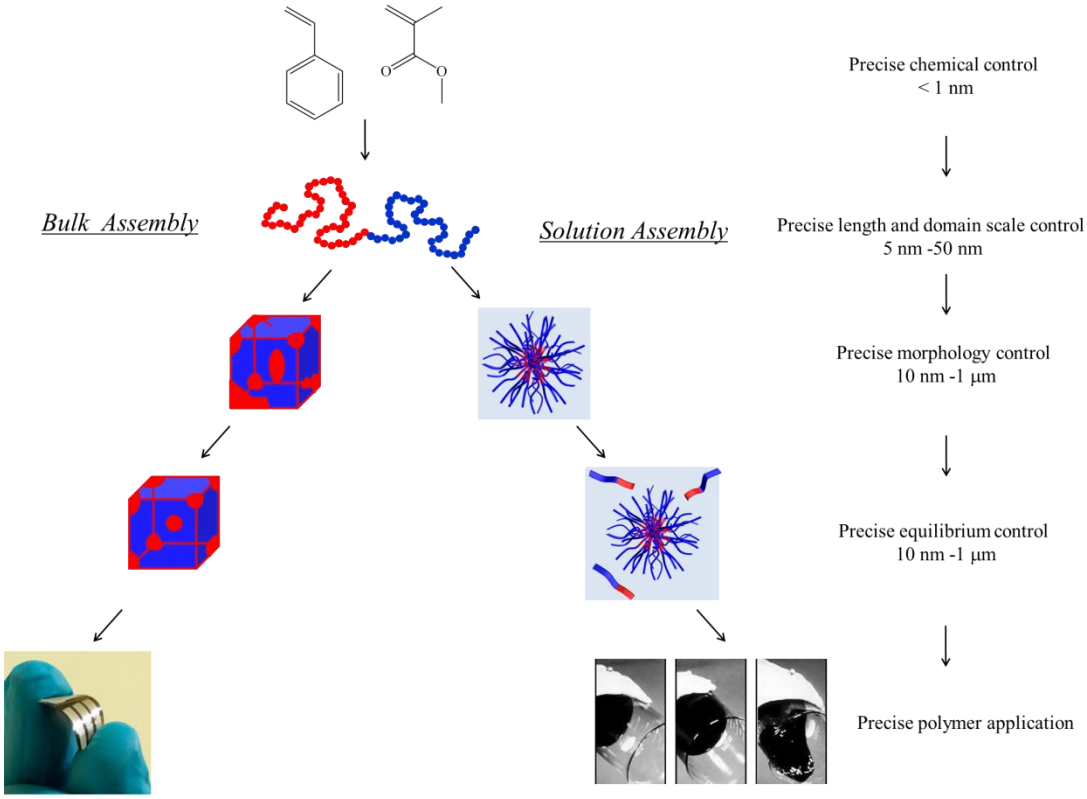

Figure 1.1. Structural hierarchies in polymer systems from a bottom up approach. Precise polymer application images adapted from ref.[2,3] Image for bulk assembly = Solar panel, image for solution assembly = Pour point additive in a lubricant formulation.

For bulk block copolymer self-assembly, extensive arrays of polymers have been produced and studied on these submicron length scales. On the other hand, for self-assemblies in solution not only must the two polymer blocks separation be understood but a further factor must be considered, the influence of the dispersion solvent of choice. Most commonly the self-assembly of diblock copolymers in solution is investigated in water based systems and mimics many of the morphologies and behaviours formed by small molecule surfactants Nevertheless, many uses of diblock copolymers in a large scale are in non-polar solvents e.g.

lubricant additives for automotive engines. Here, in this Thesis the understanding of structures formed on the nanoscale from diblock copolymers in both polar and non-polar media is explored. The aim of this Chapter is to provide an introduction on the ability to control the polymer assembly at each hierarchical level; length scale control, morphology control, domain functionality control, equilibrium control, with the principal aim towards the understanding of polymer self-assembly in solution.

1.1. Precise length scale control

Structures formed by polymers on the nanoscale have even smaller substructure domains, which can vary from a few nanometres up to 50 + nanometres.[4-7] Simply, this is achieved by making changes on much smaller length scales than the those in which the substructure domains are observed, by altering monomer structure, e.g. from a neutral to an ionic species, and / or the length of the polymer chain.[7-9]

From synthetic advances in polymer chemistry it is now suggested that any polymer architecture can be obtained, with the literature showing a plethora of examples ranging from novel peptide based polymers to large icosablock polymers, all with good control of molecular architecture.[10-13] In addition to these are polymers which have functional end groups (here to be termed "block copolymer analogues"),[14-19] that can arise from polymerisation initiators or by post polymerisation modifications, which again can produce nanoscale polymer domains with a controlled size as these end group can behave in a similar manner to a second polymer block.[20,21]

Previously polymers have been produced through living polymerisation techniques such as anionic polymerisation and as such do have the required control over chain length but will lack certain functionality such as hydroxyls, which limits the scope of these polymers to prepare controlled nanostructure domains.[1] In recent years however, the birth of reversible deactivation radical polymerisation (RDRP) has paved the way for the polymerisation of functional vinyl monomers to produce a range of polymers with functionality whilst

maintaining good control along the polymer chain.[22-26] The most prominent RDRP technique for incorporating the largest range of functionalities whilst maintaining chain length control, therefore offering potentially the most control of nanostructure, is reversible addition fragmentation termination (RAFT) polymerisation.[27]

1.1.1. RAFT Polymerisation

Although theoretically a radical technique which could give polymers of controlled molecular weight have been around since the 1950s,[28] however, it wasn't until the mid-1980s did this prediction become evident experimentally with both iniferters and reversible capping initiators.[29-33] With this discovery the control of living polymerisation could be achieved with the ease and range of functionalities from free radical polymerisation.

RAFT polymerisation is based upon the same polymerisation processes as free radical polymerisation however, with the introduction of a chain transfer agent (CTA, **1**, Figure 1.2) some processes are virtually undetectable throughout the polymerisation. Additionally in comparison to free radical polymerisation, chain transfer is now enhanced and it is now reversible if the correct CTA is used. Specifically the mechanism of RAFT polymerisation is as follows (Figure 1.2).

1.1.1.1. RAFT polymerisation mechanism

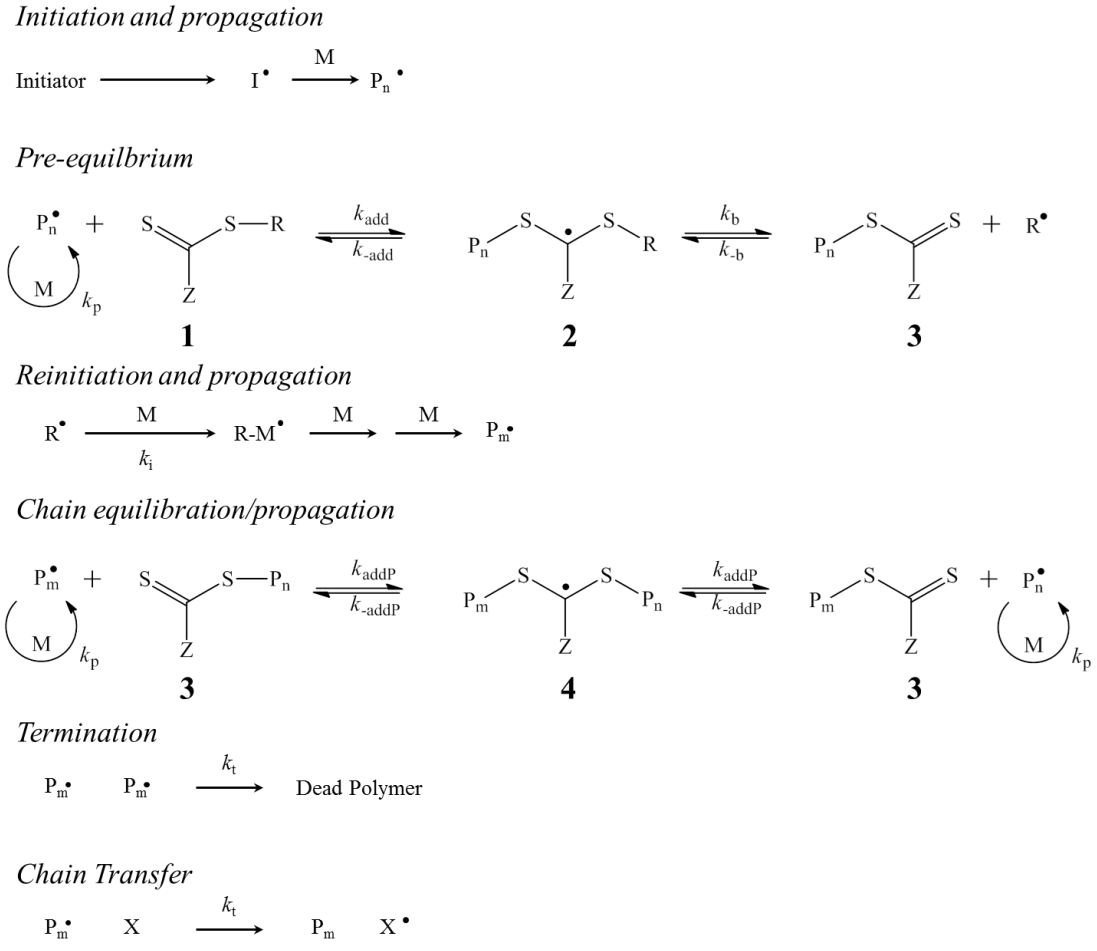

Figure 1.2 Mechanism of RAFT polymerisation.[26]

Initially a radical species is produced from the decomposition of a radical initiator. This radical species is then able to react with the chosen monomer to produce the initial monomer radical, $P_n\cdot$. RAFT polymerisation then proceeds *via* two equilibria. The first equilibrium is the reversible chain transfer / propagation. Here as the C=S bond is much more reactive to radicals than C=C bonds and therefore the growing polymer chain will rapidly add to the CTA via the C=S bond to produce the intermediate radical **2**. However, although stabilised by the Z group on the CTA the lifetime of intermediate radical **2** is very short lived and as

the R group is a good homolytic leaving group the polymer chain then stabilises to become **3**, where R· can then further reinitiate the polymerisation.

Here a rapid equilibrium is produced between the dormant Macro CTA, **3**, and the propagating radicals through the radical intermediate **4** (Figure 1.2 chain equilibrium / propagation). This degenerative transfer mechanism allows for control over molecular weight when compared to free radical polymerisation, as now the probability for each RAFT polymer to undergo propagation with a radical monomer is equal between chains and therefore all chains grow at an equivalent rate, thus giving low dispersity and good control over the molecular weight of the polymer. Furthermore it should be noted that the RAFT process neither creates nor destroys the initiated radicals and as such the rate of polymerisation is the same as free radical polymerisation under perfect conditions. Hence it can then be deduced that the rate of polymerisation is therefore pseudo first order with respect to monomer. To minimalize termination and chain transfer the concentration of radicals produced needs to be low and as the RAFT process neither creates nor destroys radicals, this can be reduced by introducing less radical initiator to the system.[10]

Given that RAFT polymerisation works on the equilibrium between the macroCTA and the radical intermediates **2** and **4**, careful selection of both the R and Z groups is needed for successful polymerisation of the selected monomer. For example if the equilibrium lies too far towards the radical intermediates **2** or **4** then the polymer chains do not grow at equal rates and broad polymer distributions are observed.

Specifically the R group must be a good homolytic leaving group with respect to P_n as poor leaving groups will cause the polymers to exist as **2** in the reversible chain transfer / propagation step for longer periods of time and cause rate retardation for the polymerisation. Additionally the R group must have a high partition coefficient (ϕ), which is the relation between the ratio between the starting materials and the products, and of the radical intermediate. Where the partition coefficient is defined using equation 1.1.

$$\phi = \frac{k_b}{k_{-add}+k_b} \qquad (1.1)$$

On the other hand the Z group controls the reactivity of the thiocarbonyl group to radical addition. The Z group maintains the stability of the radical intermediates **2** and **4**, however, for a RAFT polymerisation to be effective and have low dispersity the Z group cannot be too good as a stabilising group, as this will hinder the fragmentation of the R group towards the R· species. Although the R and Z groups can be altered to provide a range of chain transfer agent for polymerisation it should be noted that each RAFT agent should be tailored towards the monomer of interest. For example methyl methacrylate (MMA) is a more activated monomer and will therefore need an R group which can have a good leaving group when compared to the propagating radical P_n·. Furthermore, the Z group must be electron withdrawing as to ensure a good rate of radical addition towards the C=S bond on the CTA. Figure 1.3 depicts the R and Z groups matched towards each monomer.

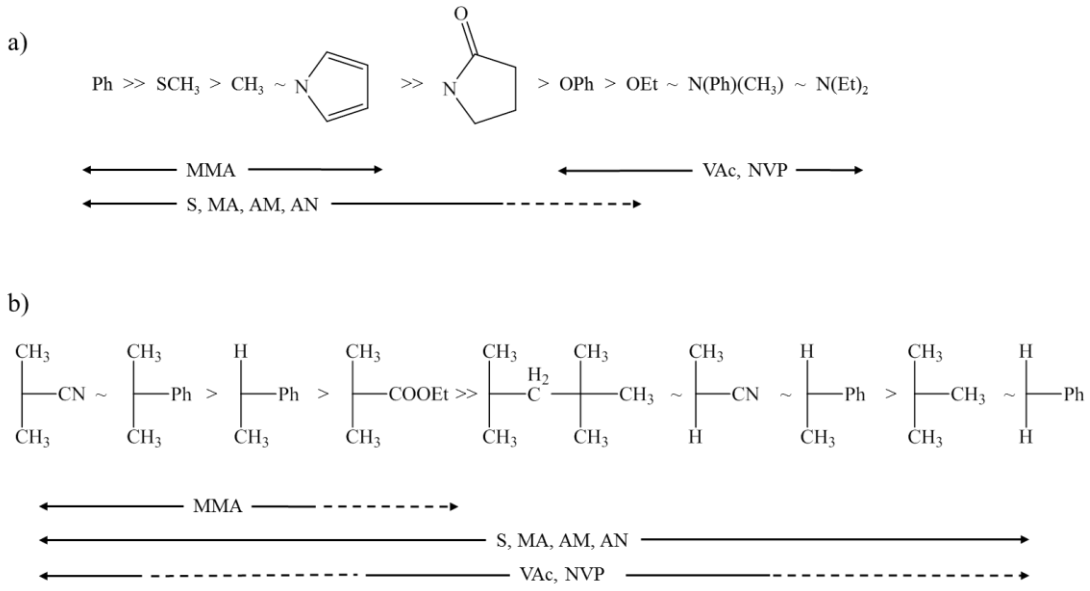

Figure 1.3. Guide to RAFT agent selection of Z and R groups. a) Z group dependent on monomer of choice. b) R group dependant on monomer choice. The dashed line indicates partial control.[26]

Another benefit of RAFT polymerisation over conventional free radical polymerisation is the ability to chain extend the polymer with a second monomer thereby producing a block copolymer. In a similar manner a novel feature of the polymers produced using a RAFT polymerisation is that the polymer chains terminated with the thiocarbonate from the CTA can be utilised further with specific chemistries post polymerisation, such as Michael addition,[17] thermolysis and radical induced removal to name a few,[34,35] and can produce block copolymer analogues.[36] Specifically the thiocarbonate group can be exploited by a range of chemistries for example the thiocarbonate group can be modified to produce second block mimics,[37] protein end groups and fluorescent tagged end groups.[17,38,39] Furthermore, these polymer end groups can result in vastly different properties to the original polymer, in some cases these end groups can induce self-assembly in solution, even if the end groups are short alky chains.[40] Winnik and co-workers have explored extensively the self-assembly of telechelic polymers in solution and have concluded that small telechelic end groups had large effects on the properties in solution, ranging from new structures formed through to changes in rheological properties.[41-47] These new end group modified polymers are interesting when compared to block copolymers, because the former will all have an end group that is identical, for instance if a long chain molecule or amino acid is added. However, the latter will have a second block which is inherently different between polymers a consequence of the second polymer block dispersity.

As previously stated, these block copolymers and block copolymer analogues can in some cases phase separate, producing a step up in hierarchy (Figure 1.1) as now larger structures with defined polymer domains can be formed.[4,48]

1.2. Precise morphology control

The next length scale to maintain control over is on the nanometer scale (Figure 1.1). It is known that in the bulk both block copolymers and block copolymer analogues can microphase separate when thermodynamically favoured.[7,49-52] This phase separation is

dependent on the interaction between the two blocks, known as the Flory-Huggins interaction parameter, $\chi_{AB,}$ and the relative degree of polymerisation, N.[51] If it is thermodynamically unfavourable for the blocks to mix the block copolymer will phase separate within the bulk to minimise this unfavourable interaction, producing defined domains composed of each block. This phase separation leads to an array of morphologies, which may also be observed in solution dependent on polymer solvent interactions (χ_{AS} and χ_{BS}), and which can be controlled by carefully synthesising the length of the polymer blocks to give specific volume fractions, f_{block} (Figure 1.4a).[50] Equilibrium morphologies can then be experimentally obtained through annealing the samples which then mimic theoretically predicted structures (Figure 1.4 b and c).

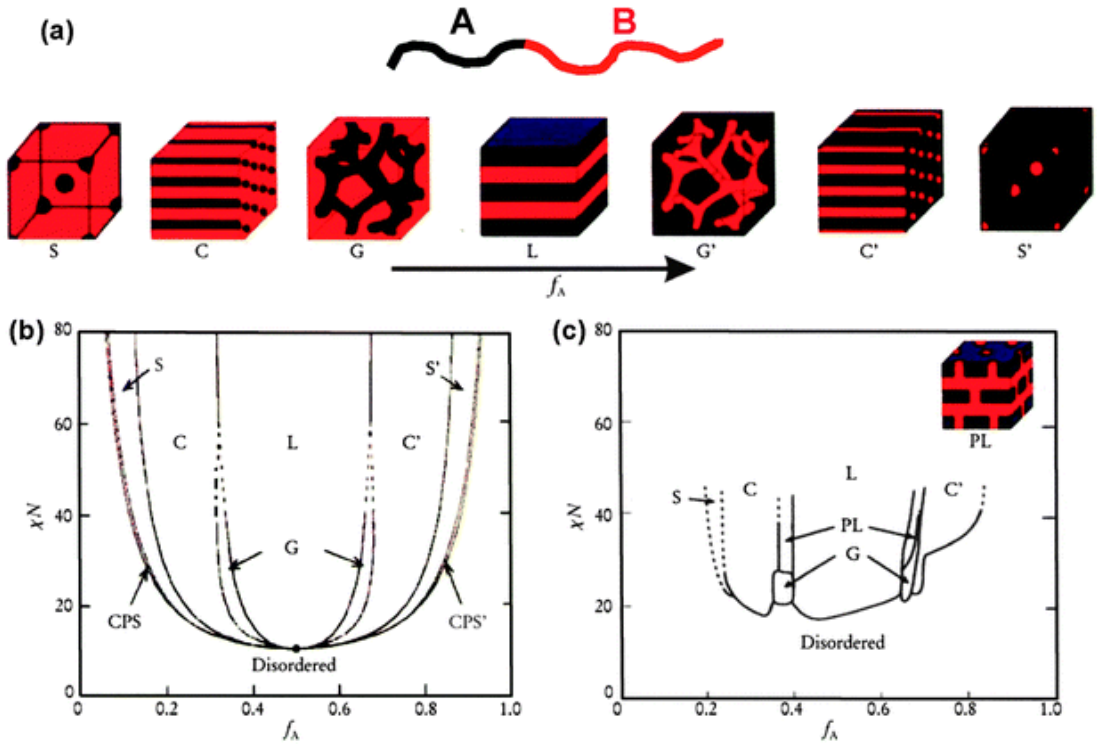

Figure 1.4. a) Morphologies formed by AB diblock copolymers in the bulk at equilibrium: S and S' body-centered-cubic spheres, C and C' = hexagonally packed cylinders, G and G' = bicontinuous gyroids, PL = perforated lamellae and L = lamellae. b) Phase diagram of AB diblock copolymers in the bulk theoretically predicted. c) Phase diagram of polyisoprene-block-polystyrene (PI-PS) diblock copolymers in the bulk obtained experimentally. Figure adapted from ref [7]

Nevertheless, even if the polymers do not phase separate in the bulk a self-assembled structure can still form in dilute solution, as the phase separation is also dependent on the polymer-solvent interactions for solution assembly, which may be more thermodynamically unfavourable than polymer-polymer interactions.[53]

These polymers are coined amphiphilic copolymers, here one block(s) of the chain is lyophilic and the other is lyophobic. When amphiphilic polymers are dispersed into selective solvent (or solvent mixture) the polymers spontaneously self-assemble in dilute solution into a range of structures on the nanoscale, similar to those structures by surfactant molecules in solution, with the most commonly formed structures being spherical micelles.[15,54,55] The vast range of nanostructures formed at equilibrium is governed by the minimisation of free energy between the two blocks in solution and, between the core forming block and the surrounding solvent.[56,57] Here this is typically dictated by the relative volume fractions (*f*), in a similar manner to bulk phase separation but the influence of solvent can alter these volumes further,[58-60] and lyophobicity of each block and can be strongly related to the packing parameter which surfactant micelles abide by.

The packing parameter of surfactant molecules as investigated by Tanford, Israelachvili, Mitchell and Ninham[61] is a simple concept which allows the relationship between surfactant molecular structure (such as head group area, a_0, tail length, l_c and tail volume, v) and the particle morphology formed to be understood using a critical packing parameter, CPP, (Figure 1.5).

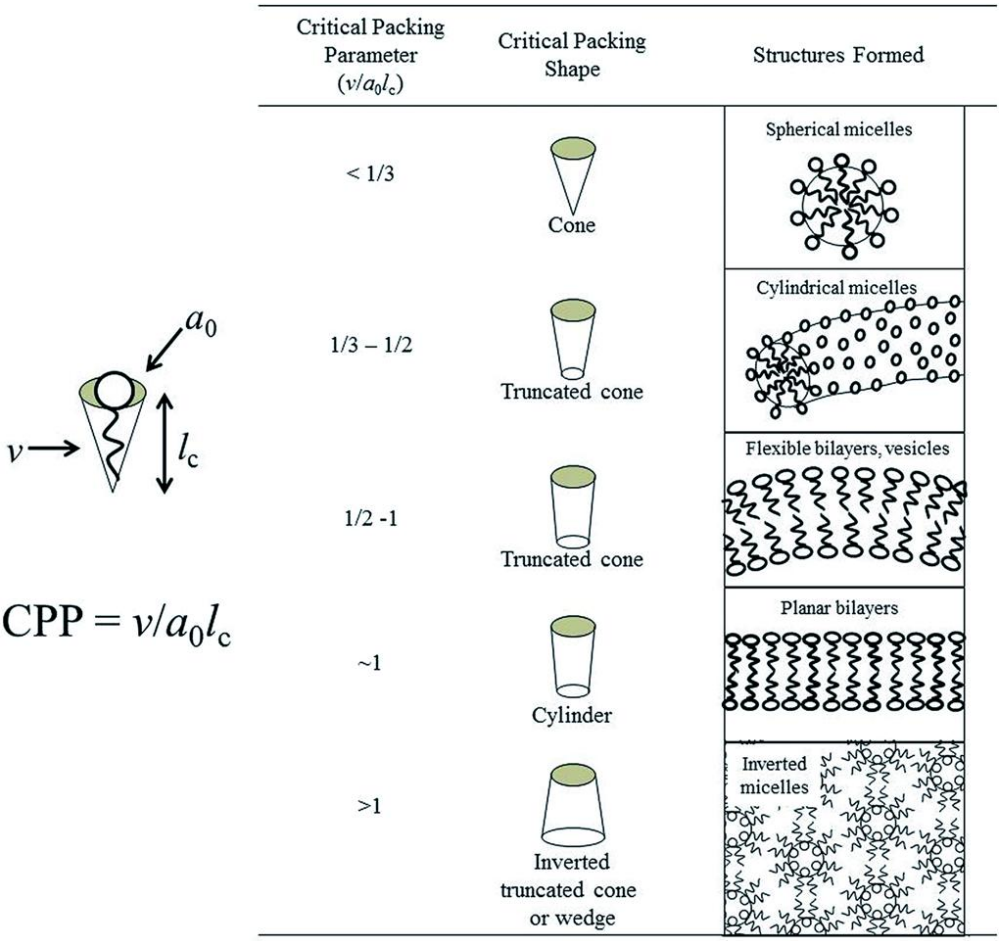

Figure 1.5. Schematic illustrating the relation of surfactant structure to the morphologies found dependant on the critical packing parameter.[62]

For example a spherical micelle will have a core volume related to its radius and aggregation number, *g*, using equation 1.2. The area of the sphere is then given by equation 1.3. Therefore by a combination of both equations 1.2 and 1.3 the radius, *R*, can be given as equation 1.4. Furthermore, it can then be understood that the core of the micelle is composed completely of surfactant tails which then indicates that the core radius cannot exceed the length of the surfactant tail. Leading to the first critical packing parameter of $v/a_0l_c < 1/3$ for spherical micelles. Understanding the other geometries e.g. cylinders and bilayers, the relation of surfactant structure to CPP can be found.

$$V = gv = \frac{4}{3}\pi R^3 \text{ (1.2)}$$

$$A = ga_0 = 4\pi R^2 \text{ (1.3)}$$

$$R = \frac{3v}{a_o} \text{ (1.4)}$$

Accordingly it can then be understood that for amphiphilic block copolymers the solvophobic block is a mimic of the surfactant tail and the solvophilic block is a mimic of the polar head group.[5,63] Here controlling the polymer chain lengths, domains sizes in the structures such as bilayer thickness or cylindrical micelle width are controlled, in addition to the resulting morphology if the structures are under thermodynamic control.[64] By controlling and targeting the correct volume fraction by polymerisation methods, specific morphologies can be easily targeted. Therefore not only can minority domains of the nanostructures be governed but also the larger morphology and hence a much richer range of nanostructure phases can be accessed in solution.

Although synthetically targeting specific block lengths can be achieved through changes in polymerisation conditions, this can be synthetically taxing. However, a much simpler approach to obtain the desired volume fractions is to simply blend two diblock copolymers together, differing in volume fractions of the blocks, as such that the average volume fractions meets that of the desired volume fraction, f, for the specific morphology and / or polymer composition.[65-69] Jain *et al* studied blends of poly(ethylene oxide)-*block*-poly(butadiene) (PEO-*b*-PB) diblock copolymers in aqueous media. Here, different block lengths of PEO and PB were targeted by blending PEO-*b*-PB diblock copolymers, the degree of polymerisation for PEO was 46 or 170 and the degree of polymerisation for PB ranged from 42 to 478, and the resulting morphologies were examined by cryo-TEM. It was observed that by blending PEO-*b*-PB diblock copolymers together, differing in the block lengths, a range of intermediate morphologies between the two pure diblock systems could be targeted if specific blending routes for assembly in solution were used.[70]

Although the assembly of polymers in the bulk has been extensively studied and is used to understand the structures formed by polymers in solution, the assembly to form polymeric nanostructures at equilibrium in solution are not as well understood, especially those with controlled functionality. Despite a huge variety in functional nanoparticles in solution found in the literature the reports of diblock copolymers at equilibrium in solution have largely been studied on block copolymers with limited functionality along the polymer chain e.g. poly(butadiene), poly(styrene) and poly(ethylene oxide) and have not been studied in great depth from polymers formed from RDRP techniques where a greater range of functionality is incorporated. From either a synthetic or blending viewpoint the next step in polymer control would therefore introduction of functionality into the structure and to have equilibrium particles with controlled functionality.

1.3. Precise control over functionality location

Although well-defined block copolymers can be produced from living polymerisation with very good length scale control in terms of chain length, these polymers and subsequently their self-assembled nanostructures typically lack functionality in the discrete domains. This lack of functionality is a result of the difficulty in having a polymerisation technique which can produce polymers of defined lengths, which is necessary to obtain morphology control, whilst tolerating functionality.

A surplus of functional polymers exists but an interesting class of functional polymers are pH responsive polymers.[71] These polymers can these exploited in two distinct ways, first pH responsive polymers can be exploited to scavenge acidic protons or hydroxide ions, for example amine based polymers are able to scavenge acidic protons in solution and consequently act as neutralising agents.[72,73] The second is that the response to pH can alter the solvophobicity or volume fraction of the polymer block in solution. For example polymers formed using a 2-(diethylamino)ethyl methacrylate (DEAEMA) monomer have been reported to undergo interesting morphology changes with respect to pH, where in a

deprotonated state the DEAEMA is hydrophobic and once protonated is hydrophilic.[74,75] In a similar manner polymers formed from a 2-(dimethylamino)ethyl methacrylate (DMAEMA) monomer do not show a change in from hydrophilic to hydrophobic upon changes in pH, DMAEMA is hydrophilic in all ionisable states when the polymer is below its lower critical solution temperature (LCST), but will indeed become more hydrophilic and possess a larger volume fraction in the protonated state.[76,77]

With respect to introducing functionality into morphologies it can be understood that, if polymer block A needs to be a specific volume fraction, f_A, to target the desired morphology (Figure 1.4). Furthermore, a specific chain length must be achieved to then target a desired domain size range, a functional monomer can be polymerised to match this specification, or a polymer in solution can produce a response to stimuli which alters the polymer block to fulfil the volume fraction needs.[78,79] Consequently a structure of precise morphology and size and with the desired functionality within phase seperated domains can be produced which could be exploited to give a desired macroscale property.

For example Wang *et al* synthesised a range of poly(styrene)-*block*-poly(ethylene oxide) diblock copolymers which form a range of structures in solution dependant on the volume fractions of the PEO block.[80] However PEO shows little response to stimuli under milder conditions (a lower critical solution temperature is observed at above 100 °C and above atmospheric pressure) and consequently the structures are unresponsive to change in solution conditions. However, Yu *et al* studied poly(styrene)-*block*-poly(acrylic acid) diblock copolymers in water and it was observed that by changing the pH of the solution the structures could produce new nanostructures in solution.[60] This was a consequence of changing the ionisation of the acrylic acid units which alters the effective volume fraction of the polymer block. Therefore by using polymerisation techniques to give a precise chain length the domain size could be controlled (for example core radius) in the micelle morphology. Therefore Yu *et al* formed similar structures to the PS-*b*-PEO polymers in

solution however, the added functionality allowed for an increase in the number phases observed for this PS-*b*-PAA diblock copolymer series.

This functionality control is not just limited to homopolymer blocks; RAFT polymerisation can produce a range of functional copolymer blocks, formed of two or more different monomers, of low dispersity.[81-83] The benefit of copolymer blocks is that they can be used to circumvent problems where a specific characteristic may be needed for a desired application, for example a targeted temperature or pH response, which could not be achieved from a polymer produce by a single monomer. Consequently by producing copolymer blocks a broader range of functionality and behaviour could be introduced into the self-assembled polymer structure.

As a copolymer is composed of two or more monomers the distribution of these two monomers throughout the block can vary. Consequently copolymers are classified accordingly to how the monomers are distributed along the polymer chain. Broadly this is subdivided into five classes:

- Alternating copolymers. Here the monomers are sequenced in an alternating fashion e.g. ABABABABAB.
- Statistical copolymers. Here the monomers are sequentially distributed along the polymer chain according to the statistical laws e.g. BAABBAABA
- Random copolymers. Here the monomers are distributed randomly as the probability of find a specific monomer at a given chain location is independent of the adjacent monomer.
- Periodic copolymer. Here the monomers are distributed in a repeating sequence along the chain e.g. AAABBBAAABBB
- Gradient copolymer. Here the monomers are distributed in a gradient fashion along the polymer chain. Where the A rich domains of the polymer chain will change to a B rich domain e.g. AAABABABBB

- Block copolymer. Here the monomers are distributed in distinct blocks. Where one monomer will be completely consumed before the polymerisation of the second monomer e.g. AAAAABBBBB

These copolymer microstructures are dependent on the reactivity ratio between the monomers of choice. Specifically this is the relation of how monomer A will polymerise in the presence of monomer B. For example if a growing polymer chain is capped with monomer A it can react in two ways a) continue to polymerise with monomer A b) alternative and polymerise with monomer B and vice versa if the polymer chain is capped with monomer B (Figure 1.6).

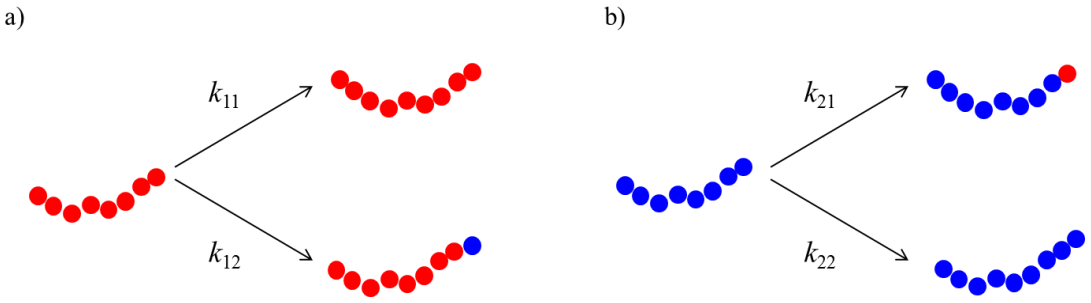

Figure 1.6. Schematic of the different ways in which a growing polymer chain can react with a selection of two monomers in solution.

The reactivity ratios, *r*, of these monomers are then dependent on the four rate constants that exist using the Mayo-Lewis equations (1.5 and 1.6).

$$r_1 = \frac{k_{11}}{k_{12}} \quad (1.5)$$

$$r_2 = \frac{k_{22}}{k_{21}} \quad (1.6)$$

The resulting r_1 and r_2 values will therefore predict which copolymer is produced. For r_1 and r_2 >> 1 then the two monomers have no affinity to react towards one another and

copolymerisation does not occur. However, for r_1 and $r_2 > 1$ then copolymerisation is still not favoured but cross polymerisation can occur to some degree. For a truly random copolymer $r_1 = r_2 \sim 1$, here both monomers are just as likely to react with each other as they are with themselves. On the other hand if $r_1 = r_2 \sim 0$ then each monomer has no tendency to react with itself and an alternating polymer is produced. The final instance is if one monomer has a reactivity ratio much higher than 1 and the second has a reactivity ratio much lower than 1. Here a gradient copolymer will be produced, one monomer is consumed very quickly and then slowly the second monomer begins to become incorporated once significant amount of the first monomer has been depleted.

Copolymers are attractive from a self-assembly aspect as they are able to introduce variable degrees of functionality into neutral domains. It is understood that the Flory interaction parameter between two blocks (χ_{AB}) and between the blocks and the solvent (χ_{AS} and χ_{BS}) can dictate the structures formed in solution; hence a novel method to change the structures would be to alter these Flory interaction parameters. A novel method to achieve this is to use copolymers as one of the blocks. Here it is predicted that the Flory interaction parameter could be altered relative to the copolymer composition.

Very recently Bendejacq *et al* studied this prediction further with a copolymer block but with additional functionality which has the potential to give a higher level of control to the polymer structures. Both a poly(styrene) - *block* – poly(acrylic acid) copolymer and a poly(styrene - *co* - acrylic acid) - *block* – poly(acrylic acid) were studied in the bulk and solution.[49,53] In the bulk it was concluded that introduction of acrylic acid units into the styrene block reduced the Flory-Huggins interaction parameter and if enough acrylic acid units are present in the styrene block then no bulk structure was observed. However, when these polymers were dispersed in aqueous solution by introducing functionality into the core forming block, micelles with a functional micelle core were produced. Moreover, Bendejacq *et al* were able to show by small angle neutron scattering (SANS) analysis in solution that

the structure factor peak for poly(styrene) – *block* – poly(acrylic acid) diblock copolymer did not change morphology upon stimuli, in this case pH, (maintained its lamellar, *L*, morphology) but only became swollen due an increase of hydration upon ionisation of the acrylic acid units and its dimensions changed. Whereas the poly(styrene - *co* - acrylic acid) - *block* – poly(acrylic acid) diblock copolymer in solution produced a broader range of morphology phases, from lamellar, *L*, to molten lamellar, *L*', to spheres, *S*, and molten spheres, *S*', from an introduction of functionality into the core domain and therefore the core hydration, which could be controlled leading to morphology changes in ionisation of the polymer in solution, where overall ionization of 0 is a neutral species (Figure 1.7).[53,84]

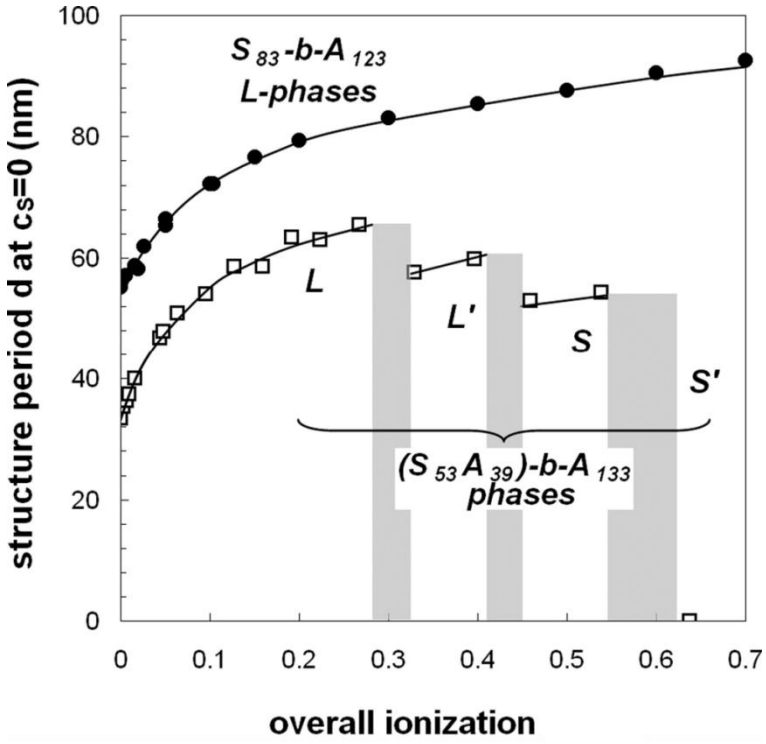

Figure 1.7. Evolution of the structure period as a function of the overall ionisation for diblocks poly(styrene -*co*- acrylic acid) - *block* – poly(acrylic acid), ($S_{53}A_{39}$)-*b*-A_{133} (□) and poly(styrene) – *block* – poly(acrylic acid), S_{83}-*b*-A_{123} (●) in solution.[53]

In a similar system, the assembly of a poly(acrylic acid-*co*-styrene) - *block* – poly(acrylic acid) in solution was explored, however in this system the core forming block is a gradient between acrylic acid and styrene as opposed to a statistical distribution.[85] Here Laruelle *et al*

demonstrated using a combination of SANS and fluorescence studies of the polymers dispersed in solution that the poly(acrylic acid-*co*-styrene) - *block* - poly(acrylic acid) diblock copolymers assembled into spherical micelle aggregates analogous to those formed by a poly(styrene) - *block* - poly(acrylic acid) system. However, this system was able to reorganise and respond to stimuli as a consequence of the introduction of functionality into the micelle aggregates. Specifically a transition between unimer chains and assembled hierarchal micelle structures was observed by lowering the pH of the solution. Although on the nanoscale functionality can be introduced into morphology domains, which in turn will respond to a specific stimuli, there can be larger macroscale behaviours produced from specifically controlling the functionality in these nanoscale domains. For example Colombani and co-workers studied the rheology of poly(*n*-butyl acrylate-*co*-acrylic acid)-*block*-poly(acrylic acid)-block- poly(*n*-butyl acrylate-*co*-acrylic acid), P(*n*BuA-*co*-AA)-*b*-PAA-*b*-P(*n*BuA-*co*-AA), triblock copolymers in aqueous media.[86] Here the block lengths were kept constant, thus domain sizes were controlled in solution, but the composition of the associating core blocks were altered by copolymerisation. From rheological measurements it could be observed that the viscoelastic relaxation time for the system could be tuned over orders of magnitude by varying the composition of the associating block and consequently the core domain (Figure 1.8). Specifically when more acrylic acid units were incorporated into the *n*-butyl acrylate blocks the average viscoelastic relaxation time decreased, which was related to the dynamic nature of the associating core forming blocks. Through copolymerisation a range of systems which can act as either a viscoelastic fluid or hydrogel on the macroscale can be produced. Furthermore, the nanoscale structure is still controlled and maintained throughout, but the changes in solution behaviour arise from introduction of functionality into the defined core domains in the micelle morphology.

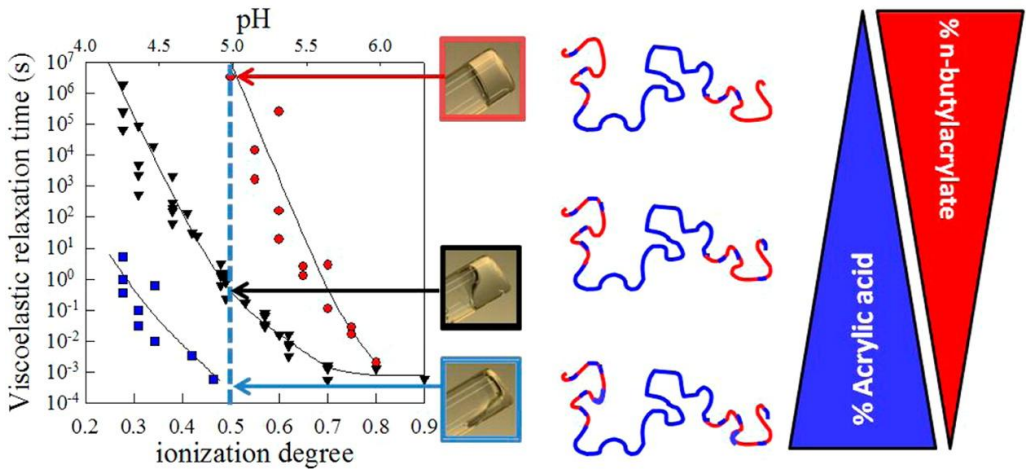

Figure 1.8. Dependence of the average viscoelastic relaxation time for P(nBuA-co-AA)-b-PAA-b-P(nBuA-co-AA), triblock copolymers with different core forming compositions.[86]

It is becoming more apparent that selective introduction of functionality to the core forming domains can offer an even larger range of morphologies with added functionality this class of copolymer diblock are relatively unexplored.

1.4. Precise control of equilibrium behaviour

The complication with amphiphilic block copolymer nanostructures in solution is that typically these polymers cannot reach thermodynamic equilibrium and therefore the structures formed are under kinetic control.[87-90] This kinetic control means that the structures dictated by the packing parameter are often never reached and intermediate morphologies are formed, which is a consequence of the slow kinetics of polymer systems in comparison to surfactant analogues.

Throughout the literature, polymeric structures are often characterised into two distinct groups with regards to their kinetics and equilibrium behaviour.[87] The first are dynamic micelle structures, these micelles are able to overcome the kinetic constraints in the system and can reach thermodynamic equilibrium.[87,88,91] The second are frozen micelles, also known

as out of equilibrium micelles, these micelles cannot overcome the kinetic restraints nor can they rearrange reversibly in solution and therefore very rarely reach thermodynamic equilibrium in solution.[87,92] Nevertheless it should be noted that although by definition there is a clear distinction, experimentally it is much more difficult to accurately determine whether a micelle is frozen or dynamic and it will crucially depend on the length scale of experimental time used.[87]

It is understood that there are two predominant mechanisms for the reorganisation of polymer micelles in solution, with regards to equilibration (Figure 1.9).[55,93,94] The first is a constant exchange of polymer chains (unimers) between the micelles.[55] This route has been concluded both experimentally and theoretically to be the most favourable mechanisms for equilibration in solution.[95] Therefore, when the dynamics of the system are discussed it will predominantly be based on the assumption that unimer exchange is the only mechanism for the equilibration of micelle structures in solution.

The second mechanism is through a fusion / fission mechanism, where polymer particles will physically collide and then rearrange by coalescence to produce a single new micelle or after collision may fissure to produce two new micelles. However, the energy barrier for this mechanism is extremely high and is therefore very unfavourable for this to occur.[94,96] Experimentally it was initially believed that these fusion events did occur during the equilibration of polymer micelles in solution.[97,98] However, recent experimental results concluded that these fusion events were predominantly from incorrect fitting of the experimental data.[88,99] Furthermore, simulations have also been conducted that again confirm that this fusion / fission mechanism is extremely unfavourable and will only happen in specific cases such as those systems extremely far from equilibrium.[93,96]

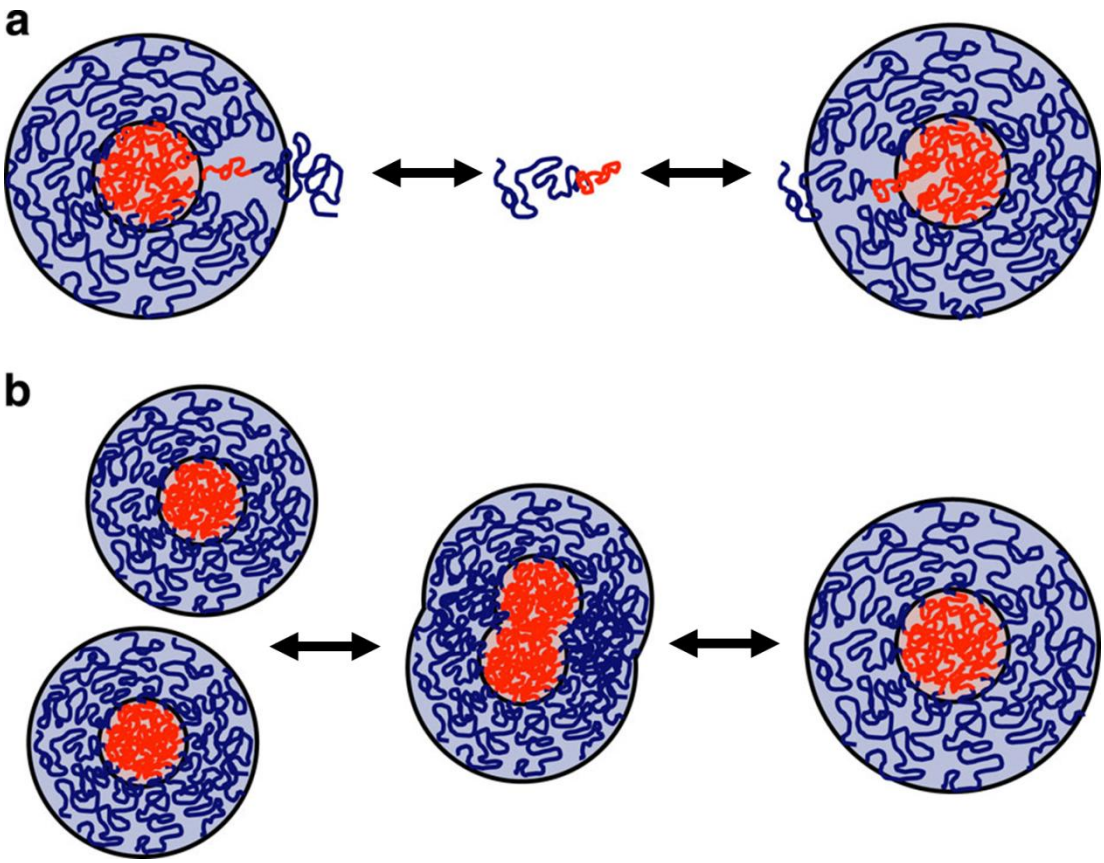

Figure 1.9. Illustration of the two primary routes for equilibration in block copolymer structures in solution. a) Unimer exchange mechanism, here a single polymer chain escapes one micelle diffuses through solution and re-enters a different micelle. b) Two micelles collide and the core domains merge to form a new micelle or will undergo fission to produce two micelles.[100]

The difference between the two systems is the ability of the micelles to reorganise in solution and exchange polymer chains between structures. The ability to do so is related to an array of factors but the predominant ones are glass transition temperature (T_g) of the core forming block, interfacial tension between the core and solvent, block length and steric hindrance of the polymer chains. All of these factors are dependent on the characteristics of the polymer chain, e.g. length and monomer(s) of choice. Therefore, although the understanding and absolute conformation of a frozen or dynamic structure is not well understood it can be suggested that a precise structure with controlled domain sizes and functionality under equilibrium could be achieved if the kinetics restraints are considered.

1.4.1.1. Influence of T_g

Firstly is the glass transition temperature, T_g, of the micelle core. The T_g of the coronal blocks can be neglected as the polymer in these domains are heavily solvated. If the T_g of the core blocks of the micelle is above the experimental temperature then the micelle cores are glassy and it is obvious that no rearrangements or exchange of polymer chains can occur, leading to morphologies under kinetic control.[66] Bendejacq *et al* studied poly(styrene)-*block*-poly(acrylic acid), PS-*b*-PAA, diblock copolymers in water and showed that although lamellar morphologies could be found with a PS core domain on initial dispersion into water, the glassy PS core of the micelles prevents any structural reorganisation and relaxation of the surface curvature, thus preventing the formation of structures that abide by the packing parameter or that would reorganise upon stimuli from the ionic acrylic acid corona domain.[49,53,84] However, once the samples were annealed at high temperatures the core became mobile and structural reorganisation could then occur, leading to structures under thermodynamic control.

This effect of T_g on morphology was also demonstrated by Choi *et al* with poly(styrene)-*block*-poly(ethylene-*alt*-propylene) diblock copolymers, PS-*b*-PEP.[101] Here on initial dispersion in sqaulene, a selective solvent for the PEP block, metastable micelle structures were formed. Once these solutions were annealed at temperatures above the glass transition of the styrene core the structures could reorganise to form more homogenous structures as observed by small angle x-ray scattering (SAXS) and dynamic light scattering (DLS), this was concluded to be an effect of the high T_g of the styrene core forming block preventing the formation of structures with controlled morphologies and domain lengths.

Nevertheless styrene is not the only monomer which can form frozen structures, Rager *et al* studied the dynamics of poly(acrylic acid)-*block*-poly(methyl methacrylate) PAA-*b*-PMMA diblock copolymers by non-radiative energy transfer (NRET).[102] Rager *et al* showed that in water the exchange of unimer chains is minimal for long PMMA blocks, however, upon

heating there is a dramatic increase in the NRET response, a consequence of the exchange of chains between micelles due to an unlocking of a glassy core.

1.4.1.2. Influence of Interfacial tension

The second influence on the exchange dynamics of polymer micelles is the energy barrier for molecular exchange. This energy barrier is related to the interfacial tension,γ, between the core forming block and the surrounding solvent and secondly the size of the collapsed core forming block, $N_b^{2/3}$.[55,94,103] This energy barrier defined as *E* is typically given as equation 1.7

$$E = \gamma N_b^{\frac{2}{3}} \quad (1.7)$$

It can therefore be understood that the effect T_g of the micelle core is independent of the energy barrier and even if the experimental temperature is above the T_g of the micelle core, unimer exchange may still be prohibited from a kinetic viewpoint. Colombani *et al* studied poly(acrylic acid)-*block*-poly(*n*-butyl acrylate), PAA-*b*-P*n*BuA, diblock copolymers in water and with a range of different solution conditions.[104,105] Using a range of scattering methods and electron microscopy it was observed that these micelles did not change structure depending on solution conditions but only on assembly pathway. Hence it was concluded that the micelles were under kinetic control and were subsequently frozen in water from the high energy barrier for unimer exchange. This polymer system was also explored by Jacquin *et al* and with deuterium labelled small angle neutron scattering (SANS) no exchange of polymer chains was observed between micelles over a time scale of 6 months confirming the conclusion that indeed these polymers are frozen due to a high interfacial tension between the core and the solvent.[106]

Another polymer with a low T_g core forming block, poly(ethylene oxide)-*block*-poly(butadiene), PEO-*b*-PB, diblock copolymers were investigated by Won *et al* using deuterium labelled small angle neutron scattering.[107] After 8 days no difference in the SANS profiles were observed for a post mixed sample, that is a sample mixed once the solutions

were assembled. Furthermore when the SANS profile was compared to a sample that was mixed prior in the bulk and then dispersed, differences between the two profiles were noted (Figure 1.10). The authors concluded that this discrepancy is from a lack of chain exchange and that the exchange of a single chain may be on the order of years owing to the poor compatibility between the PB core and solvent despite the liquid-like PB core domain. In a second report by Jain *et al*,[70] different micelle structures formed by PEO-*b*-PB were mixed, therefore causing a disruption to the system, and the evolution of structural reorganisation (equilibration) was observed by cryogenic transmission electron microscopy (cryo-TEM). It could be observed that these PEO-*b*-PB polymers did not show any evolution of structure with time which was related to the strong interfacial tension between PB and the water.

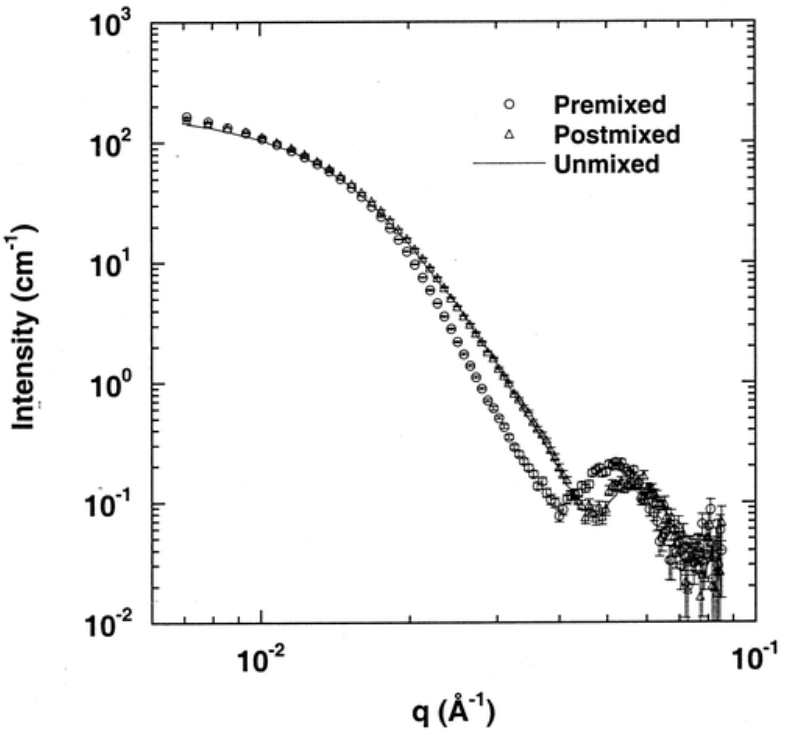

Figure 1.10. SANS profiles of PEO-*b*-PB diblock copolymers in water: premixed (circles) and postmixed (triangles). The solid line represents and arithmetic mean of the SANS profile between the two precursor samples and indicates no reorganisation of the system.[107]

However, although these examples demonstrate that the high energy barrier creates frozen micelles, this effect of interfacial tension is also evident when compared to dynamic

micelles. For example when poly(ethylene glycol)-*block*-poly(propylenesulfide)-*block*-poly(ethylene glycol), PEG-*b*-PPS-*b*-PEG, block copolymers are compared to poly(ethylene glycol)-*block*-poly(propyleneoxide)-*block*-poly(ethylene glycol), PEO-*b*-PPO-*b*-PEO, the former were shown to produce cylindrical micelles in water which over time will rearrange to spherical micelles, where the latter formed spherical micelles when dispersed in water where.[108,109] This behaviour is a consequence of the higher interfacial tension with PPS and thus slower dynamics are observed in this polymer system yet both systems are dynamic in nature.

1.4.1.3. Influence of block length

Another influence on the exchange dynamics is the length of the core forming block, as shown in equation 1.7 the energy barrier is related to both the interfacial tension and the block length of the core forming block.

For example unimer exchange in micelles from poly(ethylene oxide)-*block*-poly(styrene) polymers, consisting of a polystyrene core domain were examined by Nonradiative energy transfer (NRET). Here for NRET analysis one set of polymer micelles had a NRET donor labelled chains and the second set of polymer micelles had a NRET acceptor labelled chains. Once mixed a strong NRET response can be observed and recorded if exchange of polymer chains occurs. For the poly(ethylene oxide)-*block*-poly(styrene) system it was shown that when the core forming block had a degree of polymerisation of 45 the chains are dynamic and NRET could be observed when the solution is heated to 60 °C (Figure 1.11).[98] However, when the degree of polymerisation is 80 no exchange is observed and the micelles are consequently frozen.[110]

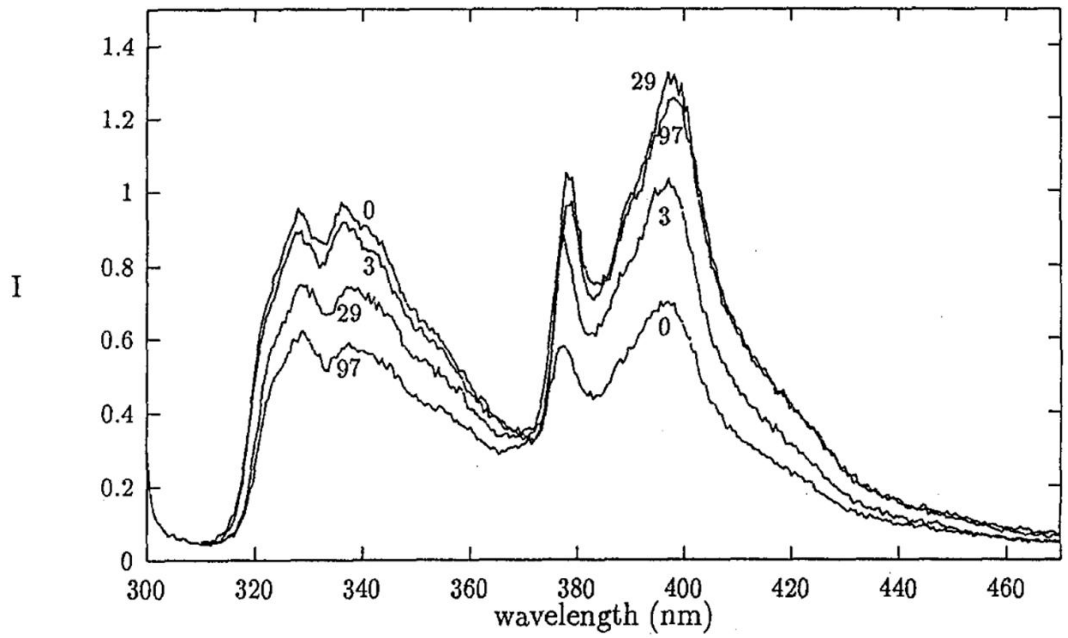

Figure 1.11. Emission spectra of NRET labelled poly(ethylene oxide)-*block*-poly(styrene) diblock copolymers in water at 60 °C after mixing donor and acceptor labelled micelle solutions when t = 0 hrs, t = 3 hrs, t = 29 hrs and t = 97 hrs. Excitation was at 290 nm, note the decrease in NRET donor emission at 340 nm and an increase in NRET acceptor emission at 400 nm with time.[98]

NRET was also used to examine the exchange dynamics of poly(sodium methacrylate)-*block*-poly((dimethylamino)ethyl methacrylate), PMANa-*b*-PDMAEMA diblock. Here two diblock copolymer systems were investigated, one had a PDMAEMA core block length of 24 and the other 15 and the coronal forming blocks were similar. As observed by NRET experiments the micelles with the smaller PDMAEMA core forming block had much faster exchange dynamics and this was due to a reduction in the energy barrier for molecular exchange, therefore less energy is required for molecular exchange.[111]

Furthermore Lu *et al* studied the equilibration on poly(styrene)-*block*-poly(ethylene-*alt*-propylene) (PS-*b*-PEP) copolymers with different PS core block lengths by time resolved small angle neutron scattering (TR-SANS) with deuterium labelling. Here it was shown that for the polystyrene chains with a smaller degree of polymerisation, the exchange of chains was faster which can then again be related to the reduction in the energy barrier for unimer exchange and less energy was required for exchange.[112]

1.4.1.4. Influence of sterics

Steric interactions can play a role in the dynamics of self-assembled polymer systems. Although not many studies have been experimentally undertaken they do nonetheless conclude that the effects of steric influences can alter the dynamics. As mentioned previously Stam *et al* studied the effect of structure on chain dynamics between micelles formed from poly(sodium methacrylate)-*block*-poly((dimethylamino)ethyl methacrylate), diblock copolymers.[113] By NRET analysis it was concluded that when the *n*-propyl groups on the amino monomer were replaced by isopropyl groups, therefore giving identical solvophobicity, the chain exchange slowed down. The authors concluded that this could be from an increase in steric interactions in the core produced from branching which causes a slower exchange rate to be observed.

Although the dynamics of self-assembled polymer systems at equilibrium are not greatly understood in detail they still have a huge impact on the behaviours observed on the macroscale and will therefore change the applications in which these polymer micelles are used. For example, the delivery of a drug molecule can be achieved using responsive polymer micelles, which would require a precise length scale control for specific domain sizes and precise control over morphology. In addition the equilibrium behaviour of the system must be accounted for to ensure efficient drug delivery at the target area.

1.5. Precise understanding of characterisation of solution morphologies

Although a range of nanostructures can be obtained in solution the nanostructures can be very different from one another, in both behaviour and structure. As mentioned previously many polymer assemblies may form frozen structures and therefore both structure and behaviour on the nanoscale will vary on assembly pathway and structures may vary between

self-assembled samples even if the same polymer was used.[6] It should then be obvious that for applications using polymer assemblies that the nanostructures must be reproducible. Although many routine analytical techniques exist for the precise analysis of polymer chains e.g. ^{1}H nuclear magnetic resonance spectroscopy (NMR), or size exclusion chromatography (SEC), these techniques may be limited in specific scenarios and even more so for block copolymers and block copolymer analogues. For example, SEC can be problematic if a good solvent for both blocks is unavailable; additionally it is often difficult to obtain composition distributions for multiblock copolymers. Although it is paramount to be able to determine the molecular characteristics of block copolymers, it could be argued that it is most beneficial to understand their *in situ* behaviours in solution, specifically for their self-assembled structures. Therefore techniques which can operate on a much larger length scale are to be sought after.

1.5.1. Small angle scattering

Scattering experiments offer a non-invasive method to characterise the structure (both morphology and domain sizes) and the dynamics of the particles (by offering an insight in how the change in the number of micelles or their specific aggregation numbers varies over time or to stimuli).[87] Commonly light, x-rays and neutrons are used as radiation sources, although each will probe the structure differently and therefore give distinct information. However, the underlying physics between each technique is similar and can be understood together.[114] Throughout this thesis light and x-ray scattering have been utilised and will be discussed further.

The small angle scattering methods used throughout this thesis all predominately work on the basis of recording the elastic scattering of particles in solution within a given length scale. Typically a sample is placed in a sample cuvette and illuminated by a radiation source (in this thesis either light or x-rays are used) and the scattering emission, which is sample dependent, is recorded at a known angle by a detector (Figure 1.12).[115] The length scale over

which particles are analysed is dependent on the q range in which the illumination source can access (1.8), when the amplitude of the scattered wave vector k_s is the same as the incident k_i then the scattering wave vector, q, is defined as (1.9). This is dependent on the wavelength (λ), angle of observation (θ) and the refractive index of the solvent (n), given in the form (1.9)[116]

$$q = k_i - k_s \quad (1.8)$$

$$q = \frac{4\pi n \sin\frac{\theta}{2}}{\lambda} \quad (1.9)$$

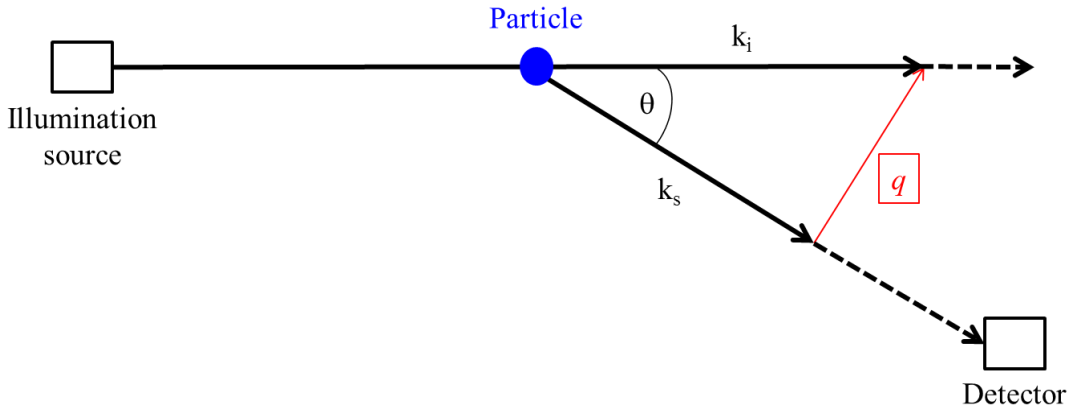

Figure 1.12 Schematic illustration of a scattering experiment.

1.5.1.1. Static light scattering (SLS)

With static light scattering (SLS) the mass, size, and interactions between particles and solvent can be obtained. SLS works on the premise of measuring the change in coherent, elastic scattering. Typically in static light scattering the average intensity of scattered light over long periods of time (typically 1000 times longer than the relaxation time (τ) of the system) is measured (Figure 1.13).[115] The long time over which the scattered light is

averaged ensures that small fluctuations in scattered light from the dynamics of the system are lost and the average intensity of scattered light is therefore time-independent and thus structural information can therefore be gained.

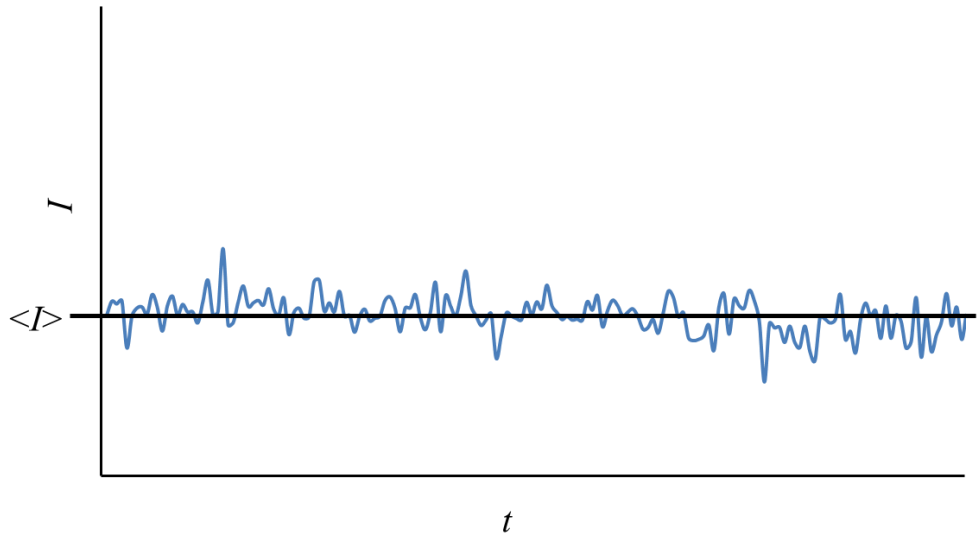

Figure 1.13 An example relationship between scattered light intensity, *I*, with time, *t*, and the average scatter intensity, <*I*>, over a much longer time period.

The most common routine for light scattering analysis of polymers in dilute solution is to perform experiments within the Zimm regime and to use the Zimm equation to obtain structural information,[117] Equation 1.10. Here the scattered radiation as a function of q^2 at a range of different concentrations is measured.

$$\frac{KC}{R_\theta} = \left(\frac{1}{M_w} + 2\mathrm{A}_2 C\right)\left(1 + \frac{q^2 {R_g}^2}{3}\right) \quad (1.10)$$

Where *K* is the contrast factor, which will account for the instrumental factors and the d*n*/d*C* of the sample given by (1.11)

$$K = \frac{4\pi^2 {n_0}^2}{\lambda^4 N_A}\left(\frac{dn}{dC}\right)^2 \quad (1.11)$$

Where n_o = 1.496 is the refractive index of the reference liquid (toluene), d*n*/d*C* is the specific refractive index increment determined by differential refractometry and N_A is Avogadro's number.[118]

R_θ is the Rayleigh ratio of the solutions measured using toluene as a reference according to (1.12).

$$R_\theta = = \frac{I_{Solution}(\theta) - I_{Solvent}(\theta)}{I_{Toluene}(\theta)} R_{Toluene} \quad (1.12)$$

Where I_i represents the intensity scattered by species *i* and $R_{toluene}$ is the Rayleigh ratio of the toluene reference.

Linear regression of KC/R_θ as a function of q^2 when c tends to 0 will provide (Figure 1.14a)

- The slope is equal to give $R_g^2/MW\sqrt{3}$ and the intercept is equal to $1/M_w$

Linear regression of KC/R_θ as a function of c when q^2 tends to 0 will provide (Figure 1.14b)

- The slope is equal to give A_2 and the intercept is equal to $1/M_w$

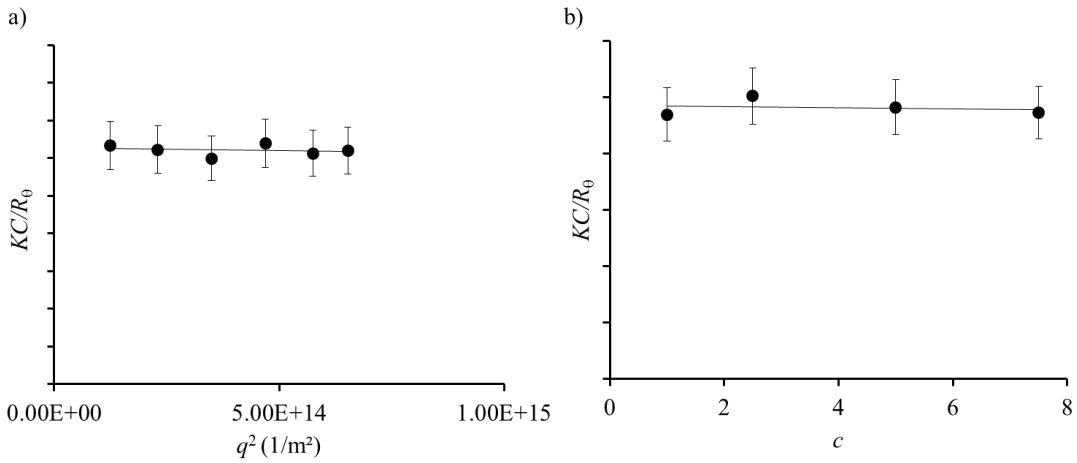

Figure 1.14. Example KC/R_θ data plots from SLS. a) Example plot of KC/R_θ vs q^2.b) Example plot of KC/R_θ vs concentration, *c*. Erros bars indicate a 10% error typically associated with light scattering.[115]

It should be noted that it is not possible to determine a value for R_g of less than 20 nm for light scattering a consequence of a lack of accuracy with respect to the scattered intensity; R_g is calculated using the slope of the KC/R_θ vs q^2 plot. The typical error for light scattering is 10%,[105,115] for example if a particle with a R_g of 17 nm is present the difference in intensity between 30° and 150° is 10%. Thus the slope of KC/R_θ vs q^2 will also give the same result as statistical error on the data and therefore for particles with an R_g of less than 20nm an average can be taken from all KC/R_θ values when plotted as a function of q^2.

Although for simple monodisperse nanoparticles the routine Zimm analysis is relatively simple for polymer solutions be it self-assembled or soluble polymer chains, a few differences and considerations must be addressed.

Firstly for the scattering of light to be related back to the concentration and shape or size of the isotropic particles, the particles must not either a) produce multiple scattering or absorb the light or b) modify the wavelength of light. Specifically for particles analysed by light scattering this is simply fulfilled by having a differential refractive index that is close to the solvent used, furthermore due to the nature of polymers typically the chains are penetrated by the solvent which helps to resolve these limitations.

Moreover, although a suitable dn/dC will allow for light scattering analysis to be undertaken the concentration of the polymer must be high enough to ensure adequate scattering of the particles above the fluctuations in solvent density. Furthermore, for polymer self-assemblies it is understood that possibly at low enough concentrations the particles will change morphology, therefore the concentration of the particles must be high enough to ensure the correct particles of interest are analysed. Moreover, if the concentration of the particles in solution is too high then multiple scattering can occur within the solution and the scattering obtained from the solution is then not representative of the single polymer particles in solution.

However, difficulties with respect the concentration can also arise from the size of the particles in solution, as the linear regression with respect to q^2 in the Zimm regime is only valid when higher order terms for R_g are negligible, specifically when $q^2R_g^2$ is <1.

1.5.1.2. Dynamic light scattering (DLS)

In the previous section it was concluded that the small changes in scattered light over short time periods can be related to changes in concentration and or density fluctuations in the q regime investigated. These fluctuation can be further understood by using a $g_2(t)$ correlator and producing an auto correlation function of the scattered light.

The auto correlation function is the intensity of light at time t = 0, I_0, multiplied by the intensity of light after a period of time I_t averaged over a much longer time point I_t (1.15a and Figure 1.15b)

$$g_2(t) = \frac{\langle I_o I_t \rangle}{\langle I_t \rangle^2} \quad (1.13)$$

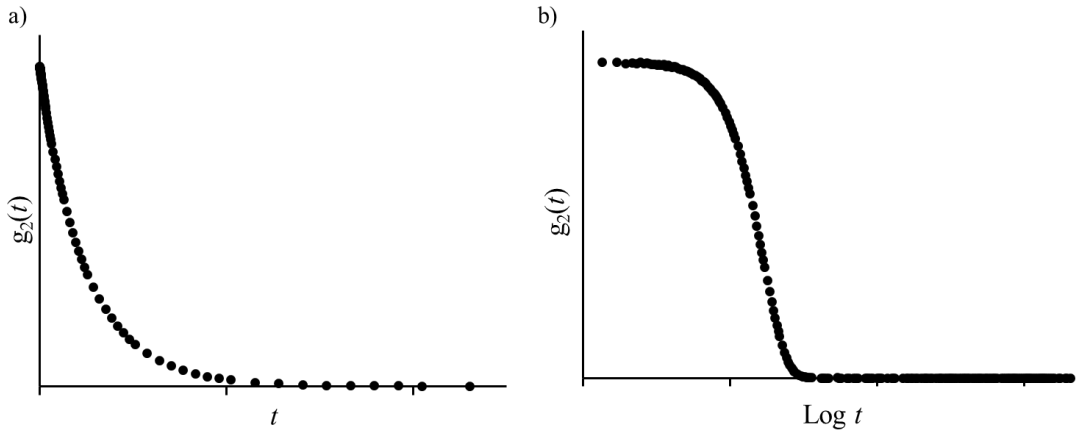

Figure 1.14 Example correlation functions obtained by DLS. a) Example plot of $g_2(t)$ versus time, t, on a linear scale. b) Example plot of $g_2(t)$ versus time, t, on a log scale.

This $g_2(t)$ intensity autocorrelation can be related to the electric field autocorrelation function $g_1(t)$ using the Seigert relation (1.14), where β is a correction factor related to the alignment of the of the laser.[119]

$$g_2(t) = 1 + \beta[g_1(t)]^2 \quad (1.14)$$

In a model system of perfect spheres under Brownian motion $g_1(t)$ is a simple single exponential decay (1.15).

$$g_1(t) = exp(-Dq^2t) \quad (1.15)$$

Where the relaxation time of the system is related to the apparent diffusion coefficient, *D*, by (1.16)

$$\tau = \frac{1}{Dq^2} \quad (1.16)$$

However, in polymer solutions the structures are often disperse, and therefore a perfect exponential in the autocorrelation function will not be observed. Then $g_1(t)$ will in fact be a weighted sum of exponential decays, which will be proportional to the mass of the particle, *M*, and the number of particles, *N* (1.17).

$$g_1(t) = \frac{\sum M^2 N exp(-Dq^2t)}{\sum M^2 N} \quad (1.17)$$

As a range of decay times exist a plot of $g_1(t)$ as a function of *t* on a log scale will yield a linear relation. However, it is more common to understand this decay as a range of relaxation times between two defined limits and therefore $g_1(t)$ is given as (1.18).

$$g_1(t) = \int_0^t A(\tau) \exp\left(-{}^{t}/_{\tau}\right) d\tau \quad (1.18)$$

To date a Laplace transformation is commonly used to calculate the relaxation time distribution for a specific correlation plot.[120,121] Computer routines exist that can extract the exact $A(\tau)d\tau$ which is the amplitude with a relaxation time in between τ and $\tau + d\tau$.[115,116]

By measuring τ over a range of q the absolute diffusion coefficient D_0 can be obtained. Its concentration dependence is given by $D = D_0(1+k_DC)$ where k_D is the dynamic second virial coefficient and D_0 the diffusion coefficient used for computing the hydrodynamic radius (R_h) of the scatterers according to the Stokes-Einstein equation (1.19).[20]

$$R_h = \frac{kT}{6\pi\eta D_0} \qquad (1.19)$$

With η the solvent viscosity, k Boltzmann's constant and T the absolute temperature. Values of R_h given in the following are then obtained after extrapolation to zero concentration.

On the other hand as mentioned polymers are inherently disperse and τ is typically then measured as an average (1.20).

$$\langle\tau\rangle = \langle\frac{1}{Dq^2}\rangle \quad (1.20)$$

It then follows that the R_h values obtained from DLS of polymer species are indeed z-averages, $\langle R_h\rangle_z$. Therefore a size distribution can be obtained from DLS. It is understood that the scattering intensity of a sample is proportional to K, c and M as understood from SLS. Therefore it follows that for particle i the intensity is as follows (1.21).[122]

$$I_i = K_i c_i M_i \quad (1.21)$$

It can be understood that consequently the hydrodynamic radius is intensity weighted and follows (1.22).

$$\langle R_h\rangle_z = \frac{\sum I_i R_{hi}}{\sum I_i} \quad (1.22)$$

It can be understood that c is *N.M* and therefore 1.22 is transformed into (1.23).

$$\langle R_h \rangle_z = \frac{\sum K_i nM.M.R_{hi}}{\sum K_i nM.M} = \frac{\sum K_i nM^2 R_{hi}}{\sum K_i nM^2} \quad (1.23)$$

Where *M* is proportional to the hydrodynamic radius scaled with the mass fractal (d_f) of the scattering particles, R_h^{df} which in DLS are assumed to be hard spheres and is 3 which leads to (1.24).

$$\langle R_h \rangle_z = \frac{\sum K_i n {R_{hi}}^7}{\sum K_i n \, {R_{hi}}^6} \quad (1.24)$$

1.5.1.3. Combination of DLS and SLS

A second consideration with polymer particles is that in some cases, two modes of relaxation could be observed in solution (Figure 1.16).

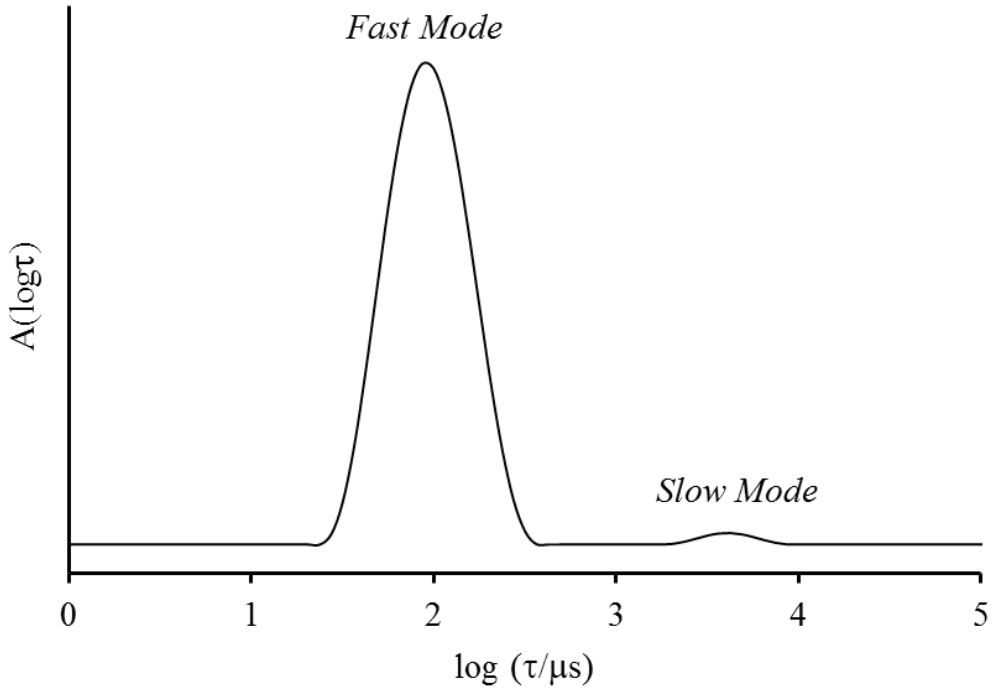

Figure 1.16 Example distribution of relaxation time obtained from DLS showing the two modes of relaxation, both fast and slow.

Therefore it can be understood that if both modes are diffusive in the solvent i.e. there is a linear relationship between <Γ> and q^2, R_θ determined by SLS can be described as the sum of the two modes according to (1.25).[20]

$$R_\theta = R_{\theta f} + R_\theta \mathrm{s} \qquad (1.25)$$

Where *f* and *s* stand respectively for fast and slow modes and using (1.26).

$$R_{\theta f}(q) = \frac{A_f(q)}{\left(A_f(q) + A_s(q)\right)} R_\theta \qquad (1.26)$$

Where A_f and A_s are the relative amplitudes of the fast and slow modes obtained by DLS using equation 1.18.

The slow mode of relaxation observed can sometimes be attributed to spurious aggregates and typically the weight fraction of these much larger particles is negligible.[119,123-125] If the fast mode can be observed then its concentration in solution must be orders above that of the slower mode given that the intensity of scattered light is proportional to the mass of the particle (1.21 and 1.10).[126]

1.5.1.4. SAXS

One of the drawbacks to laser light scattering is the length scales over which structures can be probed, which is governed by the accessible *q* range. However, X-ray scattering provides information on much smaller length scales compared to laser light scattering, typically from 0.1-100 nm as x-rays possess much smaller wavelengths and therefore a larger *q* range is accessible.[122] In addition a second difference to x-ray scattering is the way in which the illumination source will interact with particles. In x-ray scattering the x-rays are scattering by the electrons within the electron cloud of the atoms and the scattering is proportional to the atomic number of the particles and hence the number of electrons in the electron cloud. However, an assembled polymer species or a molecularly solubilised polymer chain in

solution is considered a cluster of atoms and therefore the scattering of x-rays by polymers causes additional scattering within the system, called excess scattering. This excess scattering arises as the particles have a change in electron density and therefore different scattering occurs from these with respect to the solvent. This excess scattering, in a similar manner to light scattering is considered elastic and therefore no transfer of energy from the x-ray to the electrons in the atom occurs and consequently the x-rays retain their wavelength thus producing coherent scattering which can be detected. Depending on the excess scattering pattern the structure of the particles can therefore be deduced as the scattering pattern produced can be used to understand the distance of atoms to one another and their orientation.[114]

Specifically these scattering patterns from polymer species in dilute solution are a combination of the number of particles in the x-ray beam, the particle form factor and the structure factor. Therefore in a similar manner to light scattering the total intensity of the x-rays scattered of isotropic systems is related to the contrast of the system (related to number of electrons), the structure factors, $S(q)$, and the form factor, $P(q)$, in the form (1.27).[122]

$$I = K.S(q).P(q) \quad (1.27)$$

Where the contrast factor K for SAXS is defined by 1.28.[116]

$$K = \left[\frac{0.22\ (V_s Z_m - V_m Z_s)}{V_s Z_m}\right] \quad (1.28)$$

Where z_s is the number of electrons per solvent (s) molecule and z_m is the number of electrons per monomer (m) with volume v.

The particle form factors, $P(q)$, are specific based on how the atoms are aligned within the particle morphology in solution, For example a spherical polymer structure will have a different average alignment of atoms within the morphology compared to polymer cylinders

and hence a different form factor is observed. However, often polymer particles are disperse and therefore the scattering form factor is an average of all particles in the x-ray beam.[116]

On the other hand the structure factors, $S(q)$, are specific based on how the particles are aligned in space, however, for samples in dilute solutions this is how samples interact together in solution.

When a simple plot of intensity of scattered x-rays is against q^2 is produced the shape of the plot can be related to the polymer structure in solution, an example plot of intensity versus q^2 is shown in Figure 1.17. To date many computer models exist which can fit this scattering intensity at a given q value to the particle form factor and structure factor, thus giving a range of structural characteristics such as micelle core radius, R_c, on the nanoscale for polymer assemblies.[127]

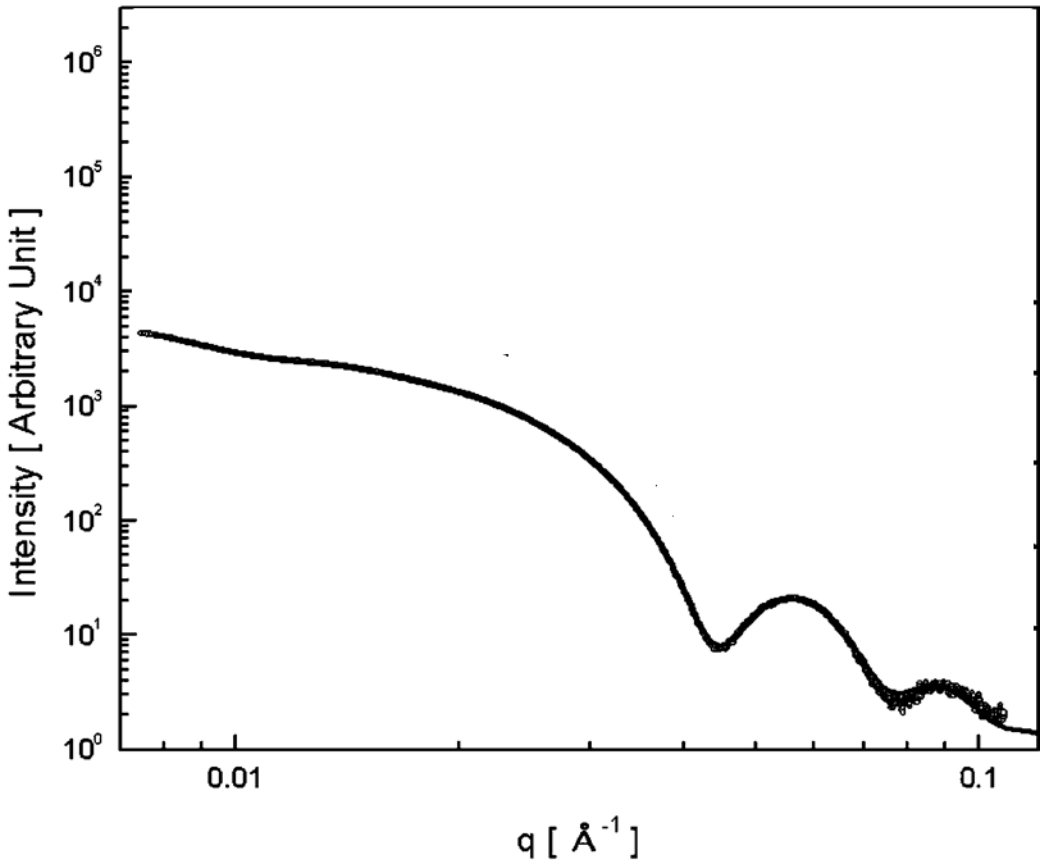

Figure 1.17 Example SAXS profile of poly(styrene)-*block*-poly(ethylene-*alt*-propylene) diblock copolymers, PS-*b*-EP, in squalene.[101]

1.6. Precise control for desired applications

Currently block copolymers in solution have the potential to be used in a variety of large scale applications, furthermore as block copolymers are typically only a minor component of a much larger formulation, the processing procedure of diblock polymers in formulations are therefore only slightly different to the processing of the current polymeric materials in formulations. Nevertheless it has been realised that the large variation of block copolymer morphologies and subsection domains produces an effective solution to an array of problems on both the nano and macro scale. For example within hydrocarbon lubricant formulations for automotive engines an array of components are utilised within the formulation to produce a desired behaviour.[128] Polymeric dispersants, are designed to encapsulate insoluble matter in the non-polar hydrocarbon solvent.[129] Specifically these dispersant molecules must be designed as to ensure specific domain functionality, size and morphology as to have a large affinity to the insoluble matter. Maintaining specific morphologies can keep other large scale properties unaffected e.g. solvent viscosity, which for lubricating formulations is vital. Similarly for solution self-assembly the use of functional diblock copolymers has been shown to produce spherical micelle nanoreactors, which not only shown an improved catalytic function compared to a polymer free system but can catalyse reaction in a media where the catalyst is not inherently soluble in.[130-133]

1.7. Summary

The theme of this introduction is to show that the control of macro scale properties is dependent on control on much smaller length scales for solution self-assembly of polymers. It can then be understood that for an improved performance of polymeric materials, delicate control on these smaller length scales is required.

As stated, it is now conceivable that control on the smallest of polymer length scales, that the monomer size, can be easily obtained from the recent developments in synthetic chemistry. However, the real challenge is to control the hierarchal structures that form in solution and

specifically controlling functional structures in solution at equilibrium with simple and accessible chemistries.

In this thesis this subject is explored further and the ability to understand these larger length scales where polymer self-assembly occurs is understood. In Chapter 2 the smallest length scales are investigated, specifically introduction of functionality into block copolymer analogues and the development of the resulting self-assembled structures with defined functional domains for lubricant additives. These systems are then understood on larger length scales for applications as lubricant additives for marine engines and the effect of nanostructure is explored with respect to the larger macroscale properties in Chapter 3. Model diblock copolymer systems were explored and the ability to obtain precise controlled self-assembled structures with controlled functional domains from pH responsive diblock copolymers in water is discussed in Chapter 4. In Chapter 5 the ability to produce functional domains in a self-assembled diblock copolymer system is explored but using a blending approach with the aim to relieve laborious synthesis on the nanometer length scale. This blending approach is then explored for the next level in hierarchy, precise equilibrium controlled structures, and the ability to form precise equilibrium structures with defined domains from a blending route.

1.8. References

(1) Lodge, T. P. *Macromol. Chem. Phys.* **2003**, *204*, 265.
(2) L. R. Rudnick *Lubricant Additives: Chemistry and Applications*; CRC Press, 2003.
(3) Docampo, P.; Ball, J. M.; Darwich, M.; Eperon, G. E.; Snaith, H. J. *Nat. Commun.* **2013**, *4*, 2761.
(4) Gröschel, A. H.; Schacher, F. H.; Schmalz, H.; Borisov, O. V.; Zhulina, E. B.; Walther, A.; Müller, A. H. E. *Nat. Commun.* **2012**, *3*, 710.
(5) Blanazs, A.; Armes, S. P.; Ryan, A. J. *Macromol. Rapid Commun.* **2009**, *30*, 267.
(6) Hayward, R. C.; Pochan, D. J. *Macromolecules* **2010**, *43*, 3577.
(7) Mai, Y.; Eisenberg, A. *Chem. Soc. Rev.* **2012**, *41*, 5969.
(8) Sun, L.; Petzetakis, N.; Pitto-Barry, A.; Schiller, T. L.; Kirby, N.; Keddie, D. J.; Boyd, B. J.; O'Reilly, R. K.; Dove, A. P. *Macromolecules* **2013**, *46*, 9074.
(9) Voulgaris, D.; Tsitsilianis, C.; Grayer, V.; Esselink, F. J.; Hadziioannou, G. *Polymer* **1999**, *40*, 5879.
(10) Gody, G.; Maschmeyer, T.; Zetterlund, P. B.; Perrier, S. *Nat. Commun.* **2013**, *4*, 2505.

(11) Blum, A. P.; Kammeyer, J. K.; Yin, J.; Crystal, D. T.; Rush, A. M.; Gilson, M. K.; Gianneschi, N. C. *J. Am. Chem. Soc.* **2014**, *136*, 15422.
(12) Gody, G.; Maschmeyer, T.; Zetterlund, P. B.; Perrier, S. *Macromolecules* **2014**, *47*, 3451.
(13) Gody, G.; Maschmeyer, T.; Zetterlund, P. B.; Perrier, S. *Macromolecules* **2014**, *47*, 639.
(14) Renou, F. d. r.; Nicolai, T.; Nicol, E.; Benyahia, L. *Langmuir* **2008**, *25*, 515.
(15) Patterson, J. P.; Kelley, E. G.; Murphy, R. P.; Moughton, A. O.; Robin, M. P.; Lu, A.; Colombani, O.; Chassenieux, C.; Cheung, D.; Sullivan, M. O.; Epps, T. H.III; O'Reilly, R. K. *Macromolecules* **2013**, *46*, 6319.
(16) Patterson, J. P.; Cotanda, P.; Kelley, E. G.; Moughton, A. O.; Lu, A.; Epps, T. H. III; O'Reilly, R. K. *Polym.Chem.* **2013**, *4*, 2033.
(17) Spruell, J. M.; Levy, B. A.; Sutherland, A.; Dichtel, W. R.; Cheng, J. Y.; Stoddart, J. F.; Nelson, A. *J. Polym. Sci. A Polym. Chem.* **2009**, *47*, 346.
(18) Castelletto, V.; Cheng, G.; Greenland, B. W.; Hamley, I. W.; Harris, P. J. F. *Langmuir* **2011**, *27*, 2980.
(19) Dehsorkhi, A.; Hamley, I. W.; Seitsonen, J.; Ruokolainen, J. *Langmuir* **2013**, *29*, 6665.
(20) Chassenieux, C.; Nicolai, T.; Durand, D. *Macromolecules* **1997**, *30*, 4952.
(21) Du, J.; Willcock, H.; Patterson, J. P.; Portman, I.; O'Reilly, R. K. *Small* **2011**, *7*, 2070.
(22) Rosen, B. M.; Percec, V. *Chem. Rev.* **2009**, *109*, 5069.
(23) Sciannamea, V.; Jérôme, R.; Detrembleur, C. *Chem. Rev.* **2008**, *108*, 1104.
(24) Ouchi, M.; Terashima, T.; Sawamoto, M. *Chem. Rev.* **2009**, *109*, 4963.
(25) Perrier, S.; Takolpuckdee, P. *J. Polym. Sci. A Polym. Chem.* **2005**, *43*, 5347.
(26) Keddie, D. J. *Chem. Soc. Rev.* **2014**, *43*, 496.
(27) G. Moad, E. R., S. Thang, *Macromolecules* **1998**, *31*, 5559.
(28) Flory, P. J. *Principles of Polymer Chemistry* Cornell Univ Pr, 1953.
(29) Solomon, D. H.; Rizzardo, E.; Cacioli, P.; US Patent 4,581,429, 1986.
(30) Cuthbertson, M.; Rizzardo, E.; Solomon, D. *Aust. J. Chem.* **1983**, *36*, 1957.
(31) Moad, G.; Rizzardo, E.; Solomon, D. H. *Macromolecules* **1982**, *15*, 909.
(32) Otsu, T. *J. Polym. Sci. A Polym. Chem.* **2000**, *38*, 2121.
(33) T. Otsu, M. Y. *Makromol. Chem Rapid Comm* **1982**, *3*, 127.
(34) Perrier, S.; Takolpuckdee, P.; Mars, C. A. *Macromolecules* **2005**, *38*, 2033.
(35) Chong, B.; Moad, G.; Rizzardo, E.; Skidmore, M.; Thang, S. H. *Aust. J. Chem.* **2006**, *59*, 755.
(36) Willcock, H.; O'Reilly, R. K. *Polym.Chem.* **2010**, *1*, 149.
(37) Boyer, C.; Granville, A.; Davis, T. P.; Bulmus, V. *J. Polym. Sci. A Polym. Chem.* **2009**, *47*, 3773.
(38) Heredia, K. L.; Grover, G. N.; Tao, L.; Maynard, H. D. *Macromolecules* **2009**, *42*, 2360.
(39) Grover, G. N.; Alconcel, S. N. S.; Matsumoto, N. M.; Maynard, H. D. *Macromolecules* **2009**, *42*, 7657.
(40) Du, J.; Willcock, H.; Patterson, J. P.; Portman, I.; O'Reilly, R. K. *Small* **2011**, n/a.
(41) Kujawa, P.; Watanabe, H.; Tanaka, F.; Winnik, F. M. *Eur. Phys. J. E* **2005**, *17*, 129.
(42) Kujawa, P.; Tanaka, F.; Winnik, F. M. *Macromolecules* **2006**, *39*, 3048.
(43) Qiu, X.-P.; Winnik, F. M. *Macromol. Rapid Comm.* **2006**, *27*, 1648.
(44) Kujawa, P.; Segui, F.; Shaban, S.; Diab, C.; Okada, Y.; Tanaka, F.; Winnik, F. M. *Macromolecules* **2006**, *39*, 341.
(45) Koga, T.; Tanaka, F.; Motokawa, R.; Koizumi, S.; Winnik, F. M. *Macromolecules* **2008**, *41*, 9413.
(46) Koga, T.; Tanaka, F.; Kaneda, I.; Winnik, F. M. *Langmuir* **2009**, *25*, 8626.
(47) Ishii, N.; Obeid, R.; Qiu, X.-P.; Mamiya, J.-i.; Ikeda, T.; Winnik, F. M. *Mol. Cryst. Liq. Cryst.* **2010**, *529*, 60.

(48) Groschel, A. H.; Walther, A.; Lobling, T. I.; Schacher, F. H.; Schmalz, H.; Muller, A. H. E. *Nature* **2013**, *503*, 247.
(49) Bendejacq, D.; Joanicot, M.; Ponsinet, V. *Eur. Phys. J. E* **2005**, *17*, 83.
(50) Hamley, I. W. *The Physics of Block Copolymers* OUP Oxford, 1998.
(51) Matsen, M. W.; Bates, F. S. *Macromolecules* **1996**, *29*, 1091.
(52) Khandpur, A. K.; Foerster, S.; Bates, F. S.; Hamley, I. W.; Ryan, A. J.; Bras, W.; Almdal, K.; Mortensen, K. *Macromolecules* **1995**, *28*, 8796.
(53) Bendejacq, D. D.; Ponsinet, V. *J. Phys. Chem. B* **2008**, *112*, 7996.
(54) Riess, G. *Prog. Polym. Sci.* **2003**, *28*, 1107.
(55) Halperin, A.; Alexander, S. *Macromolecules* **1989**, *22*, 2403.
(56) Meli, L.; Lodge, T. P. *Macromolecules* **2009**, *42*, 580.
(57) Nyrkova, I. A.; Semenov, A. N. *Faraday Discussions* **2005**, *128*, 113.
(58) Jusufi, A.; Likos, C. N.; Lowen, H. *J. Chem. Phys.* **2002**, *116*, 11011.
(59) Walther, A.; Goldmann, A. S.; Yelamanchili, R. S.; Drechsler, M.; Schmalz, H.; Eisenberg, A.; Müller, A. H. E. *Macromolecules* **2008**, *41*, 3254.
(60) Yu, Y. S.; Zhang, L. F.; Eisenberg, A. *Macromolecules* **1998**, *31*, 1144.
(61) Israelachvili, J. N.; Mitchell, D. J.; Ninham, B. W. *Biochim. Biophys. Acta* **1977**, *470*, 185.
(62) Salim, M.; Minamikawa, H.; Sugimura, A.; Hashim, R. *MedChemComm* **2014**, *5*, 1602.
(63) Jain, S.; Bates, F. S. *Science* **2003**, *300*, 460.
(64) Davis, K. P.; Lodge, T. P.; Bates, F. S. *Macromolecules* **2008**, *41*, 8289.
(65) Yoo, S. I.; Sohn, B.-H.; Zin, W.-C.; Jung, J. C.; Park, C. *Macromolecules* **2007**, *40*, 8323.
(66) Tian, M. M.; Qin, A. W.; Ramireddy, C.; Webber, S. E.; Munk, P.; Tuzar, Z.; Prochazka, K. *Langmuir* **1993**, *9*, 1741.
(67) Palyulin, V. V.; Potemkin, I. I. *Macromolecules* **2008**, *41*, 4459.
(68) Sens, P.; Marques, C. M.; Joanny, J. F. *Macromolecules* **1996**, *29*, 4880.
(69) Cantu, L.; Corti, M.; Salina, P. *J. Phys. Chem.* **1991**, *95*, 5981.
(70) Jain, S.; Bates, F. S. *Macromolecules* **2004**, *37*, 1511.
(71) Dai, S.; Ravi, P.; Tam, K. C. *Soft Matter* **2008**, *4*, 435.
(72) T. Nadasdi, W. H.; US Patent 6,235,687, 2001
(73) Tomalia, D. A.; Dewald, J. R.; US Patent 4,587,329, 1986.
(74) Lee, A. S.; Bütün, V.; Vamvakaki, M.; Armes, S. P.; Pople, J. A.; Gast, A. P. *Macromolecules* **2002**, *35*, 8540.
(75) Lee, A. S.; Gast, A. P.; Butun, V.; Armes, S. P. *Macromolecules* **1999**, *32*, 4302.
(76) Dutertre, F.; Boyron, O.; Charleux, B.; Chassenieux, C.; Colombani, O. *Macromol. Rapid Commun.* **2012**, *33*, 753.
(77) Bütün, V.; Billingham, N. C.; Armes, S. P. *Chem. Comm.* **1997**, 671.
(78) Moughton, A. O.; O'Reilly, R. K. *Chem. Comm.* **2010**, *46*, 1091.
(79) Moughton, A. O.; Patterson, J. P.; O'Reilly, R. K. *Chem. Comm.* **2011**, *47*, 355.
(80) Wang, C.; Yang, S.; Yu, X.; Zheng, J. X.; Ma, J.; Xu, J.; Zhu, M. *Soft Matter* **2012**, *8*, 10307.
(81) Cotanda, P.; Wright, D. B.; Tyler, M.; O'Reilly, R. K. *J. Polym. Sci. A Polym. Chem.* **2013**, *51*, 3333.
(82) Kang, Y.; Lu, A.; Ellington, A.; Jewett, M. C.; O'Reilly, R. K. *ACS Macro Lett.* **2013**, *2*, 581.
(83) Moore, B. L.; Lu, A.; Longbottom, D. A.; O'Reilly, R. K. *Polym.Chem.* **2013**, *4*, 2304.
(84) Bendejacq, D. D.; Ponsinet, V.; Joanicot, M. *Langmuir* **2005**, *21*, 1712.
(85) Laruelle, G.; François, J.; Billon, L. *Macromol. Rapid Commun.* **2004**, *25*, 1839.
(86) Shedge, A.; Colombani, O.; Nicolai, T.; Chassenieux, C. *Macromolecules* **2014**, *47*, 2439.
(87) Nicolai, T.; Colombani, O.; Chassenieux, C. *Soft Matter* **2010**, *6*, 3111.

(88) Lund, R.; Willner, L.; Richter, D.; Dormidontova, E. E. *Macromolecules* **2006**, *39*, 4566.
(89) Denkova, A. G.; Mendes, E.; Coppens, M.-O. *Soft Matter* **2010**, *6*, 2351.
(90) Cui, H.; Chen, Z.; Zhong, S.; Wooley, K. L.; Pochan, D. J. *Science* **2007**, *317*, 647.
(91) Lejeune, E.; Drechsler, M.; Jestin, J.; Muller, A. H. E.; Chassenieux, C.; Colombani, O. *Macromolecules* **2010**, *43*, 2667.
(92) Stejskal, J.; Hlavatá, D.; Sikora, A.; Konňák, Č.; Pleštil, J.; Kratochvíl, P. *Polymer* **1992**, *33*, 3675.
(93) Dormidontova, E. E. *Macromolecules* **1999**, *32*, 7630.
(94) Nose, T.; Iyama, K. *Comput. Theor.Polym. Sci.* **2000**, *10*, 249.
(95) Lund, R.; Willner, L.; Monkenbusch, M.; Panine, P.; Narayanan, T.; Colmenero, J.; Richter, D. *Phys. Rev. Lett.* **2009**, *102*, 188301.
(96) Nyrkova, I. A.; Semenov, A. N. *Macromol. Theory Simul.* **2005**, *14*, 569.
(97) Willner, L.; Poppe, A.; Allgaier, J.; Monkenbusch, M.; Richter, D. *Europhys. Lett.* **2001**, *55*, 667.
(98) Wang, Y.; Kausch, C. M.; Chun, M.; Quirk, R. P.; Mattice, W. L. *Macromolecules* **1995**, *28*, 904.
(99) Lund, R.; Willner, L.; Richter, D.; Iatrou, H.; Hadjichristidis, N.; Lindner, P. *J. App. Cryst.* **2007**, *40*, s327.
(100) Kelley, E. G.; Murphy, R. P.; Seppala, J. E.; Smart, T. P.; Hann, S. D.; Sullivan, M. O.; Epps, T. H. III *Nat. Commun.* **2014**, *5*, 3599.
(101) Choi, S. Y.; Bates, F. S.; Lodge, T. P. *J. Phys. Chem. B* **2009**, *113*, 13840.
(102) Rager, T.; Meyer, W. H.; Wegner, G.; Winnik, M. A. *Macromolecules* **1997**, *30*, 4911.
(103) Halperin, A. *Macromolecules* **2011**, *44*, 5072.
(104) Colombani, O.; Ruppel, M.; Schubert, F.; Zettl, H.; Pergushov, D. V.; Müller, A. H. E. *Macromolecules* **2007**, *40*, 4338.
(105) Colombani, O.; Ruppel, M.; Burkhardt, M.; Drechsler, M.; Schumacher, M.; Gradzielski, M.; Schweins, R.; Muller, A. H. E. *Macromolecules* **2007**, *40*, 4351.
(106) Jacquin, M.; Muller, P.; Talingting-Pabalan, R.; Cottet, H.; Berret, J. F.; Futterer, T.; Theodoly, O. *J. Colloid. Interface. Sci.* **2007**, *316*, 897.
(107) Won, Y. Y.; Davis, H. T.; Bates, F. S. *Macromolecules* **2003**, *36*, 953.
(108) Cerritelli, S.; Fontana, A.; Velluto, D.; Adrian, M.; Dubochet, J.; De Maria, P.; Hubbell, J. A. *Macromolecules* **2005**, *38*, 7845.
(109) Zana, R.; Marques, C.; Johner, A. *Adv Colloid Interface Sci* **2006**, *123–126*, 345.
(110) Hurtrez, G.; Dumas, P.; Riess, G. *Polym. Bull.* **1998**, *40*, 203.
(111) Creutz, S.; van Stam, J.; Antoun, S.; De Schryver, F. C.; Jérôme, R. *Macromolecules* **1997**, *30*, 4078.
(112) Lu, J.; Bates, F. S.; Lodge, T. P. *ACS Macro Lett.* **2013**, *2*, 451.
(113) Creutz, S.; van Stam, J.; De Schryver, F. C.; Jerome, R. *Macromolecules* **1998**, *31*, 681.
(114) Lodge, T. *Microchim. Acta* **1994**, *116*, 1.
(115) Patterson, J. P.; Robin, M. P.; Chassenieux, C.; Colombani, O.; O'Reilly, R. K. *Chem. Soc. Rev.* **2014**, *43*, 2412.
(116) Roe, R.-J. *Methods of X-ray and Neutron Scattering in Polymer Science*; Oxford University Press: New York, 2000.
(117) Brown, W. *Light scattering: principles and development*; Clarendon Press: Oxford, 1996.
(118) Charbonneau, C.; De Souza Lima, M. M.; Chassenieux, C.; Colombani, O.; Nicolai, T. *Phys. Chem.Chem. Phys.* **2013**, *15*, 3955.
(119) Li, J.; Ngai, T.; Wu, C. *Polym. J.* **2010**, *42*, 609.
(120) Jakes, J. *Collect. Czech. Chem. Commun.* **1995**, *60*, 1781.
(121) Provencher, S. W. *Comput. Phys. Commun.* **1982**, *27*, 229.

(122) Dautzenberg, H. J., W.; Kötz, J.; Philipp, B.; Seidel, C.;Stscherbina, D. *Polyelectrolytes: Formation, Characterization and Application*; Hanser Publishers: Munich, Germany, 1994.
(123) Sedlak, M. *J. Chem. Phys.* **1996**, *105*, 10123.
(124) Sedlak, M. *J. Chem. Phys.* **1997**, *107*, 10805.
(125) Sedlak, M. *J. Chem. Phys.* **1997**, *107*, 10799.
(126) Lejeune, E.; Chassenieux, C.; Colombani, O. Prog. Colloid Polym. Sci., **2011**, *138*,7
(127) Kline, S. *J. App. Cryst.* **2006**, *39*, 895.
(128) Rudnick, L. R. *Lubricant Additives Chemistry and Applications* 2nd ed.; CRC Press, 2009.
(129) S.N.Ahmed, A. M. N., A.Abdel-Azim, *Inter. J. of Polym. Mat.* **2007**, *57*, 114.
(130) Lu, A.; O'Reilly, R. K. *Curr. Opin. Biotechnol.* **2013**, *24*, 639.
(131) Lu, A.; Cotanda, P.; Patterson, J. P.; Longbottom, D. A.; O'Reilly, R. K. *Chem. Comm.* **2012**, *48*, 9699.
(132) Cotanda, P.; Lu, A.; Patterson, J. P.; Petzetakis, N.; O'Reilly, R. K. *Macromolecules* **2012**, *45*, 2377.
(133) Cotanda, P.; O'Reilly, R. K. *Chem. Comm.* **2012**, *48*, 10280.

2. The design and synthesis of amine containing nanostructures for applications as ashless detergents in lubricant formulations.

2.1. Abstract

Modern combustion engines have a mineral oil based lubricant formulation added to improve both the lifespan and optimal performance. To neutralise the acid compounds formed during combustion detergent nanoparticles are added. However, these detergent particles will typically produce an array of oil insoluble products from the neutralisation causing a range of problems in the engine. An alternative is to use "ashless" detergents, formed from organic bases, which do not produce these insoluble by-products of neutralisation. In this Chapter a range of amine polymers have been synthesised by RAFT, the polymers were subsequently modified using a post polymerisation Michael addition to afford amphiphilic end group modified polymers. Their structural characterisation in non-polar media has been explored by laser light scattering and indicates that these amphiphilic amine polymers can act as structural analogues to the current detergent particles.

2.2. Introduction

Since the development of the internal combustion engine lubricants have been used to ensure maximum efficiency of the engine and protect the moving parts in operation. Lubricant formulations typically consists of an array of components, where each component is used to control a specific property within the system thus improving the lifespan and performance of the engine.[1,2] Some of the most important lubricant formulation components are detergent nanoparticles, these consist of metal inorganic salts encased by surfactants to form a reverse micelle structure (Figure 2.1).[3]

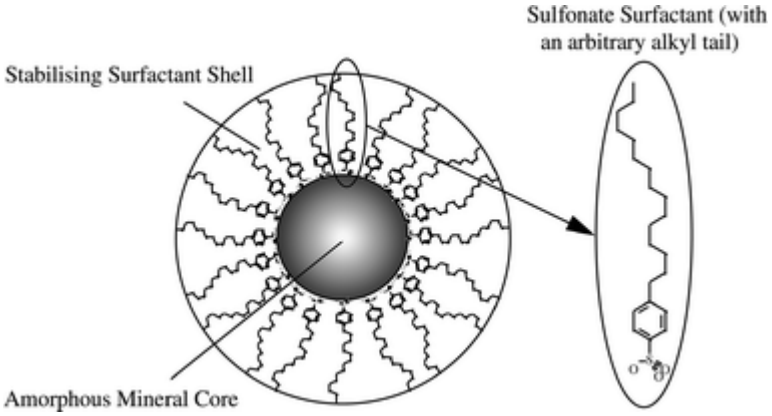

Figure 2.1. Schematic of a typical metal based detergent nanoparticle - structure shown is the reverse micelle structure of a sulfonate detergent particle.[4]

It is well documented that thermal combustion produces a range of by-products including both organic and inorganic acids, the most common of which is sulphuric acid, H_2SO_4. The primary role of these detergent nanoparticles is to provide an active base source that, upon contact with the acid products of combustion, a neutralisation reaction can occur and prevent damage to engine components.[4-6] In the crankcase these acids can build up throughout the engine lifetime and can cause a large array of problems including accelerating rust formation, corrosion and deposit formation which causes significant drops in both engine lifespan and efficiency. Similarly in piston lubrication the formation of these ash substances will cause separation from the cylinder oil and the ash will adhere to the cylinder walls.

Consequently this insoluble bulk material causes a misalignment of pistons with the cylinder walls and impaired function is a result. However, the introduction of detergent nanoparticles can alleviate these problems as they neutralise the inorganic and organic acids formed from combustion.

Although metal salt detergents work well for acid neutralisation there are many associated problems with the current detergent systems. For example, the resultant neutralisation reaction produces large amounts of solid salt products (most commonly referred to as ash). The equation in Figure 2.2 illustrates some of the reactions occurring in the calcium salt core of conventional detergent nanoparticles.

$$H_2SO_4\ (l) + Ca(OH)_2\ (s) \rightarrow CaSO_4\ (s) + 2H_2O\ (l)$$

$$H_2SO_4\ (l) + CaCO_3\ (s) \rightarrow CaSO_4\ (s) + CO_2\ (g) + H_2O\ (l)$$

Figure 2.2. Common neutralisation reactions between calcium hydroxide and calcium carbonate with sulphuric acid in lubricant formulations.

An additional problem for combustion engines is encountered by the additives in cylinder oils, here the lubricant is "burnt off" throughout operation and hence excess additive will form an additional deposit layer on the cylinder walls, lowering the engine lifespan further. Consequently the additive formulation for cylinder oils must be very well matched to the engine environment, specifically to the sulfur content in the fuel, in which it is used. A major challenge is to produce well-defined functional nanoparticles capable of acid neutralisation without the associated ash production for these highly specific cylinder oil formulations.

An alternative to inorganic overbased detergents are ashless nitrogen or oxygen-containing detergents, these provide base for neutralisation, but the benefit of ashless detergents is that they have no inorganic salt and therefore a much lower amount of ash is produced during

their operation.[7] Commonly these ashless detergents are based upon surfactant like molecules where the head group is a nitrogen containing species. Lubrizol have explored this further and identified that aromatic functionalities with an amine incorporated show the most potential for ashless detergents.[7] Similarly, Infineum have explored the use of morpholine derivatives to acts as ashless base sources in lubricant formulations.[8]

Despite the low ash content associated with these current ashless detergents there is also a low base content too, and thus larger concentrations, up to 25 wt%, of these additives are required to give similar performance to the overbased metal salt systems, which is costly from a consumer viewpoint.[7] Therefore, the challenge in the development of ashless detergents is to increase the active base strength or stoichiometric amount of base. Moreover the current ashless detergent systems from Lubrizol and Infineum are primarily based upon solubilised small molecules. The formation of discrete nanostructures, to mimic the conventional detergent structure, has not yet been explored.[1] Furthermore, these amines do not make up a large percentage in the overall composition and are typically primary or secondary amines which are of lower basicity. Thus, the exploitation of highly basic, tertiary amines polymers assembled into defined nanostructures and the investigation of their detergent properties are of interest towards the development of new high total base number (TBN) and ashless detergents.

RAFT polymerisation can produce well-defined, amphiphilic, functional amine polymers which can then self-assemble into larger hierarchical structures in a selective solvent.[9-13] Moreover it is understood that a backbone of methacrylate based polymers shows excellent thermal and oil stability which offers benefits for a detergent nanoparticle with a long lifespan.[14] Furthermore the ashless, tertiary amine functionality has been chosen to provide acid-scavenging ability a consequence of its nucleophilic nature. [15] Described in this Chapter is the synthesis of a range of methacrylate tertiary amine polymers and their self-assembly

and exploration of their properties towards their applications as ashless detergent analogues in non-polar solvents.

2.3. Results and Discussion

2.3.1. Synthesis of the tertiary amine monomers

To explore how different chemistries can change the behaviour of basicity for novel polymer ashless detergents a range of tertiary amine moieties, both alkyl and aromatic were explored. These amine moieties were incorporated into methacrylate monomers and subsequently polymerised by RAFT; Scheme 2.1 depicts the selected amine moiety targets and monomers used.

Scheme 2.1. Acid scavenging monomers investigated.

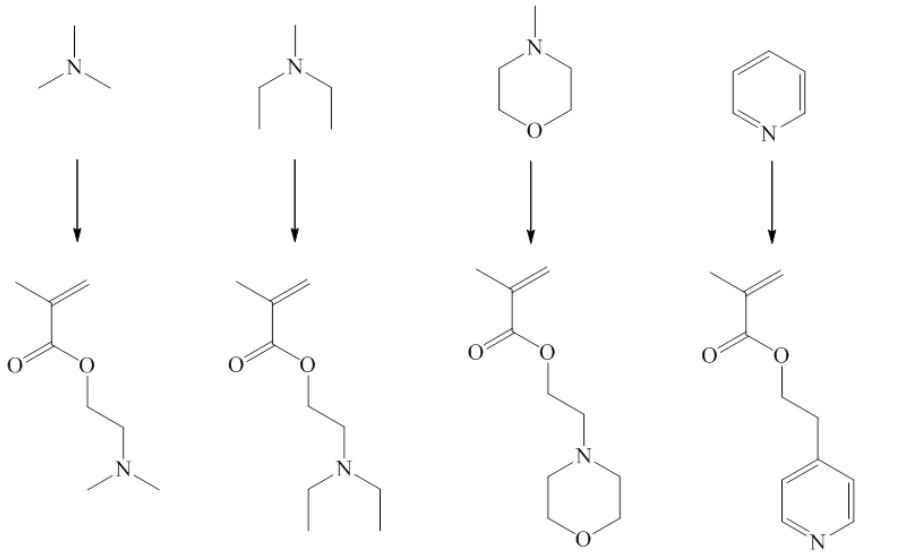

DMAEMA	DEAEMA	MEMA	PEMA
Dimethyl amine ethyl methacrylate	Diethyl amine ethyl methacrylate	2-*N*-morpholinoethyl methacrylate	Pyridinylethyl methacrylate

Dimethyl amine ethyl methacrylate (DMAEMA), Diethyl amine ethyl methacrylate (DEAEMA) and 2-*N*-morpholinoethyl methacrylate (MEMA) are all commercially available and were used as received. However, pyridinylethyl methacrylate (PEMA) was synthesised using a simple Steglich esterification; commercially available methacrylic acid was reacted with 4-pyridineethanol in the presence of 4-dimethylaminopyridine (DMAP) and 1-ethyl-3-(3-dimethylaminopropyl)carbodiimide (EDCI) with dichloromethane (CH_2Cl_2) as the solvent at room temperature, Scheme 2.2.[16]

Scheme 2.2, Synthetic route for the PEMA monomer.

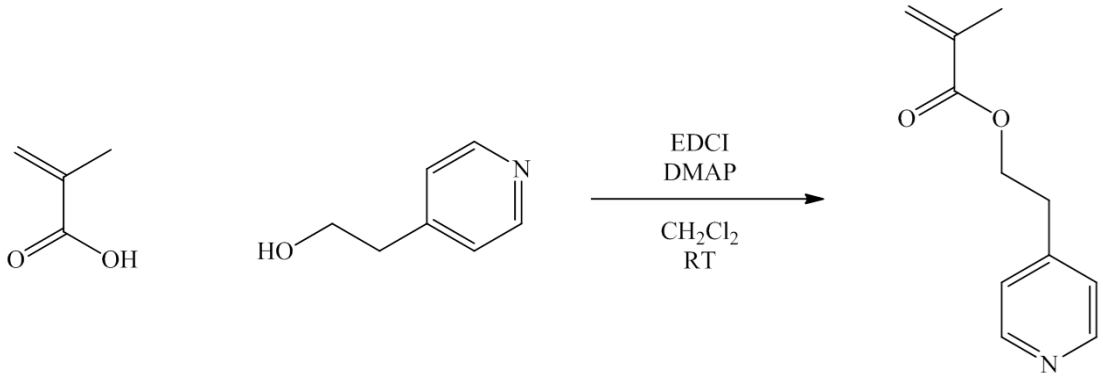

After 24 h ^{1}H nuclear magnetic resonance (NMR) spectroscopy was used to analyse the crude mixture, the resonance signal for the adjacent protons to the alcohol group (C*H*$_2$OH) at *ca*. 3.5ppm shifted to *ca.* 4.2ppm, which are the signals for the protons in the methacrylate ester bond, indicating that the product has formed. PEMA was isolated as a colourless oil by column chromatography in 65% yield, Figure 2.3 depicts the ^{1}H NMR spectrum of PEMA in $CDCl_3$.

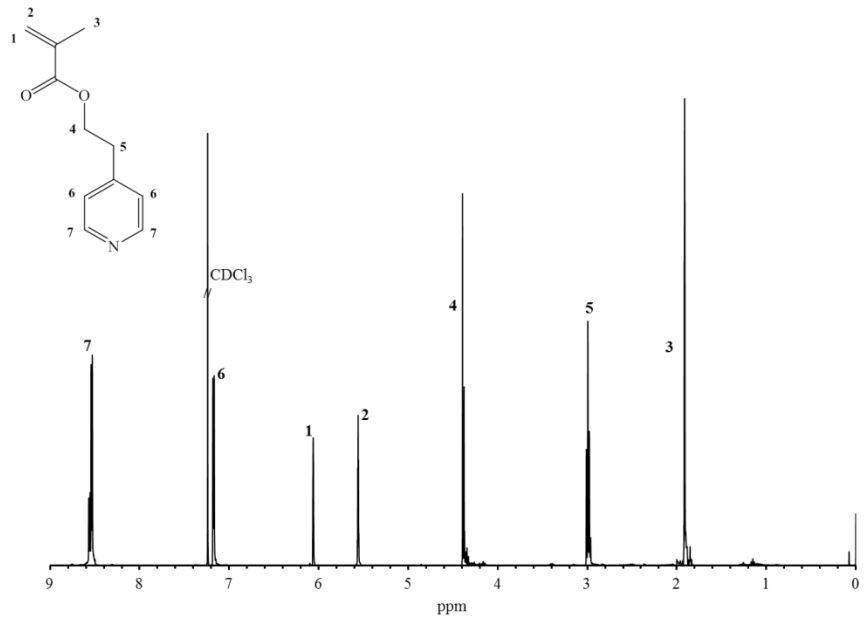

Figure 2.3 PEMA ^{1}H NMR spectrum in $CDCl_3$.

2.3.2. Homopolymerisation by RAFT polymerisation.

2.3.2.1. Synthesis of the chain transfer agent (CTA).

To successfully polymerise the methacrylate monomers by RAFT a chain transfer agent (CTA) is used.[17] Careful choice of the CTA is required to produce polymers of controlled lengths and low dispersity. Specifically the rate of monomer addition to the CTA needs to be high in relation to the rate of propagation, moreover a balance between the rates of reinitiation and fragmentation of the R group must be considered. [18] Furthermore for methacrylate polymerisation the Z group must have a high chain transfer to prevent unwanted termination and subsequently poor control with large dispersites.[19] 2-cyanoprop-2-yl dithiobenzoate (CPDB) was therefore selected as it effectively fulfils these criteria for the polymerisation of (meth)acrylate monomers (See Chapter 1 for specifics on R and Z groups for (meth)acrylate monomers).[15,20,21]

2-cyanoprop-2-yl dithiobenzoate was synthesised by a simple three step reaction (Scheme 2.3). First a bis(thiobenzoyl) disulphide was synthesised from benzyl chloride and subsequently bis(thiobenzoyl) disulphide underwent a radical addition with

azobisisobutyronitrile (AIBN) and ethyl acetate as the solvent under inert conditions. 2-cyanoprop-2-yl dithiobenzoate was isolated as a red oil by column chromatography which crystallised upon cooling in 26% yield, the CTA was characterised ^{1}H NMR spectroscopy and ^{13}C NMR spectroscopy.

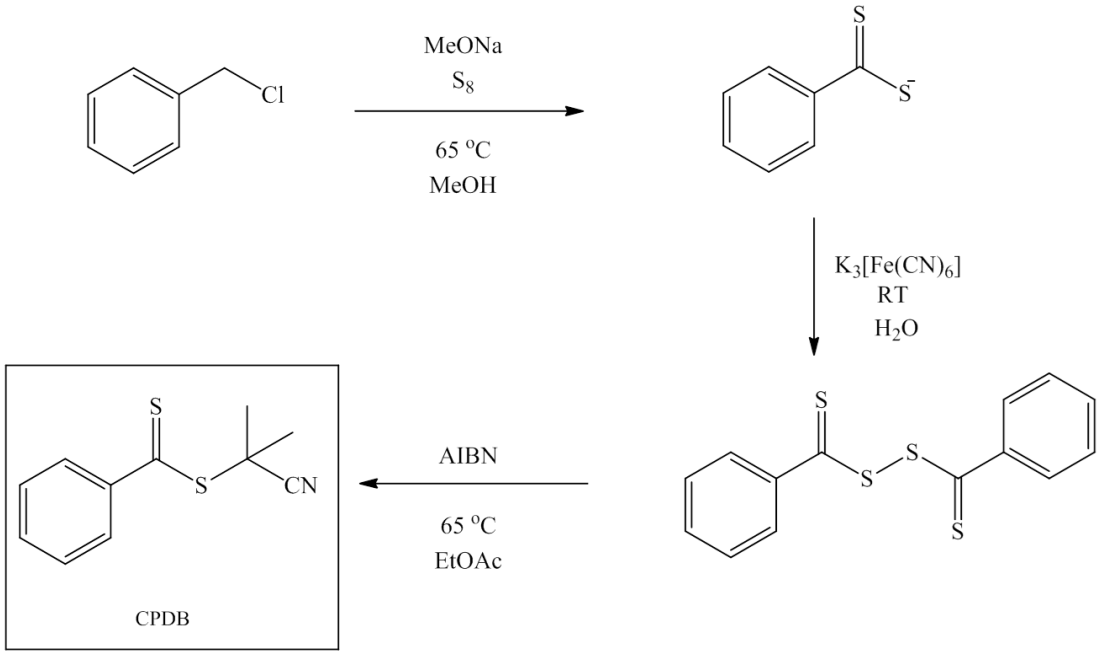

Scheme 2.3 Synthetic routes for 2-Cyanoprop-2-yl dithiobenzoate (CPDB)

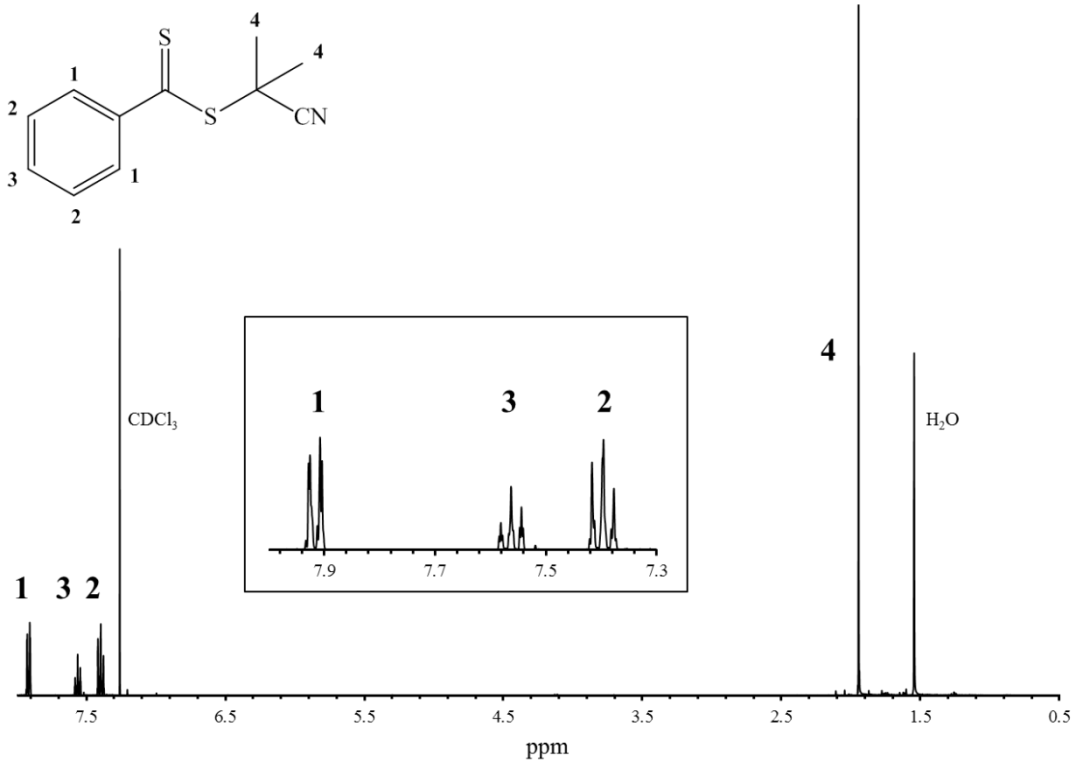

Figure 2.4 ^{1}H NMR spectrum of 2-cyanoprop-2-yl dithiobenzoate in $CDCl_3$.

2.3.2.2. Polymerisation of amine monomers

In addition to varying the amine monomer in the ashless detergent the polymer chain length was also investigated as a means to alter the behaviour of the polymers as ashless detergents. Previously it has been suggested that for ashless detergents the molecular weight of the polymer can vastly affect the performance and the mechanical properties of the oil such as the viscosity.[22] Therefore to overcome these problems low molecular weight polymers were initially targeted <5 kDa as these are believed to still show good neutralisation ability without changing the viscosity or flow properties of the oil significantly due to a significantly lower critical overlap concentration.[23] Subsequently, much larger, 85 kDa polymers were also investigated to understand if much larger chains could provide a difference in neutralisation behaviour.

The RAFT homopolymerisations of the amine monomers was explored using 2-cyanoprop-2-yl dithiobenzoate as the CTA and azobisisobutyronitrile (AIBN) as the initiator (Scheme 2.4). The first targeted polymer series was the PDMAEMA series; herein targeted molecular weights of 1, 2 and 85 kDa were chosen.

Scheme 2.4 General reaction for the polymerisation of the amine methacrylates by RAFT using CPDB as the CTA and AIBN as the radical initiator.

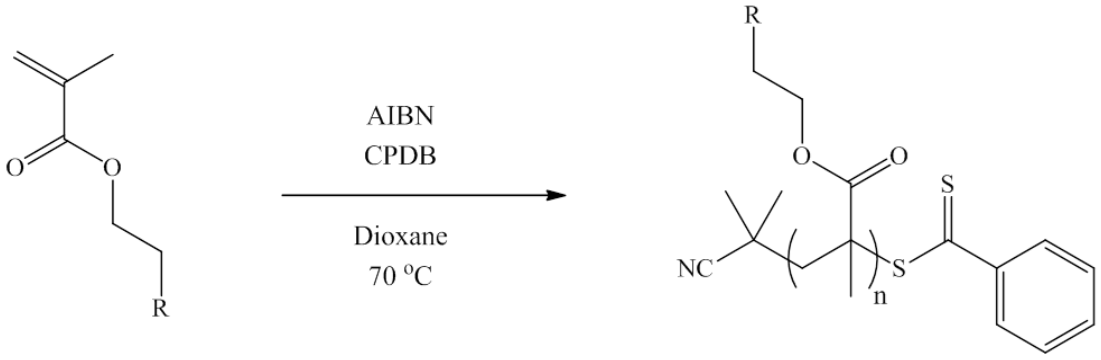

R = Amine Moiety

Polymerisations of DMAEMA was conducted at 70 ^{o}C in 1,4-dioxane with AIBN as the radical initiator. After 8 hours, (18 h for the 85 kDa polymer) the polymerisation was quenched with liquid nitrogen, purified by dialysis against deionised water and the polymer was isolated by lyophilisation to give well defined PDMAEMA with molecular weights ranging from 1- 85 kDa and good end group fidelity (Figure 2.5 and Table 2.01).

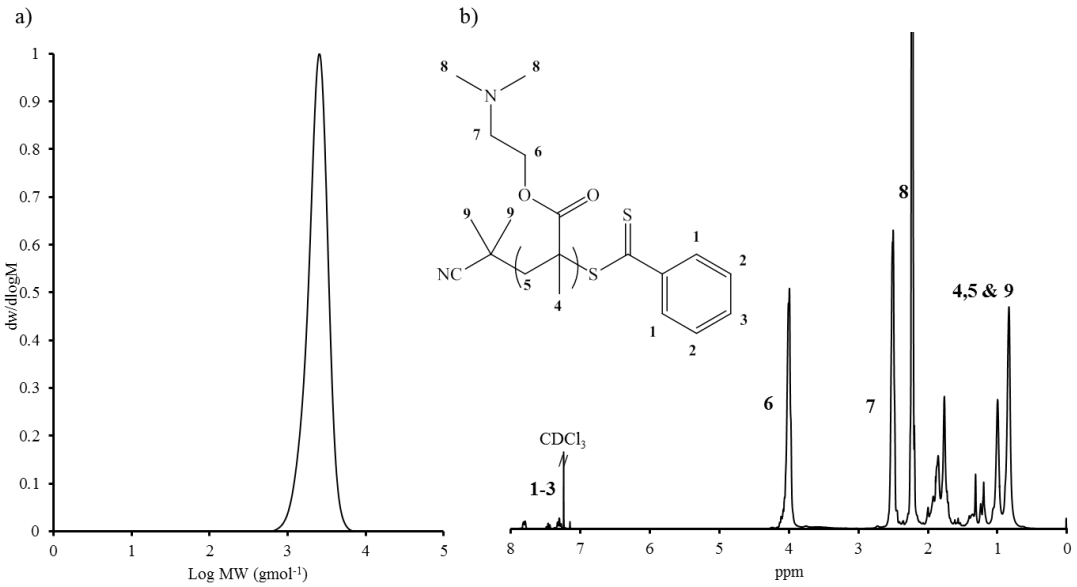

Figure 2.5 a) SEC refractive index chromatogram of **2.02** with DMF as the eluent and b) ^{1}H NMR spectrum of **2.02** in $CDCl_3$.

These polymerisation conditions were then further explored for the other amine monomers, DEAEMA (**2.04** - **2.06**), MEMA (**2.07** - **2.09**) and PEMA (**2.10** - **2.12**). Similarly all resulting polymers after purification resulted in well-defined polymers with good end group fidelity as observed by ^{1}H NMR spectroscopy from resonance signals from the RAFT end group and SEC (Table 2.1).

Table 2.1 Characterisation data of polymers **2.01**-**2.12**

Amine	Polymer	$M_{n\ NMR}$[a] (kDa)	$M_{n\ SEC}$[b] (kDa)	$Đ_{SEC}$[b]
DMAEMA	**2.01**	1.0	2.1	1.10
	2.02	2.3	3.0	1.17
	2.03	85.0	87.1	1.24
DEAEMA	**2.04**	1.2	2.1	1.08
	2.05	2.3	4.4	1.18
	2.06	86.0	88.3	1.26
MEMA	**2.07**	1.1	1.8	1.10
	2.08	2.2	2.3	1.10
	2.09	81.0	81.0	1.13
PEMA	**2.10**	1.2	2.3	1.10
	2.11	2.3	4.3	1.17
	2.12	85.0	87.2	1.20

[a] Determined by end-group analysis from ^{1}H NMR spectroscopy. [b] From SEC using DMF as the eluent based on poly(methyl methacrylate) standards.

2.3.3. Copolymerisation by RAFT.

In addition to exploring the effect of amine and molecular weight on the performance of these ashless detergents, the microstructure of the polymer was also varied and its influence on ashless detergent behaviour could then be evaluated. To further explore the effect of the amine and structure on the performance of ashless detergents a range of amine containing copolymers were synthesised. It is hypothesised that by copolymerising the amine monomers with a non-reactive monomer the properties of the polymer can be altered and selectively tuned,[24-27] which is highly attractive for lubricant additives as tailor-made additives can be produced which are specific to each environment or engine.

The choice of comonomer is important as a monomer with a similar reactivity to the amine monomer required to favour statistical copolymerisation to give a random distribution of the two monomers along the polymer backbone, thus an equal distribution of amines throughout the chain.[15,28] It has been shown previously that by altering the polymer structure via copolymerisation the behaviour of the functional monomer can be altered. Cotanda *et al* were able to show that the acid dissociation constant, pK_a, of statistical DMAEMA copolymers can be altered depending on the ratio of methyl methacrylate (MMA) and DMAEMA in the copolymer. Therefore copolymers have the ability to offer polymers with tuneable behaviours dependent on composition. The methacrylate comonomer chosen was a non-activated lauryl methacrylate, LMA, it was shown previously that LMA has a similar reactivity to the amine monomers, thus favouring statistical copolymers thus favouring statistical copolymers despite a mild compositional drift towards to amine monomer.[29] Furthermore, LMA has a long dodecyl chain which makes this monomer very solvophilic to non-polar environments and therefore it is hypothesised that the incorporation of LMA could aid the solubilisation of the polymers within the oil. For these copolymer studies only the commercially available DMAEMA, DEAEMA and MEMA monomers were explored (scheme 2.5).

Scheme 2.5 General reaction for the copolymerisation of the amine methacrylates with LMA by RAFT using CPDB as the CTA and AIBN as the radical initiator.

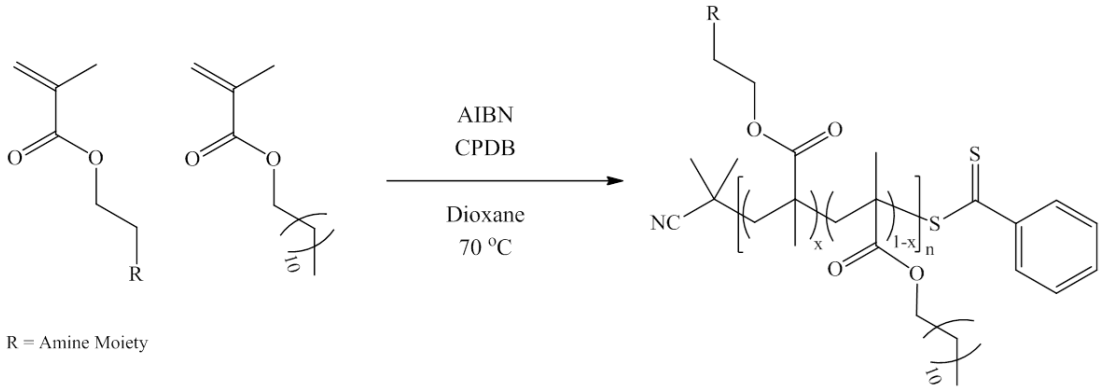

A range of copolymer incorporations were studied, ranging from 25 mol% - 75 mol% amine incorporation throughout the polymer. In a similar manner to the homopolymerisations the first targeted polymer series was a DMAEMA series, in these copolymer studies only one molecular weight was targeted, 2 kDa, and the amine content varied. Copolymerisation of DMAEMA with LMA was conducted at 70 ^{o}C in 1,4-dioxane with AIBN as the initiator, the polymerisation were quenched with liquid nitrogen and the polymer isolated by precipitation into cold methanol (MeOH). Well defined copolymers with good end group fidelity were obtained as observed by SEC and ^{1}H NMR spectroscopy, data for a representative sample **2.13** are shown in (Figure 2.6 and Table 2.2).

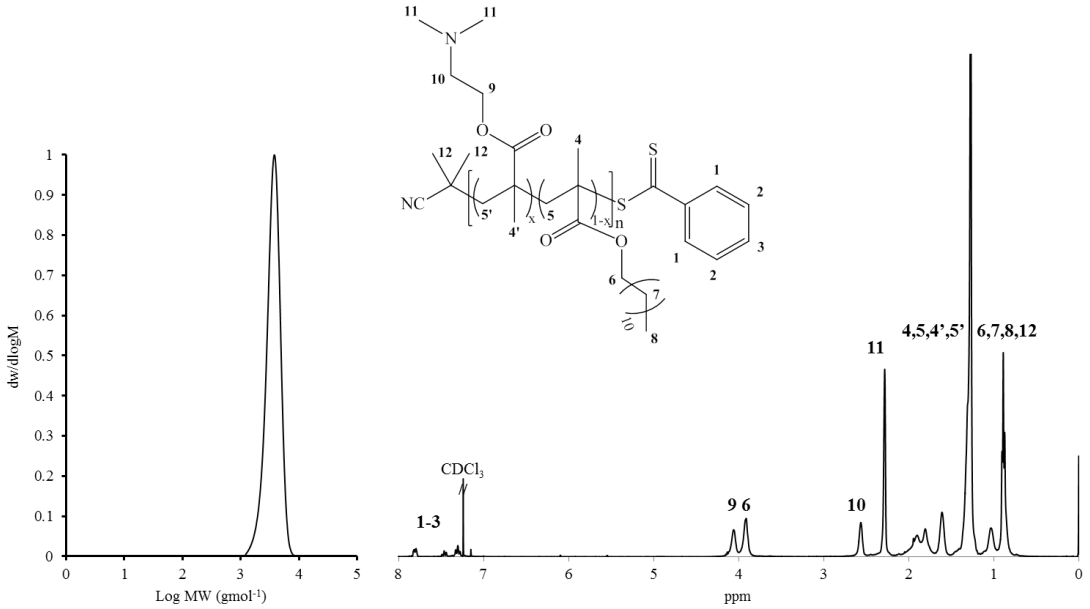

Figure 2.6 a) SEC chromatogram of **2.13** with $CHCl_3$ as the eluent and b) ^1H NMR spectrum of **2.13** in $CDCl_3$

Table 2.2 Characterisation data of copolymers **2.13**-**2.21**

Amine	Polymer	Amine mol% Feed	Amine mol%[a]	LMA mol% Feed	LMA mol%[a]	$M_{n\ NMR}$[b] (kDa)	$M_{n\ SEC}$[c] (kDa)	$Đ_{SEC}$[c]
DMAEMA	**2.13**	0.25	0.29	0.75	0.71	2.6	3.5	1.20
	2.14	0.50	0.66	0.50	0.44	2.2	3.2	1.24
	2.15	0.75	0.73	0.25	0.27	2.3	4.2	1.14
DEAEMA	**2.16**	0.25	0.33	0.75	0.67	2.0	3.1	1.28
	2.17	0.50	0.53	0.50	0.47	2.1	3.3	1.30
	2.18	0.75	0.82	0.25	0.18	2.2	3.3	1.22
MEMA	**2.19**	0.25	0.26	0.75	0.74	2.9	3.2	1.22
	2.20	0.50	0.55	0.50	0.45	2.9	2.9	1.26
	2.21	0.75	0.78	0.25	0.22	3.0	3.3	1.33

[a] Determined by ^{1}H NMR spectroscopy using the signals at 4.20 ppm and 3.90 ppm.[b] Determined by end-group analysis from ^{1}H NMR spectroscopy. [c] From SEC using based on poly(methyl methacrylate) standards in DMF.

2.3.4. End group Modification of amine polymers

To match the current metal salt detergents structurally these RAFT polymers (**2.01**-**2.21**) were then modified post polymerisation to produce an amphiphilic structure. It was proposed that these modified polymers could then self-assemble in the mineral oil and provide structures that resemble the current over-based detergents. The benefit of RAFT polymerisation is that the RAFT end groups can be further exploited with specific

chemistries. Most notably is the exploitation of the thiocarbonate group of the CTA on the terminal of the polymer chains. A wide range of chemistries are available which allow for post polymerisation modification of the theiocarboante group.

A simple Michael addition was explored as a post polymerisation reaction following reduction of the thiocarbonyl group. Spruell *et al* explored a range of Michael acceptors with RAFT polymers and demonstrated this reaction offers a simple and successful route to end group modified polymers.[30] For this study a range of Michael acceptors were explored (Figure 2.7). These Michael acceptors were chosen as they all possess a long alkyl chain which was targeted to allow the polymers to spontaneously self-assembly when in the oil formulation.

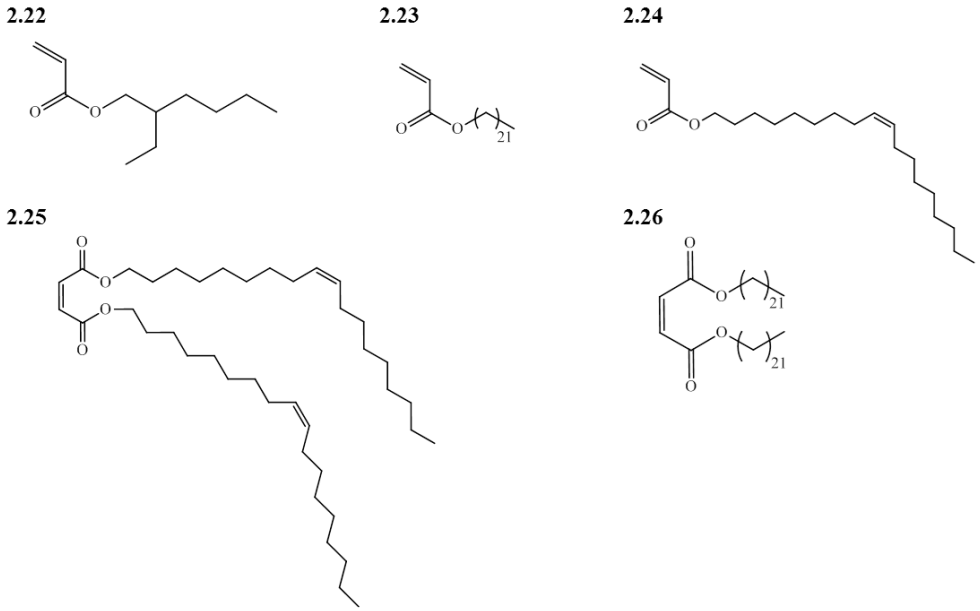

Figure 2.7. Michael acceptors explored for the end group modification of the amine polymers produced by RAFT.

Although only **2.22** is commercially available, **2.23**-**2.26** were synthesised with a simple one step reaction. Using a similar strategy to that reported in the literature the Michael acceptors **2.23** and **2.24** were synthesised by treating acryloyl chloride with the alkyl alcohol in the

presence of triethyl amine in chloroform under inert conditions.[30] For Michael acceptors **2.25** and **2.26** a Steglich esterification route was undertaken using commercially available maleic acid which was reacted with the alkyl alcohol in the presence of 4-dimethylaminopyridine (DMAP) and 1-ethyl-3-(3-dimethylaminopropyl)carbodiimide (EDCI) with dichloromethane (CH_2Cl_2) as the solvent. The Michael acceptors were purified and analysed by ^1H and ^{13}C NMR spectroscopy with yields varying between 54-79 %. Figure 2.8 shows an example ^1H NMR spectrum of **2.24** in $CDCl_3$.

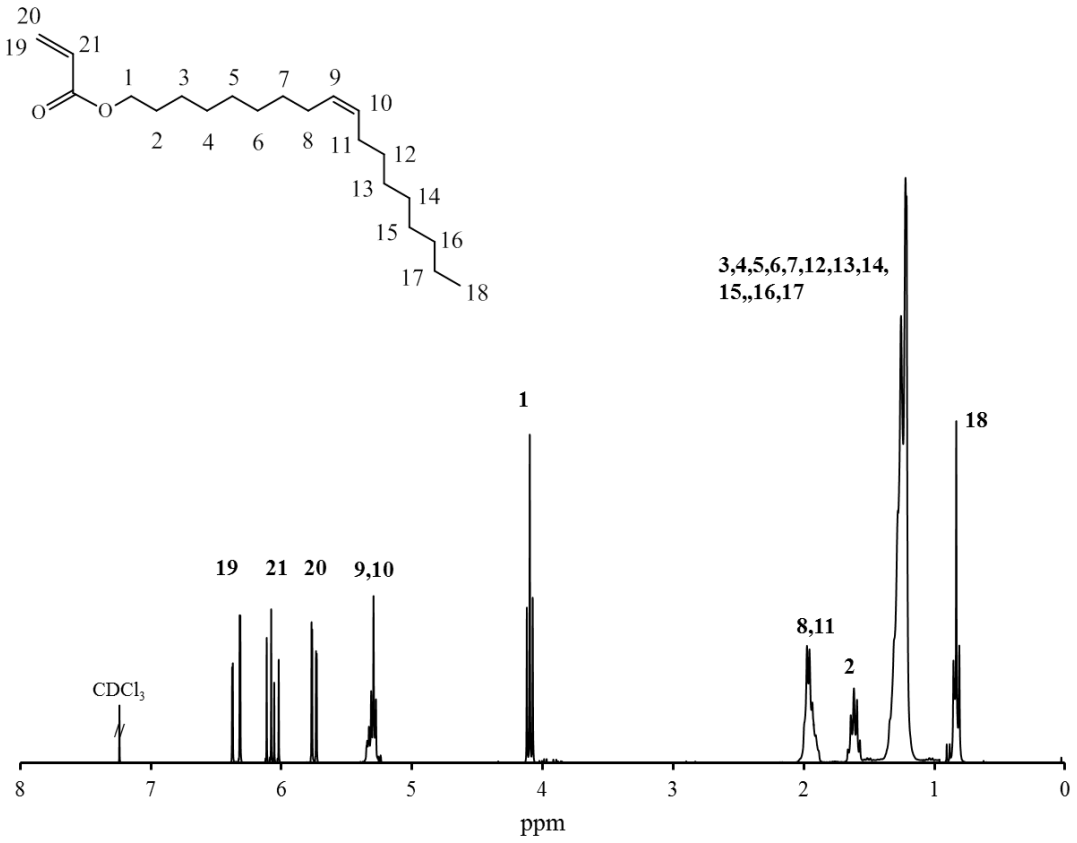

Figure 2.8. ^1H NMR spectrum of **2.24** in $CDCl_3$.

The post polymerisation Michael addition was carried out in one pot; using the chosen amine polymer, Michael acceptor, sodium borohydride ($NaBH_4$) and tributyl phosphine (PBu_3) in tetrahydrofuran (THF) were stirred at room temperature overnight (Scheme 2.6).

Scheme 2.6. General reaction for the post polymerisation modification of the amine methacrylates via a Michael addition using an alky based Michael acceptor.

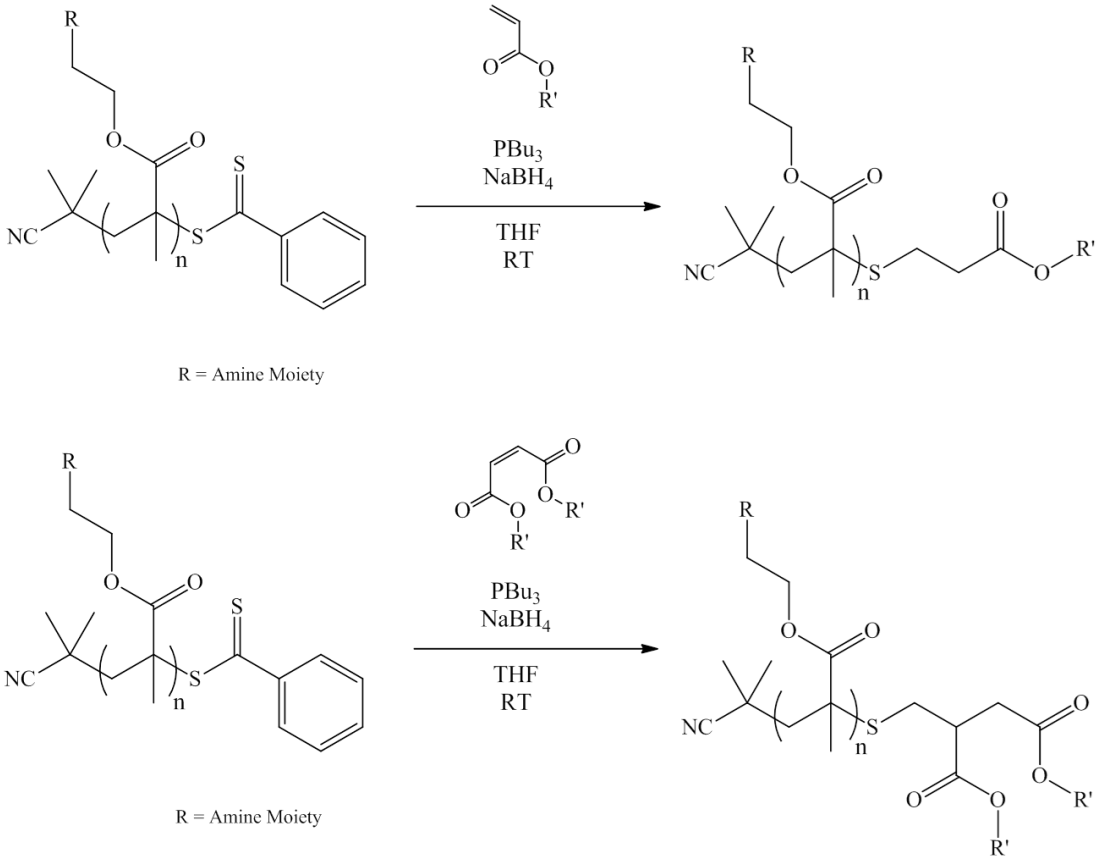

The end group modified polymers were then purified and isolated by precipitation and characterised by ^{1}H NMR spectroscopy and SEC analysis. SEC chromatograms showed no polymer-polymer coupling, and ^{1}H NMR spectra showed the disappearance of the RAFT end group as shown in Figure 2.9, for end group modified P(DMAEMA), **2.02eg**, to afford well defined end group modified amine containing polymers. Although a range of Michael acceptors were synthesised and explored the cis-9-octadecene based Michael acceptor, **2.24**, was the most readily synthesised to scale, and was most structurally similar to current detergent nanoparticles and thus was used for all further studies (see Table 2.3 for molecular weight data of end group modified polymers).

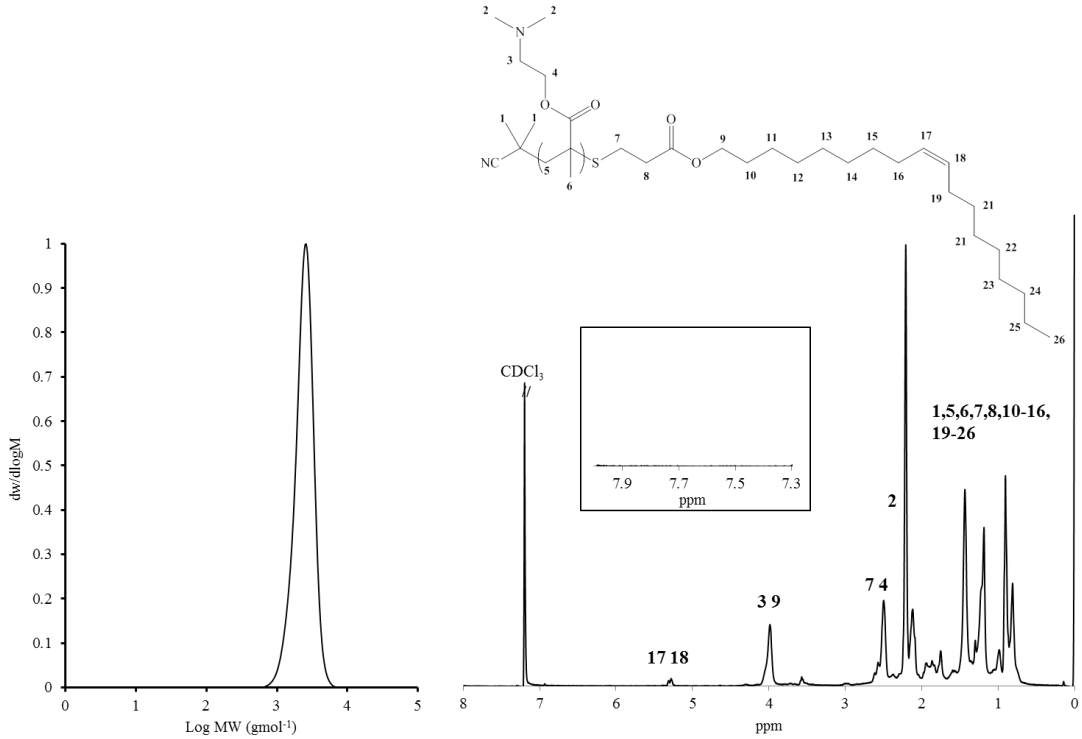

Figure 2.9 a) SEC chromatogram of **2.02eg** with DMF as the eluent and b) ^{1}H NMR spectrum of **2.02eg** in $CDCl_3$. Insert shows region where proton signals for RAFT R end group are found.

Table 2.3 Characterisation data of end group modified polymers **2.01eg - 2.12eg**.

Amine	Polymer	$M_{n\ NMR}$[a] (kDa)	$M_{n\ SEC}$[b] (kDa)	$Đ_{SEC}$[b]
DMAEMA	**2.01eg**	1.2	2.1	1.10
	2.02eg	2.5	3.0	1.17
	2.03eg	85.0	87.1	1.24
	2.13eg	2.6	3.5	1.20
	2.14eg	2.2	3.2	1.24
	2.15eg	2.3	4.2	1.14
DEAEMA	**2.04eg**	1.4	2.1	1.08
	2.05eg	2.5	4.4	1.18
	2.06eg	86.0	88.3	1.26
	2.16eg	2.0	3.1	1.28
	2.17eg	2.1	3.3	1.30
	2.18eg	2.2	3.3	1.22
MEMA	**2.07eg**	1.3	1.8	1.10
	2.08eg	2.4	2.3	1.10
	2.09eg	81.0	81.0	1.13
	2.19eg	2.9	3.2	1.22
	2.20eg	2.9	2.9	1.26
	2.21eg	3.0	3.3	1.33
PEMA	**2.10eg**	1.4	2.3	1.10
	2.11eg	2.5	4.3	1.17
	2.12eg	85.0	87.2	1.20

[a] Determined by end-group analysis from ^{1}H NMR spectroscopy. [b] From SEC using based on poly(methyl methacrylate) standards in DMF.

2.4. Self-assembly of Amine polymers in non-polar solvent.

Amphiphilic polymers can assemble in selective solvents and their nanoscale structures play a key role for their behaviour observed on the macroscale. Therefore given the amphiphilic nature of the end group modified polymers (**2.01eg**-**2.21eg**), they were investigated structurally when dispersed in a non-polar hydrocarbon solvent e.g. mineral oil. Initial experiments were conducted by direct dissolution of the polymers in mineral oil at a concentration of 0.5 g/L and at room temperature. After two days of stirring and sonication these solutions were clear to the naked eye (Figure 2.10), whereas the polymers with the RAFT end group do not soublise in the base oil, an example solution with **2.02** is shown in Figure 2.10c. Considering the amphiphilic nature of these polymers it was hypothesised that discrete reverse micelles had formed in the oil solvent, similar to those structures formed by metal salt detergents. To explore the assembly of these polymers in the oil further detailed model studies in *n*-hexane were undertaken.

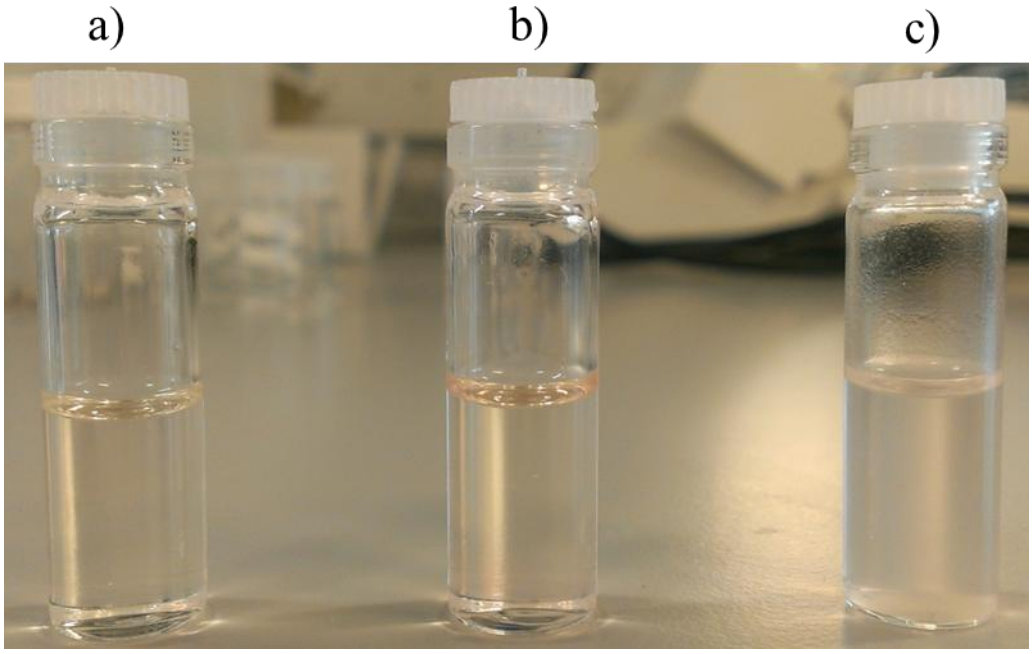

Figure 2.10. Initial dissolution studies of PDMAEMA polymers in mineral oil, a) Mineral oil solvent b) **2.02eg** in mineral oil at 0.5 g/L c) **2.02** in mineral oil at 0.5 g/L

The following results are split into two sections. In the first section the dissolution and assembly of the end group modified homopolymers (**2.01eg-2.12eg**) in non-polar solvent is studied. In the second, the dissolution of the end group modified amine copolymers (**2.13eg-2.21eg**) in non-polar solvent is explored.

2.4.1. Self-assembly of amine homopolymers in *n*-Hexane.

Although the end group modified amine polymers were shown to solubilise in the mineral oil and believed to form discrete reverse micelle structures (Figure 2.11), often these initial structures are metastable and can be representative either of structures formed in the bulk, or kinetically trapped micelles.[31] These metastable structures will often have a very different behaviour to their equilibrium analogues, therefore to deduce the influence of the structure and the amine on the detergent properties it must be ensured that all micelles are at the same energetic state, specifically micelles at equilibrium or close to equilibrium are sought.[32]

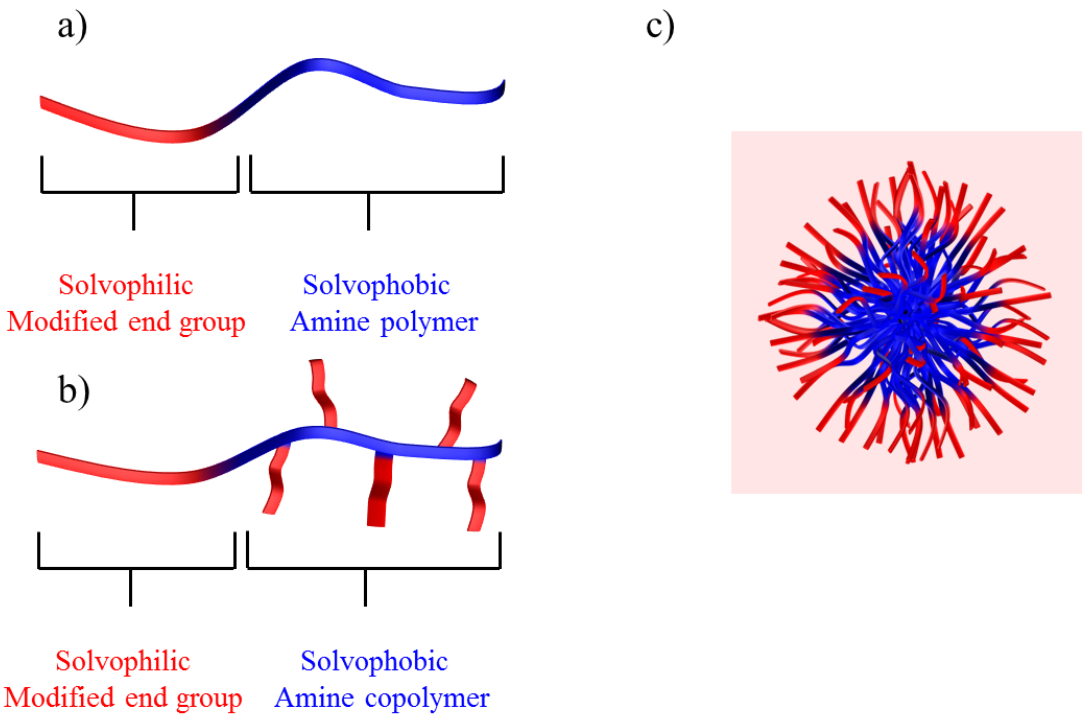

Figure 2.11) Schematic depicting the end group modified polymers a) end group modified homopolymer b) end group modified copolymer, and c) the predicted self-assembled structure in the nonpolar environment.

The topic of frozen and dynamic micelles was extensively covered in Chapter 1 and it was reported that a simple way to transform metastable or kinetically trapped micelles to micelles at equilibrium is by heating the polymer solution.[33] Briefly this is a consequence of the thermal energy altering one or both of the following parameters; 1) an increase of temperature above the glass transition temperature (T_g) of the core block, this allows for core block mobility and even global rearrangements in the system. 2) An increase in temperature reduces the energetic barrier for molecular exchange allowing polymers to equilibrate. Therefore, all polymer solutions were prepared by direct dissolution of the end group modified amine polymer (**2.01eg - 2.21eg**) into *n*-hexane at 2 g/L and once the polymer was dispersed all polymer solutions were annealed at 50 °C for 6 hours and then cooled to room temperature under ambient conditions prior to analysis.

A structural study of the self-assembled polymers was undertaken using detailed laser light scattering (LLS) studies in *n*-hexane. Both static and dynamic light scattering measurements were carried out on solutions of end group modified homopolymers after the annealing cycle at 2 g/L and at 20°C (Table 2.4). Only one concentration was used in these light scattering studies hence all values reported are apparent, as the influence of particle-particle interactions may be present.

An examination of the results from dynamic light scattering (DLS) reported a particle size in solution much larger than that of a unimer chain in solution. All polymers produced a hydrodynamic radius larger than 4.5 nm thus indicating that indeed these polymers did assemble into larger structures in the mineral oil. Moreover, an increased size in the hydrodynamic radius (R_h) was observed as the length of the amine block was increased. Since the solvophilic group is identical for all the systems, the increase in size can only weakly be attributed to the difference in the behaviour of the corona. However, as well documented, the hydrodynamic radius (R_h) is the sum of both the corona radius (R_{corona}) and core radius (R_{core}). Given the relationship between the amine block length and the alkyl chain

length, $R_{core} > R_{corona}$ it can be predicted that the self-assembled micelles formed are crew-cut micelles.[34] It is known that for crew-cut micelles the R_{core} is proportional to $N_{core}^{2/3}$ and thus, an increased block length will increase the core size, leading to a higher R_h value, which was the observed behaviour for these end group modified homopolymers.[35] Moreover, analysis of the distribution of relaxation times from DLS reveals a single mode of relaxation (Figure 2.12), which indicates that all polymers molecularly disperse to form defined nanostructures once annealed and no large bulk structures remain in solution.

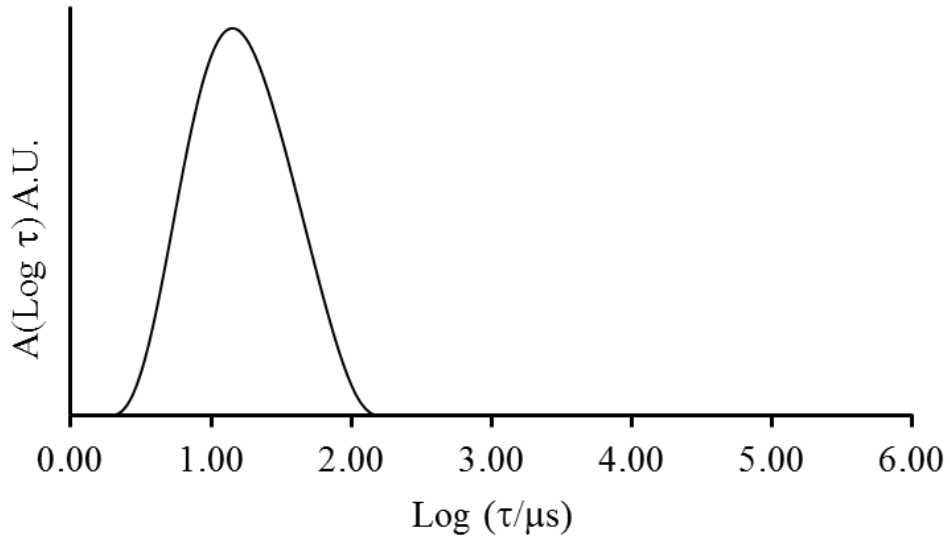

Figure 2.12. Distribution of relaxation times from DLS for **2.02eg** in n-hexane at 2 g/L at 20°C, θ = 130°.

Next the results from static light scattering (SLS) are explored. From DLS studies it was observed that a particle size larger than a molecularly dispersed unimer chain was found in solution, which indicated self-assembly of the polymer chains. The SLS results confirm this result indicating self-assembly as all aggregation numbers reported (N_{agg}) were larger than 14, indicating that the species found in solution are composed of multiple polymer chains, this SLS analysis strongly supports the conclusion that reverse crew cut micelles are formed in a non-polar solvent. Furthermore, complementing the DLS results, the SLS results showed

that as the amine block length increased the aggregation number (N_{agg}) increased (Table 2.4) in a similar trend to the relation of amine block length and R_h.

Table 2.4 Light scattering data of polymers **2.01eg - 2.12eg**

Amine	Polymer	R_h (nm)[a] ±10%	N_{agg}[b] ±10%	R_c (nm)[c]	Base units per micelle[d]	Concentration of base in each micelle (mM)[e]
DMAEMA	**2.01eg**	4.5	16	1.8	80	5.5
	2.02eg	6.0	29	2.8	348	6.0
	2.03eg	30.0	221	18.9	119340	6.9
DEAEMA	**2.04eg**	4.5	14	1.7	70	5.5
	2.05eg	5.0	32	2.9	384	6.0
	2.06eg	35.0	302	21.0	138920	5.0
MEMA	**2.07eg**	5.0	24	2.0	120	5.5
	2.08eg	6.0	40	3.1	440	5.5
	2.09eg	41.0	450	23.6	193500	3.0
PEMA	**2.10eg**	5.0	20	1.9	100	5.5
	2.11eg	6.0	38	3.0	380	5.0
	2.12eg	38.0	350	22.5	159250	4.0

[a] Determined from DLS analysis at 2 g/L. [b] Determined from SLS analysis at 2 g/L.
[c] Determined using equation 2.1. [d] Determined using degree of polymerisation × N_{agg}.
[e] Determined using equation 2.2.

This can be understood in terms of enthalpic interactions between the amine repeat units and the non-polar solvent molecules.[36] The contact of solvent molecules with the amine repeat units in the core is an unfavourable interaction and therefore the system will want to

minimise said interactions, this is achieved by an increase in the aggregation number of the polymer micelles. The increase in aggregation means a smaller surface area for unfavourable interactions at the core-corona interface, therefore minimising the solvent-amine interactions. Theoretical models were also used to extend the understanding of the core behaviour. Using equation 2.1 the core radius (R_c) can be calculated, where p is the micelle core density and N_a is Avogadro's constant.[37]

$$\frac{4\pi\rho {R_c}^3}{3} = N_{agg} \frac{M_{W\ Hydrophobic\ block}}{N_a} \quad (2.1)$$

Theoretically, as the core block length increases an increase in the core block radius is expected. However, although the data in Table 2.4 illustrate this phenomenon, if the length of the end group is accounted for within the core size then the micelle size theoretically expected is much smaller than that experimentally observed from DLS. Additionally, it is important to note that equation 2.1 used to calculate R_c assumes a completely dehydrated core which is not often the case for polymeric micelles.[35,38] However, the amine monomers used in this Chapter are soluble in non-polar solvents and the amine polymers have short block lengths, therefore the thermodynamic incompatibility between the amine and the solvent is possibly not large enough to prevent solvent penetration into the core. Thus, it can be postulated that for these amine micelles some solvent molecules can reside in the micelle core causing larger core sizes than theoretically predicted. Furthermore, this penetration of solvent indicates that the cores may be dynamic; the solvent helps to increase the mobility of the core and thermodynamic equilibrium could be reached with these micelles.

As the amine polymer chain constitutes the core of the polymer micelle, an estimated concentration of base per particle can be calculated using equation 2.2. In Table 2.4 it can be observed that despite the change in amine monomer or block length the local concentration of base per micelle is similar between all systems studied. Therefore it could be suggested that the accessibility of the base units are the same between micellar systems as the local

concentration the amine units are similar. For these end group modified amine homopolymers it can be concluded from laser light scattering that a range of structurally similar micelles are formed in solution despite the differences of amine monomer.

$$[Amine\ Base] = \frac{DP.N_{agg}}{V_{core}.N_a} \qquad (2.2)$$

2.4.2. Self-assembly of amine copolymers in *n*-Hexane.

Although experimentally it has been shown that introduction of solvophilic units into the solvophobic block can prevent any ordered bulk structures being formed the amine copolymers still underwent the same annealing cycle at 50 °C for 6 hours prior to analysis.[38] Moreover, recently the assembly of polymers where the associating block is a copolymer block has been shown to alter both the structure and assembly of the polymers in solution. Therefore, to understand how the microstructure of the polymer chain changes the structures and consequently the ashless detergent behaviour, detailed laser light scattering studies (LLS) were undertaken.

DLS studies were undertaken at 20 °C in *n*-hexane. Here the difference between the amine polymers studied is the difference in the composition of the core forming polymer block; where the compositions ranges from 25 mol% to 75 mol% amine and where the comonomer is lauryl methacrylate (LMA). However, unlike the homopolymer systems the hydrodynamic radius between systems remains constant but is nevertheless much larger than a value for a dispersed unimer chain in solution (Table 2.5 and Figure 2.13). DLS results here show that when the amine incorporation is varied the hydrodynamic radius of the micelles of the polymer micelles does not vary significantly. As mentioned previously the hydrodynamic radius of the micelles scales with block length, which for these copolymers remains constant, therefore little change in micelle size was found as the block lengths remains constant.

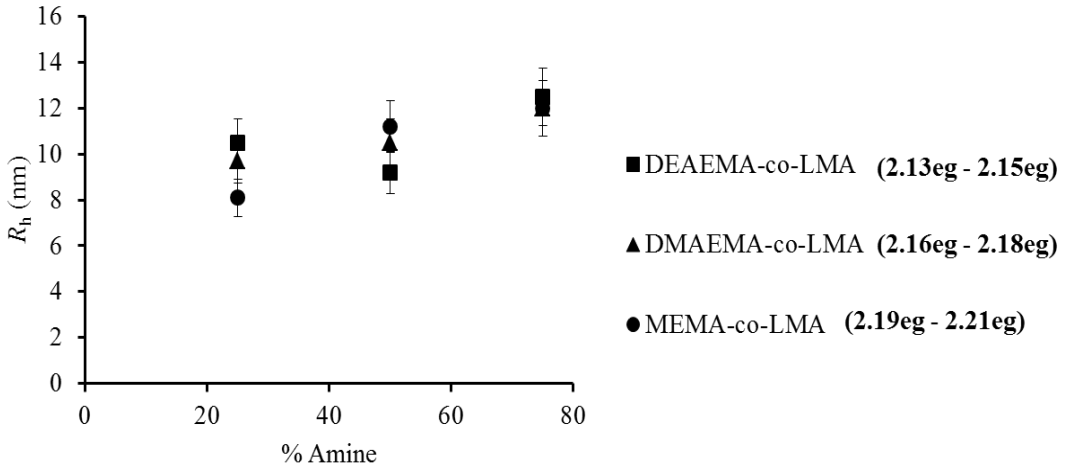

Figure 2.13. Relationship between % amine incorporation and the hydrodynamic radius, R_h, of the polymers **2.13eg - 2.21eg** in *n*-hexane. Error bars indicate 10% error in R_h.

Additionally from the distributions of relaxation times from DLS similar profiles are observed for all systems, data for an example DMAEMA-*co*-LMA series (**2.13 eg -2.15 eg**) is shown in Figure 2.14. When these copolymer distributions are compared to the homopolymer systems the dispersity of the copolymers are much smaller which indicates a more heterogeneous solution of micelles and thus these micelles may also be at equilibrium.

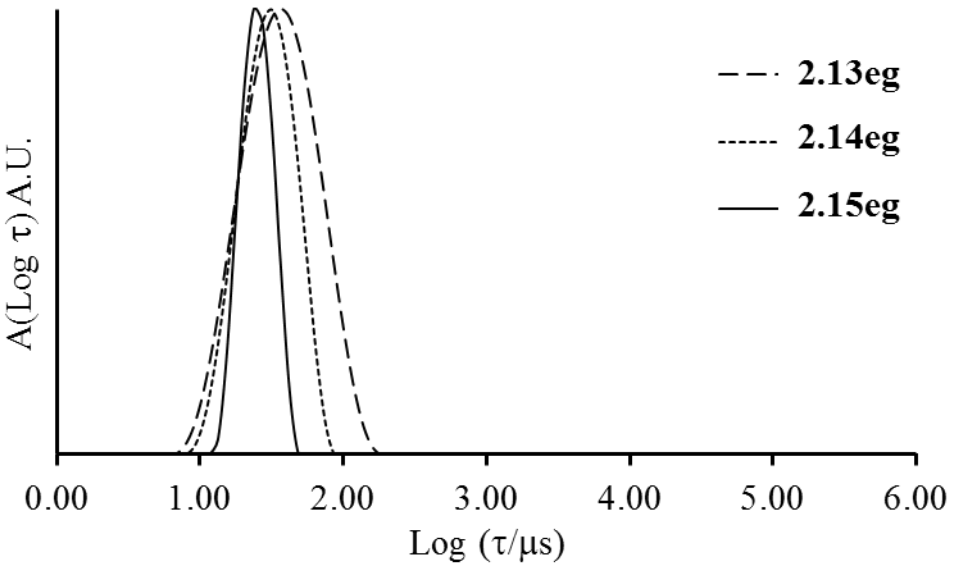

Figure 2.14. Distribution of relaxation times from DLS for **2.13eg-2.15eg** in *n*-hexane.

However, although little change in micelle size was observed this does not conclusively demonstrate that the micelles are similar in morphology or shape, SLS analysis was used to understand the nanostructures further. Firstly SLS was used to confirm that the particles observed in DLS were indeed a self-assembled particle formed from multiple polymer chains. From SLS analysis, (Table 2.5), it can be observed that the aggregation numbers are all greater than 21 which confirms the prediction from DLS that these polymer assemble into larger defined structures on the nanoscale. However, in contrast to DLS the SLS shows that between micelle aggregates the N_{agg} value does differ whilst R_h value remains similar, specifically as the amine incorporation increases the aggregation number increases. In a similar manner to section 2.3.4.1 the effect increased aggregation number is to reduce the unfavourable interactions between the increasing amine content in the core and the solvent.

For self-assembled systems Equation 2.1 can be used to understand the core sizes, assuming that a spherical micelle structure is formed and was therefore used to analyse these self-assembled diblock copolymers in solution. Here an increase in the size of the cores was observed when the amine incorporation is increased. Nevertheless understanding that $R_{total} = R_{core} + R_{corona}$ the core size (as predicted by equation 2.2) is too small to match the R_{total} values expected and similarly the R_h values observed, therefore it is predicted that these micelles are indeed solvent swollen, in a similar manner to the end group modified homopolymers. This is also explained by the presence of LMA in the micelle cores which causes a reduction in the solvent selectivity with respect to the polymer micelle core, which allows solvent to enter the cores.

Table 2.5 Light scattering data of polymers **2.13eg - 2.21eg**

Monomers	Polymer	R_h (nm)[a] ±10%	N_{agg}[b] ±10%	R_c (nm)[c]	Base units per micelle[d]	Concentration of base in each micelle (mM)[e]
DMAEMA / LMA	**2.13eg**	12.0	51	3.90	612	5.0
	2.14eg	10.5	35	3.40	210	3.0
	2.15eg	9.7	21	2.90	63	1.4
DEAEMA / LMA	**2.16eg**	12.5	45	3.50	405	3.8
	2.17eg	9.2	40	3.20	240	3.0
	2.18eg	10.5	28	2.90	84	1.4
MEMA / LMA	**2.19eg**	12.0	48	3.70	528	4.0
	2.20eg	11.2	34	3.30	238	2.6
	2.21eg	8.1	25	3.00	100	1.4

[a] Determined from DLS analysis at 2 g/L. [b] Determined from SLS analysis at 2 g/L. [c] Determined using equation 2.1. [d] Determined using degree of polymerisation × N_{agg}. [e] Determined using equation 2.2.

Furthermore, the local concentration of the amines was calculated using equation 2.2 in a similar manner to the end group modified homopolymers. Table 2.5 shows the local concentration of base in relation to the self-assembled structures. Here it can be observed that as the composition of the polymer changes the local concentration of amine units also changes, specifically as the amine incorporation is reduced the local concentration also decreases.

Interestingly these LLS results suggest that the both the end group modified amine homopolymers and copolymers self-assemble into small well-defined structures on the

nanoscale. Moreover, literature reports indicate that for metal salt detergent nanoparticles the sizes are approximately 2-7 nm for the detergent core and therefore these ashless polymeric particles shown good potential as structural analogues.

2.5. Conclusions

Novel ashless detergent structures have been produced from a series of polymeric amines. A range of well-defined amine polymers have been synthesised by RAFT polymerisation with varying degrees of polymerisation. In addition, a range of amine copolymers were also synthesised by RAFT with a non-responsive monomer lauryl methacrylate as the comonomer in varying amounts. These amine polymers and copolymers were then subsequently transformed using a simple post-polymerisation Michael addition at room temperature through conversion of the RAFT end group. In non-polar solvents the modified amine polymers spontaneously assemble into defined reverse micelle structures, where the amines aggregate to form the core domain. A combination of dynamic and static light scattering indicate these polymer micelles can be considered structural analogues of the current metal based detergents. The local concentration and type of ashless base has been varied between systems, to provide a universal template for a range of ashless detergents applicable in many different environments. These structures will be further explored in the following Chapter to elucidate their performance as ashless detergents in a lubricating oil environment.

2.6. Experimental

2.6.1. Materials

Monomers were filtered through a plug of silica prior to use and stored at 4 °C in the dark. AIBN (2,2'-azo-bis(isobutyronitrile)) was recrystallised from methanol and stored in the dark at 4 °C. The mineral oil (SN150) was used as received from BP Technology Centre in Pangbourne. All other materials were used as received from Aldrich, Fluka, and Acros. Dry solvents were used directly from a drying and degassing solvent tower delivery system.

2.6.2. Synthesis

2.6.2.1. Synthesis of 2-cyanoprop-2-yl dithiobenzoate (CPDB)

Benzyl chloride (1 eq.) was added drop wise to a solution of elemental sulfur (2 eq.), 30% sodium methoxide in methanol (2 eq.) and methanol (1:1 volume to sodium methoxide solution). Once all the benzyl chloride was added the solution was heated at reflux for 24 h. The reaction solution was subsequently cooled in an ice bath and the solution was filtered and the methanol was removed under reduced pressure. The brown solid was dissolved in deionised water (1:1 volume of methanol used) and washed three times with diethyl ether. A final addition of diethyl ether was added and the solution was acidified with 32% HCl until the top layer was a deep purple. The ether layer was then extracted three times with sodium hydroxide (NaOH 1M) to give a deep purple aqueous solution of sodium dithiobenzoate.

The dithiobenzoate solution was added drop wise to a stirring aqueous solution of potassium ferricyanide (1.5 eq.). The red precipitate is filtered and washed with deionised water until the washings were clear. The solid was dried under vacuum at room temperature overnight to give bis(thiobenzyl) disulfide.

A solution of AIBN (1.5 eq.) and bis(thiobenzyl) disulphide (1 eq.) in ethyl acetate (10:1 to total weight) was heated at reflux for 24 h under nitrogen. After 24 h the solution was cooled

in an ice bath. The ethyl acetate was removed *in vacuo* and the crude product was purified *via* column chromatography using petroleum ether to give 2-cyanoprop-2-yl dithiobenzoate as a red oil which crystallised upon standing (26 % yield). ^{1}H NMR (400 MHz, $CDCl_3$): δ (ppm) 7.85 (d, $^{3}J_{H\text{-}H}$ = 8.1 Hz, 2H, Meta-Ar*H*), 7.55 (t, $^{3}J_{H\text{-}H}$ = 7.4 Hz, 1H Para-Ar*H*), 7.40 (t, $^{3}J_{H\text{-}H}$ = 8.1 Hz, 2H, Ortho-Ar*H*), 1.95 (s, 6H, S(CH_3)$_2$). ^{13}C NMR (400 MHz, $CDCl_3$) δ (ppm) 220.0, 140.5, 135.2, 129.0, 126.8, 120.0, 40.1, 25.5 m/z [ES MS] calculated 222.0406 found 222.0404 $[M+H]^+$

2.6.2.2. Synthesis of pyridine ethyl methacrylate (PEMA)

4-(2-hydroxyethyl) pyridine (1 eq.) was stirred in dichloromethane (5:1 volume to pyridine) at 0 °C, under nitrogen. *N*-(3-dimethyl-aminopropyl)-*N*-ethylcarbodiimide hydrochloride (EDCI) (1.25 eq.) and 4-(dimethyl amino) pyridine (DMAP) (0.25 eq.) was then added and the reaction mixture stirred for 1 hour. Methacrylic acid (2 eq.) was then added and the reaction mixture was stirred at room temperature for 2 days. EDCI (1.25 eq.) and DMAP (0.25 eq.) were then added to drive the reaction to completion and the reaction mixtures stirred for a further 3 days. The reaction mixture was washed three times with a saturated brine solution, dried over magnesium sulfate and filtered. The organic solution was removed *in vacuo* and the crude product was purified *via* column chromatography using ethyl acetate to give PEMA as a colourless oil (65 % yield). ^{1}H NMR (400 MHz, $CDCl_3$): δ (ppm) 8.50 (dd, 2H, meta-Ar*H*), 7.10 (dd, 2*H*, ortho-Ar*H*), 6.10 (t, 1*H*, CH_3C*H*=CH), 5.50 (t, $^{3}J_{H\text{-}H}$ = 6.7 Hz 1H, CH_3CH=C*H*), 4.40 (t, $^{3}J_{H\text{-}H}$ = 6.6 Hz 2H, OCH_2CH_2), 3.00 (t, $^{3}J_{H\text{-}H}$ = 6.5 Hz 2H, OCH_2CH_2), 1.90 (s, 3H,CH_3CH=CH). ^{13}C NMR (400 MHz, $CDCl_3$) δ (ppm) 165.4, 136.5, 124.0, 62.5, 33.5, 14.3. m/z [ES MS] calculated 192.09 found 214.08 $[M+Na]^+$

2.6.2.3. Synthesis of 2.23

Oleyl alcohol (1 eq.) with triethylamine (1.2 eq.) was stirred in chloroform (8:1 volume to alcohol). A solution of acryloyl chloride (1.2 eq.) in chloroform (2:1 volume to chloride) was added dropwise at 0 $^{\circ}$C under inert atmosphere to the stirring oleyl alcohol solution. After 24

h the solution was washed four times with aqueous NaOH 1M, dried over magnesium sulfate and the solvent removed at reduced pressure to give **2.23** as a pale yellow oil (79 % yield). ^{1}H NMR (400 MHz, $CDCl_3$): δ (ppm) 6.4 (dd, 1H, CHC*H*=CH), 6.20 (m, 1H, C*H*CH=CH), 5.7 (dd, 1H, CHCH=C*H*), 5.35 (t, $^{3}J_{H\text{-}H}$ = 6.5 Hz 2H, C*H*=C*H*), 4.20 (t, $^{3}J_{H\text{-}H}$ = 6.7 Hz 2H, OC*H*$_2$CH$_2$), 2.10-1.90 (t, $^{3}J_{H\text{-}H}$ = 6.5, t, 2H, C*H*$_2$), 1.50 (m, 2H, OCH$_2$C*H*$_2$), 1.40-1.20 (m, 24H, C*H*$_2$) 0.85 (t, $^{3}J_{H\text{-}H}$ = 6.9 Hz, 3H, C*H*$_3$). ^{13}C NMR (400 MHz, $CDCl_3$) δ (ppm) 162.9, 131.5, 129.0, 62.5, 35.0, 32.5, 30.0, 26.8, 29.6, 26.0, 22.5, 14.6. m/z [ES MS] calculated 323.2916 found 323.2904 $[M+H]^+$

2.6.2.4. Synthesis of 2.24

Docosanol (1 eq.) with triethylamine (1.2 eq.) was stirred in chloroform (8:1 volume to alcohol). A solution of acryloyl chloride (1.2 eq.) in chloroform (2:1 volume to chloride) was added dropwise at 0 °C under inert atmosphere. After 24 h the solution was washed four times with aqueous NaOH 1M dried over magnesium sulfate and then removed the solvent at reduced pressure to give **2.24** as a white solid (67 % yield). ^{1}H NMR (400 MHz, $CDCl_3$): δ (ppm) 6.4 (dd, 1H, CHC*H*=CH), 6.20 (m, 1H, C*H*CH=CH), 5.7 (dd, 1H, CHCH=C*H*), 4.20 (t, $^{3}J_{H\text{-}H}$ = 6.7 Hz, 2H, OC*H*$_2$CH$_2$), 1.50 (m, 2H, OCH$_2$C*H*$_2$), 1.40-1.20 (m, 40H, C*H*$_2$) 0.85 (t, $^{3}J_{H\text{-}H}$ = 6.9 Hz, 3H, C*H*$_3$). ^{13}C NMR (400 MHz, $CDCl_3$) δ (ppm) 165.0, 132.0, 129.0, 64.0, 35.0, 32.5, 30.0, 26.5, 29.0, 26.0, 22.5, 14.6. m/z [ES MS] calculated 381.3796 found 323.2904 $[M+H]^+$

2.6.2.5. Synthesis of 2.25

Oleyl Alcohol (3 eq.) was stirred in dichloromethane (4:1 volume to alcohol) at 0 °C. *N*-(3-dimethyl-aminopropyl)-*N*-ethylcarbodiimide hydrochloride (EDCI) (1.25 eqv) and 4-(dimethyl amino) pyridine (DMAP) (0.25 eq.) were then added and the reaction mixture stirred for 30 mins. Maleic acid (1 eq.) was then added and the reaction mixture was stirred at room temperature for 2 days. EDCI (1.25 eq.) and DMAP (0.25 eq.) were then added to drive the reaction to completion and the reaction mixtures stirred for a further 2 days. The

reaction mixture was washed three times with a saturated brine solution, dried over magnesium sulphate and filtered. The organic solution was removed *in vacuo* and the crude product was purified *via* column chromatography using petroleum ether: ethyl acetate 9:1 to give **2,25** as a pale yellow oil (Yield 64%). ^{1}H NMR (400 MHz, $CDCl_3$): δ (ppm) 6.35 (s, 2H, C*H*=C*H*), 5.35 (t, $^{3}J_{H\text{-}H}$ = 6.5 Hz 4H, C*H*=C*H*), 4.20 (t, $^{3}J_{H\text{-}H}$ = 6.7 Hz, 2H, OCH_2CH$_2$), 2.10-1.90 (t, 4H, CH_2), 1.50 (m, 4H, OCH$_2$CH_2), 1.40-1.20 (m, 48H, CH_2) 0.85 (t, $^{3}J_{H\text{-}H}$ = 6.9 Hz, 6H, CH_3). ^{13}C NMR (400 MHz, $CDCl_3$) δ (ppm) 165.0, 164.0 132.0, 129.0, 64.0, 35.0, 32.5, 30.0, 26.5, 29.0, 26.0, 22.5, 14.6 m/z [ES MS] calculated 616.54 found 639.53 $[M+Na]^+$

2.6.2.6. Synthesis of 2.26

1-Docosanol (3 eq.) was stirred in dichloromethane (4:1 volume to alcohol) at 0 °C. *N*-(3-dimethyl-aminopropyl)-*N*-ethylcarbodiimide hydrochloride (EDCI) (1.25 eq.) and 4-(dimethyl amino) pyridine (DMAP) (0.25 eq.) were then added and the reaction mixture stirred for 30 mins. Maleic acid (1 eq.) was then added and the reaction mixture was stirred at room temperature for 2 days. EDCI (1.25 eq.) and DMAP (0.25 eq.) were then added to drive the reaction to completion and the reaction mixtures stirred for a further 2 days. The reaction mixture was washed three times with a saturated brine solution, dried over magnesium sulphate and filtered. The organic solution was removed *in vacuo* and the crude product was purified by recrystallisation from methanol to give **2.26** as a white powder (yield 54%). ^{1}H NMR (400 MHz, $CDCl_3$): δ (ppm) 6.35 (s, 2H, C*H*=C*H*), 4.20 (t, $^{3}J_{H\text{-}H}$ = 6.7 Hz, 2H, OCH_2CH$_2$), 1.50 (m, 2H, OCH$_2$CH_2), 1.40-1.20 (m, 40H, CH_2) 0.85 (t, $^{3}J_{H\text{-}H}$ = 6.9 Hz, 3H, CH_3). ^{13}C NMR (400 MHz, $CDCl_3$) δ (ppm) 166.0, 162.9, 131.5, 129.0, 62.5, 35.0, 32.5, 30.0, 26.8, 29.6, 26.0, 22.5, 14.6 m/z [ES MS] calculated 732.70 found 755.69 $[M+Na]^+$

2.6.2.7. General procedure for RAFT homopolymerisation

A solution of the amine monomer, AIBN and 2-cyano-2-propyl dithiobenzoate (CPDB) in 1,4-dioxane (1:1 volume to monomer) was added to a dry ampoule containing a stirrer bar. The solution was degassed using at least 3 freeze-pump-thaw cycles, back filled with nitrogen, sealed and placed in a pre-heated oil bath at 70 °C. After an allotted time the polymerisation was quenched by liquid nitrogen, 1,4-dioxane removed *in vacuo* and the resultant polymer dissolved with H_2O. The solution was transferred to a dialysis membrane tube with the appropriate molecular weight cut-off (MWCO 1 kDa) and dialysed against 18.2 MΩ.cm water (1.5 L) with 3 water changes. Lyophilisation resulted in a pink solid. (see Table 2.1 for molecular weight data).

PDMAEMA, **2.01** - **2.03**, δ (ppm) ^{1}H NMR (400 MHz, $CDCl_3$): δ (ppm) 7.85 (d, $^3J_{H\text{-}H}$ = 8.1 Hz, 1H Ar end group), 7.55 (t, $^3J_{H\text{-}H}$ = 7.4 Hz, 2H Ar end group), 7.41 (t, $^3J_{H\text{-}H}$ = 8.1 Hz, 2H Ar end group), 4.20 (br t, 2H, OCH_2CH_2N), 2.50 (br s, 2H, OCH_2CH_2N), 2.10 (br s, 6H, $OCH_2CH_2N(CH_3)_2$), 1.94 (s, 6H, end group) , 1.00-2.00 (br m, backbone)

PDEAEMA, **2.04** - **2.06**, δ (ppm) ^{1}H NMR (400 MHz, $CDCl_3$): δ (ppm) 7.85 (d, $^3J_{H\text{-}H}$ = 8.1 Hz, 1H Ar end group), 7.55 (t, $^3J_{H\text{-}H}$ = 7.4 Hz, 2H Ar end group), 7.41 (t, $^3J_{H\text{-}H}$ = 8.1 Hz, 2H Ar end group), 4.20 (br t, 2H, OCH_2CH_2N), 2.50 (br s, 2H, OCH_2CH_2N), 2.30 (br t, 4H, $OCH_2CH_2N(CH_2)_2(CH_3)_2$), 1.94 (s, 6H, end group), 1.10 (br t, 6H, $OCH_2CH_2N(CH_2)_2(CH_3)_2$), 1.00-2.00 (br m, backbone)

PMEMA, **2.07** - **2.09**, δ (ppm) ^{1}H NMR (400 MHz, $CDCl_3$): δ (ppm) 7.85 (d, $^3J_{H\text{-}H}$ = 8.1 Hz, 1H Ar end group), 7.55 (t, $^3J_{H\text{-}H}$ = 7.4 Hz, 2H Ar end group), 7.41 (t, $^3J_{H\text{-}H}$ = 8.1 Hz, 2H Ar end group), 4.20 (br t, 2H, OCH_2CH_2N), 3.70 (br t, 4H, $OCH_2CH_2N(CH_2)_2(CH_2)_2$) 2.50 (br s, 2H, OCH_2CH_2N), 2.40 (br t, 4H, $OCH_2CH_2N(CH_2)_2(CH_3)_2$), 1.94 (s, 6H, end group), 1.10 (br t, 6H, $OCH_2CH_2N(CH_2)_2(CH_3)_2$), 1.00-2.00 (br m, backbone)

PPEMA, **2.10** - **2.12**, δ (ppm) ^{1}H NMR (400 MHz, $CDCl_3$): δ (ppm) 8.40 (br t, 4H, OCH_2CH_2 $(CH_2)_2(CH_3)_2$ N), 7.85 (d, $^{3}J_{H\text{-}H}$ = 8.1 Hz, 1H Ar end group), 7.55 (t, $^{3}J_{H\text{-}H}$ = 7.4 Hz, 2H Ar end group), 7.41 (t, $^{3}J_{H\text{-}H}$ = 8.1 Hz, 2H Ar end group), 6.90 (br t, 4H, OCH_2CH_2 $(CH_2)_2(CH_3)_2$ N), 4.20 (br t, 2H, OCH_2CH_2N), 3.70 (br t, 4H, $OCH_2CH_2N(CH_2)_2(CH_2)_2$), 1.94 (s, 6H, end group), 1.70 (br t, 2H, end group), 1.10 (br t, 6H, $OCH_2CH_2N(CH_2)_2(CH_3)_2$), 1.00-2.00 (br m, backbone)

Table 2.6. Reaction conditions for the RAFT homopolymerisations

Amine	Polymer	Monomer (eq.)	AIBN (eq.)	CTA (eq.)	Polymerisation time (h)
DMAEMA	**2.01**	5	0.2	1	8
	2.02	12	0.2	1	8
	2.03	540	0.2	1	18
DEAEMA	**2.04**	5	0.2	1	8
	2.05	12	0.2	1	8
	2.06	460	0.2	1	18
MEMA	**2.07**	5	0.2	1	8
	2.08	11	0.2	1	8
	2.09	430	0.2	1	18
PEMA	**2.10**	5	0.2	1	8
	2.11	10	0.2	1	8
	2.12	455	0.2	1	18

2.6.2.8. General procedure for RAFT copolymerisation

A solution of the amine monomer, LMA, AIBN and 2-cyano-2-propyl dithiobenzoate (CPDB) in 1,4-dioxane (1:1 volume to monomer) was added to a dry ampoule containing a stirrer bar. The solution was degassed using at least 3 freeze-pump-thaw cycles, back filled with nitrogen, sealed and placed in a pre-heated oil bath at 70 °C. After an allotted time the polymerisation was quenched by liquid nitrogen, 1,4-dioxane removed *in vacuo* and the resultant polymer diluted with the minimum of dichloromethane (CH_2Cl_2) and the polymer was precipitated into cold methanol and isolated by filtration. Precipitation was repeated a further two times to afford a pink tacky polymer (see Table 2.2 for molecular weight data).

P(DMAEMA-*co*-LMA), **2.13** - **2.15**, δ (ppm) ^{1}H NMR (400 MHz, $CDCl_3$): δ (ppm) 7.85 (d, $^3J_{H\text{-}H}$ = 8.1 Hz, 1H Ar end group), 7.55 (t, $^3J_{H\text{-}H}$ = 7.4 Hz, 2H Ar end group), 7.41 (t, $^3J_{H\text{-}H}$ = 8.1 Hz, 2H Ar end group), 4.20 (br t, 2H, OCH_2CH$_2$N), 3.90 (br t, 2H, OCH_2CH$_{2(}$CH$_2$)$_9$CH$_3$), 2.50 (br s, 2H, OCH$_2$CH_2N), 2.10 (br s, 6H, OCH$_2$CH$_2$N(CH_3)$_2$), 1.94 (s, 6H, end group), 1.70 (br t, 2H, OCH$_2$C$H_{2(}$CH$_2$)$_9$CH$_3$), 1.20-1.30 (br t, 18H, OCH$_2$CH$_{2(}$CH_2)$_9$CH$_3$), 1.00-2.00 (br m, backbone) 0.80 (br t, 3H, OCH$_{2(}$CH$_2$)$_{10}$CH_3).

P(DEAEMA-*co*-LMA), **2.16** - **2.18**, δ (ppm) ^{1}H NMR (400 MHz, $CDCl_3$): δ (ppm) 7.85 (d, $^3J_{H\text{-}H}$ = 8.1 Hz, 1H Ar end group), 7.55 (t, $^3J_{H\text{-}H}$ = 7.4 Hz, 2H Ar end group), 7.41 (t, $^3J_{H\text{-}H}$ = 8.1 Hz, 2H Ar end group), 4.10 (br t, 2H, OCH_2CH$_2$N), 3.90 (br t, 2H, OCH_2CH$_{2(}$CH$_2$)$_9$CH$_3$), 2.50 (br s, 2H, OCH$_2$CH_2N), 2.30 (br t, 4H, OCH$_2$CH$_2$N(CH_2)$_2$(CH$_3$)$_2$), 1.94 (s, 6H, end group), 1.70 (br t, 2H, OCH$_2$C$H_{2(}$CH$_2$)$_9$CH$_3$), 1.20-1.30 (br t, 18H, OCH$_2$CH$_{2(}$CH_2)$_9$CH$_3$), 1.10 (br t, 6H, OCH$_2$CH$_2$N(CH$_2$)$_2$(CH_3)$_2$), 1.00-2.00 (br m, backbone), 0.80 (br t, 3H, OCH$_{2(}$CH$_2$)$_{10}$CH_3).

P(MEMA-*co*-LMA), **2.19** - **2.21**, δ (ppm) ^{1}H NMR (400 MHz, $CDCl_3$): δ (ppm) 7.85 (d, $^3J_{H\text{-}H}$ = 8.1 Hz, 1H Ar end group), 7.55 (t, $^3J_{H\text{-}H}$ = 7.4 Hz, 2H Ar end group), 7.41 (t, $^3J_{H\text{-}H}$ = 8.1 Hz, 2H Ar end group), 4.20 (br t, 2H, OCH_2CH$_2$N), 3.90 (br t, 2H, OCH_2CH$_{2(}$CH$_2$)$_9$CH$_3$), 3.70 (br t, 4H, OCH$_2$CH$_2$N(CH$_2$)$_2$(CH_2)$_2$) 2.50 (br s, 2H, OCH$_2$CH_2N), 2.40 (br t, 4H,

$OCH_2CH_2N(CH_2)_2(CH_3)_2$), 1.94 (s, 6H, end group), 1.70 (br t, 2H, $OCH_2CH_{2(}(CH_2)_9CH_3$), 1.20-1.30 (br t, 18H, $OCH_2CH_{2(}CH_2)_9CH_3$), 1.00-2.00 (br m, backbone), 0.80 (br t, 3H, $OCH_{2(}(CH_2)_{10}CH_3$).

Table 2.7. Reaction conditions for the RAFT copolymerisations

Amine	Polymer	Amine (eq.)	LMA (eq.)	AIBN (eq.)	CTA (eq.)	Polymerisation time (h)
DMAEMA	**2.13**	12	3	0.2	1	8
	2.14	6	5	0.2	1	8
	2.15	3	7	0.2	1	8
DEAEMA	**2.16**	9	2	0.2	1	8
	2.17	6	4	0.2	1	8
	2.18	3	6	0.2	1	8
MEMA	**2.19**	11	3	0.2	1	8
	2.20	7	6	0.2	1	8
	2.21	4	9	0.2	1	8

2.6.2.9. End group modification of tertiary amine polymers.

RAFT terminated polymer (1 eq.) was dissolved in THF (60 g/L) and the solution was purged with nitrogen for 30 minutes. The Michael acceptor (50 eq.) was then added, $NaBH_4$ (20 eq.) was then added and the solution was allowed to stir for 10 min. After which PBu_3

(10 eq.) was added. The ampoule was then sealed and allowed to stir for 20 h at room temperature. After 20 h the THF was removed *in vacuo* and the resultant polymer diluted with the minimum of dichloromethane (CH_2Cl_2) and the polymer was precipitated into cold diethyl ether and isolated by filtration. Precipitation was repeated a further two times to afford a pale yellow tacky polymer (see Table 2.2 for molecular weight data for when the Michael acceptor is **2.23**).

PDMAEMA, **2.01eg - 2.03eg**, δ (ppm) ^{1}H NMR (400 MHz, $CDCl_3$): δ (ppm) 5.35 (t, $^3J_{H\text{-}H}$ = 6.5 Hz 2H, C*H*=C*H* Oleic end group), 4.20 (br t, 2H, OCH_2CH$_2$N), 2.50 (br s, 2H, OCH$_2$CH_2N), 2.10 (br s, 6H, OCH$_2$CH$_2$N(CH_3)$_2$), 1.94 (s, 6H, end group) 1.40-1.20 (m, 24H, CH_2, oleic end group), , 1.00-2.00 (br m, backbone), 0.80 (br t, 3H, oleic end group).

PDEAEMA, **2.04eg - 2.06eg**, δ (ppm) ^{1}H NMR (400 MHz, $CDCl_3$): δ (ppm) 5.35 (t, $^3J_{H\text{-}H}$ = 6.5 Hz 2H, C*H*=C*H* Oleic end group), 4.20 (br t, 2H, OCH_2CH$_2$N), 2.50 (br s, 2H, OCH$_2$CH_2N), 2.30 (br t, 4H, OCH$_2$CH$_2$N(CH_2)$_2$(CH$_3$)$_2$), 1.94 (s, 6H, end group), 1.40-1.20 (m, 24H, CH_2, oleic end group), 1.10 (br t, 6H, OCH$_2$CH$_2$N(CH$_2$)$_2$(CH_3)$_2$), 1.00-2.00 (br m, backbone), 0.80 (br t, 3H, oleic end group).

PMEMA, **2.07eg - 2.09eg**, δ (ppm) ^{1}H NMR (400 MHz, $CDCl_3$): δ (ppm) 5.35 (t, $^3J_{H\text{-}H}$ = 6.5 Hz 2H, C*H*=C*H* Oleic end group), 4.20 (br t, 2H, OCH_2CH$_2$N), 3.70 (br t, 4H, OCH$_2$CH$_2$N(CH$_2$)$_2$(CH_2)$_2$) 2.50 (br s, 2H, OCH$_2$CH_2N), 2.40 (br t, 4H, OCH$_2$CH$_2$N(CH_2)$_2$(CH$_3$)$_2$), 1.94 (s, 6H, end group), 1.40-1.20 (m, 24H, CH_2, oleic end group). 1.10 (br t, 6H, OCH$_2$CH$_2$N(CH$_2$)$_2$(CH_3)$_2$), 1.00-2.00 (br m, backbone), 0.80 (br t, 3H, oleic end group).

PPEMA, **2.010eg - 2.12eg,** δ (ppm) ^{1}H NMR (400 MHz, $CDCl_3$): δ (ppm) 8.40 (br t, 4H, OCH$_2$CH$_2$ (CH$_2$)$_2$(CH_3)$_2$ N), 6.90 (br t, 4H, OCH$_2$CH$_2$ (CH$_2$)$_2$(CH_3)$_2$ N), 5.35 (t, $^3J_{H\text{-}H}$ = 6.5 Hz 2H, C*H*=C*H* Oleic end group), 4.20 (br t, 2H, OCH_2CH$_2$N), 3.70 (br t, 4H, OCH$_2$CH$_2$N(CH$_2$)$_2$(CH_2)$_2$), 1.94 (s, 6H, end group), 1.40-1.20 (m, 24H, CH_2, oleic end

group), 1.10 (br t, 6H, $OCH_2CH_2N(CH_2)_2(CH_3)_2$), 1.00-2.00 (br m, backbone), 0.80 (br t, 3H, oleic end group).

P(DMAEMA-*co*-LMA), **2.13eg - 2.15eg**, δ (ppm) ^{1}H NMR (400 MHz, $CDCl_3$): δ (ppm) 5.35 (t, $^3J_{H\text{-}H}$ = 6.5 Hz 2H, C*H*=C*H* Oleic end group), 4.20 (br t, 2H, OCH_2CH_2N), 3.90 (br t, 2H, $OCH_2CH_{2(}CH_2)_9CH_3$), 2.50 (br s, 2H, OCH_2CH_2N), 2.10 (br s, 6H, $OCH_2CH_2N(CH_3)_2$), 1.94 (s, 6H, end group), 1.70 (br t, 2H, $OCH_2CH_{2(}CH_2)_9CH_3$), 1.40-1.20 (m, 24H, $CH_{2,}$ oleic end group), 1.10 (br t, 6H, $OCH_2CH_2N(CH_2)_2(CH_3)_2$), 1.20-1.30 (br t, 2H, $OCH_2CH_{2(}CH_2)_9CH_3$), 1.00-2.00 (br m, backbone) 0.80 (br t, 3H, $OCH_{2(}CH_2)_{10}CH_3$), 0.80 (br t, 3H, oleic end group).

P(DEAEMA-*co*-LMA), **2.16eg - 2.18eg**, δ (ppm) ^{1}H NMR (400 MHz, $CDCl_3$): δ (ppm) 5.35 (t, $^3J_{H\text{-}H}$ = 6.5 Hz 2H, C*H*=C*H* Oleic end group), 4.10 (br t, 2H, OCH_2CH_2N), 3.90 (br t, 2H, $OCH_2CH_{2(}CH_2)_9CH_3$), 2.50 (br s, 2H, OCH_2CH_2N), 2.30 (br t, 4H, $OCH_2CH_2N(CH_2)_2(CH_3)_2$), 1.94 (s, 6H, end group), 1.70 (br t, 2H, $OCH_2CH_{2(}CH_2)_{90}CH_3$), 1.40-1.20 (m, 24H, $CH_{2,}$ oleic end group), 1.10 (br t, 6H, $OCH_2CH_2N(CH_2)_2(CH_3)_2$), 1.20-1.30 (br t, 2H, $OCH_2CH_{2(}CH_2)_9CH_3$), 1.10 (br t, 6H, $OCH_2CH_2N(CH_2)_2(CH_3)_2$), 1.00-2.00 (br m, backbone), 0.80 (br t, 3H, $OCH_{2(}CH_2)_{10}CH_3$), 0.80 (br t, 3H, oleic end group).

P(MEMA-*co*-LMA), **2.19eg - 2.21eg**, δ (ppm) ^{1}H NMR (400 MHz, $CDCl_3$): δ (ppm) 5.35 (t, $^3J_{H\text{-}H}$ = 6.5 Hz 2H, C*H*=C*H* Oleic end group), 4.20 (br t, 2H, OCH_2CH_2N), 3.90 (br t, 2H, $OCH_2CH_{2(}CH_2)_9CH_3$), 3.70 (br t, 4H, $OCH_2CH_2N(CH_2)_2(CH_2)_2$) 2.50 (br s, 2H, OCH_2CH_2N), 2.40 (br t, 4H, $OCH_2CH_2N(CH_2)_2(CH_3)_2$), 1.94 (s, 6H, end group), 1.70 (br t, 2H, $OCH_2CH_{2(}CH_2)_9CH_3$), 1.40-1.20 (m, 24H, $CH_{2,}$ oleic end group), 1.20-1.30 (br t, 2H, $OCH_2CH_{2(}CH_2)_9CH_3$), 1.10 (br t, 6H, $OCH_2CH_2N(CH_2)_2(CH_3)_2$), 1.00-2.00 (br m, backbone), 0.80 (br t, 3H, $OCH_{2(}CH_2)_{10}CH_3$), 0.80 (br t, 3H, oleic end group).

2.6.3. Polymer characterisation

2.6.3.1. ^{1}H Nuclear Magnetic Resonance (NMR) spectroscopy

^{1}H NMR spectra were recorded on a Bruker DPX-400 spectrometer in $CDCl_3$. Chemical shifts are given in ppm downfield from TMS.

2.6.3.2. Size exclusion chromatography

Size exclusion chromatography (SEC) measurements were performed with HPLC grade solvents (Fisher), dimethylformamide (DMF) with 1.06 g/L of LiCl at 40 °C as the eluent at a flow rate of 1 mL/min, on a set of two PLgel 5 μm Mixed-D columns, and one guard column. The molecular weights of the synthesised polymers were calculated relative to poly(methyl methacrylate) (PMMA) standards from refractive index chromatograms.

2.6.3.3. Refractive index increment

The specific refractive index increment (d*n*/dC) of the polymers were measured in *n*-hexane and were between 0.13 and 0.14 mL/g on a refractometer (Bischoff RI detector) operating at a wavelength of 632 nm.

2.6.4. Micelle preparation

Micelle solutions were prepared by adding solvent to the dried polymer powder at a concentration of 2 g/L and stirring overnight. After one night of stirring the solutions were heated to 50 °C for 6 hours and then allowed to cool to room temperature under ambient conditions prior to analysis.

2.6.5. Micelle characterisation

2.6.5.1. Laser light scattering

Measurements were performed at angles of observation ranging from 20° up to 150° with an ALV CGS3 setup operating at λ_0 = 632 nm and at 20 ± 1 °C. Data were collected in

duplicate with 100 s run times. Calibration was achieved with filtered toluene and the background was measured with filtered solvent (*n*-hexane).

2.6.5.2. Dynamic light scattering (DLS)

The intensity autocorrelation functions $g_2(t)$ obtained from dynamic light scattering were related to $g_1(t)$ (the normalised electric field autocorrelation functions) *via* the so-called Siegert relation. Then $g_1(t)$ was analysed in terms of a continuous distribution of relaxation times (eqn. 1.18) using the REPES routine[39] without assuming a specific mathematical shape for the distribution of the relaxation times ($A(\tau)$). The apparent diffusion coefficient *D* was calculated from eqn. 1.16 given that the average relaxation rates Γ of the scatterers were q^2 dependent, where q is the scattering vector given by $q=(4\pi n/\lambda_0).\sin(\theta/2)$ with θ the angle of observation and n = 1.373 the refractive index of the solvent (*n*-hexane). The concentration dependence of the diffusion coefficient is given by $D = D_0(1+k_DC)$ where k_D is the dynamic second virial coefficient and D_0 the diffusion coefficient used for an infinitly dilute sample, obtained by computing the hydrodynamic radius (R_h) of the scatterers according to the Stokes-Einstein eqn. 1.19. With η the solvent viscosity, k the Boltzmann's constant and T the absolute temperature. Values of R_h given in the following are then obtained after extrapolation to zero concentration.

2.6.5.3. Static light scattering (SLS)

The Rayleigh ratio of the solutions have been measured using toluene as a reference according to eqn. 1.12 where I_i represents the intensity scattered by species i and $R_{toluene}$ is the Rayleigh ratio of the reference. In dilute solutions if $R_g.q < 1$ where R_g is the radius of gyration, the q and concentration dependence of R_θ is given by eqn 1.10, where A_2 is the second virial coefficient and M_w the weight average molecular weight. *K* is an optical constant given by eqn 1.11. Where $n_o = 1.496$ is the refractive index of the reference liquid (toluene), dn/dC is the specific refractive index increment determined by differential refractometry and N_A is Avogadro's number. Values of M_w are then obtained after

extrapolation to zero concentration and zero angle and used to derive the aggregation number of the micellar aggregates $N_{agg} = M_w/M_{w,unimers}$. For spherical morphologies, it is possible to deduce the core radius, R_c, from the aggregation number, using equation (2.1) assuming the core block is dehydrated and the density matches that of the bulk value, ρ.[40] For spherical morphologies, it is possible to deduce the core radius, R_c, from the aggregation number, using equation (2.1) assuming the core block is dehydrated and the density matches that of the bulk value, ρ.[40]

2.7. References

(1) Rudnick, L. R. *Lubricant Additives Chemistry and Applications* 2nd ed.; CRC Press, 2009.
(2) Galsworthy, J.; Hammond, S.; Hone, D. *Curr. Opin. Colloid Interface Sci.* **2000**, *5*, 274.
(3) L.K.Hudson, J. E., P. J.Dowding, *Adv. Colloid Interface Sci.* **2006**, *123-126*, 425.
(4) Bearchell, C. A.; Heyes, D. M.; Moreton, D. J.; Taylor, S. E. *Phys. Chem.Chem. Phys.* **2001**, *3*, 4774.
(5) S.N.Ahmed, A. M. Nassar., A.Abdel-Azim, *Inter. J. of Polym. Mat.* **2007**, *57*, 114.
(6) J. Fu, Y. L., C. B. Campbell, K. D. Papadopoulos, *Ind. Eng. Chem. Res* **2006**, *45*, 5619.
(7) E. Delbridge, V. C., J. Pudelski, M. Gieselman, C. Friend, P. Mosier, M. Rogers, M. Tierney; US Patent 20120101012, **2012**.
(8) Jacob Emert, J. C., Jesse Dambacher, Mark Bushey, Tushar Bera, Jun Hua; European Patent 2366761, 2011.
(9) Cotanda, P.; Lu, A.; Patterson, J. P.; Petzetakis, N.; O'Reilly, R. K. *Macromolecules* **2012**, *45*, 2377.
(10) Lu, A.; Cotanda, P.; Patterson, J. P.; Longbottom, D. A.; O'Reilly, R. K. *Chem. Comm.* **2012**, *48*, 9699.
(11) Ratcliffe, L. P. D.; Ryan, A. J.; Armes, S. P. *Macromolecules* **2013**, *46*, 769.
(12) Du, J.; Willcock, H.; Patterson, J. P.; Portman, I.; O'Reilly, R. K. *Small* **2011**, *7*, 2070.
(13) Moughton, A. O.; Hillmyer, M. A.; Lodge, T. P. *Macromolecules* **2011**, *45*, 2.
(14) van de Wetering, P.; Zuidam, N. J.; van Steenbergen, M. J.; van der Houwen, O.; Underberg, W. J. M.; Hennink, W. E. *Macromolecules* **1998**, *31*, 8063.
(15) Cotanda, P.; Wright, D. B.; Tyler, M.; O'Reilly, R. K. *J. Polym. Sci. A Polym. Chem.* **2013**, *51*, 3333.
(16) Neises, B.; Steglich, W. *Angew Chem. Inr. Ed.* **1978**, *17*, 522.
(17) Keddie, D. J. *Chem. Soc. Rev.* **2014**, *43*, 496.
(18) Philipp, V. *Macromol. Symp.* **2007**, *248*, 71.
(19) Perrier, S.; Takolpuckdee, P. *J. Polym. Sci. A Polym. Chem.* **2005**, *43*, 5347.
(20) Gudipati, C. S.; Tan, M. B. H.; Hussain, H.; Liu, Y.; He, C.; Davis, T. P. *Macromol. Rapid Commun.* **2008**, *29*, 1902.
(21) Fijten, M. W. M.; Paulus, R. M.; Schubert, U. S. *J. Polym. Sci. A Polym. Chem.* **2005**, *43*, 3831.
(22) Harrison, J.; Ruhe, W.; Morris, J.; Cazin, J.US Patent 5356552, **1994**.
(23) Harrison, J.; Ruhe, W.; Morris, J.; Cazin, J. European Patent 0305087 **1994**

(24) Colombani, O.; Lejeune, E.; Charbonneau, C.; Chassenieux, C.; Nicolai, T. *J. Phys. Chem. B* **2012**, *116*, 7560.
(25) Tsitsilianis, C.; Gotzamanis, G.; Iatridi, Z. *Eur. Polym. J.* **2011**, *47*, 497.
(26) Lutz, J.-F. *J. Polym. Sci. A Polym. Chem.* **2008**, *46*, 3459.
(27) Lutz, J. F. *Polym. Int.* **2006**, *55*, 979.
(28) Lee, H.; Son, S. H.; Sharma, R.; Won, Y.-Y. *J. Phys. Chem. B* **2011**, *115*, 844.
(29) Kazantsev, O.; Kamorin, D.; Sivokhin, A.; Samodurova, S.; Orekhov, D.; Korotkova, T. *J. Polym. Res.* **2014**, *21*, 1.
(30) Spruell, J. M.; Levy, B. A.; Sutherland, A.; Dichtel, W. R.; Cheng, J. Y.; Stoddart, J. F.; Nelson, A. *J. Polym. Sci. A Polym. Chem.* **2009**, *47*, 346.
(31) Nicolai, T.; Colombani, O.; Chassenieux, C. *Soft Matter* **2010**, *6*, 3111.
(32) Lund, R.; Willner, L.; Richter, D.; Dormidontova, E. E. *Macromolecules* **2006**, *39*, 4566.
(33) Stejskal, J.; Hlavatá, D.; Sikora, A.; Konňák, Č.; Pleštil, J.; Kratochvíl, P. *Polymer* **1992**, *33*, 3675.
(34) Meli, L.; Lodge, T. P. *Macromolecules* **2009**, *42*, 580.
(35) Choi, S. Y.; Bates, F. S.; Lodge, T. P. *J. Phys. Chem. B* **2009**, *113*, 13840.
(36) Forster, S.; Abetz, V.; Muller, A. H. E. *Polyelectrolytes with Defined Molecular Architecture II* **2004**, *166*, 173.
(37) Eghbali, E.; Colombani, O.; Drechsler, M.; Muller, A. H. E.; Hoffmann, H. *Langmuir* **2006**, *22*, 4766.
(38) Bendejacq, D. D.; Ponsinet, V.; Joanicot, M. *Langmuir* **2005**, *21*, 1712.
(39) Jakes, J. *Collect. Czech. Chem. Commun.* **1995**, *60*, 1781.
(40) Patterson, J. P.; Robin, M. P.; Chassenieux, C.; Colombani, O.; O'Reilly, R. K. *Chem. Soc. Rev.* **2014**, *43*, 2412.

3. The performance of amine containing nanostructures as ashless detergents in lubricant formulations.

3.1. Abstract

In Chapter 2 a range of amine homopolymers and copolymers were synthesised and shown to form structures that mimic the current metal salt detergents found in lubricant formulations for automotive engines. In this Chapter these amine polymers are explored further and their performance as ashless detergents by a range of analytical techniques and industrial standard methods is explored further. The results indicate that these ashless detergents are able to effectively neutralise acid by-products of combustion and can act as replacements to the current metal salt detergents used in lubricant formulations.

3.2. Introduction

To ensure optimal performance within a moving engine lubricants are added. These lubricants possess many components and typically include a mineral oil and an array of additives; each additive is designed to target a specific function throughout engine use or to enhance a property already observed in the engine.[1] One of the most important components of lubricant formulations are detergents, which are designed to neutralise acidic compounds formed during fuel combustion.[2] These acidic compounds have the ability to adhere to metal surfaces and cause corrosive damage and engine wear, both of which limit engine lifespan.[3]

Currently these metal based detergents are characterised by the amount of relative base present, and are grouped into basic, overbased and superbased depending on the stoichiometric ratio of base .[4,5] A well-documented standard measurement for the basic potential of a detergent is the total base number (TBN) analysis which is the milligrams of potassium hydroxide (KOH) per one gram of the oil sample which is required to neutralise the system.[6] The TBN analysis is principally a modified titration, suited to the current industry detergents, metal inorganic salts, which is able to assess the basic nature of these additives within a lubricant formulation. However, the TBN analysis only gives the amount of base present within the system. Selected other tests can be used to analyse the detergents further for their acid neutralising ability, such as monitoring the changes in pH or carbon dioxide release with time upon contact with an acid.[7-9]

Although TBN analysis allows for an accurate determination of the base content the relative strength of the base is unknown, therefore in some cases it is plausible that high TBN values may be observed but very poor acid neutralisation ability might result. To try to understand this, potentiometric titration can be used to determine the acid dissociation constant (pK_a) or base dissociation constant (pK_b) which are quantitative measures of the strength of the investigated acid or base respectively, in solution. Therefore potentiometric titrations are able to give information on the strength of the base in the system.[10-13]

Even though the neutralisation potential of current detergents can be well characterised by the industry standard TBN analysis, the mechanisms of action are not as well characterised. Nevertheless, two mechanisms have been proposed for the neutralisation of acids in solution by detergent nanoparticles, a strong stick and weak stick mechanism (Figure 3.1).[3] A strong stick mechanism consists of the detergent particles colliding with the acid and the base core becoming directly exposed to the acid, therefore losing the detergent structure and rapid neutralisation occurring. A weak stick mechanism differs as the detergent structure is maintained and the base core is not directly exposed to the acid resulting in slower neutralisation.

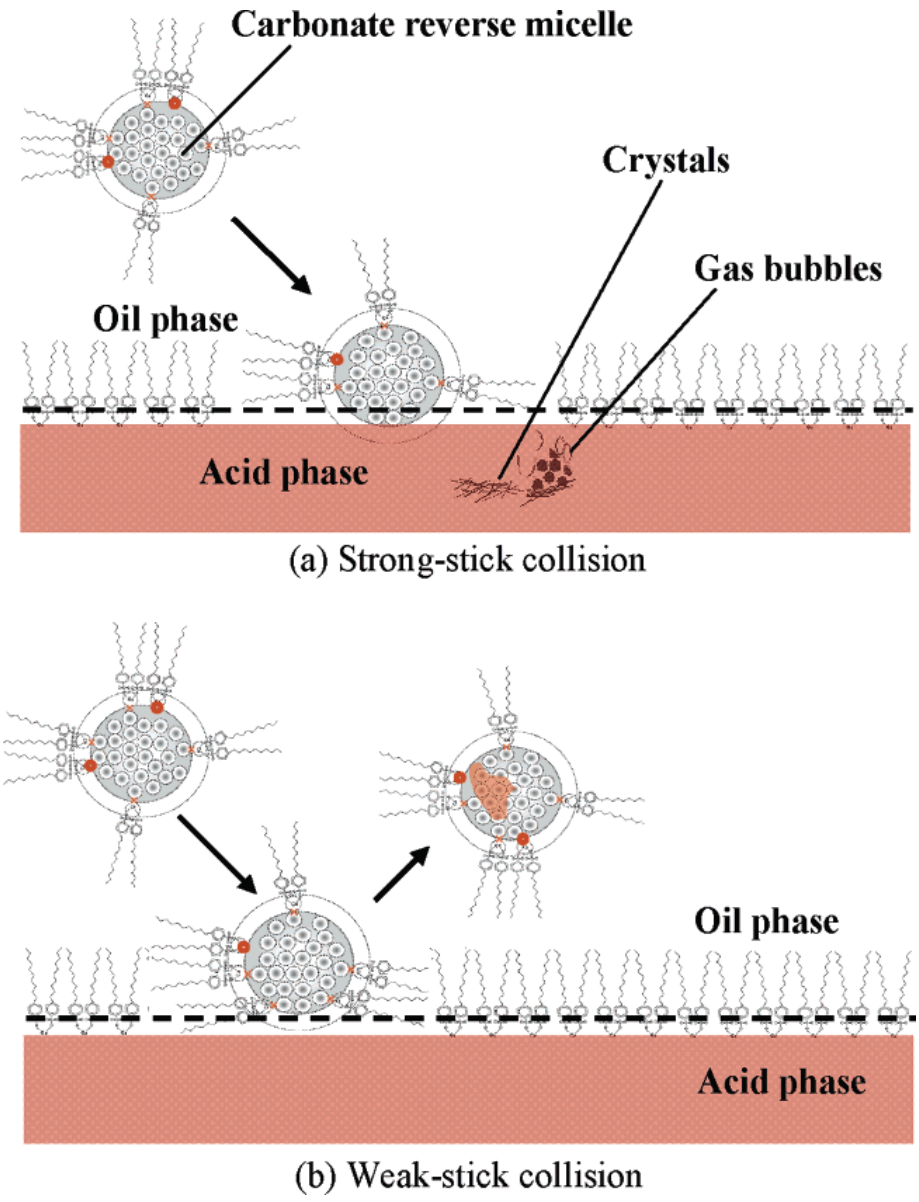

Figure 3.1 Schematic representation of the a) strong stick and b) weak stick mechanisms for acid neutralisation from detergent nanoparticles in lubricant formulations.[3]

In Chapter 2 the synthesis of a range of amine polymers was discussed and their self-assembly in non-polar solvents was considered for their potential as ashless detergents in lubricant formulations. In this Chapter the polymers from Chapter 2 are explored further as ashless detergents and their ability to neutralise acids is investigated. Specifically the TBN, pK_a and mechanism of acid neutralisation is examined for this range of self-assembled polymers.

3.3. Results and Discussion

In this Chapter polymers **2.01-2.21** and **2.01eg-2.21eg**, Scheme 3.1, are examined, using a range of analytical techniques, to explore their potential as ashless detergents in lubricant formulations. For all of the molecular characterisation and self-assembly data for these polymers please refer to Chapter 2.

Scheme 3.1. Schematic of the polymers **2.01-2.21** and **2.01eg-2.21eg**.

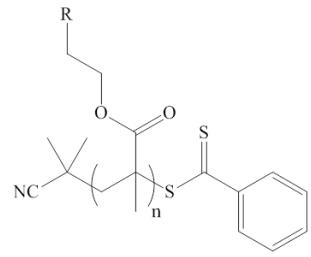

2.01-2.12

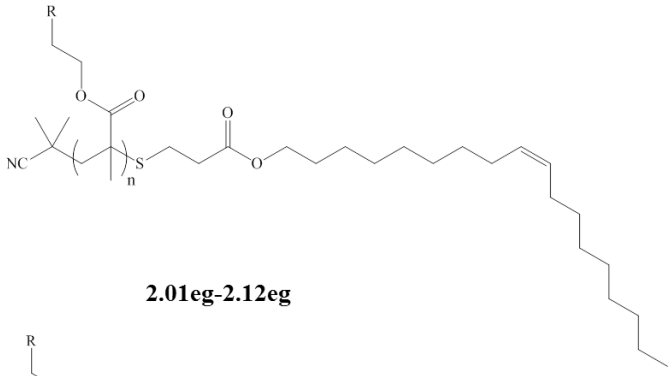

2.01eg-2.12eg

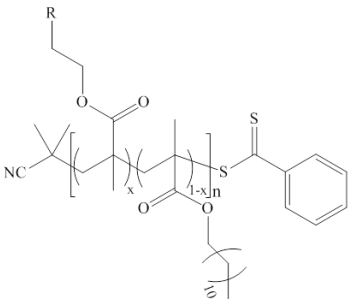

2.13-2.21

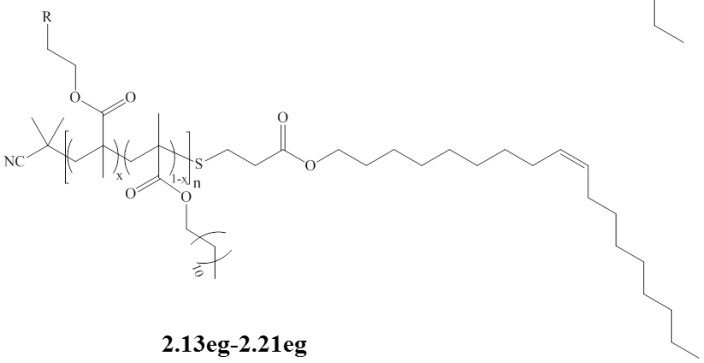

2.13eg-2.21eg

R =

DMAEMA
2.01-2.03
2.01-2.03eg
2.13-2.15
2.13-2.15eg

DEAEMA
2.04-2.06
2.04-2.06eg
2.16-2.18
2.16-2.18eg

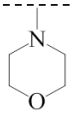

MEMA
2.07-2.09
2.07-2.09eg
2.19-2.21
2.19-2.21eg

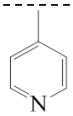

PEMA
2.10-2.12
2.10-2.12eg

3.3.1. Potentiometric titration of ashless detergents

For an ashless detergent to have the greatest performance in the engine it is hypothesised that a high affinity for acidic protons, i.e. a stronger base, would generate a faster neutralisation reaction and consequently reduce the engine wear caused from the acidic compounds. As mentioned in the introduction, potentiometric titration experiments allow for the determination of the pK_a or pK_b in solution. Here all the polymeric amines **2.01**-**2.21** and **2.01eg**-**2.21eg** were explored with potentiometric titration experiments which allowed for a simple comparison of base strength between the series of polymeric amines.

3.3.1.1. Background to potentiometric titration

The pK_a can be defined by understanding the acid-base equilibriums that exist in a system. The first is the dissociation of a strong acid (HA) into its two counter ions (H^+ and A^-), (eqn. 3.1), and therefore the acid dissociation constant K_a is defined as (eqn. 3.2):

$$HA \leftrightarrow H^+ + A^- \qquad (3.1)$$

$$K_a = \frac{[H^+][A^-]}{[HA]} \qquad (3.2)$$

The second constant to be defined is the base dissociation in water (eqn. 3.3) where the dissociation constant K_b is defined as (eqn. 3.4):

$$B + H_2O \leftrightarrow HB^+ + OH^- \qquad (3.3)$$

$$K_b = \frac{[HB^+][OH^-]}{[B]} \qquad (3.4)$$

The final equilibrium constant is the autoprotolysis of water (eqn. 3.5), where K_w is defined by (eqn. 3.6).

$$2H_2O \leftrightarrow H_3O^+ + OH^- \qquad (3.5)$$

$$K_w = [H_3O^+][OH^-] \qquad (3.6)$$

Furthermore, if pH is defined as the concentration of hydrogen ions in solution then *p*OH can be expressed as the concentration of hydroxide ions and pK_w can be expressed as (3.7):

$$pK_w = pH + pOH \qquad (3.7)$$

Although polymeric amines explored in this Chapter are known to be basic there is no need to define the base dissociation constant, K_b, as a stronger base will have a weaker conjugate acid, in this case NR_2H^+, and hence a higher pK_a will be observed.

The pK_a can be derived using the Henderson–Hasselbalch equation (eqn. 3.8).[14]

$$pK_a = pH - log_{10}\left(\frac{\alpha}{1-\alpha}\right) \qquad (3.8)$$

Where α is the degree of ionisation. It can then be understood that when α is equal to 0.5 then the equation is simplified to (eqn. 3.9):

$$pK_a = pH \qquad (3.9)$$

In this work, both water and acetonitrile (MeCN) were exploited as solvents for potentiometric titration. Acetonitrile is an interesting solvent for the titration of amines, as the autoprotolysis is much smaller than water and the dielectric constant is smaller also.[15-19] This consequently favours the dissociation of free ions in solution and allows for a stronger differentiating power between two ionic species, specifically this allows for the difference between two amino polymers to be more readily observed.

3.3.1.2. Potentiometric titration of polymeric amines

The series of polymeric amines described in Chapter 2 were titrated in two systems, an aqueous solvent system and an acetonitrile organic solvent system.

In the aqueous system the polymers were not all soluble in pure water and so the polymers were first all solubilised in a 1.1 stoichiometric excess of 1 M hydrochloric acid (HCl) to amine units. Subsequently these polymers were then back titrated with 0.1 M NaOH and the

pH of the solution was measured with respect to the volume of NaOH added. Within the acetonitrile system the polymers are titrated against glacial acetic acid and the potential of the solution with respect to volume of glacial acetic acid added was recorded. To compare the basicity of the amine polymers the pK_a of each system was measured. It is understood that a higher pK_a indicates a stronger base and therefore a more effective ashless detergent.

For titrations in acetonitrile the determination of pK_a for the amine polymers is relatively simple as when acidic protons are present, by the addition of acetic acid, the protons will react only with the tertiary amines on the polymer chain present. Assuming that the polymer in the dry powder state is at $\alpha = 0$ and acetonitrile does not ionise the amine units on the polymer once dispersed. Consequently, at the beginning of the titration the polymer is at $\alpha = 0$ and at the equivalence point (end point of the titration) the polymer is at $\alpha = 1$. Therefore the pH at which α is equal to 0.5 is defined as the pK_a. To understand α in the water systems first three scenarios must be understood. The first is when excess HCl reacts with NaOH in solution. As HCl is a strong acid this will dissociate first before the conjugate acid of the amines (eqn. 3.10).

$$HCl + NaOH = H_2O + NaCl \qquad (3.10)$$

The second is the reaction of NaOH with the conjugate acid in solution (eqn. 3.11). This reaction is the reaction of interest in the titration experiment.

$$NR_2H^+Cl^- + NaOH = H_2O + NaCl + NR_2 \qquad (3.11)$$

The final reaction is the dissociation of NaOH into free ions in solution (eqn. 3.12), this reaction will occur after the first two.

$$NaOH = Na^+ + OH^- \qquad (3.12)$$

By understanding these three reactions it can be deduced that the moles of NaOH consumed in the second scenario is equal to the number of moles of ionisable amine groups present.

Furthermore, the number of moles of NaOH added at the end of the titration is equal to the total number of moles of all three scenarios. It is known that the equivalence point of a titration curve marks the point at which there are equal stoichiometric amounts of acid and base. Therefore, for this titration the first equivalence point (V_{eqv1}) reached must signify the end of the first scenario, i.e. all the excess HCl has been neutralised. The second equivalence point (V_{eqv2}) is the end of the actual titration of interest, which represents the titration of the conjugate acid of the amines. This can be easily visible from plotting the raw data and second derivative of pH against volume of NaOH added. Therefore it can be understood the $V_{eqv2} - V_{eqv1}$ is equal to the volume of NaOH required for the titration of the amines (Figure 3.2), α can then be defined as the following (eqn. 3.13):

$$\alpha = \frac{V_{eqv2} - V_{NaOH}}{V_{eqv2} - V_{eqv1}} = \frac{Moles\ of\ NaOH}{Moles\ of\ Total\ Amine} \quad (3.13)$$

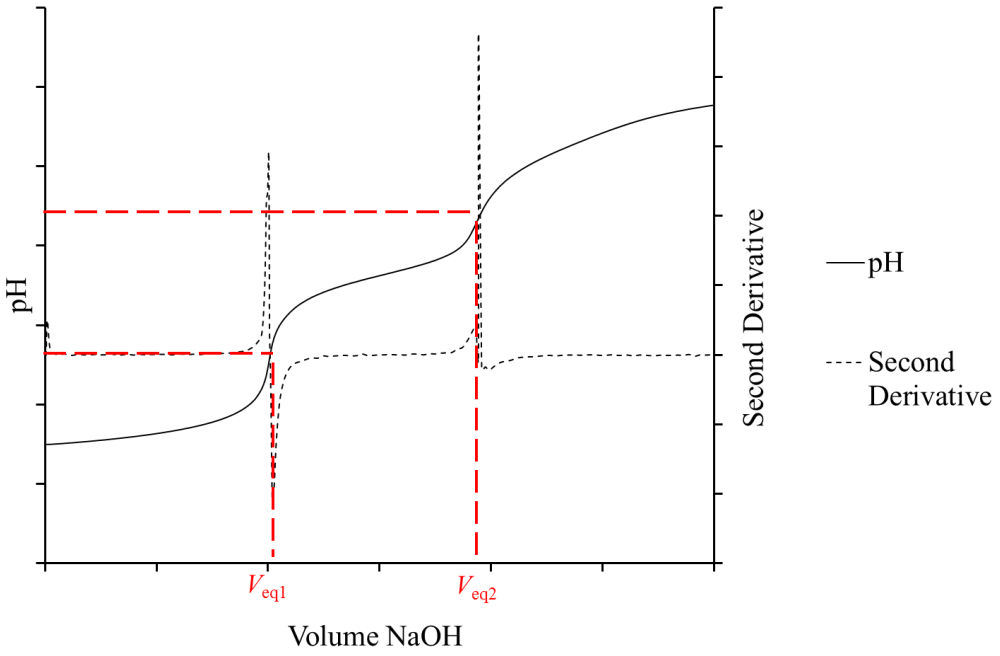

Figure 3.2. Example plot of the potentiometric back titration of a polyamine with NaOH in water, showing the relationship of pH with volume of NaOH added (solid line), and the second derivative of the pH with volume of NaOH added (dashed line).

Although pH is defined as the activity of the hydrogen ion, H^+, in aqueous system a pH value can be produced for the acetonitrile systems (MeCN) by using the Nernst equation (eqn. 3.14) and the potential measured ($E_{measured}$) in these systems.

$$E_{Measured} = E^o{}_{cell} - (0.0591)\log_{10}[H^+] \quad (3.14)$$

Within equation 3.14, $\log_{10}[H^+]$ is equal to the pH of the solution and $E^o{}_{Cell}$ is standard potential of the electrode.

3.3.1.3. Potentiometric titration of the amine homopolymers

In this first section the amine homopolymers were explored using potentiometric titration, both with RAFT end groups and with the cis-9-octadecene-based Michael acceptor end group (Scheme 3.1, **2.01**-**2.12** and **2.01eg**-**2.12eg** respectively). For the water based systems all amines were initially solubilised in 1.1 stoichiometric excess of 1M HCl and back titrated with 0.1 M NaOH. For the acetonitrile system the polymers were first solubilised directly and then titrated against glacial acetic acid. Therefore, when α = 0.5 the pK_a values were found, see Table 3.1 in the experimental for data.

As mentioned in Chapter 2, the molecular weight of the detergent is known to influence its behaviour in the lubricant. However this study was for classical metal salt detergents, where the molecular weight difference is a consequence of the increased amount of base present or a longer surfactant chain stabilising the micelle structure. For these amine polymers studied herein the molecular weight increase results in increased chain length and increased amount of amine units per particle once assembled as concluded in Chapter 2. Furthermore, for polyelectrolytes the influence of adjacent ionisable groups and therefore chain length can influence the pK_a and consequently the potential ashless detergent behaviour.[11,12,20,21] All homopolymers were titrated and the results in Figure 3.2 show the effect of molecular weight on the pK_a values obtained.

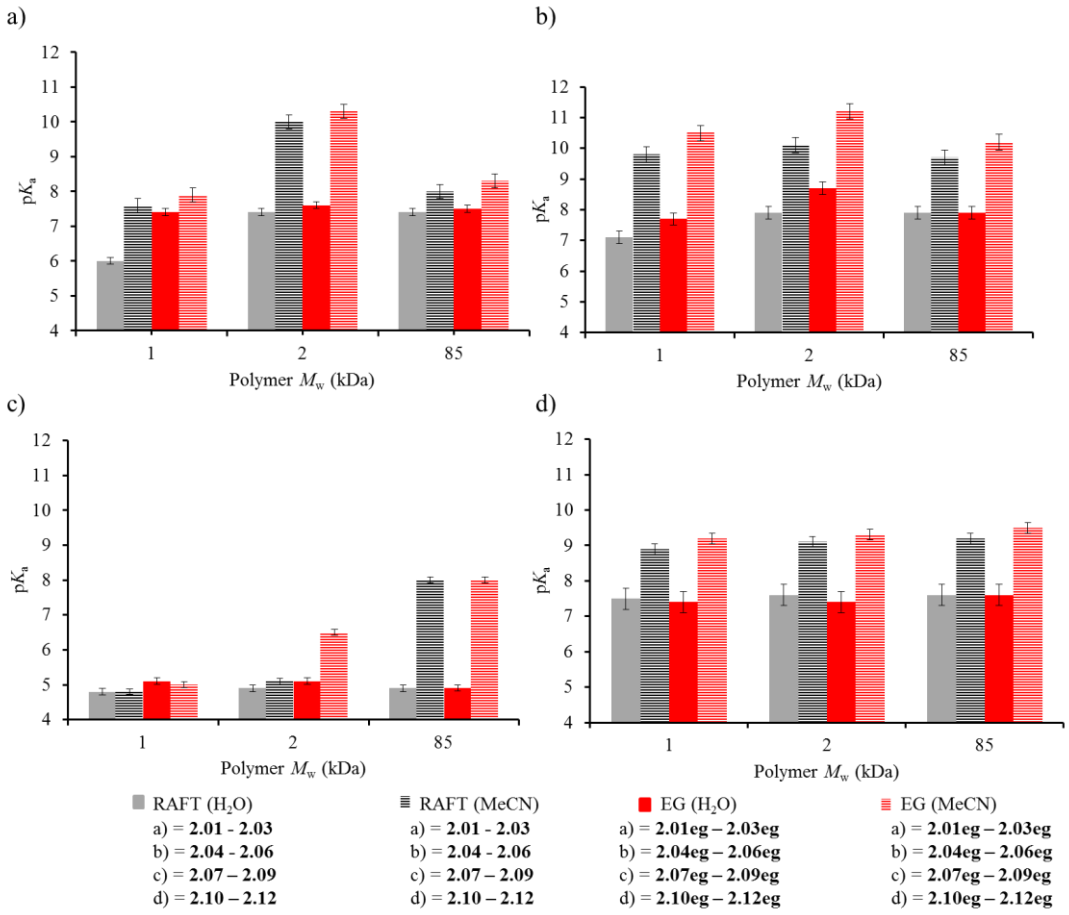

Figure 3.3. Plots to show the relationships between polymer molecular weight and pK_a value observed in both H_2O and MeCN for a) PDMAEMA **2.01-2.03** and **2.01eg-2.03eg,** b) PDEAEMA **2.04-2.06** and **2.04eg-2.06eg,** c) PMEMA **2.07-2.09** and **2.07eg-2.09eg,** d) PPEMA **2.10-2.12** and **2.10eg-2.12eg.** Labelled as RAFT, a reference to the polymer end group and labelled as EG, a reference to the modified end group polymers.

Interesting trends can be observed for these amine homopolymers; firstly for all titrations in MeCN, all systems have higher pK_a values which are attributed to the higher autoprotolysis of MeCN. Consequently equation 3.7 is adjusted as the K_w value is replaced by K_{MeCN} for acetonitrile, which is much higher than K_w, hence higher pK_a values are observed. For both the water and MeCN systems the trends are identical and therefore the results will be discussed further in parallel. For the PDMAEMA (**2.01-2.03** and **2.01eg-2.03eg**) and PDEAEMA (**2.04-2.06** and **2.04eg-2.06eg**) systems it can be observed that the 1kDa polymers gave the lowest pK_a value. This low pK_a value is a result of the charge repulsions

of adjacent amine units, as once an amine unit becomes ionised it becomes increasingly difficult to form charges on adjacent units on the same chain.[20,22,23] Given the small chain lengths here it can be deduced that for small polymer chains this effect of charge repulsion on ionisation is much more prominent throughout the entire chain. For example if one repeat unit is ionised on the 85 kDa PDMAEMA polymers, **2.03**, this equates to 0.2 % chain ionisation whereas for the 1 kDa PDMAEMA, **2.01**, system this equates to 20 % ionisation and thus the charge repulsion is much greater and hence slightly weaker bases are formed in the low molecular weight systems as indicated by a lower observed pK_a value.

On the other hand, the PMEMA (**2.07**-**2.09** and **2.07eg**-**2.09eg**) and PPEMA (**2.10**-**2.12** and **2.10eg**-**2.12eg**) systems show no significant change in pK_a with respect to chain length (Figures 3.3c and 3.3d). It is believed the lack of change between chain lengths is a consequence of the cyclic ring systems that both these polymers contain. These aromatic repeat units will already restrict the proximity of adjacent units and the influence of charge does not change this further. Therefore little to no change is observed with changing molecular weight for these systems. However, for the PMEMA **2.09** and **2.09eg** in acetonitrile there is a large increase in the pKa values observed, which could be a consequence of the reduction in charge repulsion at much larger chain lengths for the PMEMA system.

The second effect to explore was the influence of the end group modification on the pK_a values. Again, as mentioned in Chapter 2, these results are using the cis-9-octadecene based Michael acceptor as the end group as compared to the original RAFT end group from the chain transfer agent. Interestingly it can be observed that the chemical modification of the polymer with these alkyl chain end groups does indeed change the pK_a values observed. It was shown in Chapter 2 that the alkyl end group allows for the formation of discrete nanostructures in solution, therefore for these self-assembled polymer systems the increased local concentration of polymer chains results in an increased local concentration of amines.

This increased local concentration of amines means that the amine repeat units will act distinctly in two ways in comparison to a polymer chain in solution. The first is that the amines act as salts and can therefore screen the local charges on other polymer chains in local proximity and in turn the base is stronger, resulting in a higher pK_a observed by potentiometric titration.[24,25] The second is that the local concentration of these bases is very high; the high concentration of base units mean that as one base unit becomes ionised, thus forming the conjugate acid, a second base unit in close proximity can become ionised from this conjugate acid (Figure 3.4).[26]

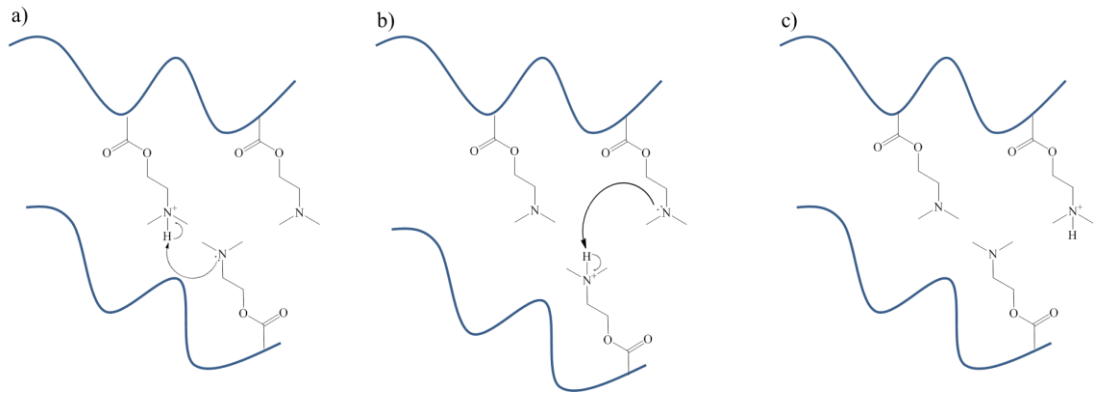

Figure 3.4. The buffering effect of PDMAEMA in a confined environment. a) Ionisation of the DMAEMA repeat unit on an adjacent chain from the conjugate acid b) subsequent ionisation of a DMAEMA repeat unit on the original polymer chain from the second DMAEMA conjugate acid c) final form of the adjacent unit ionisation, note this mechanism is reversible.

For the polymers explored in this work the influence of the end group modification is only prominent for the PDMAEMA and PDEAEMA systems in contrast to the PMEMA and PPEMA systems which show no observed difference when the polymer end group is altered. As concluded for the effects observed when changing the molecular weight of the amine polymers it is believed that the cyclic rings prevent the close proximity of the amine units and negate any potential screening of charges thus little change in pK_a is observed when the end group of the polymer is modified.

The third influence to examine is the effect of the amine on the pK_a. As a range of amines were synthesised to act as ashless detergents it is necessary to examine how different tertiary amines will alter the basicity of the resultant ashless detergent. By plotting the average pK_a of the polymers against the amine monomer repeat unit a simple comparison of amine strength can be made (Figure 3.5).

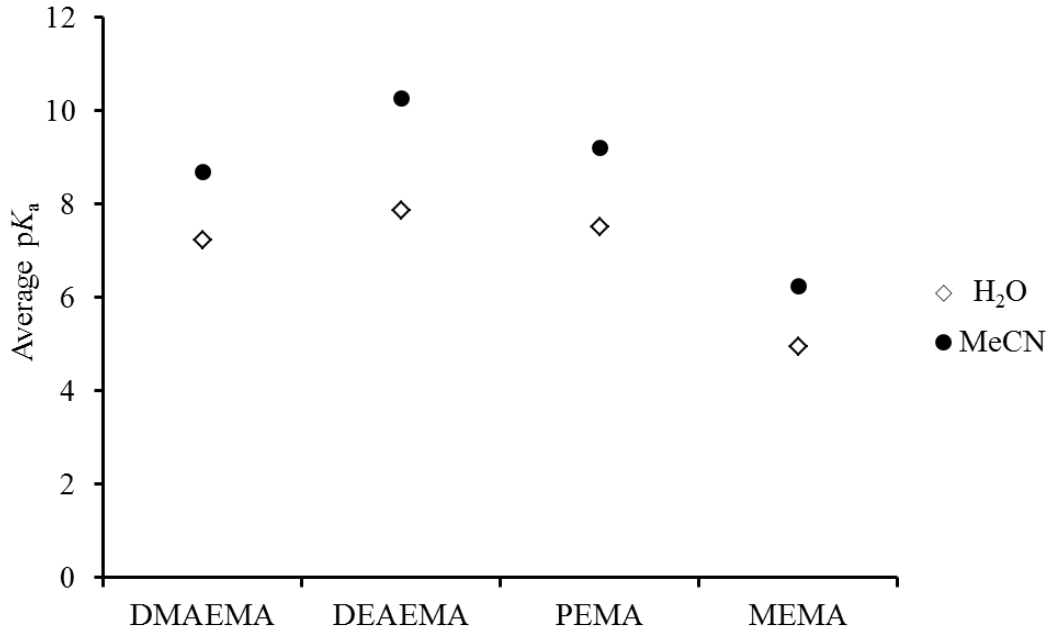

Figure 3.5. Relationships between amine and the average pK_a of the homopolymers observed in H_2O and MeCN for DMAEMA, DEAEMA, MEMA and PEMA

Overall the basicity of the amine follows the trend of DEAEMA > PEMA > DMAEMA >MEMA. Alkyl groups on the nitrogen of the tertiary amine will increase the basicity of the amine group and therefore the DEAEMA polymers results in the highest basicity of all polymer amines. Although cyclic groups can reduce the basicity of the amine, pyridine has several resonance structures which allow for the electron lone pair to reside on the nitrogen as opposed to being delocalised into the aromatic π system, allowing the nitrogen to be readily available for protonation. These resonance structures account for why the PEMA polymers are more basic than the cyclic MEMA systems.

3.3.1.4. Potentiometric titration of amine copolymers

In this second section the amine copolymers were explored by potentiometric titration, both with RAFT end groups (**2.13**-**2.21**) and the cis-9-octadecene-based Michael acceptor end group (**2.13eg**-**2.21eg)**. For the water based systems all amines were initially solubilised and back titrated with NaOH, however, during the titration the amine polymers began to precipitate from solution at low ionisation, (α), values. When these polymers begin to precipitate the polymers can no longer become deprotonated by the NaOH and thus accurate determination of the pK_a can no longer be obtained. Therefore only the results for the copolymers obtained in acetonitrile solution are reported. As described previously, for the acetonitrile system the polymers were first solubilised directly and then titrated against glacial acetic acid. The potentiometric data for all copolymers was analysed and when α = 0.5 the pK_a values were found, as listed in Table 3.2 in the experimental for data.

For these copolymers the length of the polymer chain was kept constant but the composition of the copolymer was varied. From Chapter 2 it was determined (based on the reactivity ratios) that the amine groups are statistically spaced along the polymer chain dependent on the ratios of the amine monomer and lauryl methacrylate (LMA) in the feed composition (Figure 3.6). For this first series of titrations the influence of composition on the pK_a values observed is explored (Figure 3.7).

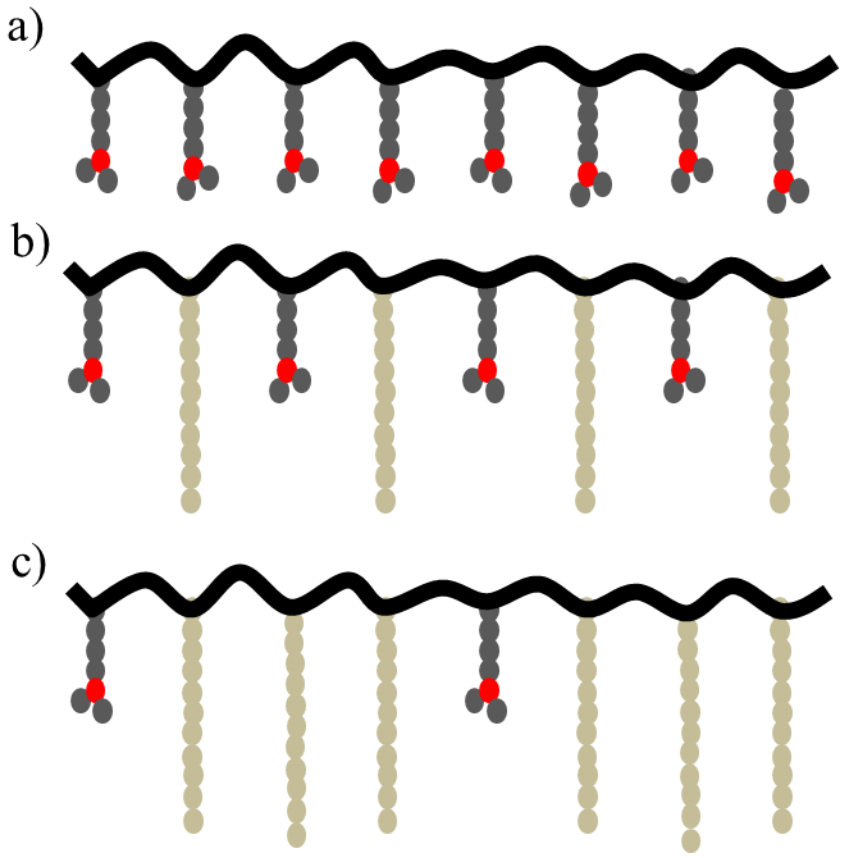

Figure 3.6. Figure depicting the increase in spacing between amine units dependent on the ratio of LMA and amine monomer. a) 100 mol% amine, b) 50 mol% amine, c) 25 mol% amine.

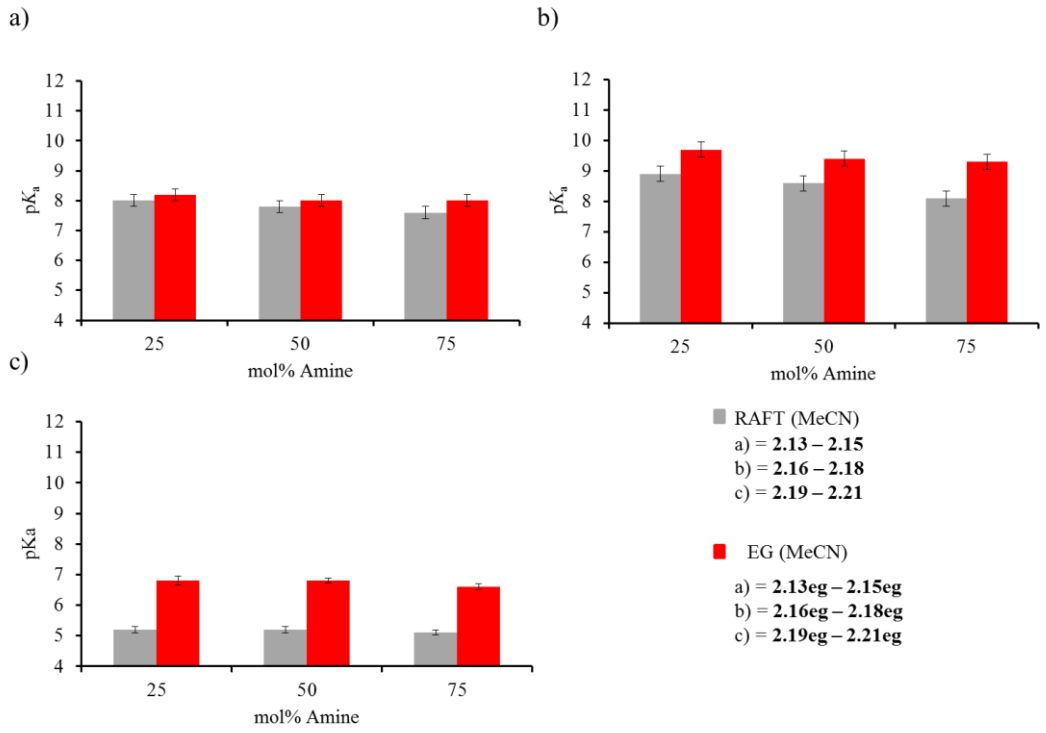

Figure 3.7 Plots to show the relationships between amine mol% and pK_a value observed in MeCN for a) P(DMAEMA-*co*-LMA) **2.13-2.15** and **2.13eg-2.15eg,** b) P(DEAEMA-*co*-LMA) **2.16-2.18** and **2.16eg-2.18eg,** c) P(MEMA-*co*-LMA) **2.19-2.21** and **2.19eg-2.21eg**. Labelled as RAFT, a reference to the polymer end group and labelled as EG, a reference to the modified end group polymers.

As shown in Figure 3.7 when the mol% incorporation of the amine is reduced the pK_a of the polymer shows a slight positive relationship. This reduction is related to the proximity of amines along the polymer chain. When the amine incorporation is high the charge repulsion of amines is high and as such the protonation of amines is more difficult.[20] On the other hand when the amines are spaced further apart the charges are separated by a large enough distance that the amine units can ionise independently, which makes protonation easier. However, for the P(MEMA-*co*-LMA) series, **2.19-2.21** and **2.19eg-2.21eg**, a large change in amine polymer loading did not result in a large change in pK_a value observed (Figure 3.7c). It is hypothesised that the cyclic structures in which the nitrogen base source is located possibly cause steric repulsions and that an increase in the spacing of the amine units does

not provide a significant increase in the spacing of the charges and thus an increased pK_a value

Additionally, likewise to the amine homopolymers these amine copolymers were end group modified through a Michael addition using the cis-9-octadecene based Michael acceptor.[27] In a similar manner to the end group modified homopolymers, **2.01eg -2.12eg**, an increase in pK_a is observed when these end group modified copolymers (**2.13eg**-**2.21eg**) are compared to the RAFT end group analogues (**2.13**-**2.21**). It is proposed that the RAFT terminated copolymers may adopt a collapsed structure in solution, however, the modification with the cis-9-octadecene based Michael acceptor is expected to alter the structure in solution and larger aggregates form (as observed by laser light scattering studies in Chapter 2). These large aggregates will have an increased local concentration of amines and therefore provide a buffering effect, screening out more charges in the local environment making deprotonation harder producing a higher pK_a. This effect of an increased local concentration of amines changing the pK_a of the polymer system are similar to reports in protein systems where hydrophobically modified pockets within the protein structure give an increased pK_a value.[26] Nevertheless this increase is most pronounced in the highest amine incorporations, 75 mol% amine copolymers (**2.15eg**, **2.17eg** and **2.21eg**). Specifically for these systems (**2.15eg**, **2.17eg** and **2.21eg**) it was believed that the possible structure formed by the end group modified polymers is much more defined in terms of segregated local environments for the amines that form the micelle core and therefore the cooperative deprotonation behaviour of the amines is increased, hence higher pK_a values are observed.

Although the results already indicate that the self-assembled structure has a much larger influence on the pK_a values than the nature of the amine moiety itself, the effect of different amine moieties was still examined. By plotting the average pK_a of the polymers against the amine monomer repeat unit a simple comparison of amine strength can be made (Figure 3.8).

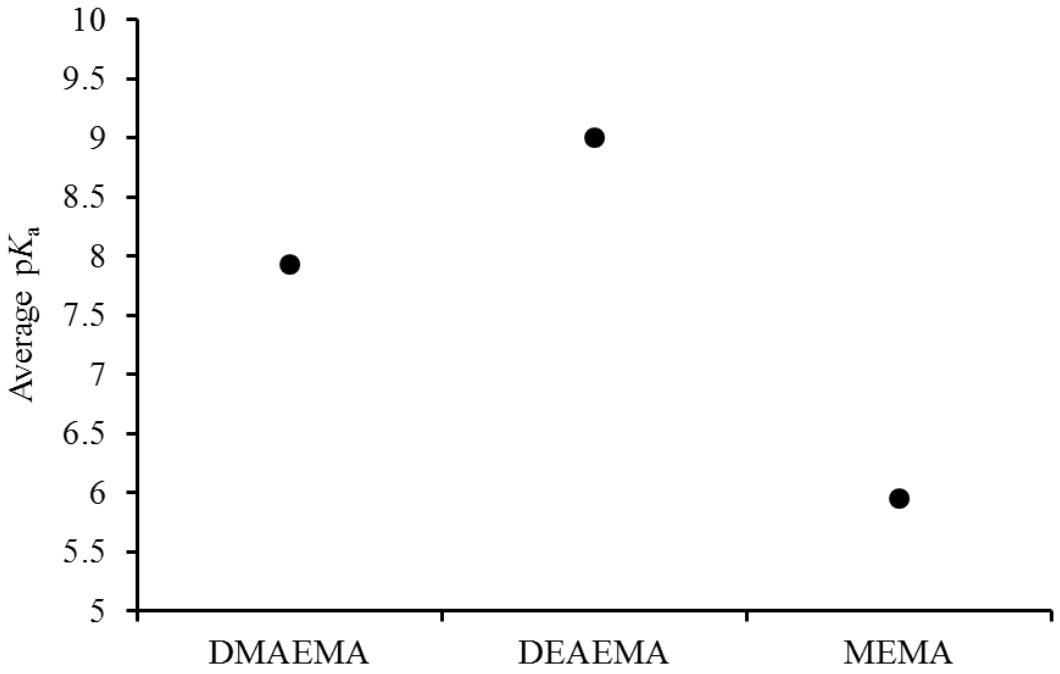

Figure 3.8. A plot to show the relationship between amine and the average pK_a of the copolymers observed in MeCN for **2.13-2.21** and **2.13eg-2.21eg**.

When the polymer structure is altered the observed pK_a greatly changed, but the overall basicity trend of the polymers followed the same basicity trend as observed for the homopolymers. Here the copolymers trend in basicity is DEAEMA > DMAEMA >MEMA, which follows a similar trend in decreasing basicity as observed for the homopolymers which was DEAEMA > PEMA > DMAEMA >MEMA. It can be therefore concluded that although the nature of the self-assembled structure can significantly alter the basic properties of these ashless detergents the overall amine basicity still follows the same trends regardless of the structure of the assembly.

These potentiometric titration experiments indicate that these amine polymers have the potential to act as ashless detergents in solution. Specifically these results demonstrate that the base source in each polymer system is capable of reacting with acid and has a strong affinity for acidic protons as indicated by the observed high pK_a values. Nevertheless, an ideal ashless detergent should also possess a very high amount of base with a high affinity

for acidic protons. In the following section the total base number (TBN) of this range of homopolymers and copolymers is explored, where the total amount of base in each of the systems is evaluated.

3.3.2. Total base number (TBN) analysis of ashless detergents

For an ashless detergent to be able to act as a replacement for the current metal salt detergent nanoparticles the polymeric materials must have high TBN to indicate a high reserve of base in the system. Although these ashless polymers show a good affinity for acidic protons the comparison of total base between amine polymer systems must also be evaluated to understand performance within the engine. To explore this all of the homopolymer and copolymer amines, **2.01**-**2.21** and **2.01eg**-**2.21eg,** were evaluated to establish their total base number (TBN) which allowed for a simple comparison between the different polymeric amine systems.

3.3.2.1. Background to TBN analysis

Potentiometric titration of detergents to obtain a pK_a value is not typically used to characterise the detergent nanoparticles in the lubricant formulation. However, in this section a similar titrimetric analysis is undertaken but for these titrations the aim is obtain the base number of a detergent nanoparticle. As mentioned in the introduction, the Total Base Number (TBN) analysis gives an indication of the amount of base present in the system. The TBN is given in mgKOH/g which represents the milligrams of KOH per one gram of an oil sample which is required to neutralise the system.

The TBN analysis is studied using a modified ASTM-D2896 method.[28] In this work the detergent nanoparticles are first solubilised in DMSO and then titrated with a solution of perchloric acid in glacial acetic acid, the electrode potential in the solution being measured with respect to the addition of perchloric acid, the end point (or equivalence point) is recorded and the TBN can be calculated from equation 3.15 in the ASTM-D2896 method:

$$TBN = \frac{[(E-F)\times N\times 56.1]}{S} \qquad (3.15)$$

Where *E* stands for the equivalence point of the titration, *F* is the blank equivalence point, N is the normality of the titrant (the equivalence of acidic protons in solution), *56.1* is the molar mass of KOH and *S* is the sample weight in g.

For a quick and simple determination of the base content of a sample, TBN analysis works well. However, the TBN analysis is primarily suited for the metal inorganic salt detergents which show an irreversible reaction between the base and acid. This irreversible reaction produces a very sharp defined end point which can then be simply related back to the amount of base present in the system. Conversely, the development of these new ashless detergents which are based upon organic base sources produces a reversible reaction between the base and the acid which means the TBN analysis may show slightly different behaviours than expected, as the original design of the test is for metal inorganic salts.

3.3.2.2. TBN analysis of the amine homopolymers

To evaluate the TBN of the amine homopolymers a modified ASTM-D2896 method was utilised, the TBN values were calculated from the end point of the titration; see Table 3.3 for the data. Furthermore, as mentioned previously, the test was not designed to analyse polymeric species which are to be used as ashless detergents, consequently some results from the TBN analysis of amine polymers may differ from expected TBN values. Each amine can react with acid in solution; therefore a theoretical TBN can be calculated (eqn. 3.16).

$$TBN_{Theoretical} = \frac{1}{(M_w\ of\ 1\ monomer\ repeat\ unit)} \times 56.1 \qquad (3.16)$$

Table 3.3. TBN analysis data for homopolymers **2.01**-**2.12** and **2.01eg**-**2.12eg** using the ASTM-D2896 analysis method.

Monomer	Polymer	M_n (kDa)[a]	$TBN_{measured}$ (mg KOH/g)[b]	$TBN_{theoretical}$ (mg KOH/g)[c]
DMAEMA	**2.01**	1.0	192	278
	2.01eg	1.2	320	207
	2.02	2.3	265	318
	2.02eg	2.5	274	282
	2.03	85	193	356
	2.03eg	85	210	356
DEAEMA	**2.04**	1.2	234	236
	2.04eg	1.4	122	175
	2.05	2.3	267	270
	2.05eg	2.5	313	239
	2.06	86	68	302
	2.06eg	86	399	302
MEMA	**2.07**	1.1	147	220
	2.07eg	1.3	374	163
	2.08	2.2	220	251
	2.08eg	2.4	239	222
	2.09	81.0	274	281
	2.09eg	81.0	172	281
PEMA	**2.10**	1.2	124	230
	2.10eg	1.4	283	171
	2.11	2.3	128	263
	2.11eg	2.5	127	233
	2.12	85.0	0	294
	2.12eg	85.0	0	294

[a]Determined by ^{1}H NMR spectroscopy. [b]Determined by ASTM-D2896 in DMSO.
[c]Determined using eqn. 3.16

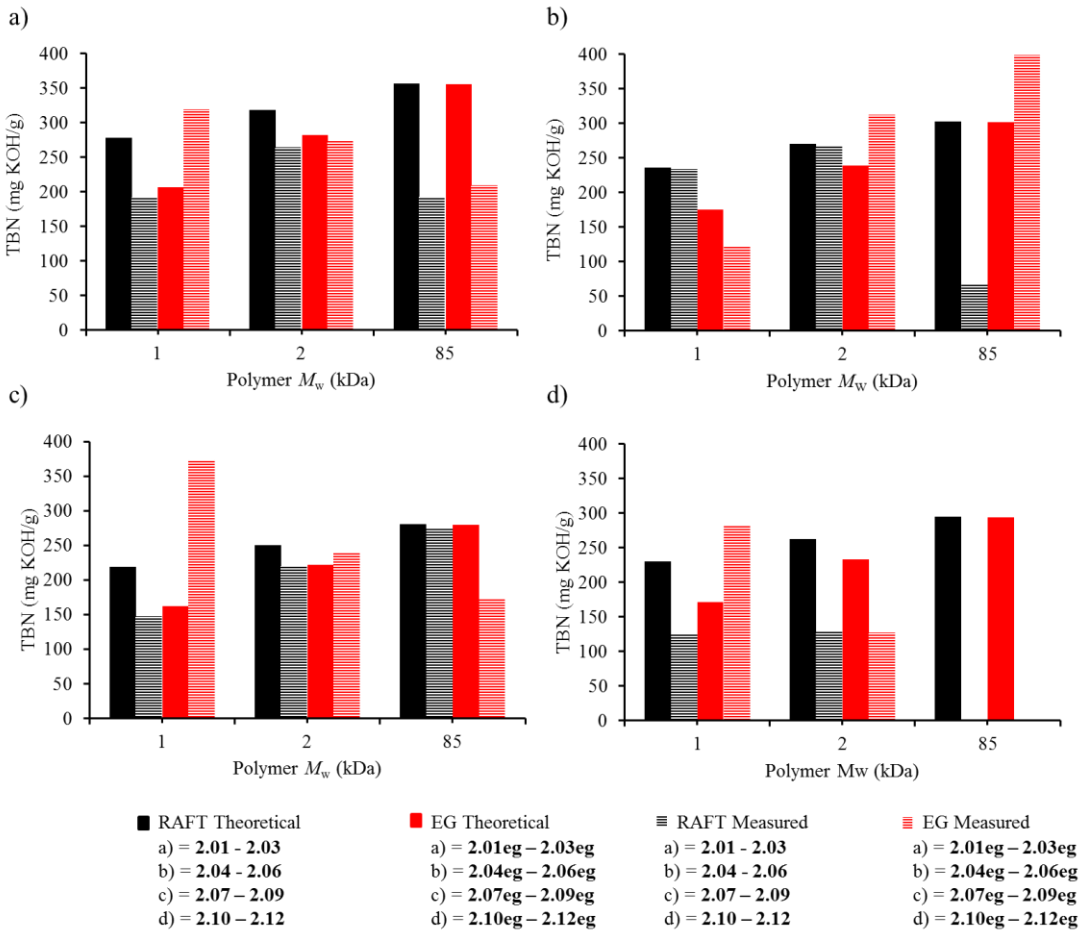

Figure 3.9. Plots to show the relationships between polymer molecular weight and TBN value measured and theoretically calculated using eqn. 3.15 for a) PDMAEMA **2.01-2.03** and **2.01eg-2.03eg,** b) PDEAEMA **2.04-2.06** and **2.04eg-2.06eg,** c) PMEMA **2.07-2.09** and **2.07eg-2.09eg,** d) PDMAEMA **2.10-2.12** and **2.10eg-2.12eg.** (Labelled as RAFT, a reference to the polymer end group and labelled as EG, a reference to the modified end group polymers).

Initially, similar to the pK_a analysis the effect of molecular weight on the TBN value was explored for this series of homopolymeric amine materials (Figure 3.9). Universally for all systems theoretically as the molecular weight of the polymer is increased the TBN values calculated by equation 3.16 increase which is as a result of the higher percentage of amines that make up the composition of the polymer with respect to the end groups. However, when this theoretical value was compared to the experimentally measured value there was a difference between the two, specifically the theoretical values predominantly show a higher

TBN value than those measured using this method (see Figure 3.9). Furthermore, it can be observed that for the TBN values measured there is no clear trend between polymer molecular weight or between polymer systems which is in contrast to the theoretical TBN values.

3.3.2.3. TBN analysis of the amine copolymers

In this second section the amine copolymers are explored by the ASTM-D2896 method and the TBN values are found, TBN values for copolymers with both RAFT end groups and the cis-9-octadecene-based Michael acceptor are explored, Table 3.4.

Table 3.4. TBN analysis data for copolymers **2.13**-**2.21** and **2.13eg**-**2.21eg** using the ASTM-D2896 analysis method.

Monomers	Polymer	mol% amine	mol% LMA	M_n (kDa)[a]	$TBN_{measured}$ (mg KOH/g)[b]	$TBN_{theoretical}$ (mg KOH/g)[c]
DMAEMA / LMA	**2.13**	25	75	3.5	41	57
	2.14	50	50	3.2	105	127
	2.15	75	25	4.2	126	293
	2.13eg	25	75	3.6	61	54
	2.14eg	50	50	3.5	102	120
	2.15eg	75	25	4.2	149	278
DEAEMA / LMA	**2.16**	25	75	2.1	49	66
	2.17	50	50	2.3	89	116
	2.18	75	25	2.3	140	251
	2.16eg	25	75	2.2	33	60
	2.17eg	50	50	2.3	70	104
	2.18eg	75	25	2.3	101	226
MEMA / LMA	**2.19**	25	75	3.2	66	54
	2.20	50	50	2.9	112	114
	2.21	75	25	3.3	138	246
	2.19eg	25	75	3.4	67	51
	2.20eg	50	50	3.1	119	107
	2.21eg	75	25	3.5	197	232

[a]Determined by ^{1}H NMR spectroscopy. [b]Determined by ASTM-D2896 in DMSO.
[c]Determined using eqn. 3.16.

For the copolymer systems it is expected that the pK_a varies when the composition changed, hence the effect of composition on the TBN values for these copolymers was initially explored (Figure 3.10).

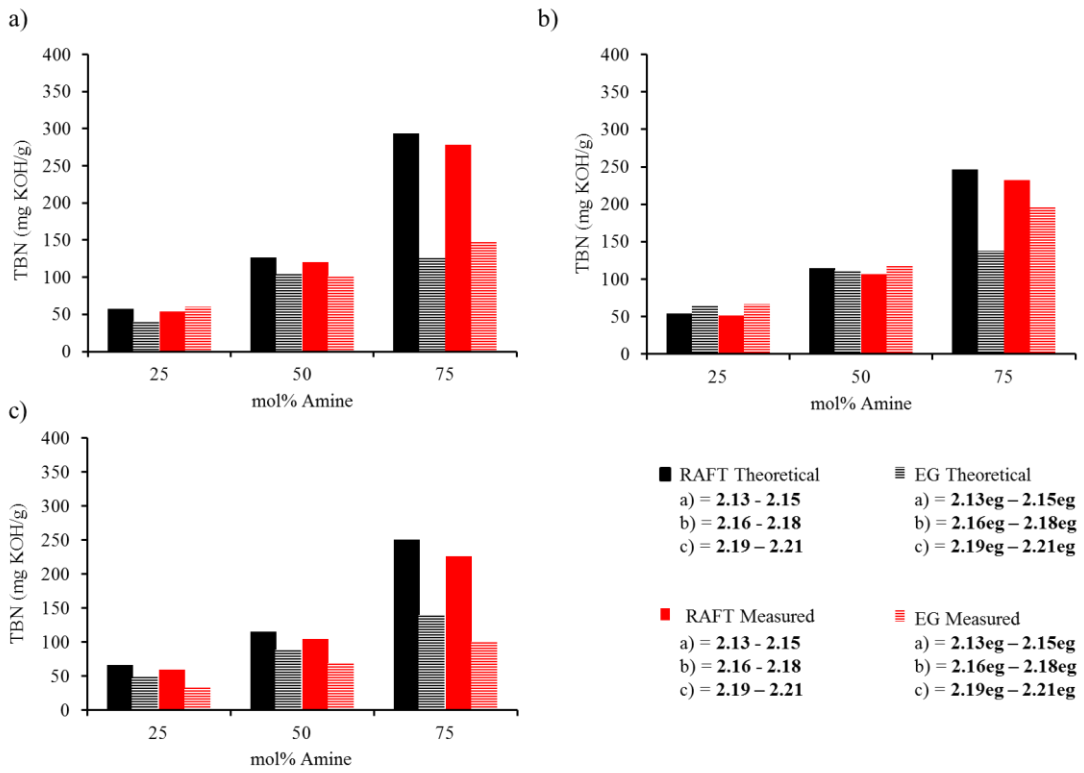

Figure 3.10. Plots to show the relationships between polymer molecular weight and TBN value measured and theoretically calculated for a) P(DMAEMA-*co*-LMA) **2.13-2.15** and **2.13eg-2.15eg,** b) P(DEAEMA-*co*-LMA) **2.16-2.18** and **2.16eg-2.18eg,** c) P(MEMA-*co*-LMA) **2.19-2.21** and **2.19eg-2.21eg**. Labelled as RAFT, a reference to the polymer end group and labelled as EG, a reference to the modified end group polymers.

By plotting the mol% of amine in the copolymer against the TBN we can see a clear linear relationship. This is to be expected as an increase in mol% of amine results in a higher concentration of base within the system and as such more acid is neutralised in the analysis method, and thus a higher TBN is measured (see Figure 3.10). Moreover, what can also be observed is that the relationship between polymer composition and theoretical TBN is also linear. Nevertheless, in all cases the theoretical TBN values are higher than the measured TBN values observed here.

The discrepancy observed between the theoretical and measured values for all polymer systems is hypothesised to be a lack of accessibility of the amines to the titrant in the TBN test method. It is believed that not all the amines can become ionised in this test method and as such, a lower TBN value is observed than the theoretical value. Furthermore, this could be a consequence of the speed of the titration, as for polymeric amines it may take a longer time for the acid molecules to diffuse successfully into the polymer structures as seen previously for potentiometric titrations of poly(styrene)-*block*-poly(acrylic acid).[29] Therefore it is believed that perhaps this increased diffusion time of protons occurs during the TBN test which results in a lower TBN value. The second is that the analysis is based on the determination of the end point of the reaction; for metal salt particles this end point is very clearly defined, but for polyamines the buffering effect of the system means that this end point is not as clearly defined and the shape of the titration curve (which is used to judge the end point for the TBN analysis) is different to metal salt detergent titration curves, possibly with polyamines possessing multiple points which could be perceived as end points to the titration.[30,31] Consequently, it might be expected that this change in the curve shape may lower the accuracy in determining the end point of the titration and therefore lower TBN values are observed throughout the series of experiments.

3.3.3. Relation of pK_a and TBN values for amine polymers.

Ideally new ashless polymer detergent particles would possess both high TBN and high pK_a values, therefore forming structures in solution which have a strong affinity for acidic protons and a high amount of base present. Although a range of acid dissociation constants (pK_a) values were found for the amine polymers and a range of TBN values, this does not mean that a polymer with a high TBN (lots of base present) will have a high pK_a value (a strong acid). To evaluate this for the series of amine homopolymers and copolymers, the comparison of pK_a and TBN was undertaken. When the pK_a of the amine homopolymers (grouped in types of monomer), both RAFT and end group modified (with the cis-9-

octadecene Michael acceptor), were plotted against TBN an easy visual comparison can be made (Figure 3.11).

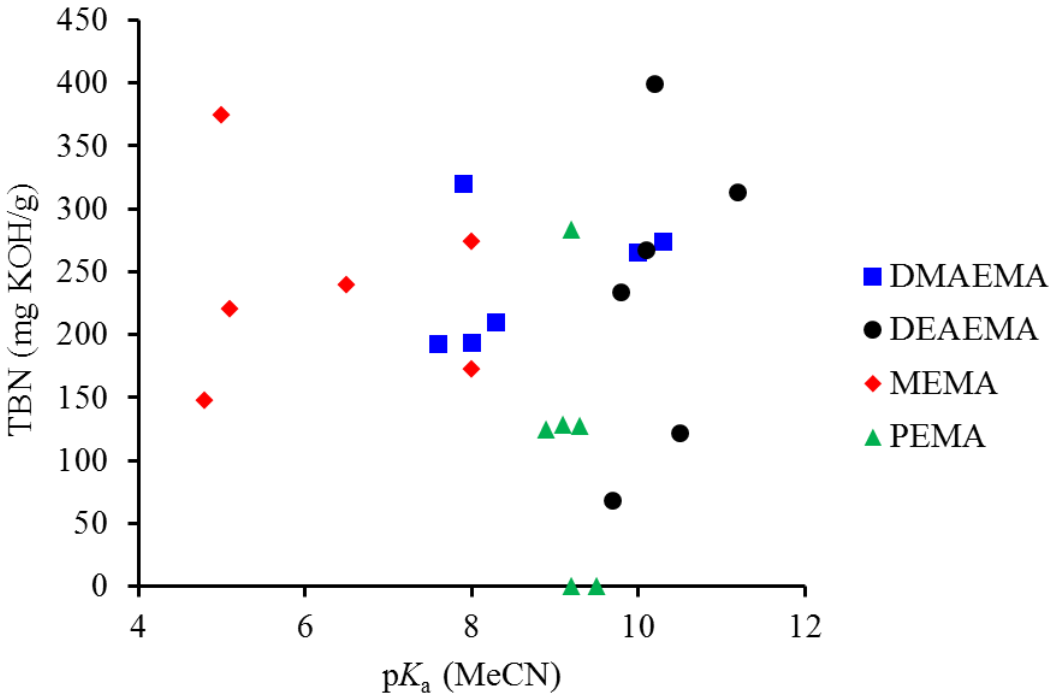

Figure 3.11. A plot to show the relationships between TBN and pK_a value for each amine homopolymer series, grouped by the monomer repeat unit, **2.01-2.12** and **2.01eg-2.12eg.**

In this plot only the pK_a results in MeCN are shown as these can be then be directly compared to the amine copolymers which were only run in MeCN. Interestingly, no obvious trend between the pK_a and TBN can be observed for the amine homopolymer series. This could be understood that because the TBN test method is based primarily on the amount of base present in the system, therefore the TBN analysis is stoichiometrically weighted to the amount of base and is irrespective of base strength. However, on the other hand the pK_a values are weighed towards the amine structure and the efficiency of the nitrogen base source, although the actual amount of base may be the same in two systems the structure of the base moiety may change and a higher pK_a may be observed for one system over another with the same amount of base.

On the other hand when the data collected for the amine copolymers pK_a value is plotted against the TBN values a different scenario is present (Figure 3.12).

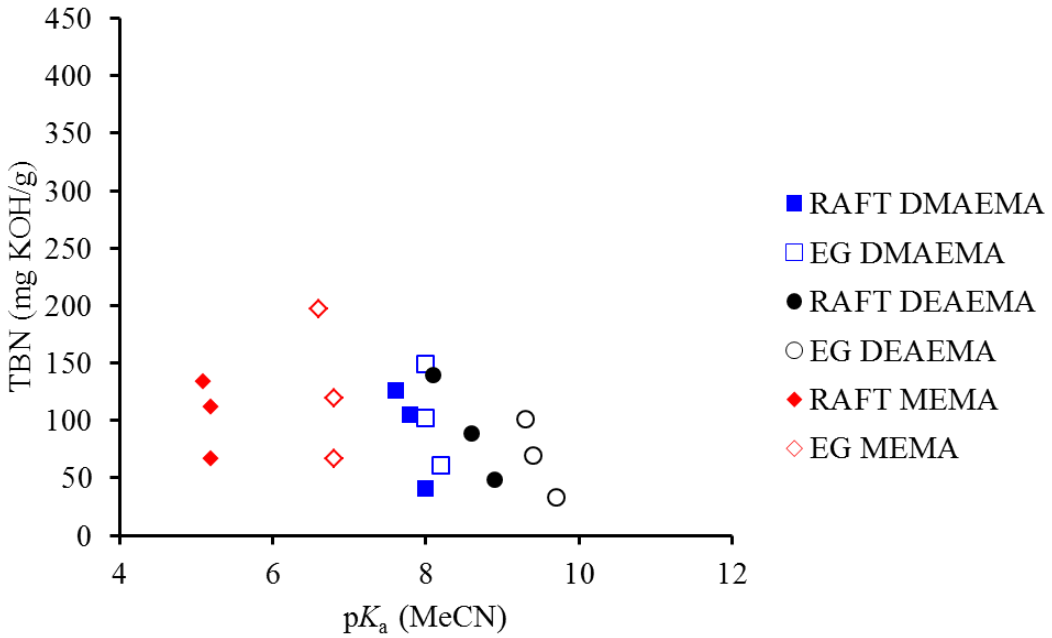

Figure 3.12. Relationships between TBN and pK_a value for each amine copolymer series, **2.13-2.21** (labelled as RAFT, a reference to the polymer end group) **2.13eg-2.21eg** (labelled, as EG a reference to the modified end group polymers).

For these amine copolymers with both RAFT end groups and also end group modified (with the cis-9-octadecene Michael acceptor), it can be observed there is a weak negative linear relationship between the pK_a and TBN. In this work it can be observed that as the pK_a value increases there is a decrease in the TBN value observed. This relation between TBN and pK_a is an effect of spacing the amines along the polymer chain, through copolymerisation, gives a higher pK_a value. However, this copolymerisation simultaneously reduces the amount of base present in the system, resulting in a lower TBN value. Interestingly this can then be used to understand that although some of these ashless copolymer detergents particles may have very low TBN values basicity may be very high.

The comparison between the pK_a and TBN data obtained indicates that both test methods provide different information on the potential for detergent behaviour, i.e. both the amount

and strength of the base present in the system. However, these tests do not conclusively show that these polymers will neutralise acid when in a mineral oil. In order to understand the potential of these polymers as ashless detergents, acid neutralisation tests were undertaken, which can mimic the conditions and environments in which these detergents would be used.

3.3.4. Acid neutralisation analysis of ashless detergents

From potentiometric titrations and TBN analysis it can be concluded that these polymeric amine systems have the potential to act as ashless detergents in solution with high pK_a values and good TBN values. To further understand the potential for the polymers to act as ashless detergents *in situ* acid neutralisation tests were undertaken.

3.3.4.1. Understanding the mechanism and rate of neutralisation for amine polymers.

As mentioned in the introduction there are two primary mechanisms for the reaction of detergent nanoparticles with acid droplets in solution. However, regardless of the mechanism the particle must still come into contact with the acid droplet. This data will assist in the understanding of the rate of reaction and the factors that increase the rate of neutralisation can be explored.

From a theoretical perspective the reaction between a detergent nanoparticle and acid in the engine oil will be dependent on both the concentration of detergent and acid thus resulting in a second order reaction. However the detergent concentration is typically much higher than the acid droplet concentration and hence the concentration of the detergent throughout the reaction does not change significantly. Therefore, it can be deduced that the reaction is *pseudo* first order and that the rate of metal salt detergent nanoparticles is given in equation 3.17.

$$Rate = k'[H_sSO_4] \qquad (3.17)$$

However, this reaction is irreversible once the product is formed. On the other hand the amine polymers, upon reaction with an acid, will undergo a reversible neutralisation reaction and therefore the derivation of the rate equation is as follows (eqn. 3.18).

$$HA + NR_3 \rightleftharpoons NR_3H^+ + A^- \qquad (3.18)$$

Similar to overbased detergents, the amine polymers are in excess and thus the reaction can be simplified to a *pseudo* first order reaction 3.19 and the rate is defined as shown in equation 3.20.

$$HA \rightarrow NR_3H^+ + A^- \qquad (3.19)$$

$$Rate = k_f[HA] \qquad (3.20)$$

However, the reverse reaction (given by eqn. 3.21) is a second order reaction (given by eqn. 3.22).

$$NR_3H^+ + A^- \rightarrow NR_3 + \mathrm{HA} \qquad (3.21)$$

$$Rate = k_r[NR_3H^+][A^-] \qquad (3.22)$$

Therefore, it can be understood that at equilibrium the rates of reaction must be equal (eqn. 3.23).

$$k_f\,[HA] = k_r[A^-][NR_3H^+] \qquad (3.23)$$

Upon rearranging the equation gives (eqn. 3.24)

$$[HA] = \frac{k_r}{k_f}[A^-][NR_3H^+] \qquad (3.24)$$

Using equation 3.20 *[HA]* can be substituted and the equation then becomes (eqn. 3.25).

$$Rate = k' \frac{k_r}{k_f}[A^-][NR_3H^+] \qquad (3.25)$$

Furthermore, using equation (3.24) k_r/k_f can be substituted and the equation evolves to become (eqn. 3.26).

$$Rate = k' \frac{[HA]}{[A^-][NR_3H^+]}\ [A^-][NR_3H^+] \qquad (3.26)$$

Which simplifies to become (eqn. 3.27)

$$Rate = k'\ [HA] \qquad (3.27)$$

From understanding both the forward and reversible reactions present for the amine homopolymers upon protonation is can be concluded that the reaction is a *pseudo* first order reaction in a similar manner to metal salt detergent nanoparticles.

3.3.4.2. Setup for the rate of acid neutralisation by polyamines

To test the rate of neutralisation a model system was produced which could mimic the environment in which these ashless detergents will be used and the acid neutralisation could be monitored over time. Hone *et al* used a stop flow model neutralisation set up and monitored the pH change during the neutralisation of H_2SO_4 by overbased detergents with UV-Vis spectroscopy over time in non-polar media.[9] Hone *et al* were able to show that using a methyl orange pH indicator a decrease in the intensity in the UV-Vis spectra at 516 nm could be observed as the neutralisation occurs. For the rate of neutralisation studies using the amine polymers a similar model micro-neutralisation set up with methyl orange and UV-Vis spectroscopy was used. In this work only the self-assembled end group modified polymers are explored (**2.01eg**-**2.21eg**) where the end group is the cis-9-octadecene based Michael acceptor. In a similar manner to Hone *et al* to analyse the rate of the neutralisation the change in the intensity at 510 nm is measured over time by UV-Vis spectroscopy. In this

model system a 0.6 μL 0.1M H_2SO_4 acid droplet, treated with methyl orange, is injected into a 250μL 1 wt% sample of amine polymer in mineral oil in a cuvette at 70 °C inside a heating block where the UV-Vis spectroscopy can be measured over time.

3.3.4.3. Rate analysis of amine polymer neutralisation

By measuring the intensity of light at 510 nm over time the rate of the reaction can then be understood. At the beginning of the reaction, t = 0, it can be assumed that all of the acid is still present in the system and the normalised concentration is of the acid is 1. Hence, the intensity of light at t = ∞ is indicative of the end of the reaction and the normalised concentration of H_2SO_4 is 0 as it has all be consumed through a neutralisation reaction.

When the normalised concentration is plotted against time for all polymer amines the rate can then be determined. For a *pseudo* first order reaction a plot of $\ln[H^+]$, where $[H^+]$ is the concentration of acid, against time, *t*, would yield a linear plot and the slope of the line would be equal to the rate of the reaction, example plots are shown for polymers **2.02eg** (Figure 3.15).

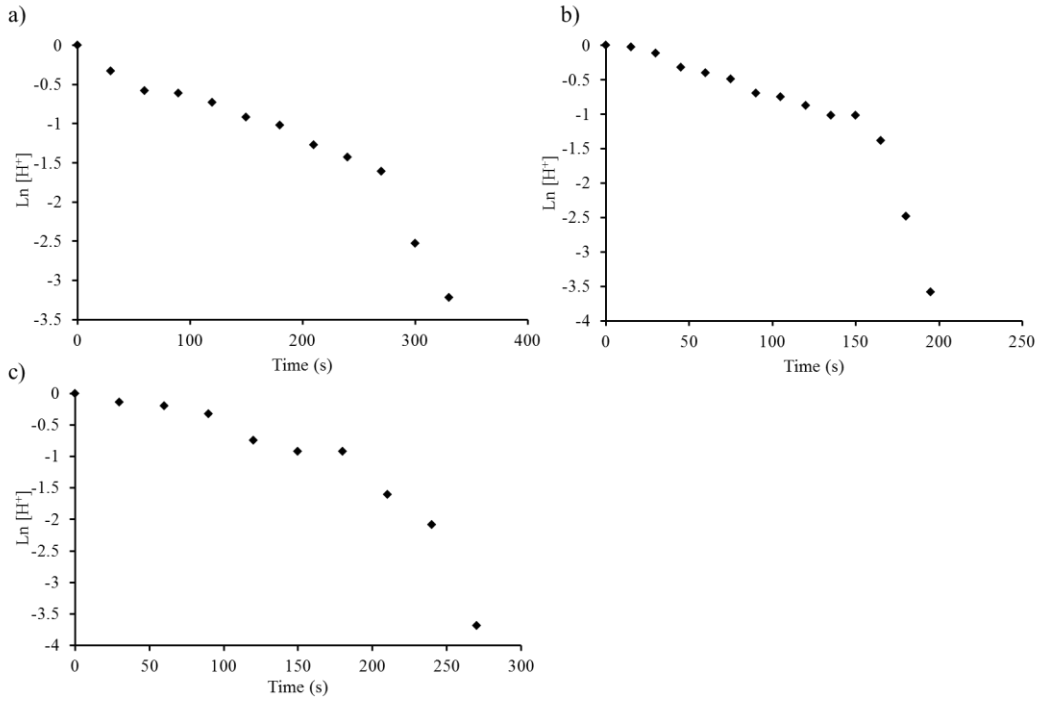

Figure 3.15. Pseudo first order kinetic plot of the neutralisation of H_2SO_4 by the amine end group polymers a) **2.02eg** b) **2.01eg** c) **2.11eg**.

However, despite theoretical predictions that a first order acid neutralisation reaction should take place for the amine polymers, experimentally this was not the case for the polyamines and the polymer systems showed a strong deviation from this prediction where at longer times the data point began to show a larger decay. It was then believed that perhaps a different rate determining step is present in the neutralisation reaction. The first thought is that the rate determining step was a second order as the may account for the decay at longer time points. For a second order reaction a plot of $1/[H^+]$, where $[H^+]$ is the normalised concentration of acid, against time, *t*, would yield a linear plot and the slope of the line would be equal to the rate of the reaction. An example plot is shown for **2.02eg** (Figure 3.16).

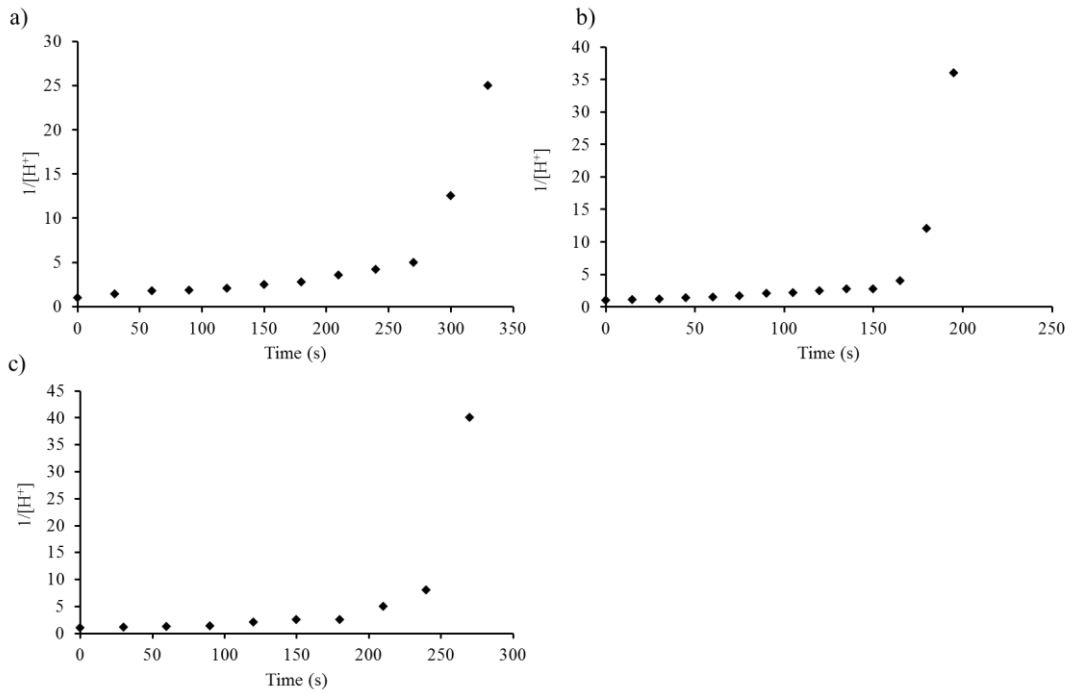

Figure 3.16. Second order kinetic plot of the neutralisation of H_2SO_4 by the amine end group polymers a) **2.02eg** b) **2.01eg** c) **2.11eg**.

All polymer systems investigated showed neither a first nor second order reaction rate. Despite the strong deviation at long time points the data shows an exponential relationship even at short time points. However, when the raw data was plotted, normalised concentration of acid, $[H^+]$, against time, *t*, on a semi-log plot a much stronger linear relationship is observed for all polymer systems.An example plot is shown for **2.02eg** (Figure 3.17).

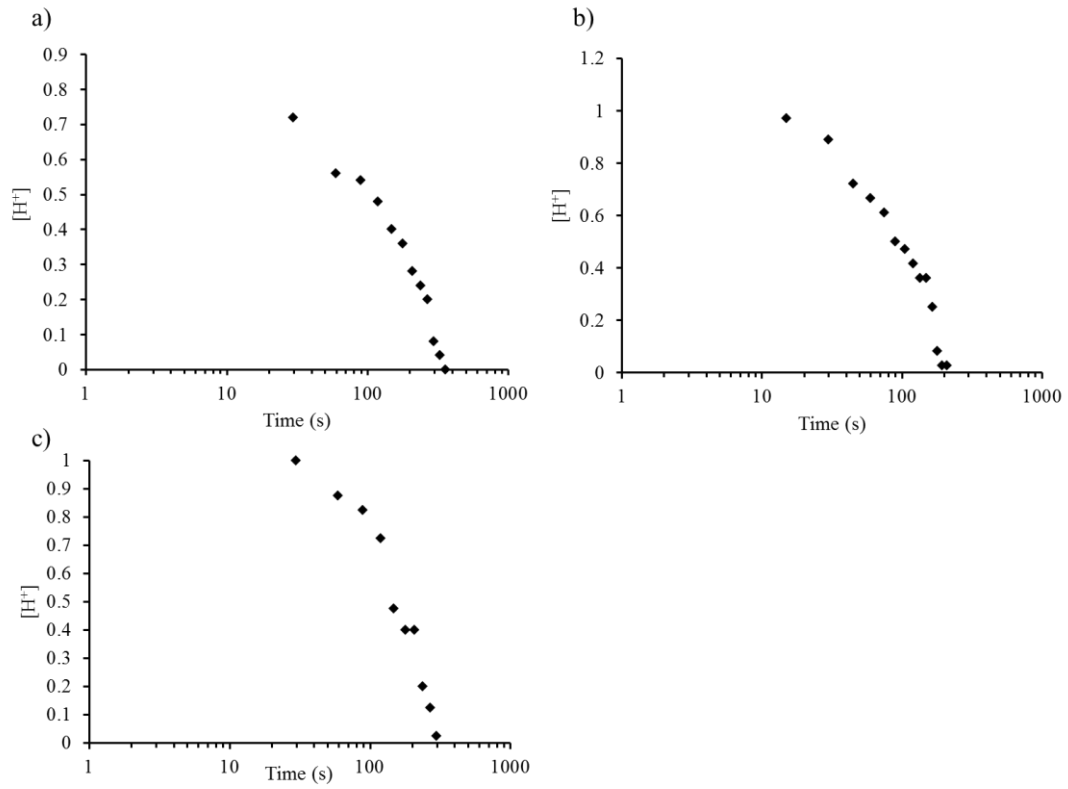

Figure 3.17. A semi-log plot of the neutralisation of H_2SO_4 by the amine end group polymers a) **2.02eg** b) **2.01eg** c) **2.11eg**.

Therefore, for these systems all polymers were compared in a semi-log scale, and the slope of the lines was evaluated. Firstly, the end group modified homopolymers were explored, **2.01eg-2.12eg** (see Figure 3.18 and Table 3.13 in the experimental section).

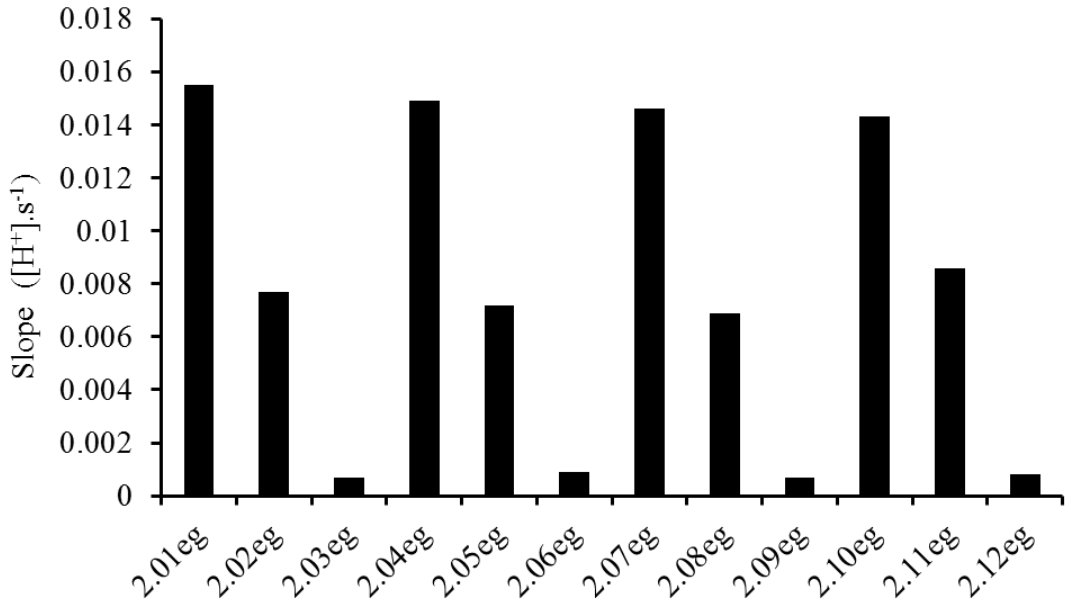

Figure 3.18. A plot to show the relationship between slope of the line from a semi-log plot of $[H^+]$ with times for the end group modified amine homopolymers; PDMAEMA **2.01eg-2.03eg**, PDEAEMA **2.04eg-2.06eg**, PMEMA **2.07eg-2.09eg** and PPEMA **2.10eg-2.12eg**.

For all polymer systems **2.01eg-2.12eg** it can be observed that as the chain length increases the slope of the line, which can be related to the rate of the reaction, decreases and thus a slower reaction is occurring. Additionally is was observed that the difference between different amine functionalities is minimal, therefore the influence of the amine does not seem to effect the rate of the reaction in this test for these end group modified homopolymers.

On the other hand, the end group modified amine copolymers **2.13eg-2.21eg**, were also evaluated but here the chain length was kept constant and the composition of the chains was varied (see Table 3.14 and figure 3.19).

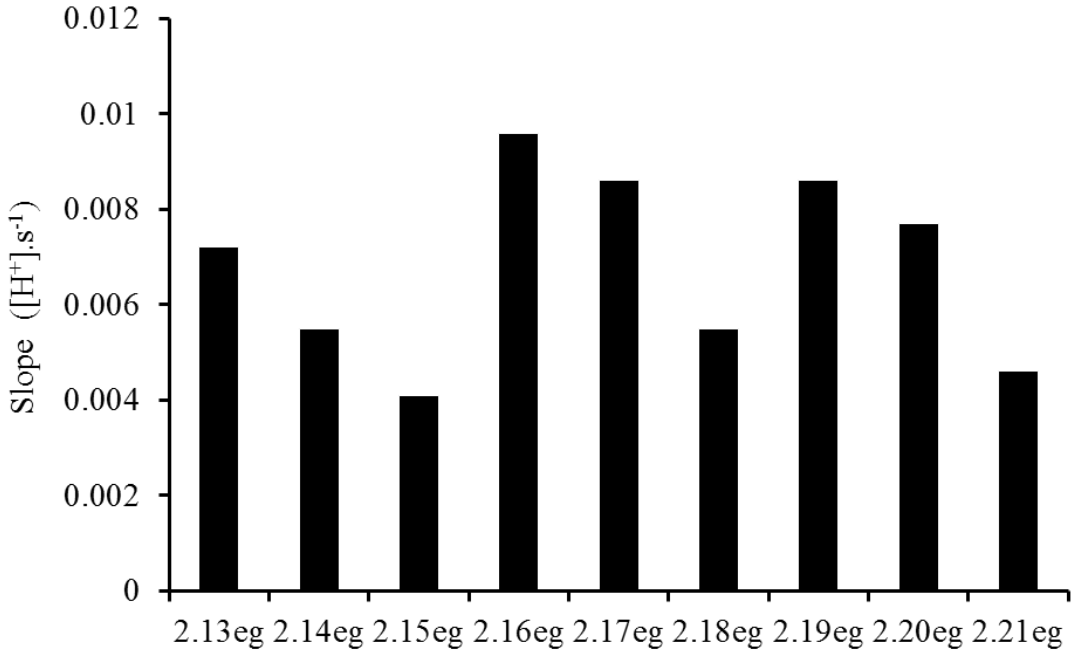

Figure 3.19. A plot to show the relationship between slope of the line from a semi-log plot of $[H^+]$ with times for the end group modified amine copolymers; P(DMAEMA-*co*-LMA) **2.13eg-2.15eg**, P(DEAEMA-*co*-LMA) **2.16eg-2.18eg**, P(MEMA-*co*-LMA) **2.19eg-2.21eg**.

It can be observed that as the amine incorporation decreases the rate of the reaction increases, which is in contrast to what would have been expected as these particles each possess the lowest amount of amine per assembly. Therefore, the rate determining step is believed to be independent of polymer nanostructure – acid droplet collisions. Furthermore, following the same trend as the end group modified homopolymers the difference between different amine functionalities is minimal.

As hypothesised, a rate limiting step that is slower than the reaction between the acidic proton and the amine base must be present in the neutralisation reaction. Moreover, the rate of the reaction is not dependent on the amount of base in each system, thus it can be deduced that particle-acid interactions are not the rate determining step. Finally, the logarithmic decay indicates that a single mean rate constant for the reaction does not exist and that multiple rate constants may be present and therefore a broad decay in acid neutralisation is observed, these assumptions are explored further in the following section.

3.3.4.4. Mechanism of ashless detergent neutralisation.

From the results in the previous section the data did not fit to a *pseudo* first order plot which would be expected for either mechanism shown in Figure 3.1. For either mechanism shown in Figure 3.1 the rate would be dependent on the detergent particles coming into contact with the acid droplet. Therefore it can be deduced that for these particles only one mean rate constant exists, which is the rate constant for the collision of an detergent particle and acid droplet.

However, the data for these ashless detergents fits best to a logarithmic decay over an order of magnitude of time. This logarithmic decay implies that a very broad distribution of rate constants exist for this system, specifically that a large range of energy barriers exist in the neutralisation process. This broad distribution of rate constants, displayed by a logarithmic decay, has been observed previously in glassy polymer domains and internal protein folding kinetics, which for this system cannot be related.[32,33] However, recently a logarithmic decay has been observed when the dynamics of polymeric micelle systems are studied in detail. In this work it was observed that the exchange of polymer chains between polymeric micelles to reach equilibrium follows a logarithmic decay.[34-37] This was studied by time resolved small angle neutron scattering (TR-SANS) experiments using two differently labelled polymers (See Chapter 1, section 1.4.1.3. for more details). [35-37] This logarithmic decay was a consequence of the polydispersity of the core forming block in these micelle systems, which results in a range of energy barrier to be overcome. For dynamic micelles, the energy barrier for molecular exchange is related to the interfacial tension, γ, of the core block and the solvent and the block length, N_b, given in the form (eqn. 1.7):[38]

Under ideal conditions a single energy barrier is present and thus an exponential decay (i.e. first order rate) is observed.[38] However, the dispersity of the core block leads to a range of energy barriers for the system and hence a much broader logarithmic decay is observed for the equilibration of the system.[37]

For these polymer systems it is believed that these polymers can indeed reach equilibrium and are therefore dynamic (an exchange of unimer chains between micelles) as shown in Chapter 2. This conclusion means that at steady state unimers are constantly in exchange between polymer micelles in the mineral oil. This dynamic behaviour produces what is believed to be a possible four step mechanism for the neutralisation of acid by these ashless detergents (Figure 3.20).

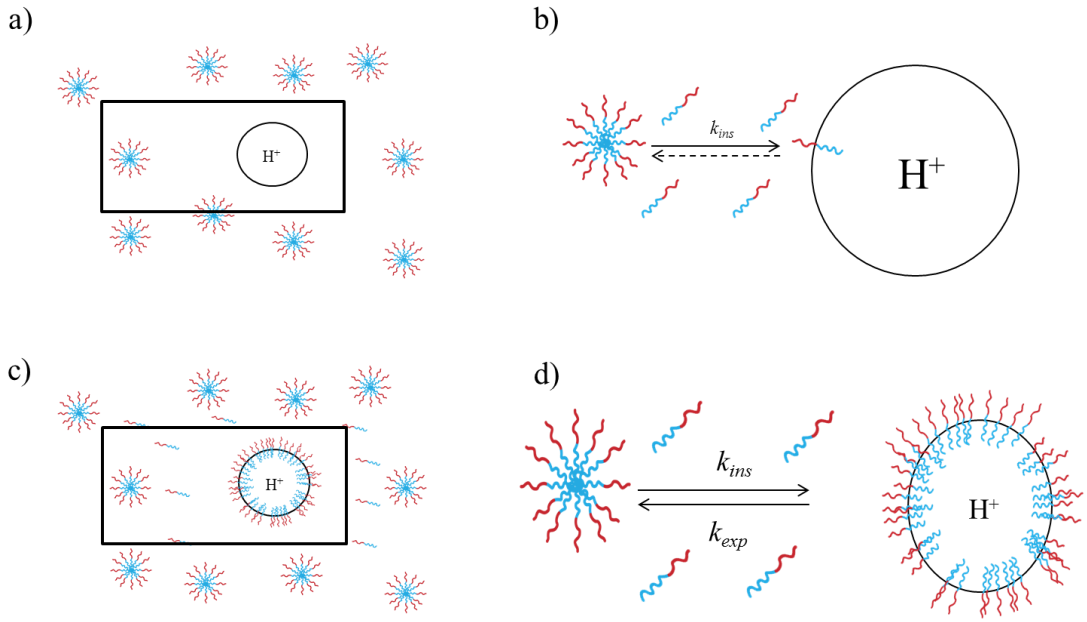

Figure 3.20 Mechanism of acid neutralisation from polyamine micelles in mineral oil. a) In mineral oil both self-assembled polymer micelles and acid droplet exist; b) initially polymer chains leave the polymer micelle and come into contact with the acid; c) surface saturation of the acid droplet by the polymer chains is reached; d) polymer chains exchange between local polymer micelles and the acid droplet.

In the first step of the possible mechanism (Figure 3.20a) self-assembled micelle structures and the acid droplet are present together in the mineral oil where the micelles are in excess in the solution. In the second step the dynamic micelles continually exchange chains between micelle structures but now begin to exchange with the acid droplet too (for simplicity only the black box region is expanded, Figure 3.20b). The dynamics of exchange of the polymer

system are expected to be very fast as the block lengths are very small and the solvent selectivity is assumed to be weak (see Chapter 2 for further details). Furthermore, the polymer micelles are in vast excess in the oil and therefore surface saturation of the acid droplet is expected to be reached almost instantly, and so no noticeable change can be detected by the rate testing set up at this point (Figure 3.20c). Once surface saturation is reached on the acid droplet the polymer chains will continue to exchange between the acid droplet and the polymer micelles in solution, therefore providing a constant reservoir of polymer chains to provide a base for neutralisation (for simplicity only the black box region is expanded, Figure 3.20d). In a similar manner to that previously seen, the exchange of polymer chains between the polymer micelles and acid droplet are dependent on the energy barrier given in equation 1.7. Therefore the dispersity of these polymers will lead to a broad range of rate constants for the exchange, and as this exchange is the rate determining step a logarithmic decay is observed for the neutralisation of acid by these polymeric materials.

Moreover, the neutralisation data in Figures 3.18 and 3.19 support this proposed mechanism further. The energy barrier for molecular exchange of the unimer chains, equation 1.7, the is related to the block length of the core forming block. As shown in Figure 3.18 as the block length increased the rate of neutralisation decreased, hence a larger core block means a higher energy barrier for unimer exchange and therefore more energy is required for the polymers to exchange leading to slower observed rates of neutralisation.

For the end group modified copolymers the block length is similar between systems but the rate does show a difference between different amine systems. However, this can be related to a difference in the interfacial tension,γ, between the amine cores and the mineral oil solvent, as the amine incorporation decreases the rate of the reaction increases. This can be related to a decrease in the interfacial tension and therefore a lower energy barrier is present and as such a fast exchange of unimers can occur and hence the rate of neutralisation was faster.

To explore this mechanism further a second model polymer system was designed and explored in the neutralisation process. Hence, a poly(lauryl methacrylate)$_{100}$-*block*-poly(4-vinyl pyridine)$_{40}$, PLMA-*b*-P4VP diblock copolymer was synthesised (see experimental for characterisation details). In the mineral oil it is expected that these polymers will self-assemble into spherical micelles given their amphiphilic nature where the PLMA forms the corona and the P4VP forms the micelle core. This polymer is believed to be frozen due to both a very high T_g of the core forming block (T_g (P4VP) = 141 °C)[39] and also having a very large energy barrier for molecular exchange, a consequence of a long core forming block and the high interfacial tension between the P4VP block and the mineral oil. Therefore it is hypothesised that these micelles do not dynamically exchange unimer chains in the mineral oil and a logarithmic decay should not be observed for the rate of acid neutralisation (Figure 3.21).

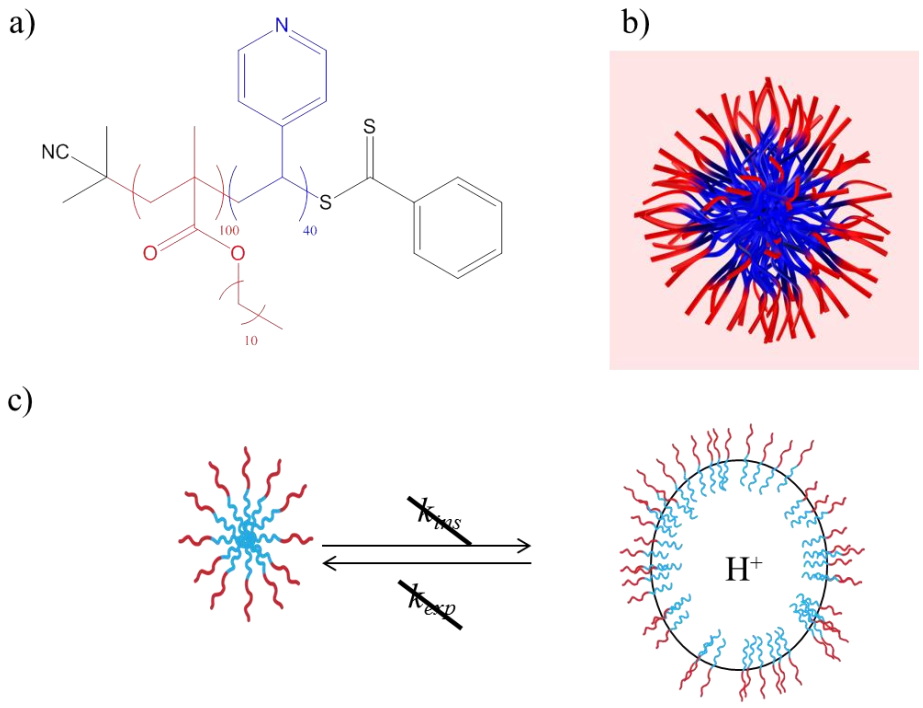

Figure 3.21. a) Schematic of the PLMA-*b*-P4VP diblock copolymer; b) schematic of the micelle structure formed by the PLMA-*b*-P4VP diblock copolymer; c) schematic of the frozen nature of these micelles highlighting no unimer exchange of polymer chains.

In support of the hypothesis the rate of acid neutralisation showed a very good fit to a *pseudo* first order reaction (R^2 = 0.9836), indicating that for these systems a single mean rate constant was present (see Figure 3.22). It can be assumed that for these frozen poly(lauryl methacrylate)$_{100}$-*block*-poly(4-vinyl pyridine)$_{40}$ diblock copolymers the mechanism of neutralisation is the same for those shown in Figure 3.1, that is the base particle must collide with the acid droplet.

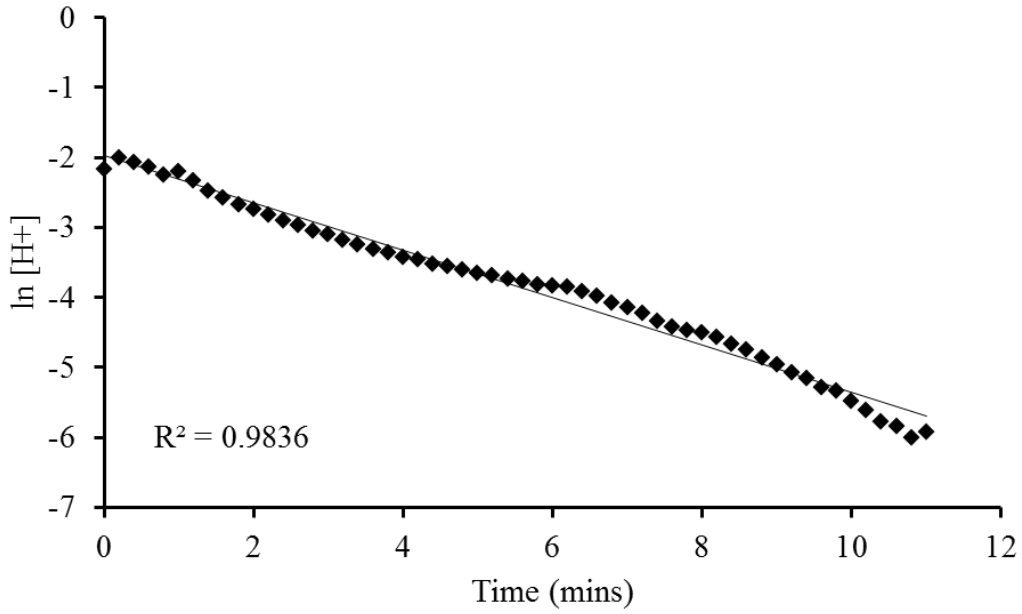

Figure 3.22. Pseudo first order kinetic plot of the neutralisation of H_2SO_4 by poly(lauryl methacrylate)$_{100}$-*block*-poly(4-vinyl pyridine)$_{40}$.

Furthermore, this frozen system does not show a logarithmic decay which supports the hypothesis that a unimer exchange mechanism is the predominant neutralisation mechanism for these polymer micelles.

3.4. Conclusions

A range of polymeric amines, both homopolymers and copolymers, were produced and their potential to act as novel ashless detergents in lubricant formulations was explored. These amine homopolymers and copolymers were then subsequently transformed using a simple post polymerisation Michael addition at room temperature which alters the RAFT end group. In non-polar solvents the amine homopolymers and copolymers spontaneously assembled into defined reverse micelle structures, where the amines aggregate to form the core. These structures were further explored with respect to their performance as ashless detergents in a hydrophobic oil environment. By using a range of techniques the acid dissociation constant (which indicates the strength of the base), total base number (which highlights the amount of base present) and the rate of acid neutralisation was explored. It was observed that the acid dissociation constant was largely governed by the discrete structures in solution and that producing nano-environments comprised of amine units an enhanced base strength was observed. From the TBN analysis it could be observed that all particles have a high amount of base present for acid neutralisation, nevertheless quantitative analysis was limited by the applicability of the established test for polymer systems. Finally, the rate of acid neutralisation was determined and was found to be extremely structure dependent and a unimer exchange process is the rate determining step for the neutralisation. All of the results in this Chapter indicate that the range of polymer micelles produced in Chapter 2 can act as ashless detergents within the mineral oil.

3.5. Acknowledgments

Dr Angela Breakspear and Dr Samir Chahine helped conduct the TBN analysis and rate of neutralisation experiments for these polymers and assisted with data analysis.

3.6. Experimental

3.6.1. Materials

Monomers were filtered through a plug of silica prior to use and stored at 4 °C in the dark. AIBN (2,2'-azo-bis(isobutyronitrile)) was recrystallised from methanol and stored in the dark at 4 °C. All mineral oils were used as received from BP Technology Centre in Pangbourne. All other materials were used as received from Aldrich, Fluka, and Acros. Dry solvents were used directly from a drying and degassing solvent tower delivery system. Polymers **2.10**-**2.21** and **2.01eg**-**2.21eg** were synthesised and assembled previously (see Chapter 2 for details).

3.6.2. Synthesis

3.6.2.1. Polymerisation of poly(lauryl methacrylate)

A solution of the lauryl methacrylate (120 eqv), AIBN (0.2 eqv) and 2-cyano-2-propyl dithiobenzoate (CPDB) (1 eqv) in 1,4-dioxane (1:1 volume to monomer) was added to a dry ampoule containing a stirrer bar. The solution was degassed using at least 3 freeze-pump-thaw cycles, back filled with nitrogen, sealed and placed in a pre-heated oil bath at 70 °C. After 6 h the polymerisation was quenched by liquid nitrogen, 1,4-dioxane removed *in* vacuo and the crude reaction was diluted with the minimum amount of dichloromethane (CH_2Cl_2) and the polymer was precipitated into cold methanol and isolated by filtration. Precipitation was repeated a further two times to afford a pink polymer. M_{nNMR} = 25.6 kDa, M_{nSEC}= 27.1 kDa, $Đ_{SEC}$= 1.12. δ (ppm) ^{1}H NMR (400 MHz, $CDCl_3$): δ (ppm) 7.85 (d, $^3J_{H\text{-}H}$ = 8.1 Hz, 1H Ar end group), 7.55 (t, $^3J_{H\text{-}H}$ = 7.4 Hz, 2H Ar end group), 7.41 (t, $^3J_{H\text{-}H}$ = 8.1 Hz, 2H Ar end group), 3.90 (br t, 2H, $OCH_2CH_2(CH_2)_9CH_3$), 1.94 (s, 6H, end group), 1.70 (br t, 2H, $OCH_2CH_2(CH_2)_9CH_3$), 1.20-1.30 (br t, 18H, $OCH_2CH_2(CH_2)_9CH_3$), 1.00-2.00 (br m, backbone) 0.80 (br t, 3H, $OCH_2(CH_2)_{10}CH_3$).

3.6.2.2. Chain extension of poly(lauryl methacrylate) with 4-vinyl pyridine.

A solution of the lauryl methacrylate (120 eqv), AIBN (0.2 eqv) and 4-vinyl pyridine (60 eqv) in 1,4-dioxane (1:1 volume to monomer) was added to a dry ampoule containing a stirrer bar. The solution was degassed using at least 3 freeze-pump-thaw cycles, back filled with nitrogen, sealed and placed in a pre-heated oil bath at 70 °C. After 6 h the polymerisation was quenched by liquid nitrogen, 1,4-dioxane removed *in* vacuo and the crude reaction was diluted with the minimum amount of dichloromethane (CH_2Cl_2) and the polymer was precipitated into cold methanol and isolated by filtration. Precipitation was repeated a further two times to afford a pink polymer. M_{nNMR} = 30.9 kDa, M_{nSEC}= 33.2 kDa, $Đ_{SEC}$= 1.16. ^{1}H NMR (400 MHz, $CDCl_3$): δ (ppm) 8.40 (br t, 4H, CH_2 $(CH_2)_2(CH_3)_2$ N), 7.85 (d, $^3J_{H\text{-}H}$ = 8.1 Hz, 1H Ar end group), 7.55 (t, $^3J_{H\text{-}H}$ = 7.4 Hz, 2H Ar end group), 7.41 (t, $^3J_{H\text{-}H}$ = 8.1 Hz, 2H Ar end group), 6.90 (br t, 4H, CH_2 $(CH_2)_2(CH_3)_2$ N), 3.90 (br t, 2H, $OCH_2CH_{2(}CH_2)_9CH_3$), 1.94 (s, 6H, end group), 1.70 (br t, 2H, $OCH_2CH_{2(}CH_2)_9CH_3$), 1.20-1.30 (br t, 18H, $OCH_2CH_{2(}CH_2)_9CH_3$), 1.00-2.00 (br m, backbone) 0.80 (br t, 3H, $OCH_{2(}CH_2)_{10}CH_3$).

3.6.3. Micelle preparation of the amine polymers in mineral oil.

Micelle solutions were prepared by adding mineral oil solvent to the dried polymer powder to a concentration of 1 wt% and were heated whilst stirring to 70 °C for 2 h and then allowed to cool to room temperature under ambient conditions prior to analysis.

3.6.4. Polymer characterisation

3.6.4.1. ^{1}H Nuclear Magnetic Resonance (NMR) spectroscopy

^{1}H NMR spectra were recorded on a Bruker DPX-400 spectrometer in $CDCl_3$. Chemical shifts are given in ppm downfield from TMS.

3.6.4.2. Size exclusion chromatography

Size exclusion chromatography (SEC) measurements were performed with chloroform ($CHCl_3$) with 2.5% volume of NEt_3 at 40 °C as an eluent at a flow rate of 1 mL/min, both on a set of two PLgel 5 μm Mixed-D columns. The molecular weights of the synthesised polymers were calculated relative to poly(styrene) (PS) standards from refractive index chromatograms.

3.6.4.3. Potentiometric titration

Potentiometric titration was performed at room temperature with an automatic titrator (Mettler Toledo G20) controlled by LabX software. 40 mL of solution was used for each potentiometric titration experiment. For the titrations in water the polymers were first dissolved at $\alpha = 1$ with 1.1 excess of 1 M HCl and then back-titrated with 0.1 M NaOH. For the titrations in acetonitrile the polymers were solubilised by direct dissolution.

For the titrations in water the addition of NaOH 0.1 M titrant was added at volume increments of 5-50 μL at 180 s intervals. For the titrations in acetonitrile the addition of glacial acetic acid titrant was added at volume increments of 0.5-5 μL and spaced with 180 s intervals. From the raw titration data the total amount of titrable amine units was calculated. Using equation 3.14 the potential of the acetonitrile solution can be related to the pH. Therefore, the change of pH could be plotted as a function of the degree of ionisation, α.

Table 3.1. Potentiometric titration data of **2.01-2.12** and **2.01eg-2.12eg** back titrated with NaOH in water and titrated with glacial acetic acid in acetonitrile.

Monomer	Polymer	M_n[a] (kDa)	pK_a[b] (aq)	pK_a[c] (MeCN)
DMAEMA	**2.01**	1.0	6	7.6
	2.01eg	1.2	7.4	7.9
	2.02	2.3	7.4	10
	2.02eg	2.5	7.6	10.3
	2.03	85	7.4	8
	2.03eg	85	7.5	8.3
DEAEMA	**2.04**	1.2	7.1	9.8
	2.04eg	1.4	7.7	10.5
	2.05	2.3	7.9	10.1
	2.05eg	2.5	8.7	11.2
	2.06	86	7.9	9.7
	2.06eg	86	7.9	10.2
MEMA	**2.07**	1.1	4.8	4.8
	2.07eg	1.3	5.1	5
	2.08	2.2	4.9	5.1
	2.08eg	2.4	5.1	6.5
	2.09	81.0	4.9	8
	2.09eg	81.0	4.9	8
PEMA	**2.10**	1.2	7.5	8.9
	2.10eg	1.4	7.4	9.2
	2.11	2.3	7.6	9.1
	2.11eg	2.5	7.4	9.3
	2.12	85.0	7.6	9.2
	2.12eg	85.0	7.6	9.5

[a]Determined by ^{1}H NMR spectroscopy. [b]Determined by potentiometric titration in water using NaOH as the titrant in water. [c]Determined by potentiometric titration in acetonitrile using glacial acetic acid as the titrant.

Table 3.2 Potentiometric titration data of **2.13-2.15** and **2.13eg-2.15eg** titrated with glacial acetic acid in acetonitrile.

Monomer	Polymer	mol% amine[a]	mol% LMA[a]	M_n[a] (kDa)	pK_a[b] (MeCN)
DMAEMA / LMA	**2.13**	25	75	3.5	8
	2.14	50	50	3.2	7.8
	2.15	75	25	4.2	7.6
	2.13eg	25	75	3.6	8.2
	2.14eg	50	50	3.5	8
	2.15eg	75	25	4.2	8
DEAEMA / LMA	**2.16**	25	75	2.1	8.9
	2.17	50	50	2.3	8.6
	2.18	75	25	2.3	8.1
	2.16eg	25	75	2.2	9.7
	2.17eg	50	50	2.3	9.4
	2.18eg	75	25	2.3	9.3
MEMA / LMA	**2.19**	25	75	3.2	5.2
	2.20	50	50	2.9	5.2
	2.21	75	25	3.3	5.1
	2.19eg	25	75	3.4	6.8
	2.20eg	50	50	3.1	6.8
	2.21eg	75	25	3.5	6.6

[a]Determined by ^{1}H NMR spectroscopy. [b]Determined by potentiometric titration in acetonitrile using glacial acetic acid as the titrant.

3.6.4.4. Total base number (TBN) analysis, ASTM-D2896.

Total base number analysis was undertaken following a modified ASTM-D2896 protocol. Here the polymers were solubilised in dimethyl sulfoxide (*DMSO*) instead of a chlorobenzene.

The polymers were titrated using an automated system with a solution of perchloric acid in glacial acetic, the potential of the solution is measured with respect to the addition of

perchloric acid and the end point is noted and the TBN can be calculated from equation (3.15)

3.6.4.5. Rate of acid neutralisation analysis by UV-Vis spectroscopy

The rate of neutralisation was undertaken with a specialised home built micro-neutralisation UV-Vis system at the BP Technology Centre in Pangbourne using a similar protocol as seen previously.[9] 250 μL of a 1 wt% amine polymer in mineral oil was added to a glass cuvette and heated to 70 °C, 0.6 μL of 0.1 M H_2SO_4 with methyl yellow is added to the cuvette at which point UV-Vis measurements are started, addition of the acid droplet indicates t = 0. UV-Vis measurements are taken at regular intervals over 30 minutes.

Table 3.5. Rate of neutralisation data of **2.01eg**-**2.12eg** by UV-Vis spectroscopy.

Polymer	Amine	M_n (kDa)[a]	Slope ($[H^+].s^{-1}$)[b]
2.01eg	DMAEMA	1.0	0.0155
2.02eg	DMAEMA	2.3	0.0077
2.03eg	DMAEMA	85.0	0.0007
2.04eg	DEAEMA	1.2	0.0149
2.05eg	DEAEMA	2.3	0.0072
2.06eg	DEAEMA	86.0	0.0009
2.07eg	MEMA	1.1	0.0146
2.08eg	MEMA	2.2	0.0069
2.09eg	MEMA	81.0	0.0007
2.10eg	PEMA	1.2	0.0143
2.11eg	PEMA	2.3	0.0086
2.12eg	PEMA	85.0	0.0008

[a]Determined by ^{1}H NMR spectroscopy. [b]Determined using a log fit to the raw neutralisation data from UV-Vis.

Table 3.6. Rate of neutralisation data of **2.13eg**-**2.21eg** by UV-Vis spectroscopy.

Polymer	mol% Amine [a]	mol% LMA [a]	M_n (kDa)[a]	Slope ($[H^+].s^{-1}$)[b]
2.13eg	25	75	2.6	0.0072
2.14eg	50	50	2.2	0.0055
2.15eg	75	25	2.3	0.0041
2.16eg	25	75	2.0	0.0096
2.17eg	50	50	2.1	0.0086
2.18eg	75	25	2.2	0.0055
2.19eg	25	75	2.9	0.0085
2.20eg	50	50	2.9	0.0077
2.21eg	75	25	3.0	0.0046

[a]Determined by ^{1}H NMR spectroscopy. [b]Determined using a log fit to the raw neutralisation data from UV-Vis.

3.7. References

(1) Rudnick, L. R. *Lubricant Additives: Chemistry and Applications*; CRC Press, 2003.
(2) Hudson, L.K.; Eastoe. J.; Dowding, P. J.; *Adv. Colloid Interface Sci*. **2006**, *123*, 425.
(3) Fu, J.; Lu, Y.; Campbell, C. B.; Papadopoulos, K. D.; *Ind. Eng. Chem. Res* **2006**, *45*, 5619.
(4) Galsworthy, J.; Hammond, S.; Hone, D. *Curr. Opin. Colloid Interface Sci.* **2000**, *5*, 274.
(5) Colyer, C. C., W.C. Gergel. *Chemistry and Technology of Lubricants*; New York: CH Publishers,, 1992.
(6) van Dam, W., Broderick, D., Freerks, R., Small, V. *SAE Technical Paper* **1997**, *972950*.
(7) Chen, Z. C.; Xiao, S.; Chen, F.; Chen, D. Z.; Fang, J. L.; Zhao, M. *J. Colloid Interface Sci*. **2011**, *359*, 56.
(8) Ahmed, S.N.; Nassar, A. M.; Abdel-Azim, A. *Inter. J. of Polym. Mat.* **2007**, *57*, 114.
(9) Hone, D. C.; Robinson, B. H.; Steytler, D. C.; Glyde, R. W.; Galsworthy, J. R. *Langmuir* **2000**, *16*, 340.
(10) Ulrich, S.; Laguecir, A.; Stoll, S. *J. Chem. Phys.* **2005**, *122*, 094911
(11) Mandel, M. *Eur. Polym. J.* **1970**, *6*, 807.
(12) Borukhov, I.; Andelman, D.; Borrega, R.; Cloitre, M.; Leibler, L.; Orland, H. *J. Phys. Chem. B* **2000**, *104*, 11027.
(13) Fritz, J. S. *Anal. Chem.* **1953**, *25*, 407.
(14) Colombani, O.; Lejeune, E.; Charbonneau, C.; Chassenieux, C.; Nicolai, T. *J. Phys. Chem. B* **2012**, *116*, 7560.
(15) Kocaoba, S.; Aydogan, F.; Afsar, H. *Rev. Anal. Chem.* **2008**, *27*, 123.
(16) Kutt, A.; Leito, I.; Kaljurand, I.; Soovali, L.; Vlasov, V. M.; Yagupolskii, L. M.; Koppel, I. A. *J. Org. Chem.* **2006**, *71*, 2829.
(17) Kaljurand, I.; Kütt, A.; Sooväli, L.; Rodima, T.; Mäemets, V.; Leito, I.; Koppel, I. A. *J. Org. Chem.* **2005**, *70*, 1019.
(18) Barbosa, J.; Sanznebot, V.; Torrero, E. *Talanta* **1991**, *38*, 425.
(19) Gundiiz, T.; Giindiiz, N.; Kill, E.; Koseoglu, F.; Oztas, S. G. *Analyst* **1988**, *113*, 715.
(20) Cotanda, P.; Wright, D. B.; Tyler, M.; O'Reilly, R. K. *J. Polym. Sci. A Polym. Chem.* **2013**, *51*, 3333.
(21) Dautzenberg, H. J., W.; Kötz, J.; Philipp, B.; Seidel, C.;Stscherbina, D. *Polyelectrolytes: Formation, Characterization and Application*; Hanser Publishers: Munich, Germany, 1994.
(22) Lee, H.; Son, S. H.; Sharma, R.; Won, Y. Y. *J. Phys. Chem. B* **2011**, *115*, 844.
(23) Colombani, O.; Ruppel, M.; Schubert, F.; Zettl, H.; Pergushov, D. V.; Müller, A. H. E. *Macromolecules* **2007**, *40*, 4338.
(24) Jusufi, A.; Likos, C. N.; Lowen, H. *J. Chem. Phys.* **2002**, *116*, 11011.
(25) Plamper, F. A.; Becker, H.; Lanzendörfer, M.; Patel, M.; Wittemann, A.; Ballauff, M.; Müller, A. H. E. *Macromol. Chem. Phys.* **2005**, *206*, 1813.
(26) Mehler, E. L.; Fuxreiter, M.; Simon, I.; Garcia-Moreno E, B. *Proteins.* **2002**, *48*, 283.
(27) Spruell, J. M.; Levy, B. A.; Sutherland, A.; Dichtel, W. R.; Cheng, J. Y.; Stoddart, J. F.; Nelson, A. *J. Polym. Sci. A Polym. Chem.* **2009**, *47*, 346.
(28) (ASTM) *Standard test method for base number of petroleum products by potentiometric perchloric acid titration*; ASTM International: West Conshohocken, PA, 2011.
(29) Štěpánek, M.; Procházka, K.; Brown, W. *Langmuir* **2000**, *16*, 2502.
(30) Manning, G. S. *J. Phys. Chem.* **1981**, *85*, 870.

(31) de Groot, J.; Koper, G. J. M.; Borkovec, M.; de Bleijser, J. *Macromolecules* **1998**, *31*, 4182.
(32) Tsiok, O. B.; Brazhkin, V. V.; Lyapin, A. G.; Khvostantsev, L. G. *Phys. Rev. Lett.* **1998**, *80*, 999.
(33) Skorobogatiy, M.; Guo, H.; Zuckermann, M. *J. Chem. Phys.* **1998**, *109*, 2528.
(34) Lund, R.; Willner, L.; Richter, D.; Dormidontova, E. E. *Macromolecules* **2006**, *39*, 4566.
(35) Lu, J.; Bates, F. S.; Lodge, T. P. *ACS Macro Lett.* **2013**, *2*, 451.
(36) Lu, J.; Choi, S.; Bates, F. S.; Lodge, T. P. *ACS Macro Lett.* **2012**, *1*, 982.
(37) Choi, S.; Lodge, T. P.; Bates, F. S. *Phys. Rev. Lett.* **2010**, *104*, 047802.
(38) Halperin, A.; Alexander, S. *Macromolecules* **1989**, *22*, 2403.
(39) Kuo, S.-W.; Wu, C.; Chang, F.-C. *Macromolecules* **2004**, *37*, 192.

4. Tuning the aggregation behaviour of pH responsive polymers by copolymerisation

4.1. Abstract

Amphiphilic diblock copolymers, poly(2-(diethylamino)ethyl methacrylate–*co*–2-(dimethylamino)ethyl methacrylate)–*block*–poly(2-(dimethylamino)ethyl methacrylate, P(DEAEMA-*co*-DMAEMA)-*b*-PDMAEMA with various amounts of DEAEMA have been synthesised by RAFT polymerisation. In water their micelle formation has been investigated by scattering measurements over a wide pH range. It appeared that the polymers self-assembled into pH sensitive star like micelles. For a given composition, when the pH is varied the extent of polymer aggregation can be adjusted reversibly over orders of magnitude. When the copolymer composition in the hydrophobic block was varied, the onset and extent of aggregation was shifted with respect to pH. This class of diblock copolymers, with a copolymer associating block offers the possibility to select the range of stimuli-responsiveness that is useful for a given application, which can rarely be achieved with conventional diblock copolymers consisting of homopolymer blocks.

4.2. Introduction

In a selective solvent, and above a critical aggregation concentration (CAC), amphiphilic block copolymers aggregate by the association of the solvophobic blocks into micellar cores, surrounded by a corona made of the solvated solvophilic blocks, which can minimise the enthalpic costs of the contact between solvent and solvophobic monomer.[1-3]

It has been shown both theoretically and experimentally that the physical natures of both the solvophobic and solvophilic blocks influence the aggregation and the equilibrium behaviour of such polymer micelles. Longer core solvophobic blocks cause increased aggregation numbers, because of the decreased head group area which alters the packing parameter, and slower exchange kinetics.[4,5] Slower exchange kinetics occur as a consequence of increased chain entanglements, increased friction between chains and a larger energy barrier for exchange.[6-8] Longer solvophilic corona blocks give decreased aggregation numbers since the relative area of the head group becomes larger which modifies the core-solvent interactions and packing parameters.[9] Chemically the influence on aggregation is much more varied but in general increasing the solvophobicity of the core forming block through monomer chemistry will cause an increase in the aggregation number from the increased surface energy of the micelle core which is reduced by aggregation, and a reduction in the exchange kinetics at equilibrium,[10,11] resulting from a higher interfacial tension between the solvophobic block and the solvent, which causes a higher energy barrier for unimer exchange. [12-14]

The extensive literature on block copolymer micelles in the literature has focused on pure homopolymeric blocks, however, as mentioned the self-assembly behaviour is relative to the associating block and as such these homopolymeric blocks severely restrict said behaviour. Despite the relative success of these homopolymeric diblocks the predominant limitation is that for each application a new polymer should be synthesised.

It should be noted that homopolymeric amphiphilic block copolymers will often form "frozen" out of equilibrium structures and rarely show true enthalpy governed assembly with dynamic behaviour and critical micelles concentrations (CMCs) like surfactant micelles.[14,15] These "frozen" structures are largely a result of two factors; the first is a glass transition temperature (T_g) above experimental conditions; which will restrict core block mobility and prevent coalescence of particles,[3,16,17] the second is due to large solvophobicity of the core forming block or large block length, producing a large activation energy barrier for molecular exchange regardless of T_g.[7,18,19] Consequently the structures formed by "frozen" micelles are largely dependent on the dispersion of the polymer and show little or an irreversible response to external stimuli.[16,20,21]

A promising new strategy has been proposed to circumvent these problems, by simply copolymerising the solvophilic monomer into the solvophobic block, a moderately solvophobic block can be formed. Throughout the literature it is known that stimuli responsive monomers can be copolymerised with non-responsive or differently responsive monomers to produce a broad range of behaviours.[22] For example, statistical copolymers of pH sensitive and inert monomers exhibited an ionisation behaviour dependent on the non-responsive monomer content.[23,24] Lutz *et al* showed that lower critical solubility temperature (LCST) values could also be selectively targeted by controlling the statistical copolymer composition.[25,26]

Given the exciting possibilities of these new systems only a few reports exist where a stimuli responsive copolymer block forms the solvophobic block(s) of the polymer. Moreover these reports study polymers which all contain permanently hydrophobic units present, e.g. styrene and butyl (meth)acrylate, within the moderately solvophobic copolymer block.[27-36] Nevertheless these reports show that the moderately solvophobic copolymer block can vastly change the properties of the self-assembled micelles. By varying the copolymer composition in the core forming block the effective solvophobicity is changed and accordingly the free

energy of the micelle system also changes. These parameters are key in the behaviour of self-assembled structures. Moreover, unlike thermodynamically frozen micelles the aggregation and dynamics of self-assembly for this new class of diblock copolymer could be controlled by stimuli, in these cases pH.[27,28,30-32] Therefore by introducing responsive units into the associating block the effective solvophobicity is reduced and these copolymer diblock polymers can overcome the kinetic restraints and form structures that are under thermodynamic control, offering improved behaviour over conventional amphiphilic homopolymeric blocks as equilibrium structures are reproduced irrespective of assembly pathway. For example Lejuene *et al* synthesised a poly(*n*-butyl acrylate-*co*-acrylic acid)-*block*-poly(acrylic acid), P(*n*BA-*co*-AA)-*b*-PAA, diblock copolymer and analysed the structures by SANS using different pathways for assembly (Figure 4.1).[27,34]

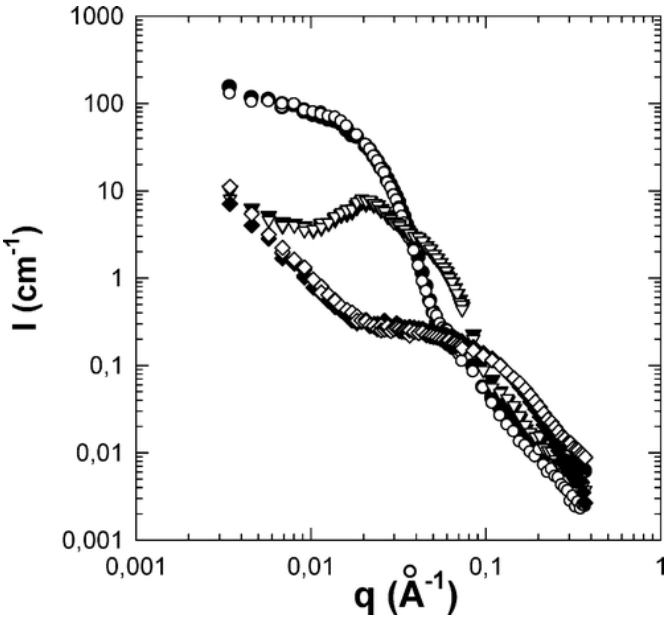

Figure 4.1. SANS curves for P(*n*BA-*co*-AA)-*b*-PAA diblock copolymer at 20 g/L in the presence of 0.3 M NaCl and at α = 0.1 (Direct dissolution ●, lowered from α = 0.5 ○), α = 0.5 (raised from α = 0.3 ▼, lowered from α = 0.9 ▽), α = 0.9 (raised from α = 0.1 brought to 0.9 in 3 steps ◇, raised from α = 0.1 brought to 0.9 in 2 steps ◆).[32] Note: regardless of pathway when α is targeted the structures are identical.

PDEAEMA, poly(diethylaminoethyl)methacrylate containing diblock copolymers are widely used as pH responsive diblock copolymers in aqueous media, as a consequence of the increase in hydrophobicity upon deprotonation. Gast and co-workers studied poly(dimethylaminoethyl)methacrylate-*block*-poly(diethylaminoethyl)methacrylate, PDMAEMA-*b*-PDEAEMA, polymers in depth using an array of assembly methods and have shown that these polymers form spherical micelles in aqueous solution depending on the degree of ionisation of the polymer.[37,38] Analysis of DEAEMA diblock copolymers by stop flow techniques concluded that the polymers micellise *via* a two-step fusion/fission mechanism which is incredibly similar to the formation of frozen micelles.[39-41] Adams and co-workers have also used different pathway preparation techniques to show that different structures can be formed depending on the pathway used for Poly(ethylene oxide) – block – poly(diethylaminoethyl)methacrylate, PEO-*b*-PDEAMA, diblock copolymer (Figure 4.2).[42] Although the results regarding pH responsive micelles with a DEAEMA core suggest that they form out of equilibrium structures the dynamics of the system are still unknown.

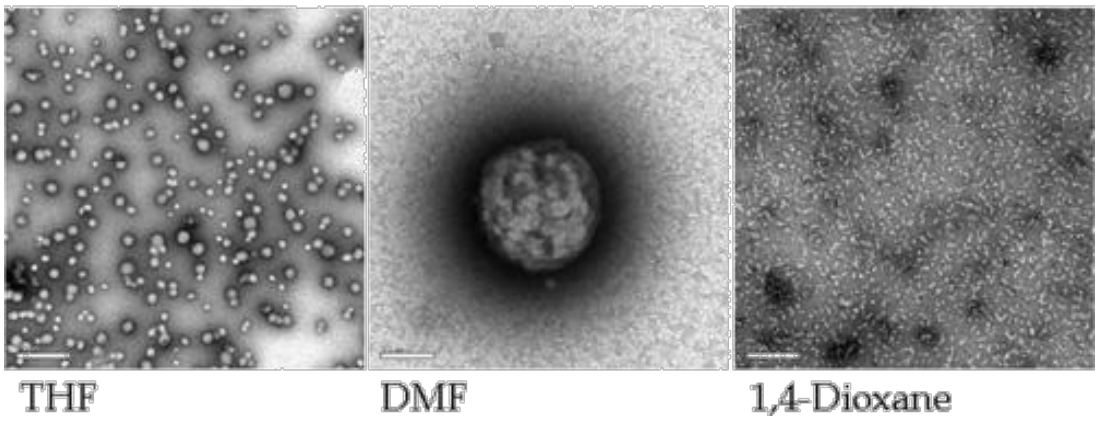

Figure 4.2. TEM images of PEO-*b*-PDEAMA diblock copolymer prepared by quenching a solution in an organic solvent with pH 12 water. The scale bar is 200 nm.[42]

Therefore, in this chapter the introduction of solvophilic units into the solvophobic blocks is discussed in particular for a series of P(DEAEMA-*co*-DMAEMA)-*b*-PDMAEMA diblock copolymer with a moderately responsive PDEAEMA containing block. Thus it is predicted

that the pH region where the polymer micelles exist can be shifted with respect to the relative copolymer composition of the associative block. Furthermore the extent of aggregation can be tuned over larger orders of magnitude by slight variations in stimulus, owing to the high pH sensitivity of the core. Given the responsive nature of this proposed system it is necessary to distinguish the difference between reversibility from stimuli and dynamic exchange at equilibrium. Although the dynamics of systems with a PDEAEMA core block is unknown, observations show that the aggregation number and structure can vary with ionisation. It cannot be concluded that different ionisation values gave frozen or dynamic micelles, as the system could indeed be frozen at both ionisations but dynamic at an intermediate value. On the other hand the small changes seen in the micelle structure over a range of changes in stimuli one could assume that the system has reorganised within the given range, but it might be uncertain if this change is reversible.[14]

By synthesising a series of polymers with varying degrees of responsive monomer present, it is possible to understand and quantify the nature of a moderately responsive block. To truly understand the effect of moderating the responsive block, the core block length must be kept constant. As mentioned before the physical properties of the polymer blocks can have great implications on self-assembly. For that reason, the synthesis of the polymers must be controlled to allow for similar block lengths and to minimise the energy barrier difference between different polymers.[18,43] Additionally, the need for a polymerisation technique to afford copolymers of controlled length and tolerance to functional groups was desired. In order to achieve this, reversible addition fragmentation chain transfer, RAFT, polymerisation was selected for polymer synthesis in this Chapter.[44,45]

The objective of this work was to develop a new system with responsive units to modify the nature of the solvophobic block in polymer micelles. To both tune the aggregation and the equilibrium behaviour of polymeric micelles in aqueous media, which produces a larger scope for polymeric micelles applications. To understand the polymeric micelle morphology

and dynamics with respect to ionisation dynamic light scattering (DLS), static light scattering (SLS), small angle X-ray scattering (SAXS) and cryogenic transmission electron microscopy (cryo-TEM), were to be used

4.3. Results and Discussion

4.3.1. Synthesis and Molecular Characterisation of P(DEAEMA-*co*-DMAEMA)-*b*-PDMAEMA diblock copolymers

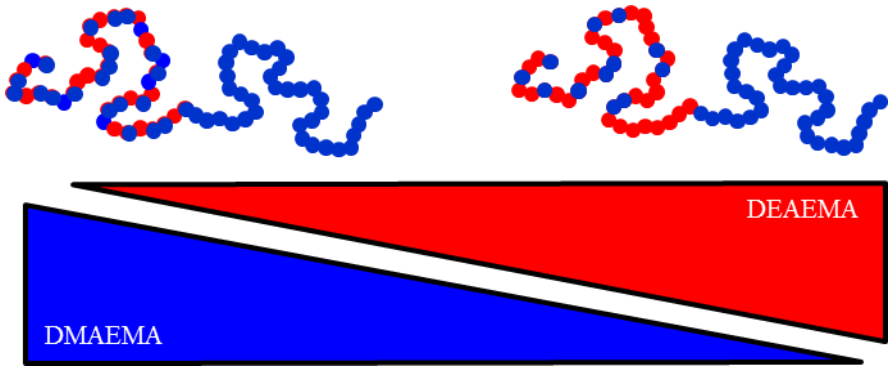

Figure 4.3. Diagram representing how the composition of the core block was varying by changing the ratios of DEAEMA and DMAEMA.

4.3.1.1. Synthesis of P(DEAEMA-co-DMAEMA)-b-PDMAEMA diblock copolymers by RAFT polymerisation

The P(DEAEMA-*co*-DMAEMA)-*b*-PDMAEMA diblock copolymers were synthesised in two steps. First, various copolymer PDEAEMA-*co*-PDMAEMA macroCTAs were synthesised with equal block lengths by RAFT polymerisation using various ratios of DMAEMA and DEAEMA, AIBN as a radical initiator, 1,4-dioxane as the solvent at 70 °C and 2-cyano-2-propyl benzodithioate (CPDB) as the CTA (Scheme 4.1). After 7 h of reaction the polymerisation reactions were quenched in liquid nitrogen, dialysed against nanopure water and the products isolated by lyophilisation.

Scheme 4.1. Copolymerisation of DMAEMA and DEAEMA and chain extension with DMAEMA by RAFT polymerisation.

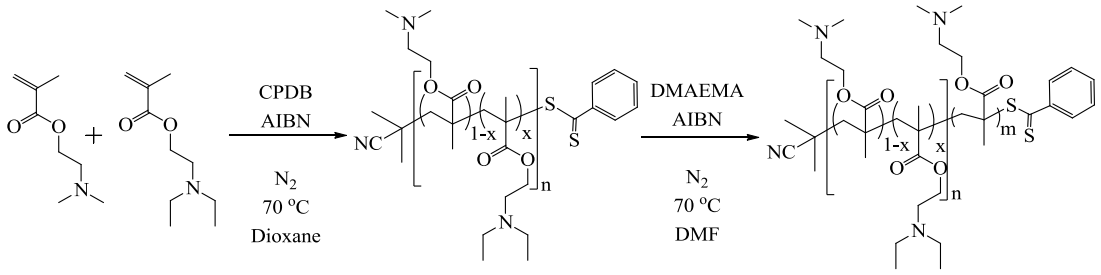

To confirm the composition of the copolymer macroCTAs, reactivity ratios were calculated using a method developed by van Herk.[46] Both F_1 (mol fraction in the copolymer) and f_1 (mol fraction in monomer feed) values were used to determine the reactivity ratio of the monomers for the macroCTAs. The values for r_1 and r_2 were as follows; DMAEMA/DEAEMA r_1= 1.140, r_2=0.824 r_1r_2 = 0.939 (Figure 4.4).[47] This shows a near ideal copolymerisation, it can be deduced that there is no block or gradient like nature for this copolymer. The responsive monomer, DEAEMA, is evenly distributed throughout the block, RAFT polymerisation allows for the living chains to grow simultaneously to one another and as such the assumption is that all chains will have the same microstructure.[48]

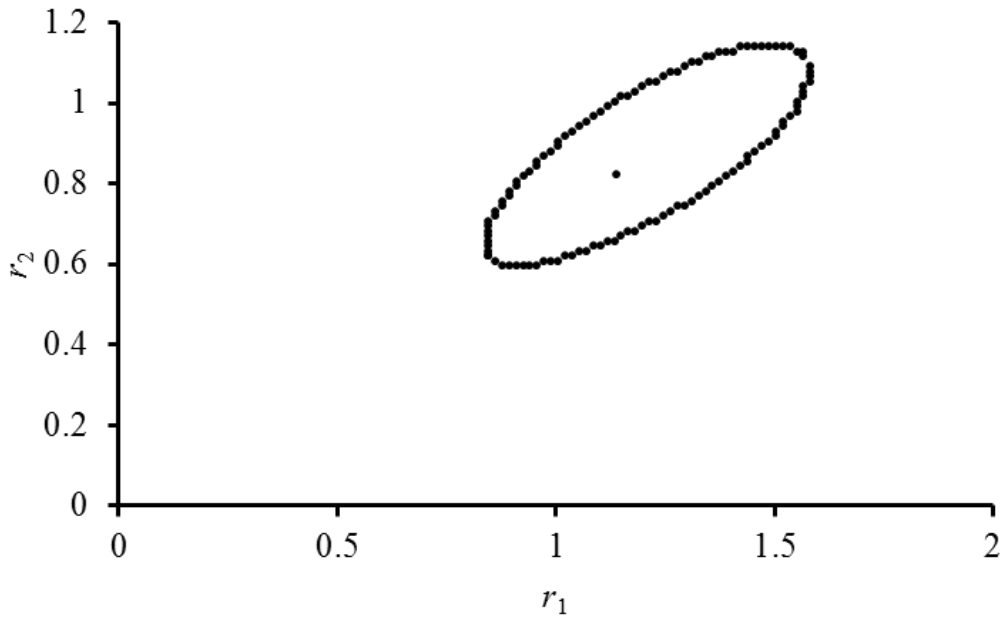

Figure 4.4. 95% joint confidence intervals of the r_1 and r_2 values for the DMAEMA/DEAEMA copolymerisation

All polymers were subsequently chain extended with DMAEMA, Scheme 4.1, which gave diblock copolymers with a controlled incorporation of responsive monomer, known molecular weights and low dispersity ($Đ < 1.2$). Similar blocks lengths (30-35) were synthesised for all polymers, Table 4.1.

Table 4.1. Molecular characteristics of the P(DEAEMA-*co*-DMAEMA)-*b*-PDMAEMA diblock copolymers**.**

Diblock Copolymer	**x**[a]	**n**[b]	**m**[b]	$M_{n,NMR}$[b] **(kDa)**	$M_{n,SEC}$ **(kDa)**	$Đ_{,SEC}$[c]	d***n***/d***C***[c] **(mL/g)**
4.1	0.32	35	30	10.7	13.8	1.16	0.125
4.2	0.65	36	35	12.3	14.2	1.12	0.122
4.3	0.76	25	34	10.0	12.8	1.18	0.127
4.4	0.91	28	32	10.4	13.5	1.10	0.127

[a] Determined by ^{1}H NMR spectroscopy using the signals at 4.20 ppm and 2.10 ppm.[b] Determined by end-group analysis from ^{1}H NMR spectroscopy. [c] From SEC based on poly(methyl methacrylate) standards.[d] By differential refractometry.

4.3.1.2. Ionisation behaviour

For diblock copolyelectrolytes it has been concluded that ionisation behaviour is different to that of simple homopolyelectrolytes.[29] Moreover for the system studied here both monomers in both blocks can be ionised. Therefore we explored how the microstructure of the diblock copolymers altered their ionisation behaviour *via* potentiometric titration experiments.

Knowing the molecular weight and DP of the diblock copolymers, the moles of ionisable units in solution can be calculated. All of the polymers were soluble in pure water with a 1.1 stoichiometric excess of HCl 1M to ionisable units. Subsequently these solutions (approximately 2.4×10^{-4} M) were back titrated with NaOH 0.1 M. This allows for the evolution of ionisation degree, α, with respect to pH to be observed. We define α as the

degree of ionisation following equation (4.1) and the equilibrium that exists between the ionisable groups in solution and the acidic protons (4.2).

$$\alpha = \frac{[NR_2H^+Cl^-]}{[NR_{2_{total}}]} \qquad (4.1)$$

For complete protonation of amine units, α = 1 and for complete deprotonation of amine units, α = 0.

$$NR_2H^+Cl^- \leftrightarrow HCl + NR_2 \qquad (4.2)$$

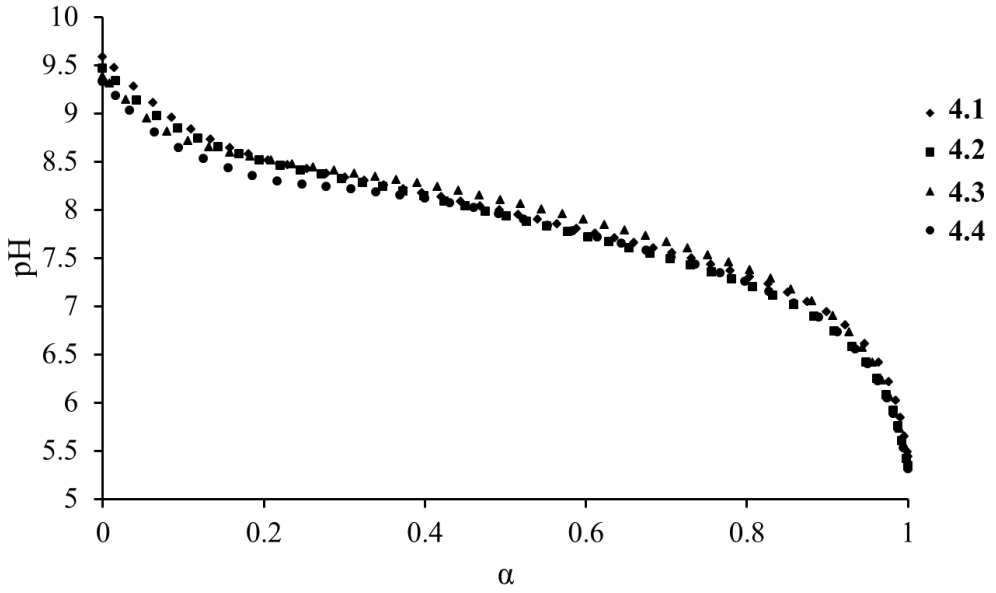

Figure 4.5. Evolution of ionisation degree α, with pH for the diblock copolymers, **4.1** - **4.4**.

On inspection of the evolution of α with pH for each diblock copolymer (Figure 4.5, **4.1** to **4.4**) one can observe the ionisation behaviour of each system. Interestingly for all polymers herein regardless of the amine location on the chain, core or coronal forming blocks, all amines can become ionised and subsequently deionised. Nonetheless, at low ionisation values it was observed that deprotonation of the amines is more difficult as it requires a higher pH. Considering the amphiphilic nature of the polymer at low ionisation values this observation can be ascribed to the presence of star shaped micelles at low ionisation values,[49] which will condense greater amounts of counter ions to decrease the associated free energy

cost of repulsive charges.[50] The condensation of counter ions causes the Debye length in this region to increase and causes a screening of the charges on the repeat units, impeding the subsequent deprotonation of the adjacent units.[51]

However, although the ease of protonation varies with pH it should be noted that the overall acidity does not vastly change between systems although the copolymer composition does (Figure 4.6). It can be concluded that the relationship of composition to ionisation is relatively weak for this series of diblock copolymers despite being structurally very different to homopolyelectrolytes.

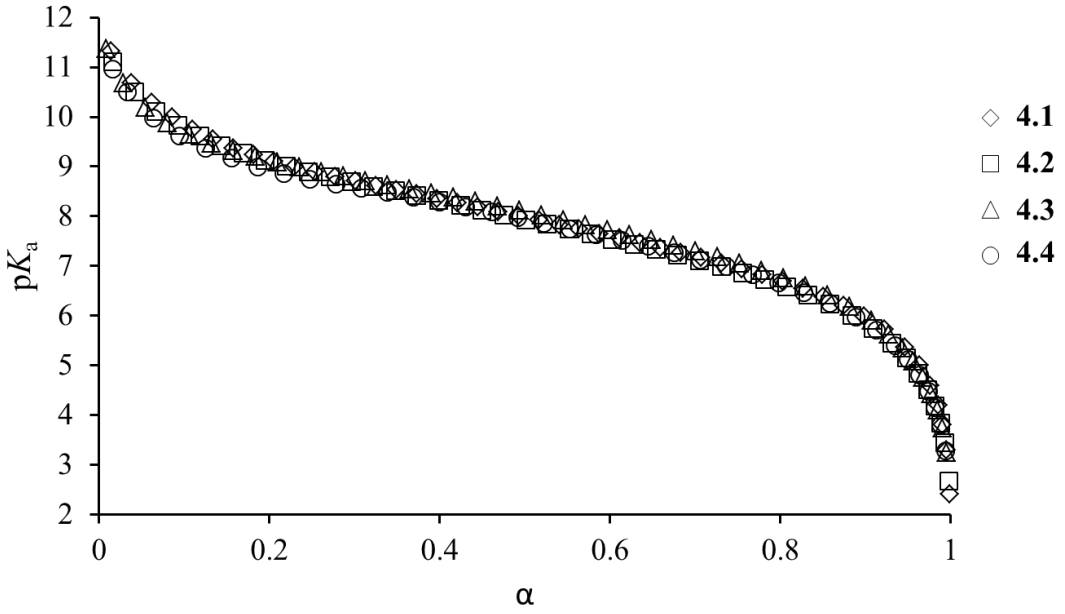

Figure 4.6. Evolution of ionisation degree α, with apparent pK_a for the diblock copolymers, **4.1** - **4.4**.

4.3.2. Aqueous Solution Properties

4.3.2.1. Pathway dependence on the self-assembly

As mentioned in the introduction, although a system may reorganise after a perturbation to the system this does not necessarily conclude that the change is reversible or that the system is at thermodynamic equilibrium. In a previous report by Jacquin[52] with poly(*n*-butyl

acrylate)-*block*-poly(acrylic acid) diblock copolymers respectively, demonstrated that morphology changes arose when then ionisation of the polyelectrolyte was varied, however, the changes in the morphology of the aggregates was irreversible, indicating that the system is indeed still frozen. Consequently if non-reversible pH-sensitive behaviour is observed then it can be deduced that the aggregates in solution are indeed out-of-equilibrium "frozen" structures. These structures would have characteristics and properties on both the nano and macro scale that are strongly dependent on the method of dispersion.[4,20]

Therefore it is highly important to understand if the perturbation by pH on the system is reversible, and also if the influence of composition influences this behaviour further. To analyse if the reorganisation of the system with pH is reversible two pathways of pH change were used and the structures analysed by LLS. Figure 4.7 shows the two pathways for understanding the reversibility (see the experimental section for details of sample preparation). Briefly, the pathways consist of reaching a target ionisation either from raising the ionisation by subsequent protonation of the system (pathway B) or by lowering the ionisation by incremental deprotonation by base additions (pathway A). All the experiments for these reversibility tests were done at 2.5 g/L and are thus apparent N_{agg} values were calculated.

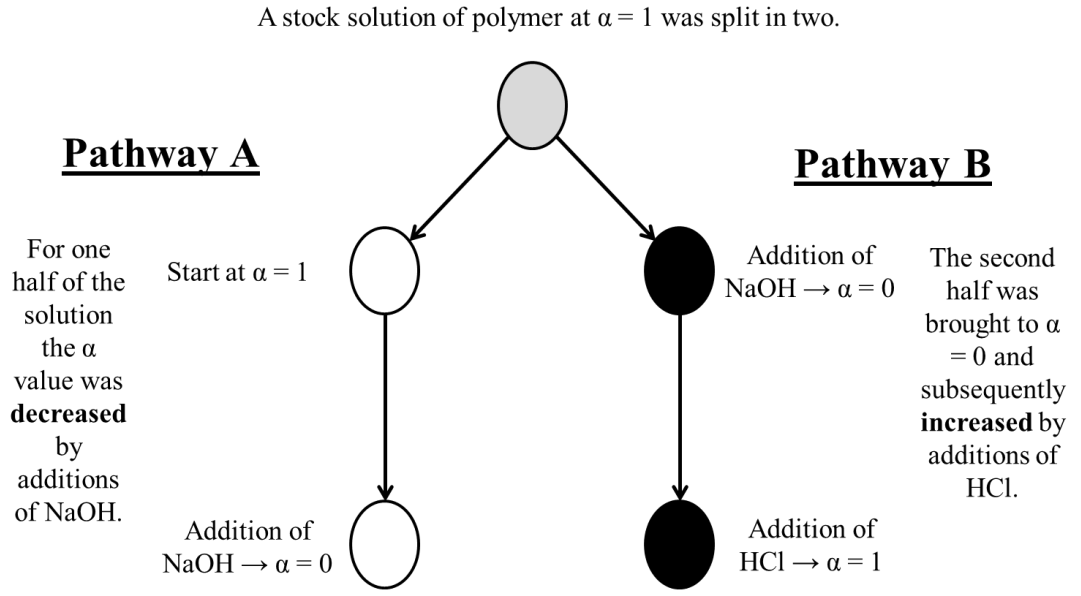

Figure 4.7. Schematic showing the two pathways (A and B) used for the reversibility testing.

As can be seen in Figure 4.8, regardless of pathway for the aggregates the N_{agg} for the aggregates varies with both ionisation and copolymer composition. It can be observed that for some ionisation values the two pathways do not lead to identical structures, this is highlighted strongly for polymer **4.4**, but the both structures are very similar from either pathway. This similarity between structures regardless of pathway shows that the pH induced perturbation is reversible and moreover the system appears to be under thermodynamic control. This thermodynamic control renders these polymers highly interesting for different applications as no pathway dependence exists.

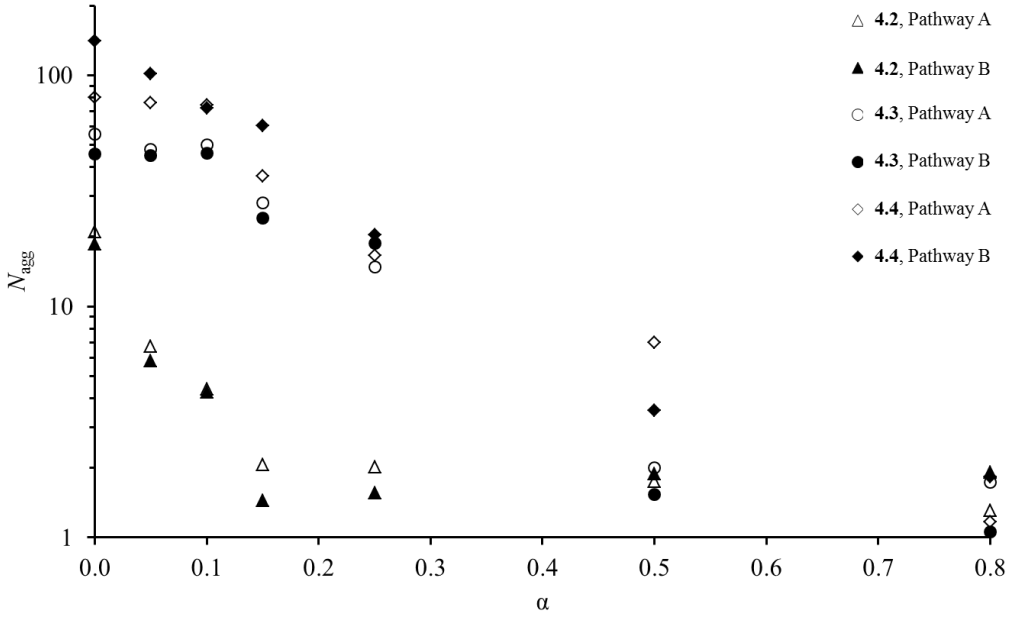

Figure 4.8. Evolution of N_{agg} with increasing (pathway B) or decreasing (pathway A) the ionisation for **4.2**, **4.3** and **4.4** at 2.5 g/L 0.1 M NaCl solution.

This reversible behaviour and thermodynamic control for all of the diblock copolymers suggests that the aggregates are dynamic in nature. Therefore it is proposed that the hydrophobic blocks can escape the micelle core, diffuse through the solvent and re-enter a new micelle until the thermodynamically preferred structure is obtained. However, further studies using rheology,[28] time-resolved SANS[6,11] or fluorescence[53,54] would be needed to probe quantitatively the dynamics of the unimer exchange mechanism but it can be concluded, however, that the system is dynamic and no preparation pathway dependence exists.

It should be noted that in these studies the salt concentration (NaCl) was adjusted after α was reached. However, it was also explored how the polymer would disperse and how the structures would change when the polymers were assembled in the presence of salt, 0.1 M NaCl, whilst reaching the targeted α value (Figure 4.9).

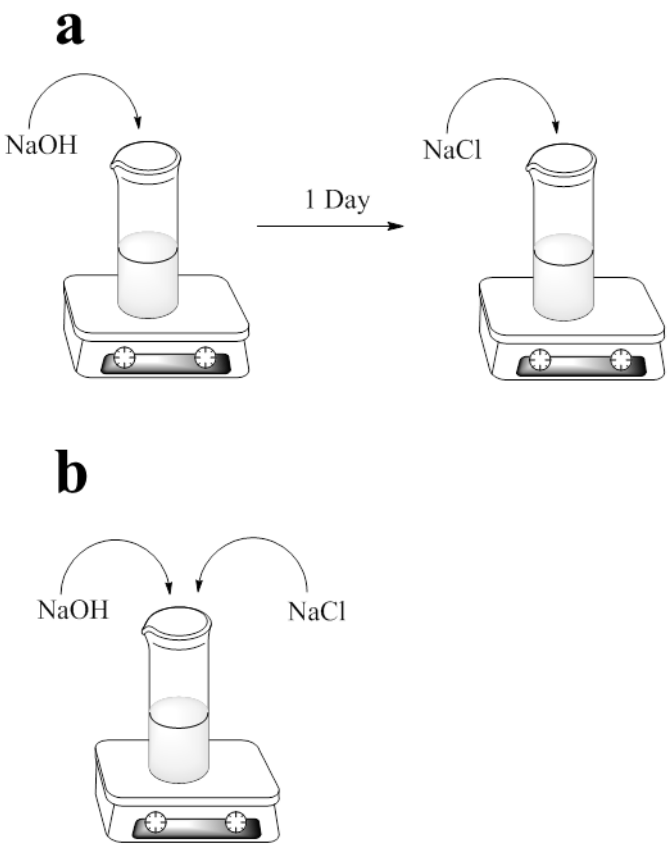

Figure 4.9. Diagram to represent the two pathways to understand the influence of salt. a) Salt added after α was reached. b) salt added whilst α was reached.

From Table 4.2 it is noted that although the size of the micelle aggregates are very similar within experimental error, the N_{agg} values obtained for the addition of salt during self-assembly are much larger in comparison to the addition of salt after self-assembly, up to 3 times larger. It was initially believed that the presence of salt slows down the kinetics of exchange and thus longer times are needed for the polymer micelles to reach equilibrium and as such larger disperse structures are observed, Figure 4.10.

Table 4.2. Characteristics of **4.2** and **4.3** at α = 0 and with salt added during or after assembly.

Polymer	N_{agg} salt after	R_h salt after (nm)	N_{agg} salt during	R_h salt during (nm)
4.2	21	9.5	82	12.3
4.3	46	10.5	143	15.3

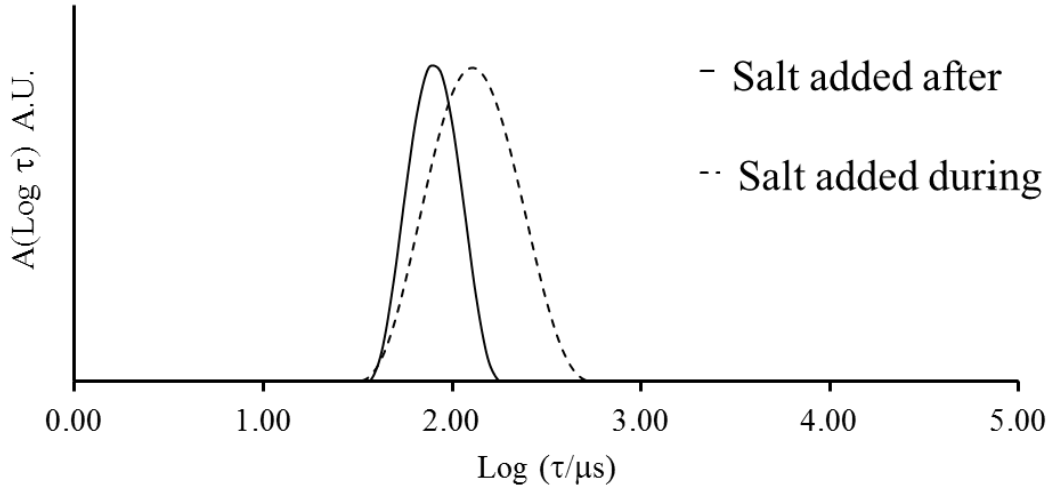

Figure 4.10. Relaxation time distributions for **4.3** at α = 0 with salt added after or during assembly.

However, after extended periods of time (approximately 2 months) no significant change was observed from the initial N_{agg} value (both values are within 10%). It can be deduced that in the presence of salt long lasting metastable aggregates are formed, similar to results observed by Colombani *et al* for poly(*n*-butyl acrylate)-*block*-poly(acrylic acid), P*n*Ba-*b*-PAA, diblock copolymers.[9] These metastable states are produced due to the poor dispersion of the polymer chains in the presence of salt. The solvation of the polyelectrolyte chains is largely due to the entropic gain upon the dissociation of counter ions into the solution. However, when salt is present in solution this entropic gain is thus reduced or even

prevented, causing large stable aggregates to remain in solution. Therefore for all further experiments the salt concentration was adjusted after the targeted α value was reached.

4.3.2.2. Influence of DEAEMA incorporation

For the following section all polymers were prepared by firstly completely protonating the sample and then subsequently deprotonating the sample, thus lowering α from 1 to 0 through addition of 1 M NaOH. Although the system shows no pathway dependence, the same sample pathway using method 1 was used for all samples.

For some of the polymer systems, typically at high α when the scattering of the polymer aggregates is relatively low, relaxation distributions from DLS showed two modes of relaxation. The first mode is the polymer of interest and the second mode can be attributed to spurious aggregates with a negligible weight fraction but larger scattering intensity.[55-57] The intensity auto correlation function, $g_2(t)$, was analysed using an inverse Laplace transformation (REPES) assuming a continuous distribution of relaxation times.[58] Therefore with REPES multiple modes of relaxation can be examined. By taking the concentration of the fast mode to be that of the concentration of the solution detailed light scattering analysis on solely the fast mode can be obtained (Figure 4.11).

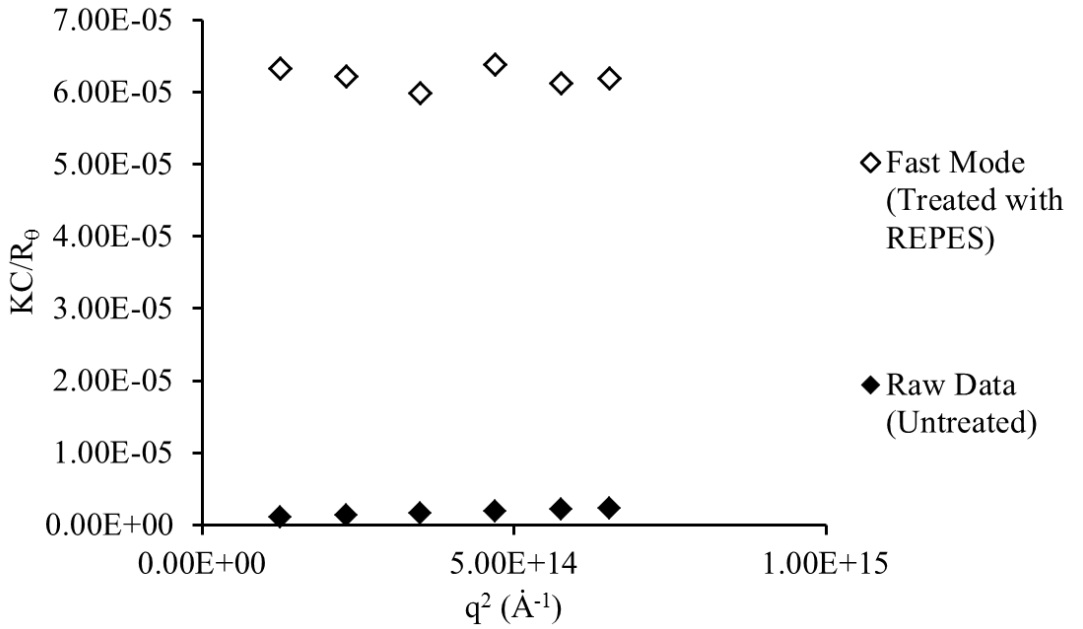

Figure 4.11. Plot of KC/R_θ vs q^2 for treated and raw data for polymer **4.3** at 10 g/L, $\alpha = 0.8$ in 0.1 M NaCl.

To investigate the influence of DEAEMA in the core forming block on the solution self-assembly behaviour a range of solutions for each DEAEMA content were prepared to specific α values, and the solution properties were analysed. Figures 4.12 a and b represent respectively the evolution of the aggregation number and the hydrodynamic radius of the polymers with the ionisation degree as measured by static and dynamic light scattering. For the polymer with the lowest DEAEMA incorporation, polymer **4.1**, regardless of ionisation there is no observed significant change in the R_h and N_{agg}. Furthermore for this polymer system N_{agg} is *ca* 1 within experimental error for all α values studied; because of this the values of R_h can then act as a reference for single unimer chains in solution as at all other compositions the block lengths are similar.

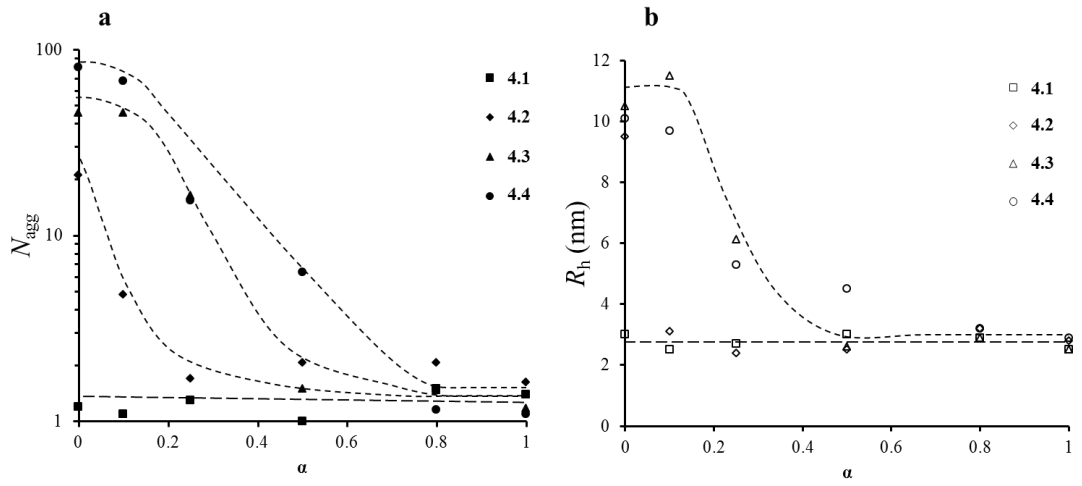

Figure 4.12. a) Evolutions of N_{agg} with α for polymers **4.1**, **4.2**, **4.3** and **4.4**. b) Evolutions of R_h with α for polymers **4.1, 4.2, 4.3** and **4.4**. Lines are to serve as guides.

On the other hand, all other polymers **4.2 - 4.4** show that when ionisation is varied both R_h and N_{agg} change significantly. Notably, large changes in the behaviour were observed although there are only subtle differences in the composition of the core forming block. What is most prominent is that the onset of aggregation with respect to ionisation is dependent on the DEAEMA content, explicitly as the DEAEMA content is increased the onset of aggregation is shifted to higher α values.

Polymer **4.2** only self assembles once the degree of ionisation is less than 0.1 and this polymer does not show an upper limit for its aggregation in the ionisation regime studied herein. Similarly this behaviour is exhibited with both **4.3** and **4.4**, again when the DEAEMA content is increased the onset of aggregation is increased, as the aggregation of **4.4** starts below α = 0.8, whereas α must be lower than 0.5 for aggregation of polymer **4.3**. However, in contrast to **4.2**, **4.3** and **4.4** both present a plateau and upper limit to their aggregation which is observed when ionisation is less than 0.1.

From the potentiometric studies and understanding the Henderson–Hasselbalch equation, 3.8, the variation of structure with respect to pH can then be plotted and observed. It was

observed that a wide pH regime exists (pH 7 – 10) where the aggregation of the polymers can be precisely controlled (Figure 4.11). Furthermore these polymers exhibit highly pH-sensitive aggregation as large changes in aggregation are produced from slight changes in pH and in turn ionisation degree, α. These diblock copolymers with a statistical associating block offer great benefits over conventional diblock copolymers as the pH sensitive structures can be elegantly controlled by small variations in core block composition.

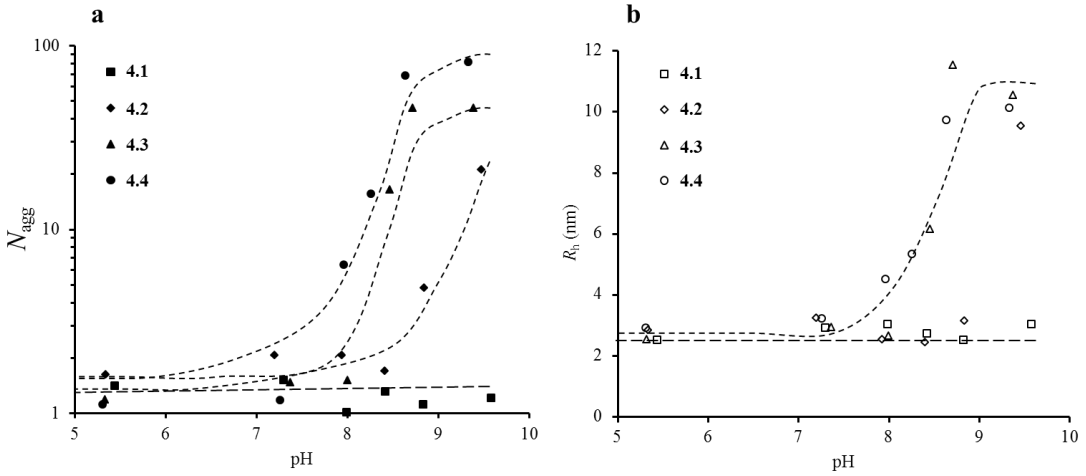

Fig. 4.13. a) Evolutions of N_{agg} with pH for polymers **4.1**, **4.2**, **4.3** and **4.4**. b) Evolutions of R_h with pH for polymers **4.1**, **4.2**, **4.3** and **4.4**. Lines are included as a guide for the reader.

DLS measurements of the solutions at 2.5 g/L showed a gradual shift in the distribution of relaxation times for the fast mode versus ionisation after a critical ionisation degree is reached (Figure 4.14a example is for **4.3**). This is attributed to the aggregation of the polymer chains in star like micelles where P(DMAEMA-*co*-DEAEMA) forms the core. Additionally the dispersity of the fast mode of relaxation does not increase but remains constant or drops which is indicative of the closed micelle association mechanism.[59] On the other hand the gradual increase in the relaxation time for the fast mode is related to an open association mechanism.[55] From analysis of the distribution of relaxation times for the

polymers at $\alpha = 0$ for different concentrations we can begin to understand the mechanism further.

From the relaxation distributions of the fast mode it is evident that an increase in concentration gave a decrease in the dispersity of the polymeric micelles for all polymers examined, example shown is for **4.3**, Figure 4.14b. This is strong evidence of a closed association of micelle formation. The higher dispersity value is a consequence of free unimer chains in solution in equilibrium with the micelles, as the concentration increases the contribution of scattering intensity of these free chains diminishes and thus the dispersity decreases. This phenomenon is much weaker at higher DEAEMA incorporations. Hence this behaviour is a consequence of a lower critical aggregation concentration (CAC) due to the increase in hydrophobicity. The decrease in CAC would produce fewer free unimer chains in solution and as such the dispersity of the distribution shows little change with concentration.

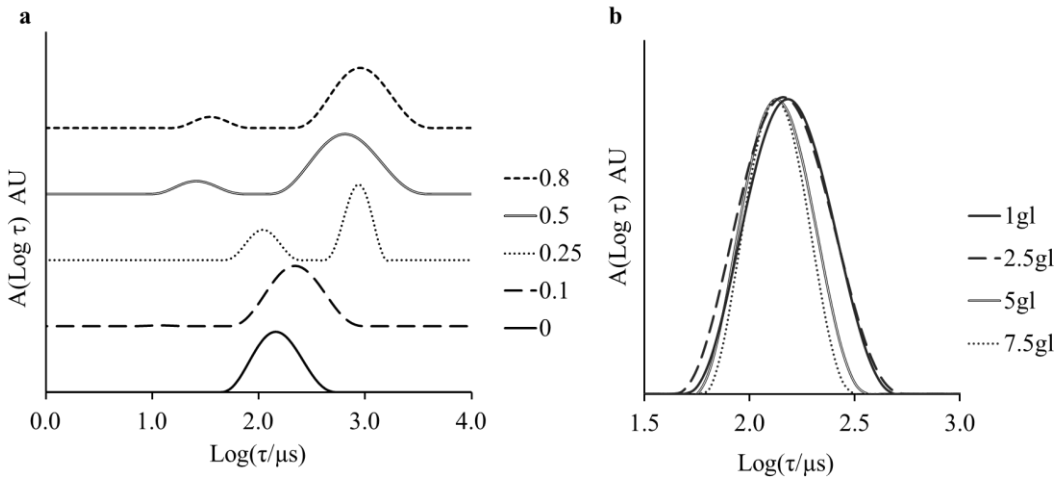

Figure 4.14. a) Intensity weighted distribution of relaxation times for **4.3** at 2.5 g/L in a 0.1M NaCl solution with varying the ionisation, $\alpha = 0 – 0.8$, measured at $\theta = 130°$. b) Effect of concentration on the intensity weighted distribution of relaxation times for **4.3**, measured at $\theta = 130°$, $\alpha = 0$.

Although the α-sensitive aggregation behaviour may appear expected where an increase in hydrophobic DEAEMA content increased aggregation, aggregation of polymer chains into defined nanostructures is a result of both kinetic and thermodynamic factors, and

consequently many polymers will not follow such aggregation trends. For this diblock copolymer system the aggregation is driven by the balance between two opposing factors. The first is an increase in charges along the polymer backbone, these charges which gives increased hydrophilicity to the polymer and also cause solvation of the core. The second effect is that as the DEAEMA incorporation is reduced the effective hydrophobicity of the polymer is reduced. This in turn leads to a lower α value being needed for the polymers to aggregate. The subtle balance between these factors allows a wide range of structures to be easily accessed over a precise pH range.

From the structure of the polymer and the N_{agg} and R_h values obtained, it is reasonable to expect that the polymers will aggregate forming a spherical core-shell micelle morphology.[60,61] From knowledge of micelle geometry and understanding that the copolymer would block would form the micelle core and the DMAEMA homopolymer block would form the corona the use of theoretical models (see experimental for model details) can be used. Consequently, structural characteristics can be calculated and therefore it can be deduced that these polymers do indeed form star like micelles, involving a dense core composed of the copolymer block surrounded by a partially extended corona formed by the homopolymer DMAEMA (see Tables 4.3 – 4.5).

The first polymer system investigated was **4.1**, here the DEAEMA content is the lowest, 32%. As observed from LLS this polymer did not assemble at any α values investigated. Therefore the core-corona micelle model could not be applied to this system as the polymer remained as unimers. (table 4.3)

Table 4.3. Characteristics of **4.1** with varying ionisation.

α	M_w [a] (kg.mol^{-1}) ± 10%	N_{agg} [a] ± 10%	R_h [b] (nm) ± 10%
0	13	1.2	3.0
0.1	12	1.1	2.5
0.25	13	1.3	2.7
0.5	12	1	3.0
0.8	13	1.5	2.9
1	13	1.4	2.5

[a] Determined by SLS, M_w is the weight-average molecular weight of the scatterers. [b] Determined from DLS.

The second polymer system was **4.2**, here the DEAEMA content is 65% in the core forming block. For this polymer system the polymers do aggregate to form micelles but only at α = 0. From the core-coronal model it can be observed that polymers form a start like micelle and the coronal chains are mildly stretched, 64% as a result of the densely packed chains.

Table 4.4. Characteristics of 4.2 with varying ionisation.

α	M_w (kg.mol^{-1}) [a] ± 10%	N_{agg} [a] ± 10%	R_h [b] (nm) ± 10%	R_c [c] (nm)	*Corona Stretching* (%)[d]
0	256	21	9.5	3.9	64
0.1	58	5	3.1	[e]	[e]
0.25	21	2	2.4	[e]	[e]
0.5	25	2	2.5	[e]	[e]
0.8	25	2	3.2	[e]	[e]
1	20	2	2.8	[e]	[e]

[a] From SLS, M_w is the weight-average molecular weight of the scatterers. [b] Determined from DLS. [c] Calculated from equation 7 assuming a core density of 1. [d] (R_{hDLS}-R_{cSLS})/$L_{contour}$,DMAEMA. [e]For polymers above α = 0 the model of "core-corona" is no longer applicable.

The third system was **4.3** where the DEAEMA content is 76%. For this system additional SAXS analysis was also undertaken and the results corroborated with LLS. For this system the polymers assemble below α = 0.25 and the characteristics fit well to a star like micelle. It can be observed that as the ionisation degree is lowered the micelles core expands and the coronal chains become more stretched, a result of increased chain density.

Table 4.5. Characteristics of **4.3** with varying ionisation.

α	M_w (kg.mol^{-1}) [a] ± 10%	N_{agg} [a] ± 10%	R_h [b] (nm) ± 10%	R_g [c] (nm)	R_c [c] (nm)	R_c [f] (nm)	*Corona Stretching* (%)[g]
0	556	46	10.5	8.5[d]	4.9	4.6	70
0.1	556	46	11.5	-	-	4.6	81
0.25	200	16	6.1	7.5[d]	5.3	3.2	34
0.5	18	1	2.6	-	-	[h]	[h]
0.8	18	1	2.9	3.7[e]	-	[h]	[h]
1	14	1	2.5	3.5[e]	-	[h]	[h]

[a] From SLS, M_w is the weight-average molecular weight of the scatterers. [b] Determined from DLS. [c] From SAXS at a concentrations of 2.5 gL^{-1} using method1. [d] Determined with the Guinier-Porod model. [e] Determined with the Debye model. [f] Calculated from equation 7 assuming a core density of 1. [g] $(R_{hDLS}-R_{cSLS})/L_{contour,DMAEMA}$. [h]For polymers above α = 0.25 the model of "core-corona" is no longer applicable.

The final system was **4.4**, this system has the highest DEAEMA content, 91% in the core forming block. Similar to **4.3** this polymer only assembles into star like micelles for α < 0.25. However, for this system larger core sizes were calculated, a result of an increased aggregation number and thus more polymers form the densely packed core for these micelles. Furthermore the chain stretching of this system is lower than that of **4.3** which indicates that the space occupied by each coronal chain is less and thus less stretching is needed to balance the enthalpy. It can also be observed that the N_{agg} and R_h for α = 0.5 is larger than unimers, although the star like micelle does not fit well here it is believed that this is a small aggregate but not a well-defined structure.

Table 4.6. Characteristics of **4.4** with varying ionisation.

α	M_w (kg.mol^{-1}) [a] ± 10%	N_{agg} [a] ± 10%	R_h [b] (nm) ± 10%	R_c [c] (nm)	*Corona Stretching* (%)[d]
0	1086	80	10.1	5.6	56
0.1	915	68	9.7	5.3	55
0.25	209	15	5.3	3.2	26
0.5	86	6	4.5	[e]	[e]
0.8	16	1	3.2	[e]	[e]
1	16	1	2.9	[e]	[e]

[a] From SLS, M_w is the weight-average molecular weight of the scatterers. [b] Determined from DLS. [c] Calculated from equation 7 assuming a core density of 1. [d] (R_{hDLS}-R_{cSLS})/$L_{contour}$,DMAEMA. [e]For polymers above α = 0.25 the model of "core-corona" is no longer applicable.

Polymers **4.2** - **4.4** all assemble into star like micelles and further corroboration of this model with cryo-TEM and SAXS confirm the presence of star like polymer micelles. Cryo-TEM images, Figure 4.15, reveal that the micelles confirm the assembly into star like micelles. The cryo-TEM images do have slightly larger cores than that from SLS analysis but this believed to be due to the poor contrast from the core and corona and consequently part of the coronal chains near the core-corona interface are also observed. SAXs analysis allows structures to be examined on smaller length scales; therefore we can compare directly theoretical models obtained from LLS with those directly examined from SAXS.

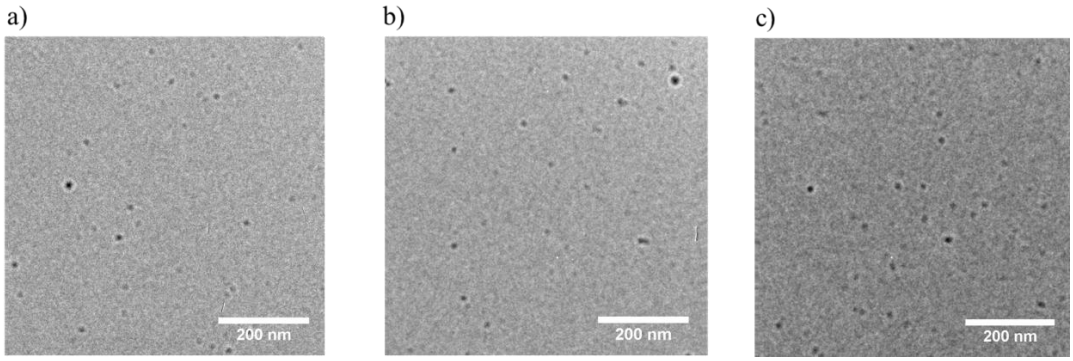

Figure 4.15. Cryo-TEM images at α = 0, 2 g/L and in 0.1 M NaCl solution. a) **4.2**, b) **4.3**, c) **4.4**. Scale bar 200nm.

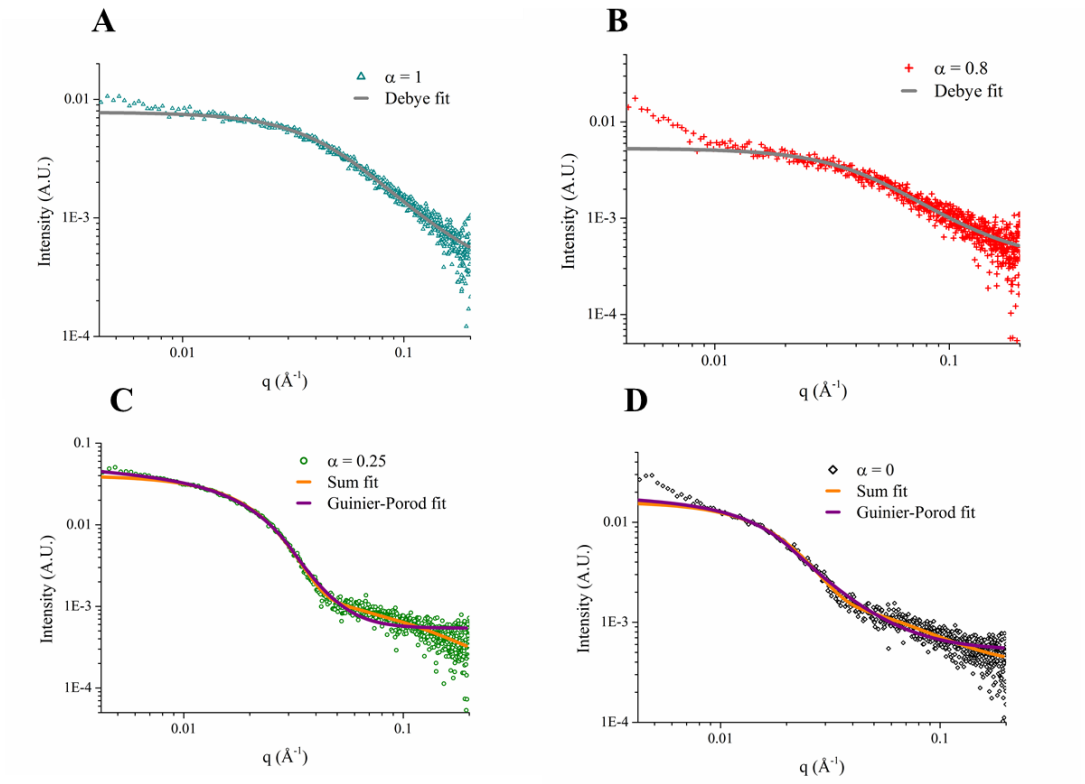

Figure 4.16. Small-angle X-ray scattering (SAXS) profiles of **4.3** with varying α. A) α = 1, B) α = 0.8, C) α = 0.25, D) α = 0, all at 2.5 g/L and in 0.1 M NaCl solution.

SAXS analysis can deduce that identical trends are observed to those found from LLS (Figure 4.16). That is, an increase in α causes the micelles to begin to disassemble and consequently transition to a solution of free unimers in solution. The shape of the SAXS

profile is related to the morphology of the aggregate in solution, furthermore the slope of the curve as q→0 is related to the R_g of the aggregate. As the ionisation is increased it can be observed that the slope of the curves greatly reduces, indicating a decrease in the size of the aggregate. The change in the shape of the curve is indicates a change of the particle form factor which confirms the progressive disassembly of the micelles upon an increase in ionisation. Nevertheless SAXS does indicate a larger core size when compared to LLS, Table 4.5. This core difference is believed to be attributed to the small contrast difference between the core and corona for SAXS in comparison to LLS; due to similar chemical composition and small differences in scattering length density (SLD). Consequently it is understood that the crowded corona at the core-corona interface is partially observed.[62]

Polymers **4.1** - **4.4** all have quasi identical block lengths, and therefore when $\alpha = 0$ the N_{agg} and R_h values can be depicted as a function of DEAEMA content. Here only the polymers that self-assembled, **4.2** - **4.4**, were plotted and the influence of DEAEMA content was further examined. It is clear that the aggregation number varies significantly with DEAEMA content whereas the R_h values do not. Specifically N_{agg} can vary up to 4 times whereas the R_h values vary less than 1 nm between DEAEMA incorporation (Figure 4.17).

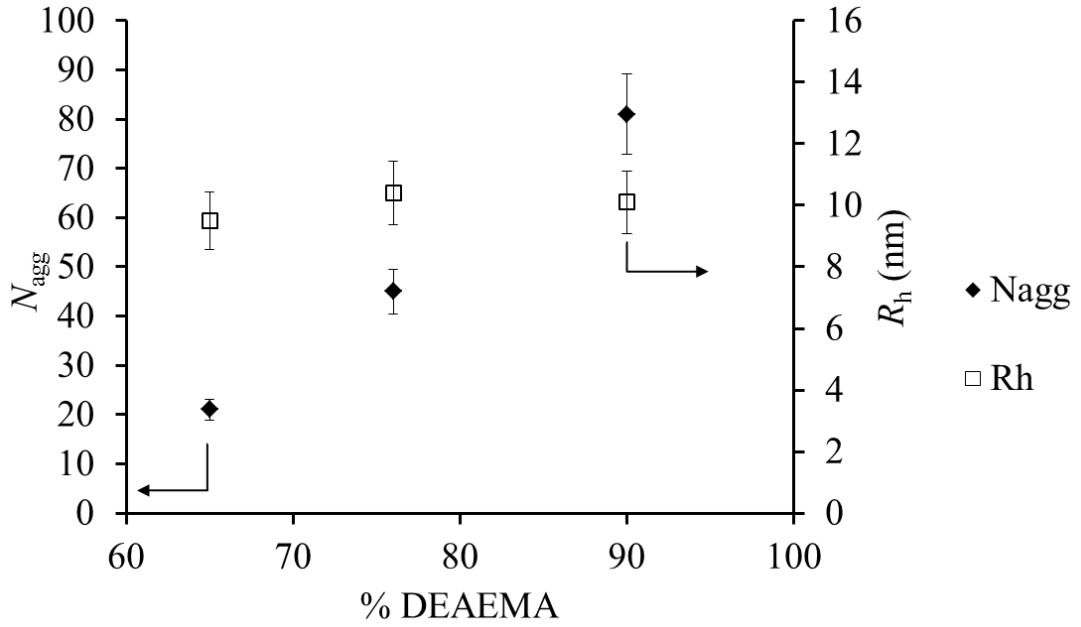

Figure 4.17. Effect of the DEAEMA loading on the N_{agg} and R_h for polymers **4.2**, **4.3** and **4.4** at $\alpha = 0$. Error bars represent 10% error for both N_{agg} and R_h.

This behaviour highlights the strong relationship of core character on the aggregates formed on the nanoscale in solution. Slight adjustments and tuning of the associating block by incorporation of solvophilic units can have a pronounced change on the final aggregate formed in solution, despite being similar in size. For applications of self-assembled nanostructures such as catalysis[63-65] and nanomedicine,[63,66,67] the ability to significantly change performance of the aggregate but to maintain precise control of structure is of great importance and therefore these novel copolymer associating blocks offer a unique new protocol for this structural control.

4.4. Conclusions

A series of P(DEAEMA-*co*-DMAEMA)-*b*-PDMAEMA diblock copolymers have been synthesised with varying degrees of DEAEMA in the core block. In aqueous media, below a given ionisation degree, the polymers self-assemble into pH sensitive star like micelles, similar to the behaviour to the analogous PDEAEMA-*b*-PDMAEMA diblock copolymer. However, contrary to what was observed for the analogous diblock, the pH region of aggregation for these P(DEAEMA-*co*-DMAEMA)-*b*-PDMAEMA diblock copolymers can be shifted by modifying the composition of the statistical hydrophobic block. The apparent aggregation number was shown to change reversibly for the micelles irrespective of the preparation pathway, which indicates that there is reorganisation of the system and that the system is under thermodynamic control. Furthermore the aggregation number of these star-like micelles can be increased up to 4 times by varying the incorporation of DEAEMA (from 65 mol% to 91 mol%) in the core block, whilst maintaining equal block lengths and micelle sizes in solution. The ability to selectively tune the aggregation behaviour of responsive polymers by making subtle changes to polymer composition stresses the great sensitivity and ability to decisively tune diblock copolymer assemblies. However, as mentioned earlier in this chapter, synthesis is a limiting factor in producing a range of polymer structures. Therefore to mitigate this factor a simpler protocol to prepare nanoscale assemblies has been explored and is detailed in the following Chapters.

4.5. Acknowledgements

Dr Joseph Patterson conducted the cryo-TEM experiments and assisted with data analysis. Dr Anaïs Pitto-Barry conducted the SAXS experiments and did the model fitting.

4.6. Experimental

4.6.1. Materials

Monomers were filtered through a plug of silica prior to use and stored in the dark at 4 °C. AIBN (2,2'-azo-bis(isobutyronitrile)) was recrystallised from methanol and stored in the dark at 4 °C. All other materials were used as received from Aldrich, Fluka, and Acros. HCl (1 M) and NaOH (1 M) were calibrated and using tris(hydroxymethyl)-aminomethane and potassium hydrogen phthalate respectively.

4.6.2. Synthesis

4.6.2.1. General procedure for copolymerisation of DMAEMA with DEAEMA (MacroCTA)

A solution of 40 equivalents of a combination of the two monomers (DMAEMA = x, DEAEMA = 40 - x), 0.2 equivalents of AIBN and 1 equivalent of 2-cyano-2-propyl dithiobenzoate (CPDB) in 1,4-dioxane (1:1 volume compared to monomer) was added to a dry ampoule containing a stirrer bar. The solution was degassed using at least 3 freeze-pump-thaw cycles, back filled with nitrogen, sealed and placed in a pre-heated oil bath at 70 °C. After 7 hours the polymerisation was quenched by liquid nitrogen, dioxane removed *in vacuo* and the resultant polymer dissolved with H_2O. The solution was transferred to a dialysis membrane tube with the appropriate molecular weight cut-off (MWCO 3.5 kDa) and dialysed against 18.2 MΩ.cm water (1.5 L) with 3 water changes. Lyophilisation resulted in a pink solid. ^{1}H NMR (400 MHz, $CDCl_3$): δ (ppm) 7.85 (d, $^3J_{H\text{-}H}$ = 8.1 Hz, 1H Ar end group), 7.55 (t, $^3J_{H\text{-}H}$ = 7.4 Hz, 2H Ar end group), 7.41 (t, $^3J_{H\text{-}H}$ = 8.1 Hz, 2H Ar end group), 4.20 (br t, 2H, OCH_2CH_2N), 2.50 (br s, 2H, OCH_2CH_2N), 2.30 (br t, 4H, $OCH_2CH_2N(CH_2)_2(CH_3)_2$), 2.10 (br s, 6H, $OCH_2CH_2N(CH_3)_2$), 1.94 (s, 6H, end group), 1.10 (br t, 6H, $OCH_2CH_2N(CH_2)_2(CH_3)_2$), 1.00-2.00 (br m, backbone) (See Table 4.1 for molecular weight data).

4.6.2.2. General procedure for chain extension of the copolymers with DMAEMA

MacroCTA (1.0 eq), AIBN (0.2 eq) and DMAEMA (40 eq) were dissolved in DMF (1:1 volume compared to the monomer) and were added to a dry ampoule containing a stirrer bar. The solution was degassed using at least 3 freeze-pump-thaw cycles, back filled with nitrogen, sealed and placed in a pre-heated oil bath at 70 °C. After 7 hours the polymerisation was quenched by liquid nitrogen, DMF was removed *in vacuo* and the resultant polymer diluted with H_2O and transferred to a dialysis membrane tube with the appropriate molecular weight cut off (MWCO 6 - 8 kDa) and dialysed against 18.2 MΩ.cm water (1.5 L) with 3 water changes. Lyophilisation resulted in a pink solid. ^{1}H NMR (400 MHz, $CDCl_3$): δ (ppm) 7.85 (d, $^3J_{H\text{-}H}$ = 8.1 Hz, 1H Ar end group), 7.55 (t, $^3J_{H\text{-}H}$ = 7.4 Hz, 2H end group), 7.41 (t, $^3J_{H\text{-}H}$ = 8.1 Hz, 2H, end group), 4.20 (br t, 2H, OCH_2CH_2N), 2.50 (br s, 2H, OCH_2CH_2N), 2.30 (br t, 4H, $OCH_2CH_2N(CH_2)_2(CH_3)_2$), 2.10 (br s, 6H, $OCH_2CH_2N(CH_3)_2$), 1.94 (s, 6H, end group), 1.10 (br t, 6H, $OCH_2CH_2N(CH_2)_2(CH_3)_2$), 1.00-2.00 (br m, backbone) (See Table 4.1 for molecular weight data).

4.6.2.3. Reactivity ratios of DMAEMA and DEAEMA

DMAEMA and DEAEMA at different molar ratios, CPDB and AIBN were dissolved in 1,4-dioxane. The ratio of [monomers]: [CTA]: [AIBN] was 40: 1: 0.2, the solution was degassed using at least 3 freeze-pump-thaw cycles, back filled with nitrogen, sealed and placed in a pre-heated oil bath at 70 °C. The conversion was kept below 10% and the reaction was quenched by liquid nitrogen. Aliquots were taken and characterised by ^{1}H NMR spectroscopy in $CDCl_3$. f_1 and F_1 values for the copolymerisation of DMAEMA(f_1) and DEAEMA(f_2) are given in table 4.7.

Table 4.7. f_1 and F_1 values for the copolymerisation of DMAEMA(f_1) and DEAEMA(f_2).

Experiment	Mol fraction in initial feed (f_1)	Mol fraction in copolymer (F_1)
1	0.09	0.09
2	0.25	0.32
3	0.32	0.35
4	0.37	0.41
5	0.54	0.55
6	0.60	0.63
7	0.71	0.76
8	0.83	0.86

4.6.3. Polymer characterisation

4.6.3.1. ^{1}H Nuclear Magnetic Resonance (NMR) spectroscopy

^{1}H NMR spectra were recorded on a Bruker DPX-400 spectrometer in $CDCl_3$. Chemical shifts are given in ppm downfield from TMS.

4.6.3.2. Size exclusion chromatography

Size exclusion chromatography (SEC) measurements were performed with HPLC grade solvents (Fisher), dimethylformamide (DMF) with 1.06 g/L of LiCl at 40 °C as the eluent at

a flow rate of 1 mL/min, on a set of two PLgel 5 μm Mixed-D columns, and one guard column. The molecular weights of the synthesised polymers were calculated relative to poly(methyl methacrylate) (PMMA) standards from refractive index chromatograms.

4.6.3.3. Potentiometric titration

Potentiometric titration was performed at room temperature with an automatic titrator (Mettler Toledo G20) controlled by LabX software. 40 mL of solution (approximately 2.3×10^{-4} M) was used for each potentiometric titration experiment. The polymers were first dissolved at $\alpha = 1$ with 1.1 excess of 1 M HCl and then back-titrated with 0.1 M NaOH. We define α as the degree of ionisation following equation (4.1),

The addition of NaOH 0.1 M titrant was added at volume increments of 5-50 μL and spaced with 180 s intervals. From the raw titration data the total amount of titrable amine units was calculated. Therefore, the change of pH could be plotted as a function of the degree of ionisation, α.

4.6.3.4. Refractive index increment

The specific refractive index increment (d*n*/dC) of the polymers were measured on a refractometer (Bischoff RI detector) operating at a wavelength of 632 nm.

4.6.4. Micelle preparation

Three methods for the preparation of the solutions were used. Method 1 consisted of diluting polymer stock solutions that were prepared at 20 g/L by dispersing the polymer in 18.2 MΩ.cm water containing the appropriate amount of HCl to reach $\alpha = 1$. After one night of stirring α was lowered with the required amount of 1 M NaOH and the solutions were stirred again overnight, after which time the NaCl concentration was adjusted to 0.1 M by the addition of 4 M NaCl. The solutions were further stirred overnight before use. Samples at lower concentrations were subsequently diluted with 0.1 M NaCl to reach the desired concentrations (10 g/L – 0.5 g/L).

For reversibility tests method 2 was used. Method 2 consisted of making a polymer solution at $\alpha = 1$ as for method 1 at a concentration of 2.5 g/L. Subsequently this solution was split in two. One half of the solution was brought to lower α values by the addition of 1 M NaOH (this will be referred to as Pathway A), whereas the second half was first brought to $\alpha = 0$ from the addition of 1 M NaOH, knowing the chemical structure of the polymers and considering that all units are ionisable as verified by potentiometric titration. Then α values were raised by the addition of 1 M HCl (referred to as Pathway B). Each change in α was spaced by at least one night of stirring.

For the tests on the influence of salt method 3 was used. Here the polymer powder was dispersed directly at the targeted α in 0.1 M NaCl at 2.5 g/L the solutions were left to stir for 24 h before analysis.

4.6.5. Micelle characterisation

4.6.5.1. Laser light scattering

Measurements were performed at angles of observation ranging from 20° up to 150° with an ALV CGS3 setup operating at $\lambda_0 = 632$ nm and at 20 ± 1 °C. Data were collected in duplicate with 240 s run times. Calibration was achieved with filtered toluene and the background was measured with filtered solvent (NaCl 0.1 M).

4.6.5.2. Dynamic light scattering (DLS)

The intensity autocorrelation functions $g_2(t)$ obtained from dynamic light scattering were related to $g_1(t)$ (the normalised electric field autocorrelation functions) *via* the so-called Siegert relation. Then $g_1(t)$ was analysed in terms of a continuous distribution of relaxation times (eqn. 1.18 using the REPES routine[58] without assuming a specific mathematical shape for the distribution of the relaxation times ($A(\tau)$). The apparent diffusion coefficient *D* was calculated from eqn. 1.16 given that the average relaxation rates Γ of the scatterers were q^2 dependent, where q is the scattering vector given by $q=(4\pi n/\lambda_0).\sin(\theta/2)$ with θ the angle of

observation and n = 1.333 the refractive index of the solvent (water). Its concentration dependence is given by $D = D_0(1+k_DC)$ where k_D is the dynamic second virial coefficient and D_0 the diffusion coefficient used for computing the hydrodynamic radius (R_h) of the scatterers according to the Stokes-Einstein eqn. 1.19. With η the solvent viscosity, k the Boltzmann's constant and T the absolute temperature. Values of R_h given in the following are then obtained after extrapolation to zero concentration.

4.6.5.3. Static light scattering (SLS)

The Rayleigh ratio of the solutions have been measured using toluene as a reference according to eqn. 1.12 where I_i represents the intensity scattered by species i and $R_{toluene}$ is the Rayleigh ratio of the reference. In dilute solutions if $R_g.q < 1$ where R_g is the radius of gyration, the q and concentration dependence of R_θ is given by eqn 1.10, where A_2 is the second virial coefficient and M_w the weight average molecular weight. K is an optical constant given by eqn 1.11. Where $n_o = 1.496$ is the refractive index of the reference liquid (toluene), dn/dC is the specific refractive index increment determined by differential refractometry (see Table 4.1) and N_A is Avogadro's number. Values of M_w are then obtained after extrapolation to zero concentration and zero angle and used to derive the aggregation number of the micellar aggregates $N_{agg} = M_w/M_{w,unimers}$. For spherical morphologies, it is possible to deduce the core radius, R_c, from the aggregation number, using equation (2.1) assuming the core block is dehydrated and the density matches that of the bulk value, ρ.[68] When in some cases two modes of relaxation were observed by DLS measurements, R_θ was described as the sum of two contributions according to eqn. 1.25, where f and s stand respectively for fast and slow modes and using 1.26. Where A_f and A_s are the relative amplitudes of the fast and slow modes obtained by DLS. The slow mode of relaxation observed can be attributed to spurious aggregates with a negligible weight fraction but larger scattering intensity.[55,69]

4.6.5.4. Small angle X-ray scattering (SAXS)

Measurements were performed at the Australian Synchrotron facility at a photon energy of 11 keV. The samples in solutions of 0.1 M NaCl were analysed at a sample to detector distance of 3.252 m to give a q range of 0.004 to 0.2 $Å^{-1}$. The scattering from a blank (aqueous solution of NaCl 0.1 M) was measured in the same location as the sample collection and was subtracted for each measurement. Data was normalised for total transmitted flux using a quantitative beamstop detector and absolute scaled using water as an absolute intensity standard. The two-dimensional isotropic SAXS images were converted in one-dimensional SAXS scattered intensity profiles (I(q) versus q) by circular averaging. The functions used for the fitting from NCNR package[70] were "Guinier-Porod"[71,72] "Core-Shell"[72] and "Debye".[73] Scattering length densities (SLD) were calculated using the "Scattering Length Density Calculator" provided by the NIST Center for Neutron Research. A linear summation of the PolyCoreShell ratio model and the Debye model is used and has the following parameters (K0 to K7 for the PCR model, K8 to K10 for the Debye model):

K0 scale

K1 average core radius (Å)

K2 average shell thickness (Å), not used in this model

K3 overall polydispersity

K4 scattering length density (SLD) core (Å-2)

K5 SLD shell (Å-2), not used in this model

K6 SLD solvent (Å-2)

K7 background (cm-1)

K8 scale

K9 Rg (Å), used in this model as a hydrated thickness, and as unimers in solution for the kinetics early data points

K10 background (cm-1)

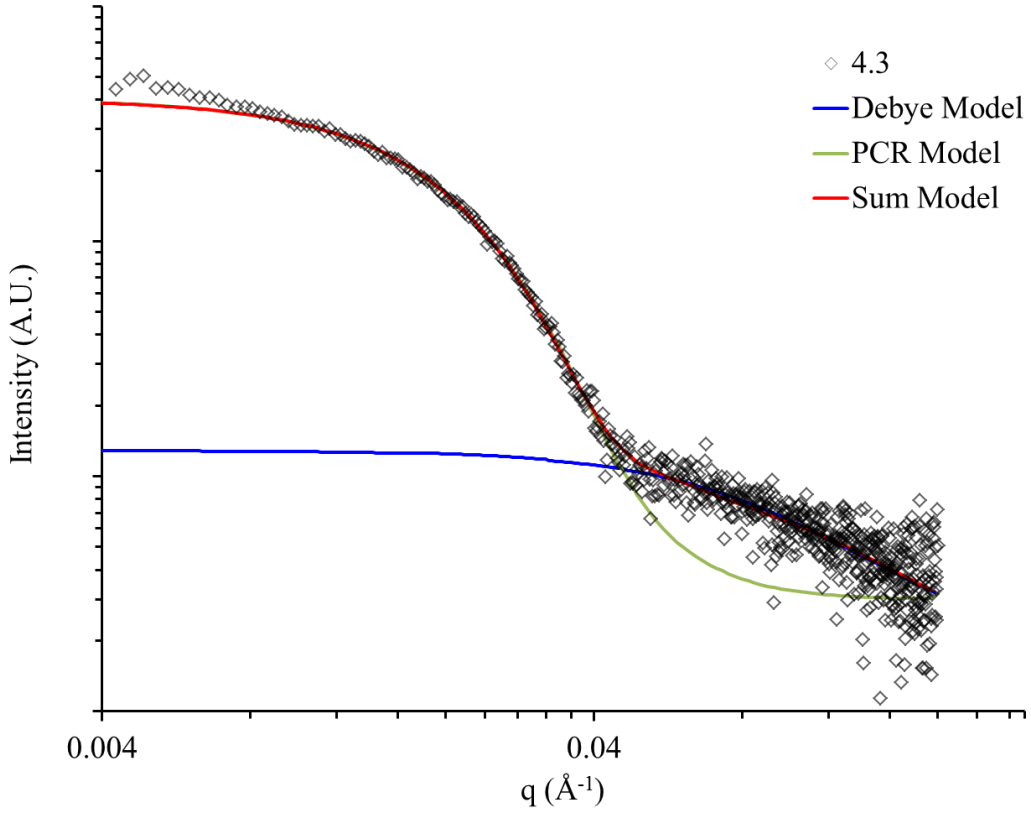

Figure 4.18. SAXS profile of 4.3 at α = 0, 2.5 g/L and in 0.1 M NaCl solution showing the Debye model fit, PolyCoreShell model fit and a linear summation of the PolyCoreShell and Debye model fit.

4.6.5.5. Cryogenic transmission electron microscopy samples (cryo-TEM)

Cryo-TEM images were taken on a FEI Sphera microscope operated at 200 keV. 3.5 μL of sample were added to freshly glow discharged Quantifoil R2/2 TEM grids. The grids were blotted with filter paper under high humidity to create thin films and rapidly plunged into liquid ethane. The grids were transferred to the microscope under liquid nitrogen and kept at < -175 °C while imaging.

4.7. References

(1) Hamley, I. W. *The Physics of Block Copolymers* OUP Oxford, 1998.
(2) Hamley, I. W. *Block Copolymers in Solution: Fundamentals and Applications*; Wiley, 2005.
(3) Mai, Y.; Eisenberg, A. *Chem. Soc. Rev.* **2012**, *41*, 5969.
(4) Choi, S. Y.; Bates, F. S.; Lodge, T. P. *J. Phys. Chem. B* **2009**, *113*, 13840.
(5) Li, Z.; Dormidontova, E. E. *Soft Matter* **2011**, *7*, 4179.
(6) Choi, S.-H.; Lodge, T. P.; Bates, F. S. *Phys. Rev. Lett.* **2010**, *104*, 047802.
(7) Won, Y. Y.; Davis, H. T.; Bates, F. S. *Macromolecules* **2003**, *36*, 953.
(8) Rager, T.; Meyer, W. H.; Wegner, G.; Winnik, M. A. *Macromolecules* **1997**, *30*, 4911.
(9) Colombani, O.; Ruppel, M.; Burkhardt, M.; Drechsler, M.; Schumacher, M.; Gradzielski, M.; Schweins, R.; Muller, A. H. E. *Macromolecules* **2007**, *40*, 4351.
(10) Meli, L.; Santiago, J. M.; Lodge, T. P. *Macromolecules* **2010**, *43*, 2018.
(11) Lund, R.; Willner, L.; Richter, D.; Dormidontova, E. E. *Macromolecules* **2006**, *39*, 4566.
(12) Nyrkova, I. A.; Semenov, A. N. *Macromol. Theory Simul.* **2005**, *14*, 569.
(13) von Gottberg, F. K.; Smith, K. A.; Hatton, T. A. *J. Chem. Phys.* **1998**, *108*, 2232.
(14) Nicolai, T.; Colombani, O.; Chassenieux, C. *Soft Matter* **2010**, *6*, 3111.
(15) Hadgiivanova, R.; Diamant, H.; Andelman, D. *J. Phys. Chem. B* **2011**, *115*, 7268.
(16) Stejskal, J.; Hlavatá, D.; Sikora, A.; Konňák, Č.; Pleštil, J.; Kratochvíl, P. *Polymer* **1992**, *33*, 3675.
(17) Zhang, L.; Shen, H.; Eisenberg, A. *Macromolecules* **1997**, *30*, 1001.
(18) Halperin, A.; Alexander, S. *Macromolecules* **1989**, *22*, 2403.
(19) Nose, T.; Iyama, K. *Comput. Theor.Polym. Sci.* **2000**, *10*, 249.
(20) Hayward, R. C.; Pochan, D. J. *Macromolecules* **2010**, *43*, 3577.
(21) Save, M.; Manguian, M.; Chassenieux, C.; Charleux, B. *Macromolecules* **2004**, *38*, 280.
(22) Gibson, M. I.; O'Reilly, R. K. *Chem. Soc. Rev.* **2013**, *42*, 7204.
(23) Cotanda, P.; Wright, D. B.; Tyler, M.; O'Reilly, R. K. *J. Polym. Sci. A Polym. Chem.* **2013**, *51*, 3333.
(24) Lee, H.; Son, S. H.; Sharma, R.; Won, Y.-Y. *J. Phys. Chem. B* **2011**, *115*, 844.
(25) Lutz, J.-F. *J. Polym. Sci. A Polym. Chem.* **2008**, *46*, 3459.
(26) Lutz, J.-F.; Akdemir, Ö.; Hoth, A. *J. Am. Chem. Soc.* **2006**, *128*, 13046.
(27) Charbonneau, C.; De Souza Lima, M. M.; Chassenieux, C.; Colombani, O.; Nicolai, T. *Phys. Chem.Chem. Phys.* **2013**, *15*, 3955.
(28) Charbonneau, C.; Chassenieux, C.; Colombani, O.; Nicolai, T. *Macromolecules* **2011**, *44*, 4487.
(29) Colombani, O.; Lejeune, E.; Charbonneau, C.; Chassenieux, C.; Nicolai, T. *J. Phys. Chem. B* **2012**, *116*, 7560.
(30) Dutertre, F.; Boyron, O.; Charleux, B.; Chassenieux, C.; Colombani, O. *Macromol. Rapid Commun.* **2012**, *33*, 753.
(31) Lejeune, E.; Chassenieux, C.; Colombani, O. *Prog. Colloid Polym. Sci.* **2011**, 138, 7.
(32) Lejeune, E.; Drechsler, M.; Jestin, J.; Muller, A. H. E.; Chassenieux, C.; Colombani, O. *Macromolecules* **2010**, *43*, 2667.
(33) Shedge, A.; Colombani, O.; Nicolai, T.; Chassenieux, C. *Macromolecules* **2014**, *47*, 2439.
(34) Bendejacq, D. D.; Ponsinet, V. *J. Phys. Chem. B* **2008**, *112*, 7996.
(35) Bendejacq, D. D.; Ponsinet, V.; Joanicot, M. *Langmuir* **2005**, *21*, 1712.
(36) Ribaut, T.; Oberdisse, J.; Annighofer, B.; Stoychev, I.; Fournel, B.; Sarrade, S.; Lacroix-Desmazes, P. *Soft Matter* **2009**, *5*, 4962.

(37) Lee, A. S.; Bütün, V.; Vamvakaki, M.; Armes, S. P.; Pople, J. A.; Gast, A. P. *Macromolecules* **2002**, *35*, 8540.
(38) Lee, A. S.; Gast, A. P.; Butun, V.; Armes, S. P. *Macromolecules* **1999**, *32*, 4302.
(39) Zhang, J.; Xu, J.; Liu, S. *J. Phys. Chem. B* **2008**, *112*, 11284.
(40) Zhu, Z.; Armes, S. P.; Liu, S. *Macromolecules* **2005**, *38*, 9803.
(41) Johnson, B. K.; Prud'homme, R. K. *Phys. Rev. Lett.* **2003**, *91*, 118302.
(42) Adams, D. J.; Butler, M. F.; Weaver, A. C. *Langmuir* **2006**, *22*, 4534.
(43) Halperin, A. *Macromolecules* **2011**, *44*, 5072.
(44) G. Moad, E. Rizzardo., S. Thang, *Macromolecules* **1998**, *31*, 5559.
(45) Keddie, D. J. *Chem. Soc. Rev.* **2014**, *43*, 496.
(46) Van Herk, A. M.; Dröge, T. *Macromol. Theory Simul.* **1997**, *6*, 1263.
(47) Flory, P. J. *Principles of Polymer Chemistry* Cornell Univ Pr, 1953.
(48) Philipp, V. *Macromol. Symp.* **2007**, *248*, 71.
(49) Plamper, F. A.; Becker, H.; Lanzendörfer, M.; Patel, M.; Wittemann, A.; Ballauff, M.; Müller, A. H. E. *Macromol. Chem. Phys.* **2005**, *206*, 1813.
(50) Manning, G. S. *J. Phys. Chem.* **1981**, *85*, 870.
(51) Nyrkova, I. A.; Semenov, A. N. *Faraday Discussions* **2005**, *128*, 113.
(52) Jacquin, M.; Muller, P.; Talingting-Pabalan, R.; Cottet, H.; Berret, J. F.; Futterer, T.; Theodoly, O. *J. Colloid. Interface. Sci.* **2007**, *316*, 897.
(53) van Stam, J.; Creutz, S.; De Schryver, F. C.; Jerome, R. *Macromolecules* **2000**, *33*, 6388.
(54) Creutz, S.; van Stam, J.; De Schryver, F. C.; Jerome, R. *Macromolecules* **1998**, *31*, 681.
(55) Chassenieux, C.; Nicolai, T.; Durand, D. *Macromolecules* **1997**, *30*, 4952.
(56) Sedlak, M. *J. Chem. Phys.* **1997**, *107*, 10805.
(57) Sedlak, M. *J. Chem. Phys.* **1997**, *107*, 10799.
(58) Jakes, J. *Collect. Czech. Chem. Commun.* **1995**, *60*, 1781.
(59) Nyrkova, I. A.; Semenov, A. N. *Eur. Phys. J. E* **2005**, *17*, 327.
(60) Eghbali, E.; Colombani, O.; Drechsler, M.; Muller, A. H. E.; Hoffmann, H. *Langmuir* **2006**, *22*, 4766.
(61) Daoud, M.; Cotton, J. P. *J. Phys. I* **1982**, *43*, 531.
(62) Patterson, J. P.; Kelley, E. G.; Murphy, R. P.; Moughton, A. O.; Robin, M. P.; Lu, A.; Colombani, O.; Chassenieux, C.; Cheung, D.; Sullivan, M. O.; Epps, T. H.III; O'Reilly, R. K. *Macromolecules* **2013**, *46*, 6319.
(63) Lu, A.; O'Reilly, R. K. *Curr. Opin. Biotechnol.* **2013**, *24*, 639.
(64) Cotanda, P.; Lu, A.; Patterson, J. P.; Petzetakis, N.; O'Reilly, R. K. *Macromolecules* **2012**, *45*, 2377.
(65) Cotanda, P.; O'Reilly, R. K. *Chem. Comm.* **2012**, *48*, 10280.
(66) Park, J. H.; Lee, S.; Kim, J.-H.; Park, K.; Kim, K.; Kwon, I. C. *Prog. Polym. Sci.* **2008**, *33*, 113.
(67) Rush, A. M.; Nelles, D. A.; Blum, A. P.; Barnhill, S. A.; Tatro, E. T.; Yeo, G. W.; Gianneschi, N. C. *J. Am. Chem. Soc.* **2014**, *136*, 7615.
(68) Patterson, J. P.; Robin, M. P.; Chassenieux, C.; Colombani, O.; O'Reilly, R. K. *Chem. Soc. Rev.* **2014**, *43*, 2412.
(69) Sedlak, M. *J. Chem. Phys.* **1996**, *105*, 10123.
(70) Kline, S. *J. Appl. Crystallogr.* **2006**, *39*, 895.
(71) Glatter, O.; Kratky, O. *Small-Angle X-Ray Scattering*; Academic Press, 1982.
(72) Guinier, A.; Fournet, G. *Small-angle scattering of X-rays*; John Wiley & Sons: New York, 1955.
(73) Roe, R.-J. *Methods of X-ray and Neutron Scattering in Polymer Science*; Oxford University Press: New York, 2000.

5. The copolymer blending method for targeted assemblies

5.1. Abstract

Polymer self-assembly in solution offers a simple strategy for the production of elegant complex nanomaterials. Similar to low molecular weight surfactants tailoring specific structures is typically attempted by incremental modification of both molecular weight and composition in order to alter the self-assembly in order to target desired morphologies. However due to thermodynamic, kinetic and synthetic limitations the ability to produce defined and reproducible equilibrium structures remains elusive. Here a simple blending protocol for diblock copolymers with identical block lengths but varying hydrophobic monomer incorporation can be used to overcome thermodynamic and kinetic limitations whilst being robust enough to suppress synthetic difficulties producing well defined tuneable nanostructures. The results demonstrate that a range of equilibrium structures can be produced from blending just two polymers; these blended structures are identical to those formed from the pure synthetic analogue at the same composition.

5.2. Introduction

In soft nanotechnology, attempts have been made to replicate these complex nanostructures by using amphiphilic block copolymers which spontaneously self-assemble in selective solvents.[1-3] In dilute solution, the most commonly studied nanostructures are spherical micelles.[4] These man-made nanostructures have enormous potential in a variety of applications, but are particularly interesting for biological systems as they can mimic segregated environments similar to those found in eukaryotic cells which have lipid bilayers such as mitochondria. Although a plethora of polymer nanostructures can be obtained, an array of thermodynamic and kinetic constraints exists which severely limits both the precision and purpose so easily obtained by nature. Moreover, it is now well established that many amphiphilic block copolymers self-assemble into out-of-equilibrium or "frozen" structures because exchange of single chains (unimers) between the assemblies is kinetically prohibited, either because of a high glass transition temperature (T_g) of the solvophobic block or because of the highly hydrophobic character of the solvophobic block despite a low T_g.[5-12]

There are three possible routes to modify nanoscale polymer assemblies in solution. First, as previously shown in the literature and Chapter 4 diblock copolymers can be synthesised with varying block ratios or solvophobicity of one of the blocks through copolymerisation.[13-21] However, there are limitations associated with this method being able to precisely synthesise and target exact molecular weights coupled with the difficulties of polymerising comonomers of different functionalities in a reproducible manner.[22] Moreover targeting specific nanoscale structures via this method requires the use of a phase diagram, and these phase diagrams take vast amounts of time and synthesis to determine. Second, the manipulation of the assembly conditions, by controlling the solvent composition during assembly and hence supporting or severely restricting unimer exchange can cause certain structures to be kinetically trapped. Such approaches prohibit equilibrium being reached,

resulting in frozen micelles without unimer exchange, preventing the formation of defined segregated environments.[2,23-25]

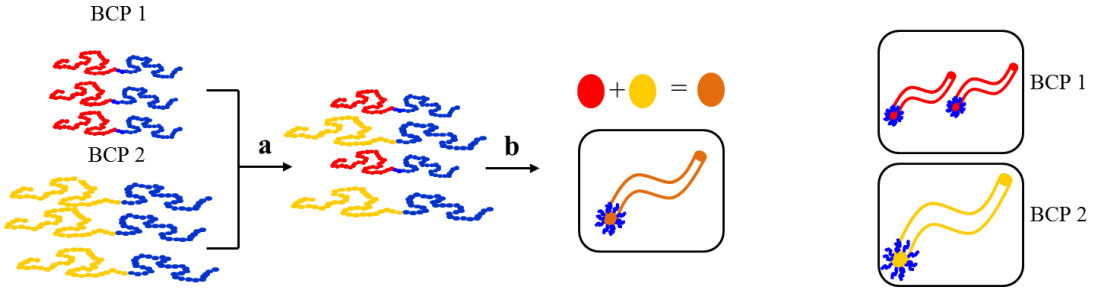

Figure 5.1 Schematic demonstrating the blending of two diblock copolymers together to reach the desired composition. a) Diblock copolymers are first blended together as powders and b) subsequently assembled in aqueous solution. Note that individually the diblock copolymers form different cylinder structures once assembled, once blended the structure is an intermediate between the two. Figure adapted from reference [9].

Finally, a simpler and more elegant route exists involving the blending of two different copolymers together in a binary mixture to obtain the desired composition or structure (Figure 5.1).[9,10,26-29] Here a blend structure is composed of two or more pure polymers, where pure refers to a system with only one polymer type and the polymer is synthesised to the desired composition. For example in Figure 5.1 the blend structure is formed from pure block copolymers (BCP) 1 and BCP 2. Where the pure BCP 1 will form a cylinder structure with specific lengths and widths and BCP 2 a cylinder structure with different dimensions, but the blend structure will be a cylinder with lengths and widths of intermediate values between the two observed for BCP1 and BCP2. In this specific example the BCP can indeed mix and therefor this blending strategy would allow the formation of nanostructures with a range of compositions in an effortless manner using only two polymers in contrast to a self-sorting system with coexistence of two different particles. This is opposes the required synthesis of the polymer to the desired composition for a desired application. However this is only true if the structures can overcome the kinetic obstacles in place and thermodynamic equilibrium is reached. For example Lu *et al* studied the equilibration of poly(styrene)-*block*-

poly(ethylene propylene), PS-*b*-PEP, diblock copolymer with different PS block lengths in sqaulene (a good solvent for PEP) and concluded that unimers must overcome a kinetic energy barrier for molecular exchange to successfully blend (Figure 5.2).[30] Here, chain exchange was measured by time resolved SANS in a sample of spherical micelles formed by mixing pairs of *h*PS-*b*-PEP (proton labelled) and *d*PS-*b*-PEP (deuterium labelled) containing two different molecular weight PS blocks. Complete chain exchange results in a uniform distribution of the four types of PS blocks and a blend micelle is formed. Additionally, as mentioned in previous Chapters, amphiphilic block copolymers often form frozen structures in water and molecular reorganisation is prevented which stops any reorganisation of the system. It is obvious that in the absence of unimer exchange, two different types of micelles formed by two different amphiphilic block copolymers cannot rearrange spontaneously into blended micelles.[9] However, the formation of blended micelles may also be prevented in dynamic assemblies if the two different block copolymers are too different to allow thermodynamic compatibility between polymer chains.[31-33]

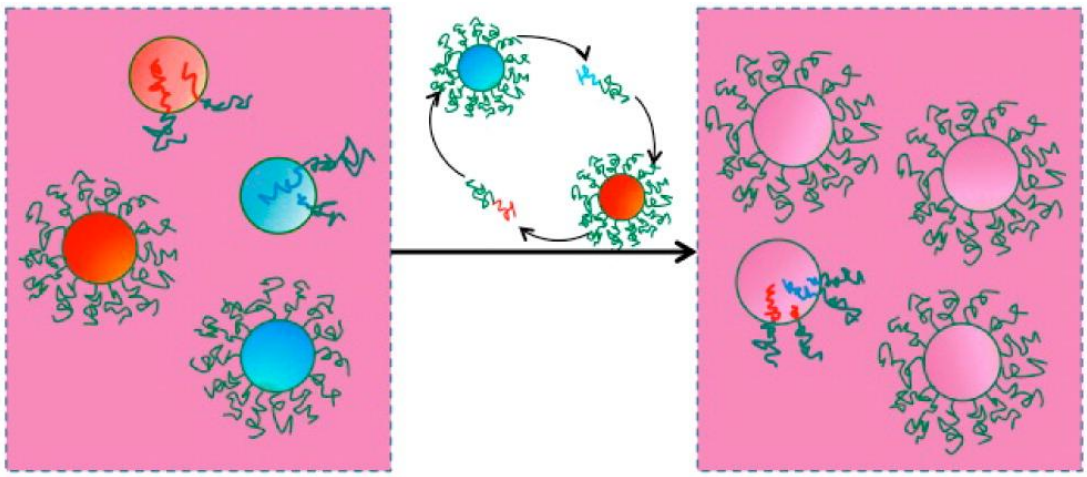

Figure 5.2 Equilibration of PS-*b*-PEP micelles with hydrogenated (blue) and deuterated (red) PS cores in sqaulene.[30]

Experimentally and theoretically binary mixtures of self-assembled systems have not been widely explored in solution.[31-36] Despite exploring different variables (specifically the length

of the blocks or the nature of the core forming block) the authors of these studies all agreed that mixed micelles may form when both individual polymers could self-assemble, or if specific pathways for mixed assembly are used.[32,35,36] Nevertheless spontaneous mixing only occurs if it is thermodynamically favourable, meaning that core forming blocks are not too thermodynamically dissimilar to one another and can mix.[31] To date only one report exists to our knowledge comparing a binary polymer mixture to pure polymer samples, that is a single polymer system) with the same composition.[26] Although these reports on blending suggest that similar properties could be targeted, the structures formed from binary mixtures differed structurally to those theoretically predicted and observed by pure samples (as determined by laser light scattering and TEM). The difference between the two systems may be due to the out of equilibrium behaviour polymeric micelles often exhibit,[5] thus prohibiting the reorganisation and cooperative assembly of the polymer mixture.[9,23] Still, theoretical studies by Palyulin *et al* did indicate that if equilibrium can be obtained, allowing structures to reach the true Gibbs free energy minima, plus the incompatibility between the two polymers is weak, then entropically stable mixed micelle structures could form (Figure 5.3).[32]

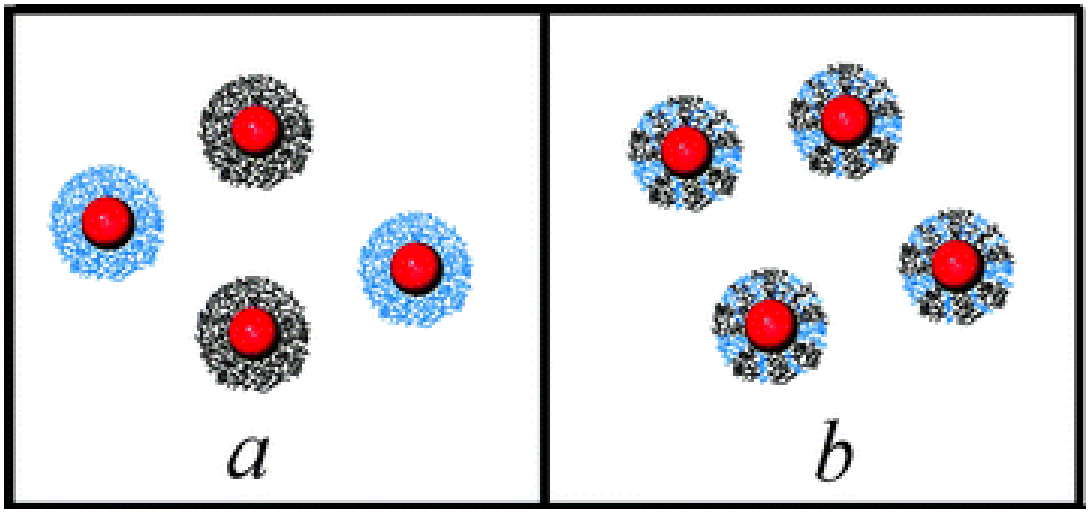

Figure 5.3 Simulation of a) Mixed micellar structures with high thermodynamic incompatibility. b) Mixed micellar structures with low thermodynamic incompatibility, for AB and BC diblock copolymers.[32]

In this Chapter the strategy was to blend two diblock copolymers, differing only in the ratio of co-monomers in the associating block and to analyse the blended micelles formed in comparison to the micelles formed by a single polymeric series at the same average composition (Figure 5.4). This simple blending protocol allows the characteristics of blended micelles to be elegantly tuned whilst achieving structurally identical micelles to that of pure micelles at the desired composition. This robust yet simple blending strategy for assembly offers great potential to obtain predictable structures of low dispersity on the nanoscale and providing a simple route to produce particles where precise catalytic or drug loadings are required.[37-43]

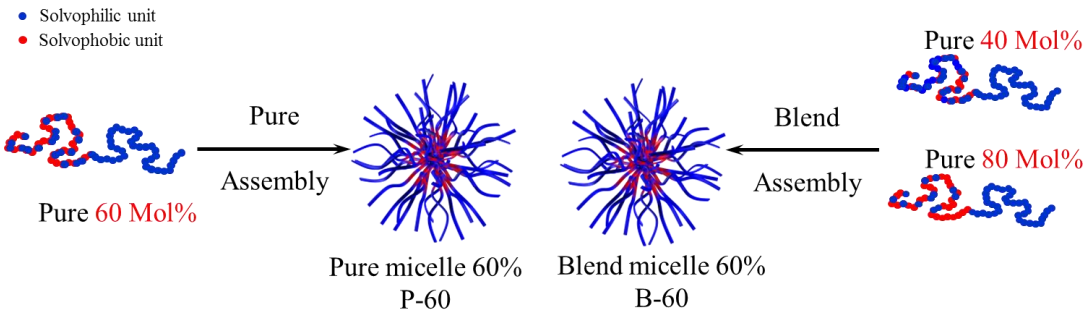

50 Mol% of Pure 80% + 50 Mol% of Pure 40% = **Blend micelle 60%**

Figure 5.4. Schematic demonstrating the blending of two diblock copolymers together to form blended nanoscale assemblies at the desired composition.

5.3. Results and Discussion

5.3.1. Synthesis and molecular characterisation of the diblock copolymers

5.3.1.1. Synthesis of P(DEAEMA-co-DMAEMA)-b-PDMAEMA diblock copolymers

The synthesis and self-assembly of the pure poly(dimethylaminoethyl)methacrylate-co-(diethylaminoethyl)methacrylate*)-block*-poly(diethylaminoethyl)methacrylate, P(DEAEMA-*co*-DMAEMA)-*b*-PDMAEMA, diblock copolymers with respect to DEAEMA incorporation and ionisation was explored in Chapter 4. These polymers were then further used in this Chapter along with two additional (DEAEMA-*co*-DMAEMA)-*b*-PDMAEMA diblock copolymers, one with 50% DEAEMA and one with 85% DEAEMA in the core forming block (Table 5.1) characterised by ^{1}H nuclear magnetic resonance (NMR) spectroscopy and size exclusion chromatography (SEC).

To distinguish between the blend and pure systems within this Chapter the following notation is used; blended systems (systems with two diblock copolymers blended together) with *n*% DEAEMA in the core are presented as B-*n* and pure systems (systems with only one diblock copolymer series in the system) with *n*% DEAEMA in the core are denoted as P-*n*.

Scheme 5.1. Structure of the P(DEAEMA-*co*-DMAEMA)-*b*-PDMAEMA diblock copolymers used.

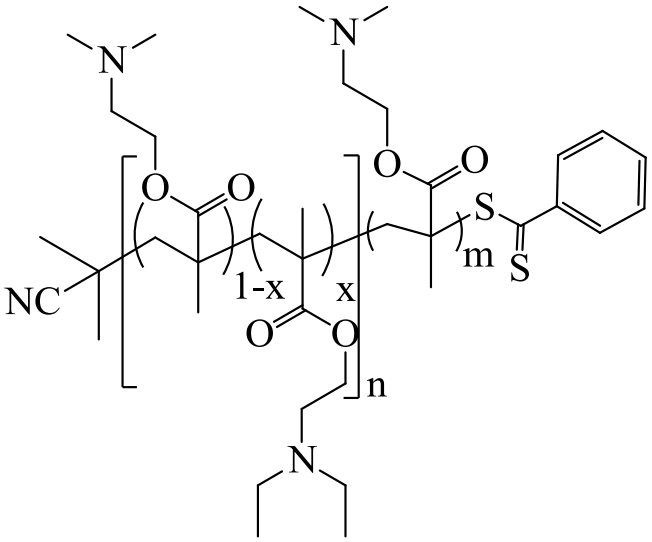

Table 5.1. Characteristics of the P(DMAEMA$_{1-x}$-*co*-DEAEMA$_x$)$_n$-*b*-PDMAEMA$_m$ diblock copolymers.

Diblock copolymer	x[a]	n[b]	m[b]	$M_{n,NMR}$[b] (kDa)	$M_{n,SEC}$[c] (kDa)	$Đ_{,SEC}$[c]
P-32	0.32	35	30	10.7	13.8	1.16
P-50	0.50	34	32	11.1	13.4	1.18
P-65	0.65	36	35	12.3	14.2	1.12
P-76	0.76	25	34	10.0	12.8	1.18
P-85	0.85	31	35	11.4	13.9	1.17
P-91	0.91	28	32	10.4	13.5	1.10

[a] Determined by ^{1}H NMR spectroscopy using the signals at δ = 4.20 ppm and 2.10 ppm. [b] Determined by end-group analysis from ^{1}H NMR spectroscopy. [c] From SEC based on poly(methyl methacrylate) standards in DMF.

5.3.2. Blending of diblock copolymers

Herein the self-assembly in aqueous solution of diblock copolymer blends was investigated. Altering the ratio of the two diblock polymers in the blend allowed a range of different compositions to be targeted. These blend micelles were then further compared to pure systems at the same average composition. The pure systems were produced by synthesising the pure system to have similar block lengths but the ratio of monomers in the core forming block was targeted to give the desired composition.

5.3.2.1. P(DEAEMA-co-DMAEMA)-b-PDMAEMA diblock copolymer blends

For the P(DMAEMA-*co*-DEAEMA)-*b*-PDMAEMA diblock copolymer blends the block copolymers **P-32** (32% DEAEMA in the core) and **P-91** (91% DEAEMA in the core) were blended together in different ratios to obtain intermediate compositions between the two, Table 5.2.

Table 5.2. Molar mixing ratios for the blended block copolymer systems.

Blended diblock copolymer	Mole fraction **P-91**	Mole fraction **P-32**	Theoretical DEAEMA in core block
B-50	0.40	0.60	50%
B-65	0.60	0.40	65%
B-76	0.75	0.25	76%
B-85	0.90	0.10	85%

5.3.3. Formation of blend micelles of pH responsive P(DMAEMA-*co*-DEAEMA)-*b*-PDMAEMA

As observed in Chapter 4 the aggregation behaviour of P(DMAEMA-*co*-DEAEMA)-*b*-PDMAEMA diblock copolymers could be tuned by varying the core composition through altering the ratio of DMAEMA and DEAEMA in the copolymer associating block. Here aggregation behaviour is explored by varying the composition of the core block by blending two P(DMAEMA-*co*-DEAEMA)-*b*-PDMAEMA diblock copolymers together.

Two methods of preparation were explored to understand if equilibrium can be reached and therefore allow successful blending, Figure 5.5. Method A entails forming blend micelles by mixing the copolymers as unimers in two steps. First the bulk powders were mixed and solubilised at $\alpha = 1$, at this point the solution is molecularly dissolved unimers. Once solubilised the α value is subsequently lowered until $\alpha = 0$ and stirred for 24 hrs at which point the polymers have assembled into spherical micelles. α represents the overall ionisation degree of the DEAEMA and DMAEMA units, which is the percentage of these units which are cationically charged. As these polymers have assembled from a solution of unimers it can be believed that this system should be under thermodynamic control as equilibrium is reached before chain exchange is eventually stopped and the structures are locked in. For method B, micelle blending, the copolymers are first solubilised separately at $\alpha = 1$ and then α is slowly lowered until $\alpha = 0$ is reached. Only once the polymers have reached $\alpha = 0$ are the solutions then blended together. For this route thermodynamic structures can only form if the unimers can exchange between micelles and overcome the kinetic obstacles hindering exchange.

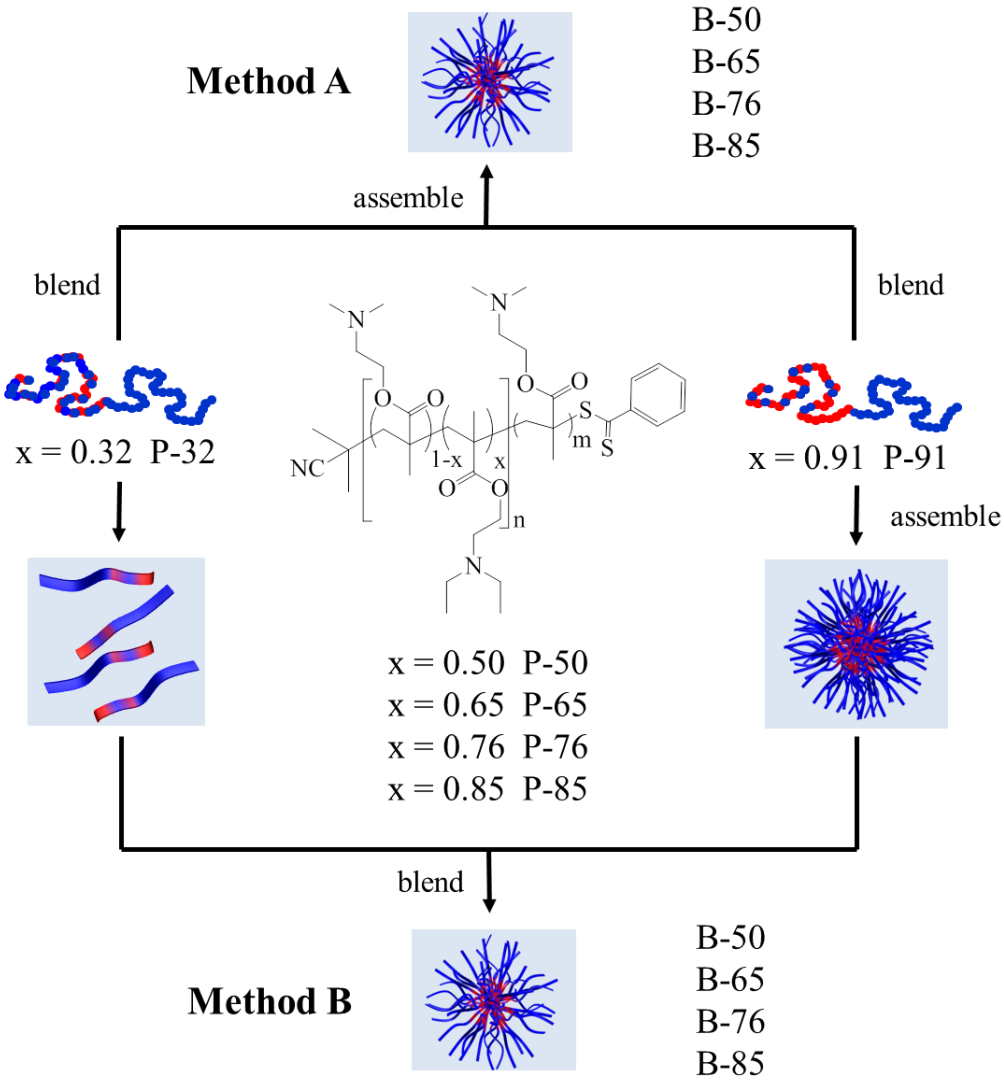

Figure 5.5 Schematic demonstrating the blending protocols employed. Method A, dry powder mixing (unimer blending), polymer powders are first mixed to match the desired DEAMEA *n*% and then subsequently assembled. Method B, solution blending (micelle blending), polymers are first solubilised and then subsequently mixed to match the desired DEAEMA *n*%.

Here two solutions were solubilised individually and then the solutions were blended once α = 0. Once the solutions were mixed LLS and SAXS measurements were taken at defined time intervals. Laser light scattering (LLS) measurements over time reveal that with Method B a reorganisation of the system occurs and then a steady state is reached several days after the initial mixing of the two solutions, Figure 5.6. From Figure 5.6 it can be observed that

eventually steady state is reached and no further change in the structure of the micelles was observed up to 14 days.

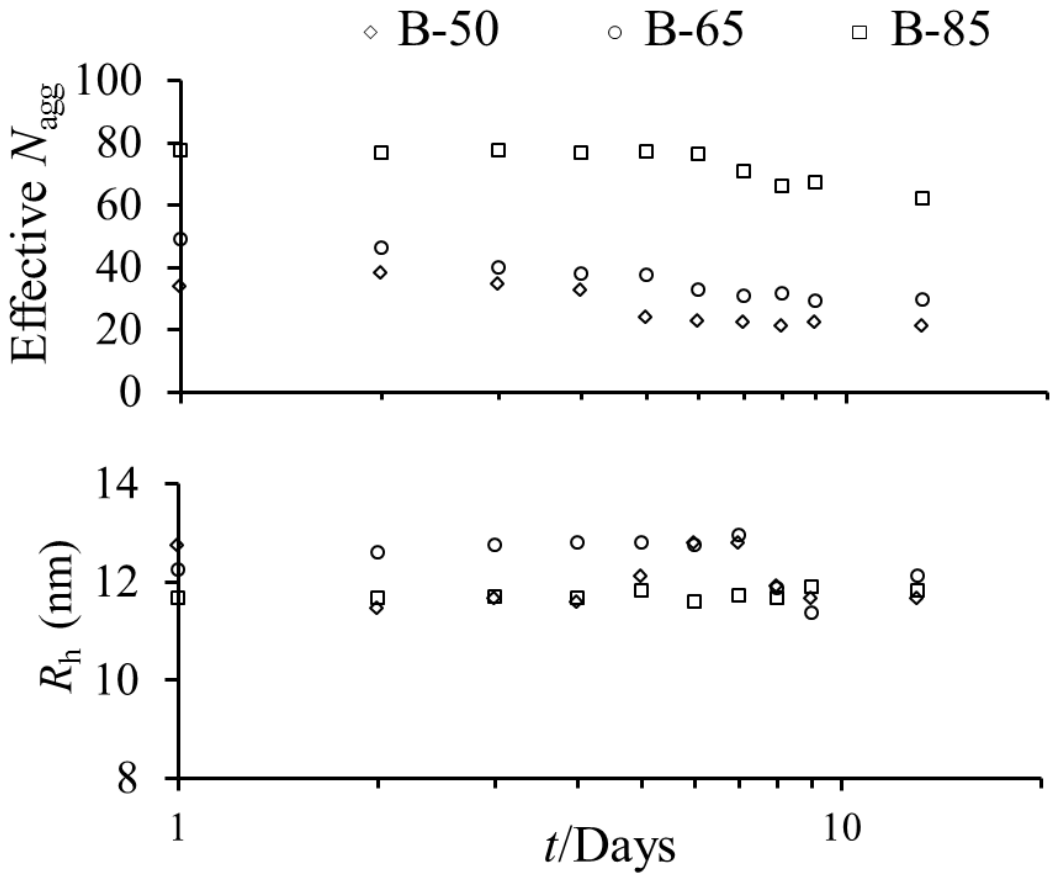

Figure 5.6. Evolution of aggregation number (N_{agg}) and hydrodynamic radius R_h with time upon blending using Method B;

As shown from the LLS results of Method B the polymer micelles must reorganise to form micelles composed of both P-91 and P32, Figure 5.6. An effective aggregation number is used to describe the combined scattering of the two polymer species in solution during the reorganisation, where a larger intensity of scattering will arise from the P-91 micelles. From Figure 5.6 the micelles initially present in solution are shown to decrease in effective aggregation number. A decrease in the effective N_{agg} value observed represents the decrease in the concentration of the larger P-91 micelles as these will have a larger scattering intensity in these light scattering experiments (eqn. 1.21). The decrease in the effective aggregation

number observed whilst maintaining a similar micelle size suggested that the reorganisation of the system occurs through a unimer exchange mechanism as opposed to a fusion of two micelles.

As confirmed in Chapter 4 the system is indeed not frozen but exchanges on a reasonable experimental time scale. Although the rate constants for the exchange dynamics were not extracted for the reorganisation of these blend systems it can still be observed that the reorganisation of chains, which occurred over days (Figure 5.6), is orders of magnitude slower than molecular surfactants, which typically occurs of minutes.[44] Moreover, it can be observed that the time needed to reach steady state differs between systems, for low DEAEMA incorporations (50%) the exchange dynamics are faster and steady state is reached earlier, whereas for higher DEAEMA loadings (85%) the time needed is longer, 4 and 8 days respectively. As previously mentioned it is believed that this reorganisation occurs through a unimer exchange mechanism.[30,45] With this hypothesis of a unimer exchange mechanism SAXS measurements over time were undertaken. SAXS analysis was used as it is able to probe much smaller length scales than light scattering, specifically the ability to probe the micelle cores directly which are believed to reorganise once the two polymer solutions, P-32 and P-91, are blended together. SAXS analysis was undertaken on the solution over time at defined time intervals once the solutions, P-32 and P-91, have been blended according to method B where $t = 0$ corresponds to the point of blending (Figure 5.7). When the SAXS profiles are compared with respect to time the first oscillation shows a shift to larger q values (For example from 0.042 $\dot{A}^{-1}$ to 0.046 $\dot{A}^{-1}$, Figure 5.7b).

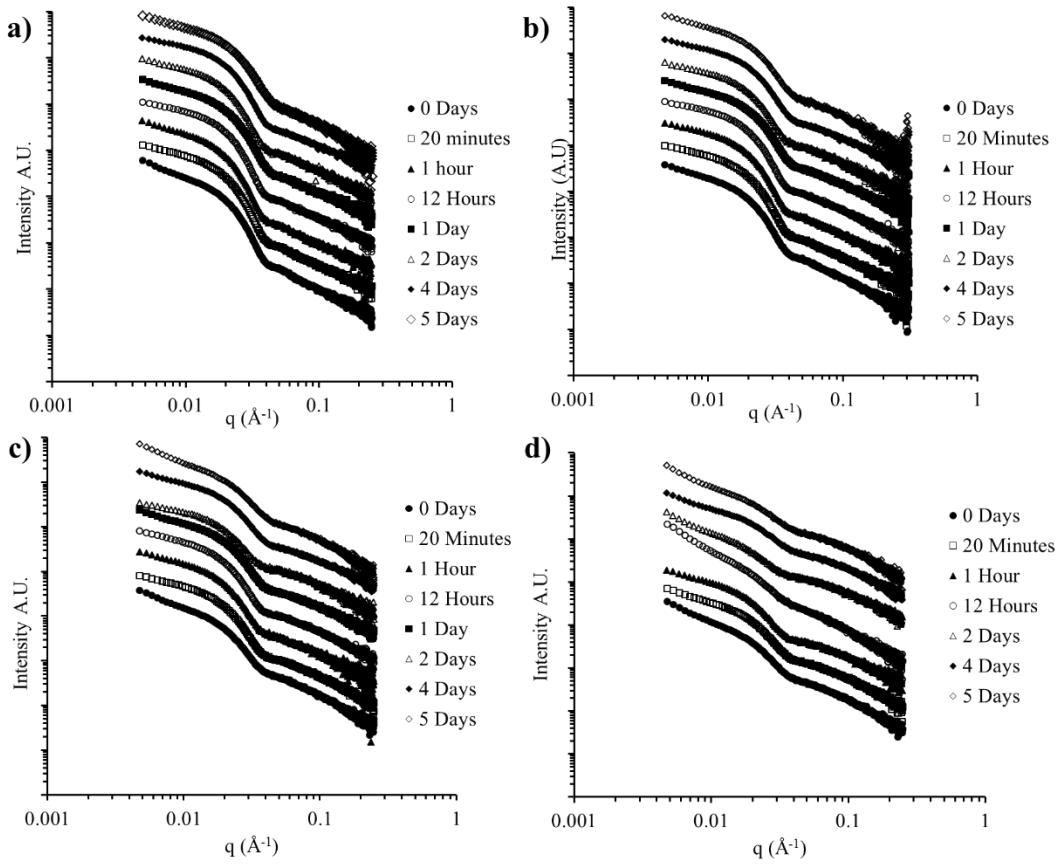

Figure 5.7 SAXS profiles of blend micelles formed by method B with time, 0 days indicates the start of the blending with method B. Plots have been shifted vertically for clarity. a) B-85, b) B-76, c) B-65, d) B-50.

By plotting the data with a Porod representation the shift in the first oscillation with time is much easier to observe, clearly highlighting the reorganisation, Figure 5.8. Moreover, the SAXS profiles show that the shapes of the profiles are similar throughout the reorganisation of the system, suggesting that the shape of the micelles remains similar throughout. The shift in the first minima in intensity is related to a change in core size. This shift in core size can then be related to a decrease in aggregation number for the formation of blended micelles using equation (2.1) which is then in agreement with the results obtained from laser light scattering.

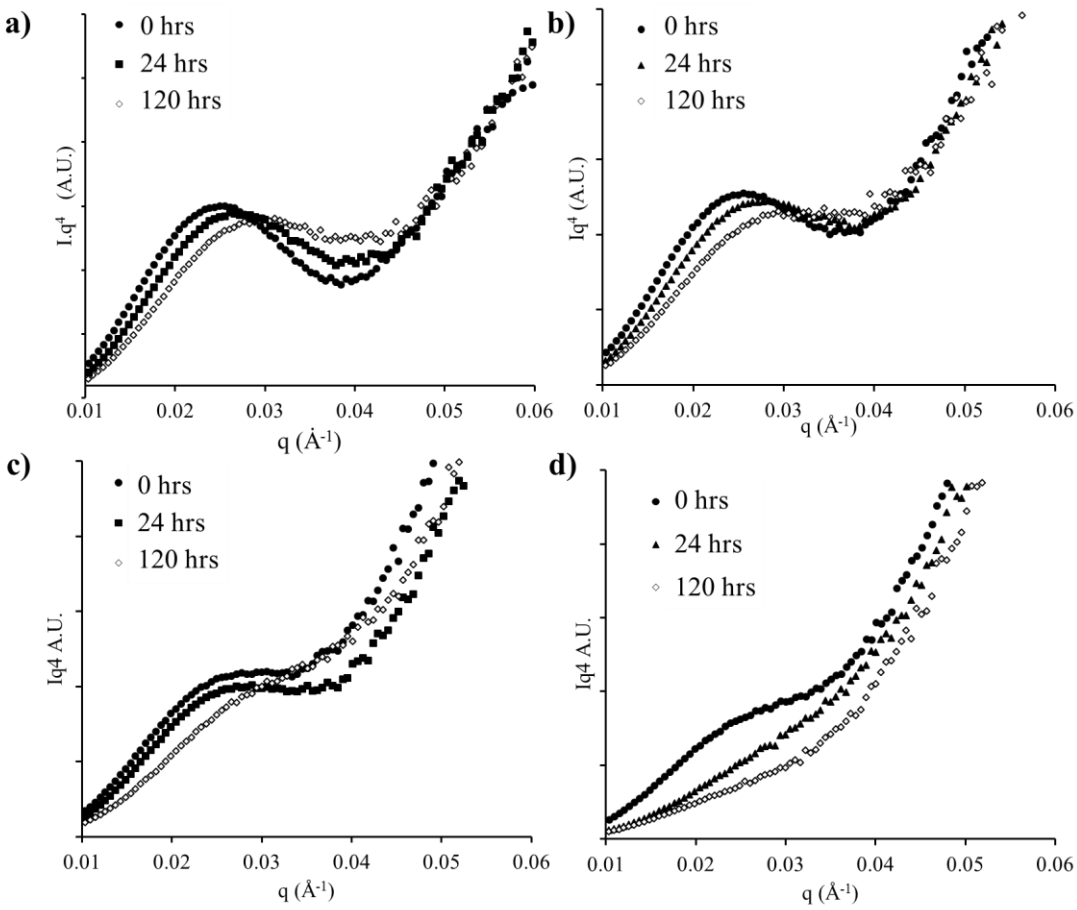

Figure 5.8. Porod representations of the SAXS data with time for Method B, some points have been omitted for clarity. a) B-85, b) B-76, c) B-65, d) B-50.

With the hypothesis of unimer exchange it is then proposed that the difference in kinetics in the reorganisation between the systems is a consequence of the concentration of the P-91 unimers and the rate limiting step is the exchange of P-91 between micelles, as these polymers have a much greater hydrophobicity and will have slower exchange times between micelles. As mentioned in the introduction Halperin and Alexander[46] documented that the energy barrier for unimer exchange for polymeric micelles is proportional to the length of the collapsed core block, $N_b^{2/3}$, and its interfacial tension between the associating block and the solvent, γ, in the form $E = \gamma N_b^{2/3}$. Therefore an increase hydrophobicity of the core forming block will lead to a higher energy barrier for molecular exchange and therefore slower kinetics.

Furthermore, after 14 days the structures formed from Method B were compared to those formed by Method A after 24 hrs, Figure 5.9 and as observed the structures formed are identical regardless of pathway. In addition these blend micelles were then compared to pure systems at the same core composition. As observed in Figure 5.9 regardless of pathway or if the system is pure or blended the micelle structures are identical.

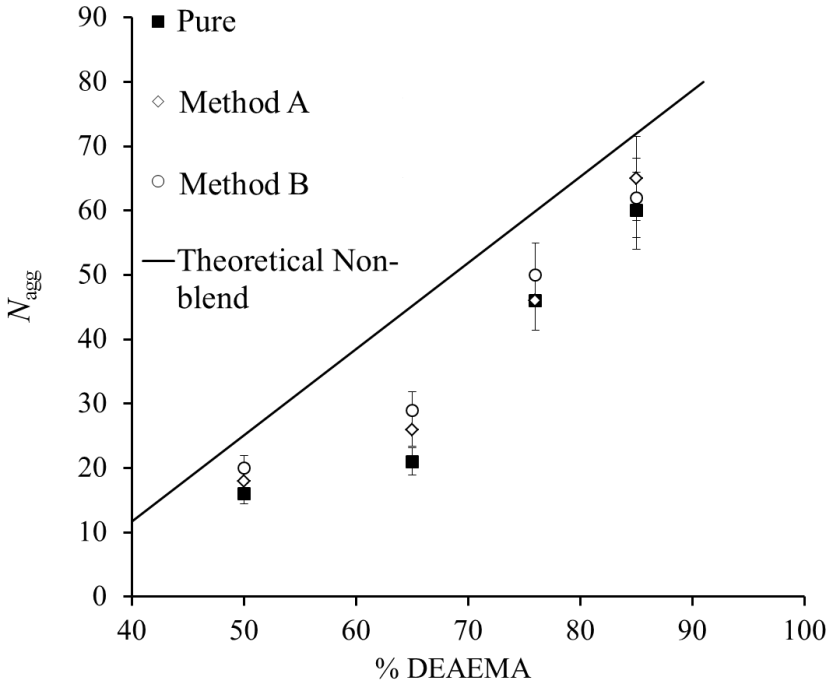

Figure 5. 9 a) Relationship of the aggregation number (N_{agg}) with % DEAEMA in the core for both assembly Methods A and B and theoretical aggregation number for non-blended micelles (straight line) from equation 5.2. Errors bars represent10% of the N_{agg} values

Although these blend micelles are structurally identical regardless of pathway, the solution may in fact be a mixture of pure micelles which have not blended, which is micelles that have only one polymer present. From light scattering a theoretical weight average aggregation number, which is a Theoretical non-blend value can be calculated (Equation 5.2) where C is the weight concentration of the solution, this value represents a solution of non-blended polymer micelles. When this value is compared to the values observed by the blend micelles in the final state the values strongly differ (Figure 5.9). Therefore it can be

concluded that, regardless of preparation pathway, these polymers can form blended micelles at $\alpha = 0$, which are identical to pure micelles formed at the same composition

$$N_{agg\ mix} = \frac{(C_{P-91}N_{agg\ P-91}) + (C_{P-32}N_{agg\ P-32})}{(C_{P-91} + C_{P-32})} \qquad (5.2)$$

5.3.4. Comparison of blend and pure micelles

5.3.4.1. Pyrene fluorescence critical aggregation concentration experiments on the P(DMAEMA-co-DEAEMA)-b-PDMAEMA diblock copolymers.

By using the steady state fluorescence spectroscopy of pyrene the formation of both the pure and blended micelles can be understood.[47,48] The critical aggregation concentration (CAC) of the pure and blend micelles were determined as the inflection point of the intensity ratio between 339 nm and 335 nm in the fluorescence emission spectra, an example plot for P-65 and B-65 is shown Figure 5.10. A clear difference in the steady state fluorescence results of pyrene between pure and blended systems with respect to DEAEMA mol% in the micelle core was observed Figure 5.11a. For the pure micelles as the DEAEMA content increased the critical aggregation concentration (CAC) decreased. However, the contrary is seen for the blended systems as all DEAEMA core loadings show very similar CAC values, approximately 4.9×10^{-4} mol/dm^3, which is comparable to the pure micelle system for P-91 (Figure 5.11a).

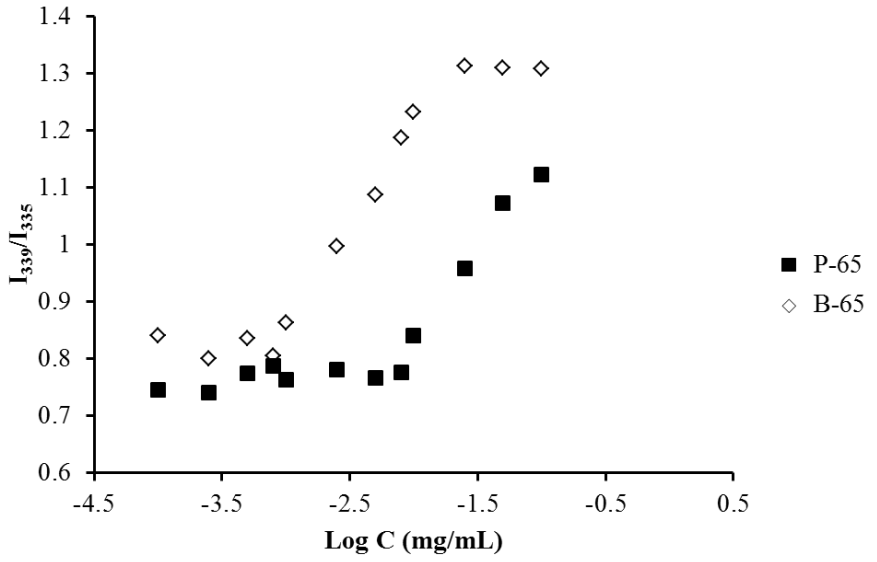

Figure 5.10. Intensity ratio I_{339}/I_{335} from the steady state fluorescence of pyrene as a function of polymer concentration data shown is for B-65 and P-65.

Plotting the concentration of P-91 in the blended system at the CAC for the micelles we observe that the values are extremely similar to one another (Figure 5.11b). At this point these results indicate that two scenarios are possible, the first is that the behaviour represents a true CAC and the second is that apparent CAC values may be due to the partition equilibrium of pyrene between the micelle cores and the aqueous solvent.[49]

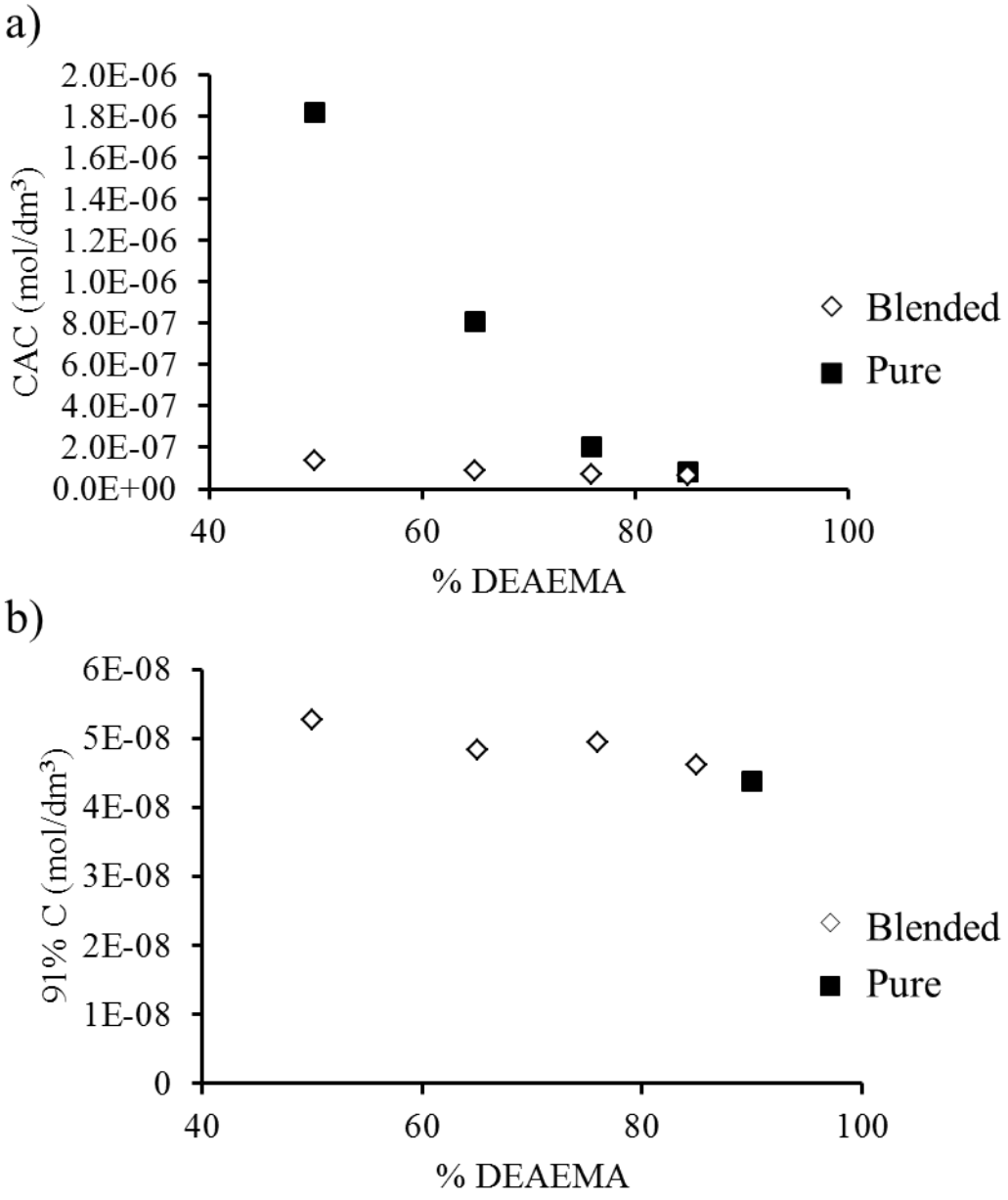

Figure 5.11 a) Relation of % DEAEMA in the core with critical aggregation concentration (CAC) values for pure and blended samples; b) Relation of % DEAEMA with the concentration of 91 % DEAEMA at the critical aggregation concentration (CAC).

Firstly, as the DEAEMA content decreases in the pure micelles there is a decrease in the core hydrophobicity. This decrease in core hydrophobicity means that pyrene is less efficiently encapsulated within the cores and the partition equilibrium is shifted and a higher CAC is observed. However for the blended system a different scenario is present, here it can be deduced that the P-32 polymer can encapsulate negligible levels of pyrene whereas the P-91 polymer can encapsulate much larger amounts of pyrene. Therefore only when P-91 polymer micelles are present can pyrene effectively partition into the core. The second scenario which could occur is that the true CAC for the micelles is observed. For the pure system a decrease in CAC with DEAEMA is to be expected due to the increased hydrophobicity of the polymer chains and incompatibility with the solvent. Hence, micelles with high DEAEMA content form at lower concentrations. However, the results from Figure 5.11b for the blended micelle systems show a different CAC behaviour, specifically a distinct two step mechanism. Firstly, the association of the polymers with the highest DEAEMA core block incorporation (P-91) occurs, followed secondly by the incorporation of the copolymer with the lower DEAEMA content (P-32) to form the blended micelle. In this final scenario a true CAC was observed but is that for blended micelles, the highly hydrophobic character of P-91 triggers the formation of blended micelles, as soon as P-91 beings to form P-32 simultaneously assembles cooperatively. Similar two step mechanisms for the association of blend micelles have been observed before.[33]

5.3.4.2. Comparisons of micelle structures for P(DMAEMA-co-DEAEMA)-b-PDMAEMA diblock copolymers

The P(DMAEMA-*co*-DEAEMA)-*b*-PDMAEMA diblock copolymers which successfully form blend micelles once equilibrium was reached were structurally compared further to those micelles obtained with a pure diblock copolymer matching the average chemical composition of the blend.

Figure 5.12 contains representative cryo-TEM micrographs of both pure and blend micelles for 85-50 % DEAEMA incorporation in the micelle core. The cryo-TEM images clearly show irrespective of whether the blend or direct synthesis method is utilised that spherical star-like micelles are formed in both cases (Figure 5.12 a-h). Furthermore these micelles exhibit low dispersity and no difference in the size distribution of micelles was observed indicating that all micelles reach the same energetic state (Figure 5.2 i and j show example distributions and radial plot profiles of P-85 and B-85). Similar core sizes were observed between pure and blended micelles for these DEAEMA core block incorporations. Therefore given the similarities between the core sizes it can be assumed that both diblock copolymers are evenly distributed throughout the blend micelles in solution, as differences in the distribution of chains would lead to bimodal populations or clustering, thus indicating cooperative micellization.[36] Moreover, as both systems are observed to be identical and one population is observed, cooperative micellization is believed to be a consequence of these systems reaching equilibrium.[50,51] To understand the dimensions and nanostructure of both the core and corona of these star-like micelles further detailed laser light scattering and small angle X-ray scattering techniques (LLS and SAXS) were undertaken.

a)

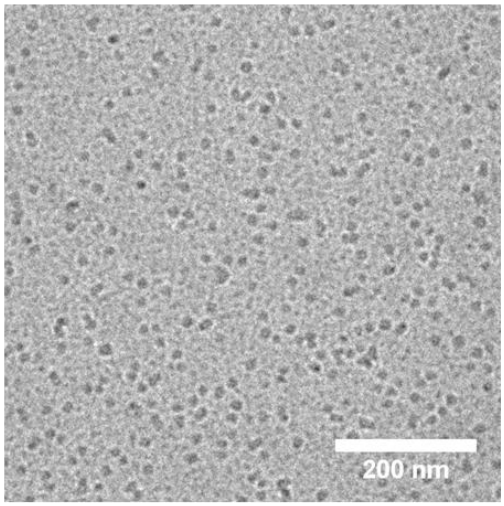

b)

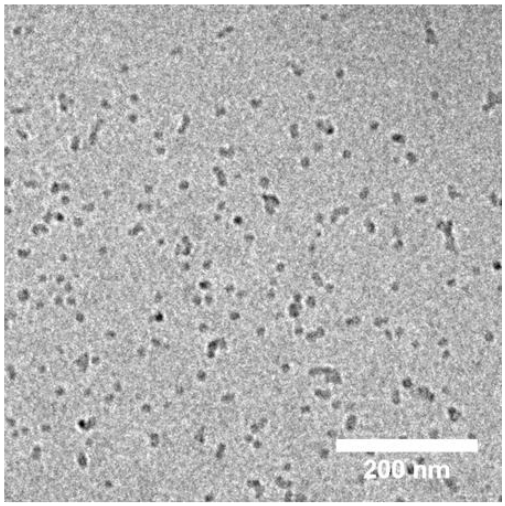

c)

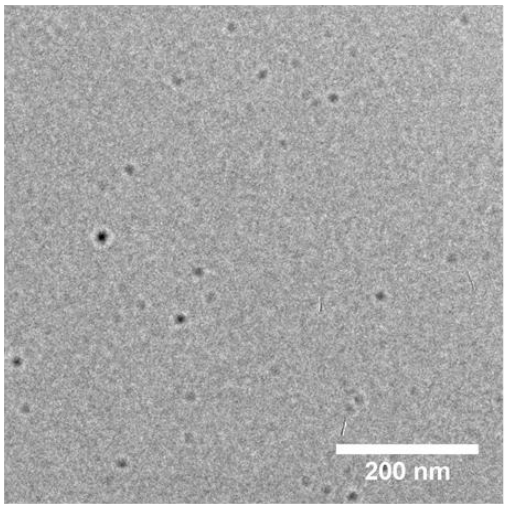

d)

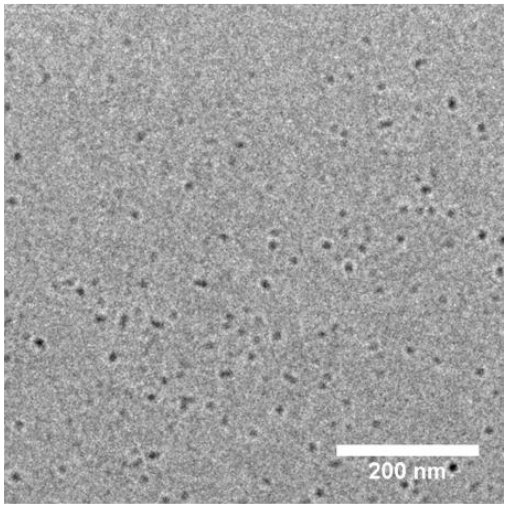

e)

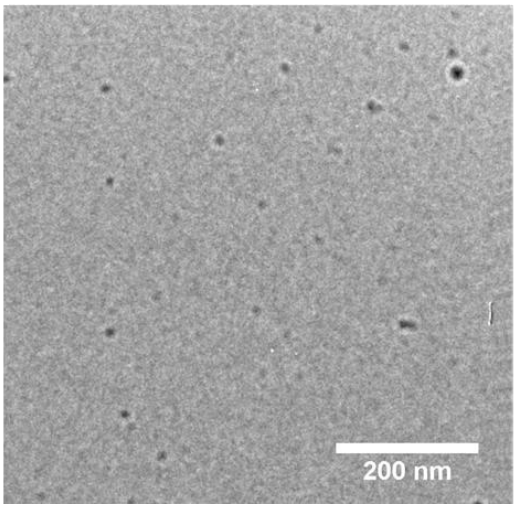

f)

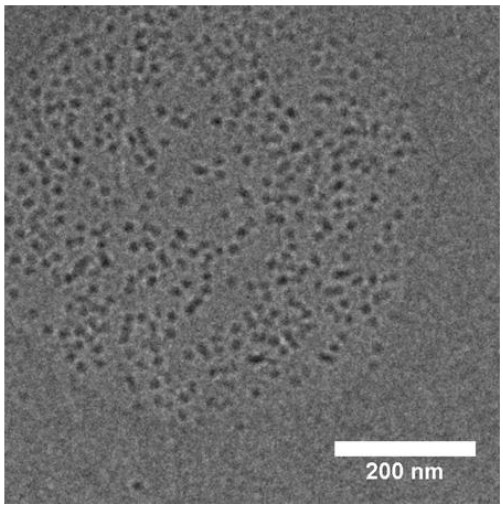

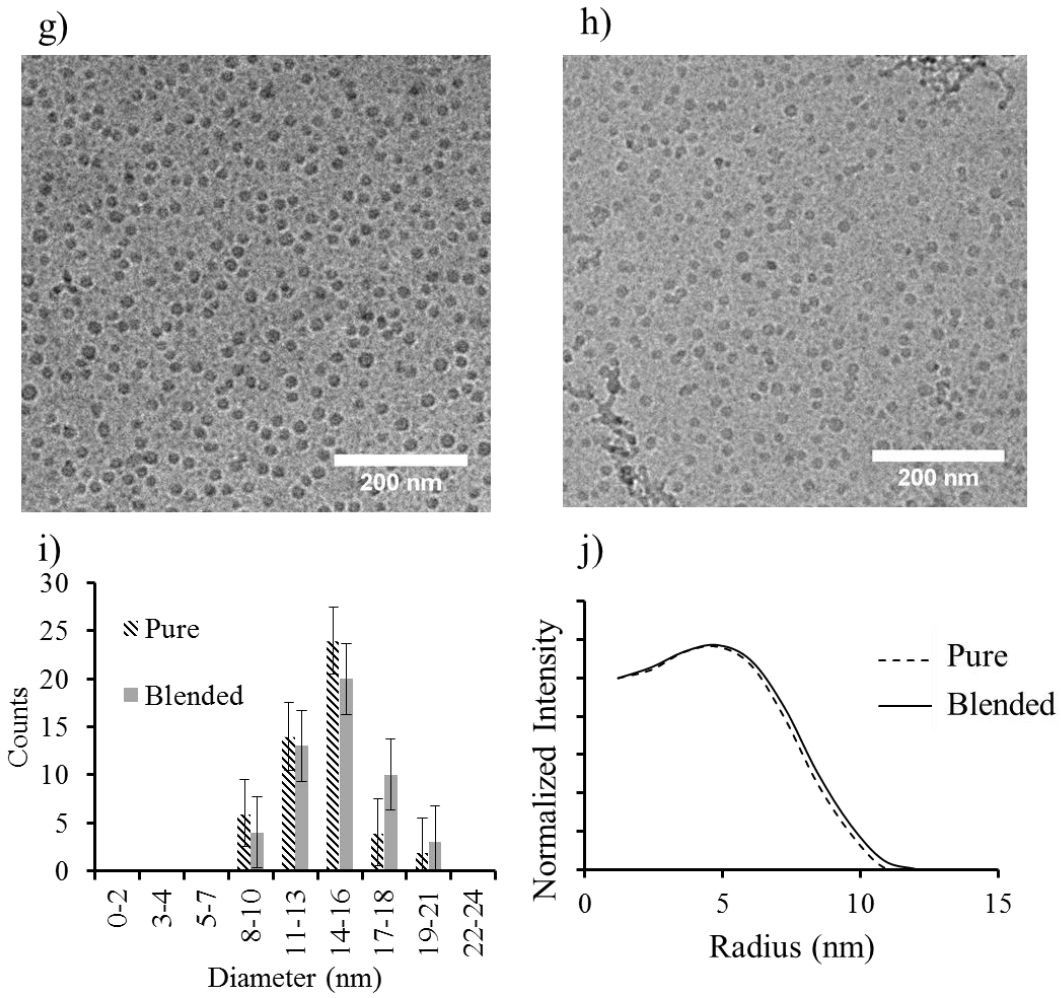

Figure 5.12 Cryo-TEM analysis of both pure and blend micelles; a) image of P-50; b) image of B-50; c) image of P-65; d) image of B-65; e) image of P-76; f) image of B-76; g) image of P-85; h) image of B-85; i) histograms of the core diameter for both P-85 and B-85 samples, error bars calculated from Poisson error. j) Radial plot profiles from cryo-TEM for both P-85 and B-85 samples (averaged over 50 particles).

Detailed laser light scattering and small angle X-ray scattering analysis reveals that the blend micelles are structurally indistinguishable from a pure micelle sample as shown in Figures 5.13 and 5.14. Dynamic light scattering (DLS) was used to analyse the distribution of relaxation times for the micelles in solution, Figure 5.13. The Gaus-Gex routine[52] was used to determine the distribution of relaxation times of these systems. Only one mode of relaxation is seen for all systems which can be attributed to the single micelle population in solution. By analysing the relaxation time distributions from both the blended and pure assembly, as shown in Figure 5.13a-5.13d, it can be observed that the blend and pure

systems gave very similar distributions in solution, yet most notable is the fact that the blended sample shows a lower dispersity (for example 1.08 *versus* 1.10 for the B-76 and P-76 systems respectively) than the synthesised diblock. Moreover, from DLS studies of both the blend and pure micelles no difference was observed in the size of the aggregates in solution between the blend and the pure micelle samples (Figure 5.13e). The slight decrease in R_h with lower DEAEMA content can be attributed to a reduction of coronal chain stretching from a lower aggregation number.[53,54]

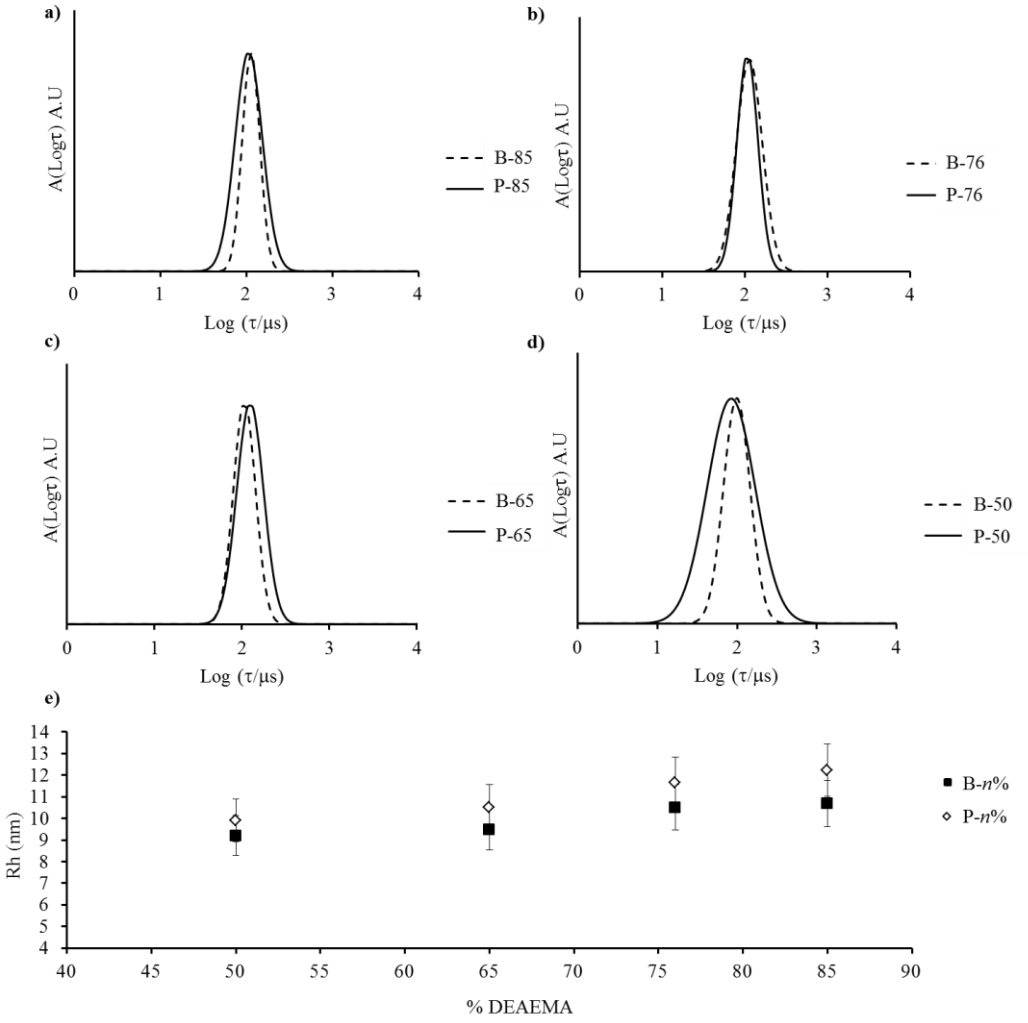

Figure 5.13 a) Relaxation time distribution of P-85 and B-85 at α = 0 in 0.1 M NaCl, θ = 130° b) Relaxation time distribution of P-76 and B-76 at α = 0 in 0.1 M NaCl, θ = 130° c) Relaxation time distribution of P-65 and B-65 at α = 0 in 0.1 M NaCl, θ = 130° d) Relaxation time distribution of P-50 and B-50 at α = 0 in 0.1 M NaCl, θ = 130°e) dependence of hydrodynamic radius (R_h) with % DEAEMA in the core domain. Errors bars are calculated from 10% of the R_h values;

Again small angle X-ray scattering analysis reveals that the blend micelles are structurally indistinguishable from a pure micelle sample (Figure 5.14). In Figure 5.14, it should be noted that 50% DEAEMA does show a difference between the blend and pure micelles by SAXS analysis. At this composition, the pure micelles have a very hydrophilic core and will subsequently only weakly associate with a very weak contrast between the core and corona. On the other hand, the blend micelles are composed of P-91 which is a highly aggregating species at $\alpha = 0$, and as such it is possible that P-91 gives a platform for assembly providing an increased core-corona contrast for the blend assembly. Other analysis techniques confirm the structural similarity between blend and pure micelles at 50% DEAEMA. It can then be deduced that equilibrium is reached for these P(DMAEMA-*co*-DEAEMA)-*b*-PDMAEMA diblock copolymers as only one population is observed throughout, which when the DEAEMA content is above 50%, is identical regardless of pathway and for a range of compositions.[50,51]

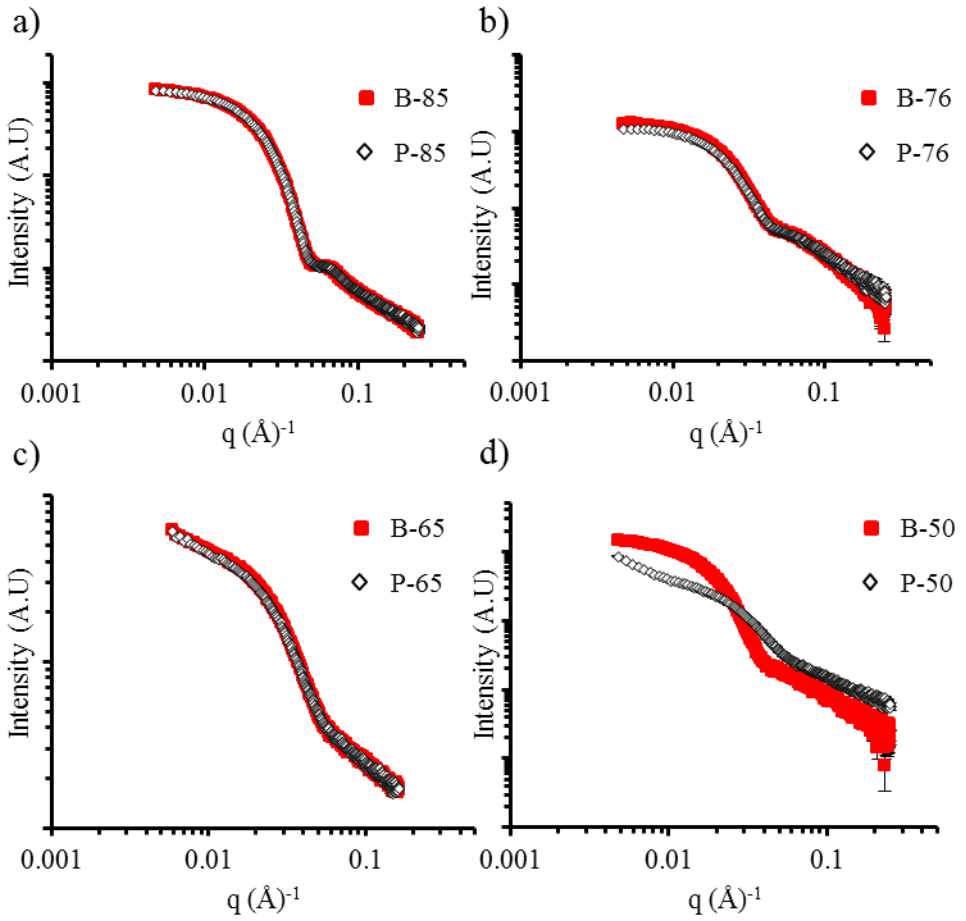

Figure 5.14) SAXS profiles of blended and pure samples in NaCl 0.1 M. a) 85% DEAEMA; b) 76% DEAEMA; c) 65% DEAEMA; d), 50% DEAEMA. Note that for the 85%, 76% and 65% samples, the profiles superimpose for the blended and pure solutions.

Both SAXS and cryo-TEM have the benefit of being able to directly probe the core size of the micellar aggregates compared to LLS which allows a theoretical core size to be calculated using equation 2.1. This allows a comparison of three techniques (LLS, cryo-TEM and SAXS) to fully analyse the blended and pure micelles. As observed in figure 5.15 the core sizes from cryo-TEM and SAXS give very similar results and trends, that regardless of core composition the core size remains constant. However, larger sizes are observed by cryo-TEM and SAXS when compared to the core size calculated from N_{agg} determined by LLS. It is believed that this difference in core size from LLS can be attributed to the small contrast

difference between the core and corona, therefore the corona is partially seen in cryo-TEM and SAXS.[55]

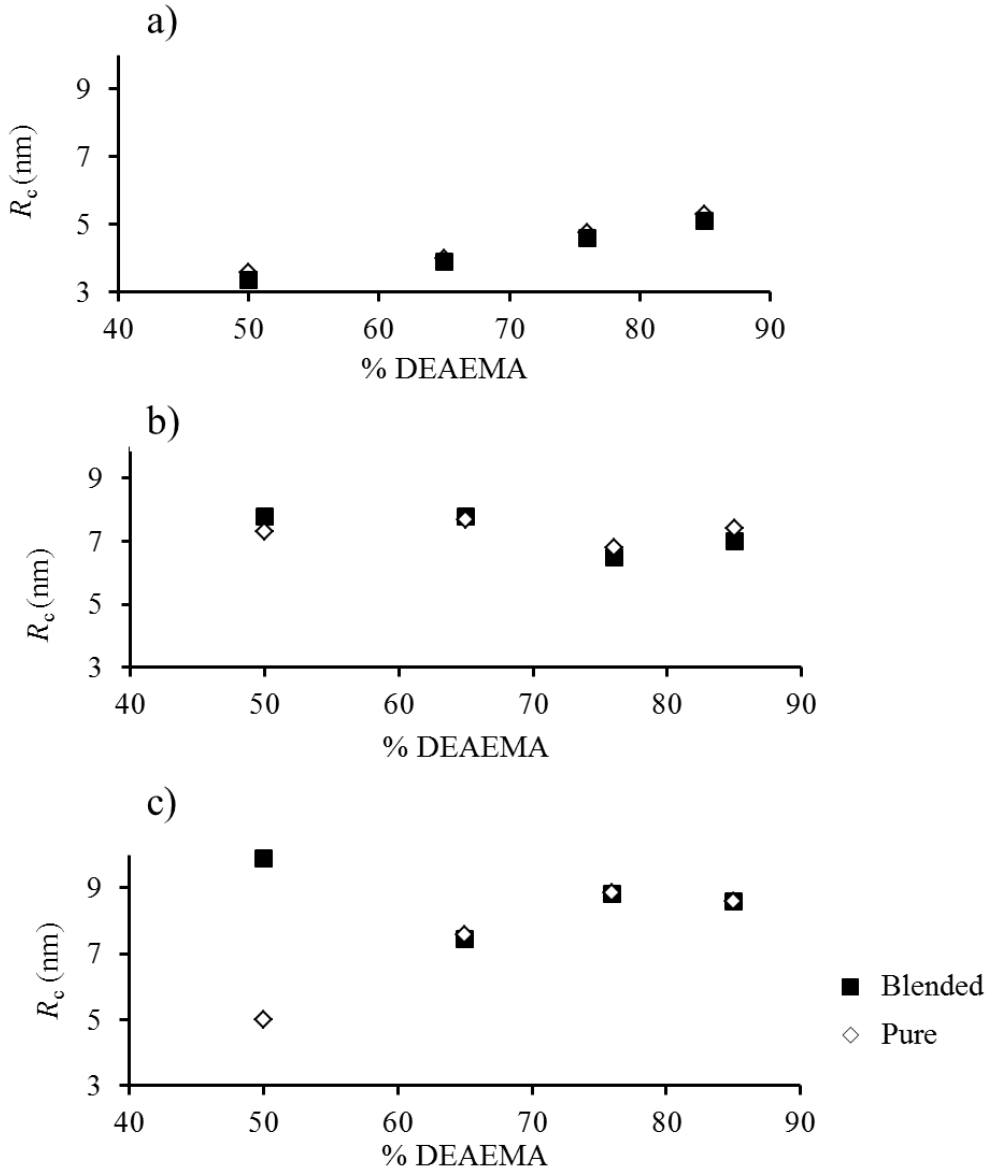

Figure 5.15. Comparison of core sizes from a) LLS b) cryo-TEM, and c) SAXS for blend and pure micelles.

A general trend observed from the core size determined by LLS is that a decrease in DEAEMA content (from 85% to 50%) gave smaller core sizes (Figure 5.15a). The core size determined from LLS is calculated assuming that the density of the core is equal to that of

the bulk density of the two monomers and is assumed to be independent of copolymer composition. However, by using a combination of LLS and cryo-TEM the core density can be explored further with equation 2.1; specifically a decrease in core density is attributed to an increase in the hydration of the core. This core density analysis was explored using a combination of *Z*-average core sizes from cryo-TEM and N_{agg} values from LLS to predict the core density using equation 2.1 in a similar manner to Piogé *et al*.[56] However, the calculated core densities, approximately < 0.2 g/mL (Table 5.3), are surprisingly much lower than the density of the monomers (approximately 1.08 g/mL). The low density is believed to then be too low to provide significant contrast for cryo-TEM, it can be suggested that the crowded coronal chains near the core-corona interface may be visible and account for the larger core sizes observed. Moreover, the difference in the scattering length densities between the two components for SAXS analysis is extremely small too (4.8×10^{-8} $\dot{A}^{-2}$) which results in a portion of the coronal chains being included in the core size when analysed by SAXS.

Table 5.3. Additional micelle scattering characterisation data for all blend and pure samples at α = 0 in 0.1 M NaCl solution.

	N_{agg} ±10 %	R_h (nm) ±10 %	$R_{c\ LLS}$ (nm)[a]	Coronal Stretching (%)[b]	$R_{c\ cryo\text{-}TEM}$ (nm)	$R_{c\ SAXS}$ (nm)	Core density based on cryo-TEM (g/L) [c]
P-85	60	10.7	5.1	64	7.8	8.6	0.17
P-76	46	10.5	4.6	70	7.8	8.8	0.12
P-65	21	9.5	3.9	64	6.5	7.6	0.09
P-50	16	9.2	3.3	73	7.0	5.0	0.05
B-85	65	12.2	5.3	87	7.3	8.6	0.20
B-76	46	11.7	4.8	86	7.7	8.8	0.14
B-65	26	10.5	3.9	74	6.8	7.5	0.09
B-50	18	9.9	3.5	87	7.4	9.9	0.06

[a]Calculated from equation 2.1 assuming a core density of 1 g/L. [b](R_{hDLS}-R_{cSLS})/$L_{contour,DMAEMA}$ [c] Calculated from equation 2.1 using R_c from cryo-TEM and N_{agg} from SLS.

Using the combination of cryo-TEM, SAXS and LLS a spherical morphology can be further confirmed. As observed by cryo-TEM the particles are clearly spherical in nature, however, due to contrast variations the true nature of these spherical particles cannot be further deduced from microscopy. Therefore a simple core-corona model can be used with LLS; as such the dimensions from this model are consistent with a spherical micelle morphology where the coronal chains are moderately stretched but most notable is that structurally with this model the pure and blend micelles show almost identical structural characteristics (Table 5.3).

5.4. Conclusions

The blending method for micelle assembly introduced in this Chapter provides a simple and effective route to modifying and achieving a range of defined nanoscale assemblies in aqueous solution without laborious synthetic approaches. By blending two copolymers with high and low incorporations of hydrophobic monomer a variety of polymeric micelles with varying hydrophobic compositions can be obtained. This strategy could in particular be used to screen rapidly the effect of the co-monomer composition on the characteristics of the self-assembled nanostructures without the need of a phase diagram, by only synthesising two polymers with significantly differing compositions and then blending them. By a combination of cryo-TEM, laser light and small angle X-ray scattering methods, these blended micelles were found to be structurally identical to pure micelles with the same composition formed from a single polymer system. This work represents a significant advantage over traditional approaches for the preparation of spherical nanostructures with specific structural characteristics as it requires minimal synthesis and allows for access to the full range of copolymer compositions through a simple blending approach.

5.5. Acknowledgements

Dr Joseph Patterson conducted the cryo-TEM experiments and assisted with data analysis. Dr Anaïs Pitto-Barry conducted the SAXS experiments and did the model fitting.

5.6. Experimental

5.6.1. Materials

Monomers were filtered through a plug of silica prior to use and stored at 4 °C. AIBN (2,2'-azo-bis(isobutyronitrile)) was recrystallised from methanol and stored in the dark at 4 °C. All other materials were used as received from Aldrich, Fluka, or Acros. HCl (1 M) and NaOH (1 M) were calibrated and standardised using tris(hydroxymethyl)-aminomethane and potassium hydrogen phthalate respectively. P(DMAEMA-*co*-DEAEMA)-*b*-PDMAEMA diblock copolymers were synthesised by RAFT and characterised by ^{1}H NMR spectroscopy and SEC as previously reported in Chapter 4.

5.6.2. Preparation of the aqueous solutions

5.6.2.1. Preparation of P(DEAEMA-co-DMAEMA)-b-PDMAEMA diblock copolymer micelles

5.6.2.1.1. Pure micelle samples

Pure micelle assembly was performed by diluting stock polymer solutions that were prepared at 20 g/L by dispersing the polymer in 18.2 MΩ.cm water containing the appropriate amount of HCl to reach α = 1, where α is defined as $\alpha = [NR_2H^+]/[NR_{2Total}]$. After one night of stirring α was lowered to α = 0 by the addition of the required amount of 1 M NaOH and the solutions were stirred again overnight, after which time the NaCl concentration was adjusted to 0.1 M by the addition of 4 M NaCl. The solutions were further stirred overnight before analysis.

5.6.2.1.2. Blended micelle samples

Two methods for the preparation of the binary solutions were used.

Method A (unimer blending) consisted of mixing dry bulk polymer samples together. These dry powders were then used to produce polymer solutions at 10 g/L which were prepared by

dispersing the two polymer powders in 18.2 MΩ water containing the appropriate amount of HCl to reach α = 1 to give a solution of blended unimers in a good solvent. After one night of stirring α was lowered to 0 by the addition of the required amount of 1 M NaOH and the solutions were stirred again overnight, after which time the NaCl concentration was adjusted to 0.1 M by the addition of 4 M NaCl. The solutions were further stirred overnight before being analysed.

Method B (micelle blending) involved making individual polymer solutions of 32% DEAEMA or 91% DEAEMA copolymers at α = 0 using the same protocol as for the pure micelle samples, at a concentration of 2.5 g/L. These solutions were then mixed together at desired stoichiometric ratios and stirred to give the targeted % DEAEMA and then stored at room temperature.

5.6.3. Micelle Characterisation

5.6.3.1. Refractive index increment

The specific refractive index increments (dn/dC) of the polymers in water were measured on a refractometer (Bischoff RI detector and a Shodex RI−101 RI detector) operating at a wavelength of 632 nm.

5.6.3.2. Laser light scattering

Measurements were performed at angles of observation ranging from 20° up to 130° with an ALV CGS3 setup operating at λ_0 = 632 nm and at 20 °C ± 1 °C. Data were collected in duplicate with 240 s run times. Calibration was achieved with filtered toluene and the background was measured with filtered solvent (NaCl 0.1 M solution).

5.6.3.3. Dynamic light scattering (DLS)

The intensity autocorrelation functions $g_2(t)$ obtained from dynamic light scattering were related to $g_1(t)$ (the normalised electric field autocorrelation functions) *via* the so-called Siegert relation. Then $g_1(t)$ was analysed in terms of a continuous distribution of relaxation

times (eqn. 1.18 using the REPES routine[58] without assuming a specific mathematical shape for the distribution of the relaxation times (A(τ)).When comparing micelle distributions directly to one another the Gaus-GEX routine was used.[52] The apparent diffusion coefficient *D* was calculated from eqn. 1.16 given that the average relaxation rates Γ of the scatterers were q^2 dependent, where q is the scattering vector given by $q=(4\pi n/\lambda_0).\sin(\theta/2)$ with θ the angle of observation and n = 1.333 the refractive index of the solvent (water). Its concentration dependence is given by $D = D_0(1+k_DC)$ where k_D is the dynamic second virial coefficient and D_0 the diffusion coefficient used for computing the hydrodynamic radius (R_h) of the scatterers according to the Stokes-Einstein eqn. 1.19. With η the solvent viscosity, k the Boltzmann's constant and T the absolute temperature. Values of R_h given in the following are then obtained after extrapolation to zero concentration.

5.6.3.4. Static light scattering (SLS)

The Rayleigh ratio of the solutions have been measured using toluene as a reference according to eqn. 1.12 where I_i represents the intensity scattered by species i and $R_{toluene}$ is the Rayleigh ratio of the reference. In dilute solutions if $R_g.q < 1$ where R_g is the radius of gyration, the q and concentration dependence of R_θ is given by eqn 1.10, where A_2 is the second virial coefficient and M_w the weight average molecular weight. *K* is an optical constant given by eqn 1.11. Where $n_o = 1.496$ is the refractive index of the reference liquid (toluene), dn/dC is the specific refractive index increment determined by differential refractometry (see Table 4.1) and N_A is Avogadro's number. Values of M_w are then obtained after extrapolation to zero concentration and zero angle and used to derive the aggregation number of the micellar aggregates $N_{agg} = M_w/M_{w,unimers}$. For spherical morphologies, it is possible to deduce the core radius, R_c, from the aggregation number, using equation (2.1) assuming the core block is dehydrated and the density matches that of the bulk value, ρ.[68] When in some cases two modes of relaxation were observed by DLS measurements, R_θ was described as the sum of two contributions according to eqn. 1.25, where f and s stand

respectively for fast and slow modes and using 1.26. Where A_f and A_s are the relative amplitudes of the fast and slow modes obtained by DLS. The slow mode of relaxation observed can be attributed to spurious aggregates with a negligible weight fraction but larger scattering intensity.[55,69]

5.6.3.5. Small angle X-ray scattering (SAXS)

Measurements were performed at the Australian Synchrotron facility at a photon energy of 11 keV. The samples in solutions of 0.1 M NaCl were analysed at a sample to detector distance of 3.252 m to give a q range of 0.004 to 0.2 $Å^{-1}$. The scattering from a blank (aqueous solution of NaCl 0.1 M) was measured in the same location as the sample collection and was subtracted for each measurement. Data were normalised for total transmitted flux using a quantitative beamstop detector and absolute scaled using water as an absolute intensity standard. The two-dimensional isotropic SAXS images were converted into one-dimensional SAXS scattered intensity profiles ($I(q)$ versus q) by circular averaging. The functions used for the fitting from the NCNR package[62] were "Guinier-Porod"[63,64], "Polycore Form"[64] and "Debye".[65] Scattering length densities (SLD) were calculated using the "Scattering Length Density Calculator"[66] provided by the NIST Center for Neutron Research. A linear summation of the PolyCoreShell ratio model and the Debye model is used and has the following parameters (K0 to K7 for the PCR model, K8 to K10 for the Debye model):

K0 scale

K1 average core radius (Å)

K2 average shell thickness (Å), not used in this model

K3 overall polydispersity

K4 scattering length density (SLD) core (Å-2)

K5 SLD shell (Å-2), not used in this model

K6 SLD solvent (Å-2)

K7 background (cm-1)

K8 scale

K9 Rg (Å), used in this model as a hydrated thickness, and as unimers in solution for the kinetics early data points

K10 background (cm-1)

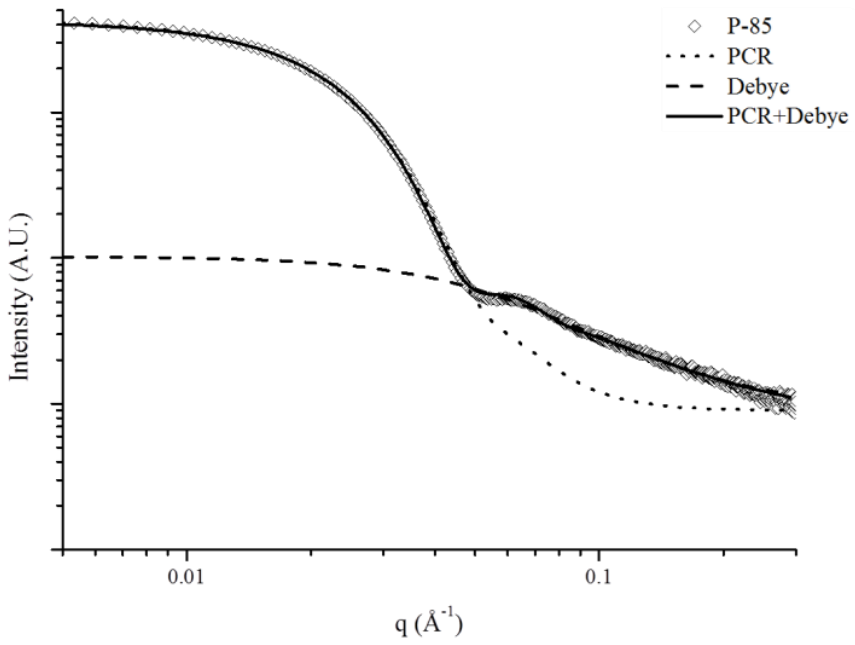

Figure 5.16. SAXS profile of P-85 showing the Debye model fit, PolyCoreShell model fit and a linear summation of the PolyCoreShell and Debye model fit.

5.6.3.6. Cryogenic transmission electron microscopy samples (cryo-TEM)

Cryo-TEM was conducted on a FEI Sphera microscope operated at 200 keV. 3.5 μL of sample were added to freshly glow discharged Quantifoil R2/2 TEM grids. The grids were blotted with filter paper under high humidity to create thin films and rapidly plunged into liquid ethane. The grids were transferred to the microscope under liquid nitrogen and kept at < -175 ^{o}C while imaging.

5.7. References

(1) Moughton, A. O.; Hillmyer, M. A.; Lodge, T. P. *Macromolecules* **2011**, *45*, 2.
(2) Gröschel, A. H.; Schacher, F. H.; Schmalz, H.; Borisov, O. V.; Zhulina, E. B.; Walther, A.; Müller, A. H. E. *Nat. Commun.* **2012**, *3*, 710.
(3) Rees, P.; Wills, J. W.; Brown, M. R.; Tonkin, J.; Holton, M. D.; Hondow, N.; Brown, A. P.; Brydson, R.; Millar, V.; Carpenter, A. E.; Summers, H. D. *Nat. Methods* **2014**, *11*, 1177.
(4) Hamley, I. W. *The Physics of Block Copolymers* OUP Oxford, 1998.
(5) Nicolai, T.; Colombani, O.; Chassenieux, C. *Soft Matter* **2010**, *6*, 3111.
(6) Lund, R.; Willner, L.; Richter, D.; Dormidontova, E. E. *Macromolecules* **2006**, *39*, 4566.
(7) Stejskal, J.; Hlavatá, D.; Sikora, A.; Konňák, Č.; Pleštil, J.; Kratochvíl, P. *Polymer* **1992**, *33*, 3675.
(8) Choi, S.-H.; Lodge, T. P.; Bates, F. S. *Phys. Rev. Lett.* **2010**, *104*, 047802.
(9) Jain, S.; Bates, F. S. *Macromolecules* **2004**, *37*, 1511.
(10) Won, Y. Y.; Davis, H. T.; Bates, F. S. *Macromolecules* **2003**, *36*, 953.
(11) Petzetakis, N.; Walker, D.; Dove, A. P.; O'Reilly, R. K. *Soft Matter* **2012**, *8*, 7408.
(12) Petzetakis, N.; Dove, A. P.; O'Reilly, R. K. *Chem. Sci.* **2011**, *2*, 955.
(13) Shedge, A.; Colombani, O.; Nicolai, T.; Chassenieux, C. *Macromolecules* **2014**, *47*, 2439.
(14) Charbonneau, C.; De Souza Lima, M. M.; Chassenieux, C.; Colombani, O.; Nicolai, T. *Phys. Chem.Chem. Phys.* **2013**, *15*, 3955.
(15) Colombani, O.; Lejeune, E.; Charbonneau, C.; Chassenieux, C.; Nicolai, T. *J. Phys. Chem. B* **2012**, *116*, 7560.
(16) Dutertre, F.; Boyron, O.; Charleux, B.; Chassenieux, C.; Colombani, O. *Macromol. Rapid Commun.* **2012**, *33*, 753.
(17) Charbonneau, C. ; Chassenieux, C.; Colombani, O.; Nicolai, T. *Macromolecules* **2011**, *44*, 4487.
(18) Lejeune, E.; Chassenieux, C.; Colombani, O. *Prog. Colloid Polym. Sci.* **2011**, 138, 7
(19) Lejeune, E.; Drechsler, M.; Jestin, J.; Muller, A. H. E.; Chassenieux, C.; Colombani, O. *Macromolecules* **2010**, *43*, 2667.
(20) Bendejacq, D. D.; Ponsinet, V. *J. Phys. Chem. B* **2008**, *112*, 7996.
(21) Bendejacq, D. D.; Ponsinet, V.; Joanicot, M. *Langmuir* **2005**, *21*, 1712.
(22) Moore, B. L.; O'Reilly, R. K. *J. Polym. Sci. A Polym. Chem.* **2012**, *50*, 3567.
(23) Hayward, R. C.; Pochan, D. J. *Macromolecules* **2010**, *43*, 3577.
(24) Yu, Y. S.; Zhang, L. F.; Eisenberg, A. *Macromolecules* **1998**, *31*, 1144.
(25) Mai, Y.; Eisenberg, A. *Chem. Soc. Rev.* **2012**, *41*, 5969.
(26) Renou, F.; Nicolai, T.; Nicol, E.; Benyahia, L. *Langmuir* **2008**, *25*, 515.
(27) Repollet-Pedrosa, M. H.; Mahanthappa, M. K. *Soft Matter* **2013**, *9*, 7684.
(28) Borovinskii, A. L.; Khokhlov, A. R. *Macromolecules* **1998**, *31*, 7636.
(29) Hillmyer, M. A. *J. Polym. Sci. B Polym. Phys.* **2007**, *45*, 3249.
(30) Lu, J.; Bates, F. S.; Lodge, T. P. *ACS Macro Lett.* **2013**, *2*, 451.
(31) Tian, M. M.; Qin, A. W.; Ramireddy, C.; Webber, S. E.; Munk, P.; Tuzar, Z.; Prochazka, K. *Langmuir* **1993**, *9*, 1741.
(32) Palyulin, V. V.; Potemkin, I. I. *Macromolecules* **2008**, *41*, 4459.
(33) Sens, P.; Marques, C. M.; Joanny, J. F. *Macromolecules* **1996**, *29*, 4880.
(34) Cantu, L.; Corti, M.; Salina, P. *J. Phys. Chem.* **1991**, *95*, 5981.
(35) Calderara, F.; Riess, G. *Macromol. Chem. Phys.* **1996**, *197*, 2115.
(36) Yoo, S. I.; Sohn, B.-H.; Zin, W.-C.; Jung, J. C.; Park, C. *Macromolecules* **2007**, *40*, 8323.
(37) Lu, A.; O'Reilly, R. K. *Curr. Opin. Biotechnol.* **2013**, *24*, 639.
(38) Lu, A.; Moatsou, D.; Longbottom, D. A.; O'Reilly, R. K. *Chem. Sci.* **2013**, *4*, 965.

(39) Patterson, J. P.; Cotanda, P.; Kelley, E. G.; Moughton, A. O.; Lu, A.; Epps, T. H. III; O'Reilly, R. K. *Polym.Chem.* **2013**, *4*, 2033.
(40) Cotanda, P.; Lu, A.; Patterson, J. P.; Petzetakis, N.; O'Reilly, R. K. *Macromolecules* **2012**, *45*, 2377.
(41) Lu, A.; Smart, T. P.; Epps, T. H. III; Longbottom, D. A.; O'Reilly, R. K. *Macromolecules* **2011**, *44*, 7233.
(42) Haag, R. *Angew. Chem. Int. Ed.* **2004**, *43*, 278.
(43) Cotanda, P.; O'Reilly, R. K. *Chem. Comm.* **2012**, *48*, 10280.
(44) Creutz, S.; van Stam, J.; Antoun, S.; De Schryver, F. C.; Jérôme, R. *Macromolecules* **1997**, *30*, 4078.
(45) Nyrkova, I. A.; Semenov, A. N. *Macromol. Theory Simul.* **2005**, *14*, 569.
(46) Halperin, A.; Alexander, S. *Macromolecules* **1989**, *22*, 2403.
(47) Thurmond, K. B.; Kowalewski, T.; Wooley, K. L. *J. Am. Chem. Soc.* **1996**, *118*, 7239.
(48) Goddard, E. D.; Turro, N. J.; Kuo, P. L.; Ananthapadmanabhan, K. P. *Langmuir* **1985**, *1*, 352.
(49) Wilhelm, M.; Zhao, C. L.; Wang, Y.; Xu, R.; Winnik, M. A.; Mura, J. L.; Riess, G.; Croucher, M. D. *Macromolecules* **1991**, *24*, 1033.
(50) Eghbali, E.; Colombani, O.; Drechsler, M.; Muller, A. H. E.; Hoffmann, H. *Langmuir* **2006**, *22*, 4766.
(51) Jain, S.; Bates, F. S. *Science* **2003**, *300*, 460.
(52) Nicolai, T.; Gimel, J. C.; Johnsen, R. *J. Phys. II* **1996**, *6*, 695.
(53) Choi, S. Y.; Bates, F. S.; Lodge, T. P. *J. Phys. Chem. B* **2009**, *113*, 13840.
(54) Colombani, O.; Ruppel, M.; Burkhardt, M.; Drechsler, M.; Schumacher, M.; Gradzielski, M.; Schweins, R.; Muller, A. H. E. *Macromolecules* **2007**, *40*, 4351.
(55) Patterson, J. P.; Kelley, E. G.; Murphy, R. P.; Moughton, A. O.; Robin, M. P.; Lu, A.; Colombani, O.; Chassenieux, C.; Cheung, D.; Sullivan, M. O.; Epps, T. H. III; O'Reilly, R. K. *Macromolecules* **2013**, *46*, 6319.
(56) Piogé, S.; Fontaine, L.; Gaillard, C.; Nicol, E.; Pascual, S. *Macromolecules* **2009**, *42*, 4262.
(57) Jakes, J. *Collect. Czech. Chem. Commun.* **1995**, *60*, 1781.
(58) Patterson, J. P.; Robin, M. P.; Chassenieux, C.; Colombani, O.; O'Reilly, R. K. *Chem. Soc. Rev.* **2014**, *43*, 2412.
(59) Chassenieux, C.; Nicolai, T.; Durand, D. *Macromolecules* **1997**, *30*, 4952.
(60) Sedlak, M. *J. Chem. Phys.* **1997**, *107*, 10805.
(61) Sedlak, M. *J. Chem. Phys.* **1997**, *107*, 10799.
(62) Kline, S. *J. App. Crystallogra.* **2006**, *39*, 895.
(63) Glatter, O.; Kratky, O. *Small-Angle X-Ray Scattering*; Academic Press, 1982.
(64) Guinier, A.; Fournet, G. *Small-angle scattering of X-rays*; John Wiley & Sons: New York, 1955.
(65) Roe, R.-J. *Methods of X-ray and Neutron Scattering in Polymer Science*; Oxford University Press: New York, 2000.
(66) NIST SLD calculator http://www.ncnr.nist.gov/resources/sldcalc.html.

6. Amphiphilic block copolymer micelles: Blending and structural understanding

6.1. Abstract

Amphiphilic block copolymers can assemble into a variety of structures on the nanoscale in a selective solvent. The micelle blending protocol explored in Chapter 5 offers a simple unique route to reproducibly produce structures on the nanoscale. Here this blending protocol is expanded to a range of polymer micelle systems and self-assembly routes. It was reported in Chapter 5 by a exploring a range of variables that the systems must be able to reach equilibrium at some point for the blending protocol to be successful. The results concern the thermodynamics and mechanism for the blending protocol which can then be applied to a wide range of self-assembling polymers.

6.2. Introduction

Much like small molecule surfactants amphiphilic block copolymers will spontaneously self-assemble when dispersed in a selective solvent for one of the copolymer blocks.[1] Although small molecule surfactants and amphiphilic block copolymers both exhibit similar behaviour in solution, once the molecules have assembled into micelles there are some solution behaviours which are vastly different between the two. The most prevalent behavioural difference in solution is that surfactant micelles will typically reach thermodynamic equilibrium, through a constant exchange of surfactant molecules between structures.[2-4] Here once the surfactant micelle has formed (when the concentration of surfactant molecules is above the critical micelle concentration, CMC) at any one time surfactant molecules are either within the self-assembled structure or free in solution; often this association mechanisms is an "all or nothing" response and this is termed the closed association model (Figure 6.1).[5]

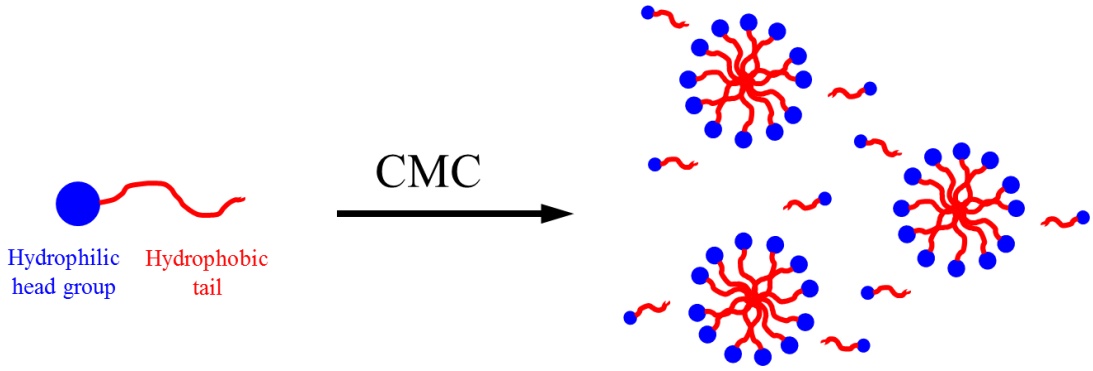

Figure 6.1. Formation of surfactant micelles above the CMC. Below the CMC surfactant molecules are free in solution and once the CMC is reached discrete nanostructures are formed with a fraction of surfactant molecules free in solution.

However, amphiphilic block copolymers only rarely reach the true Gibbs free energy minima and hence thermodynamic equilibrium.[6,7] Predominantly the exchange of polymer chains between structures is often kinetically hindered because the energy barrier for unimer exchange is too great and the concentration of polymer chains free in solution is most commonly negligible.[8,9] This inability to reach equilibrium, specifically during micelle

formation for diblock copolymers, was explored by Johnson *et al*.[10] A poly(*n*-butylacrylate)-*block*-poly(acrylic acid), P*n*BuA-*b*-PAA diblock copolymer was molecularly dissolved in methanol and subsequently quenched with water (a poor solvent for *n*BuA); effectively a similar to increasing the concentration of diblock copolymer in solution. Johnson *et al* were able to conclude with stop flow light scattering experiments that once the system was quenched with water the polymers instantly nucleate and form a stable particle which does not reorganise over time. It was understood that upon quenching with water a copolymer insertion barrier to the micelle is created and that this barrier grows rapidly whilst the particles nucleate, consuming unimer chains. This rapid energy barrier increase from quenching with water subsequently traps the structures in solution before equilibrium is reached and no further rearrangements occur, leading to out-of-equilibrium micelles which do not reorganise in solution (Figure 6.2).[10]

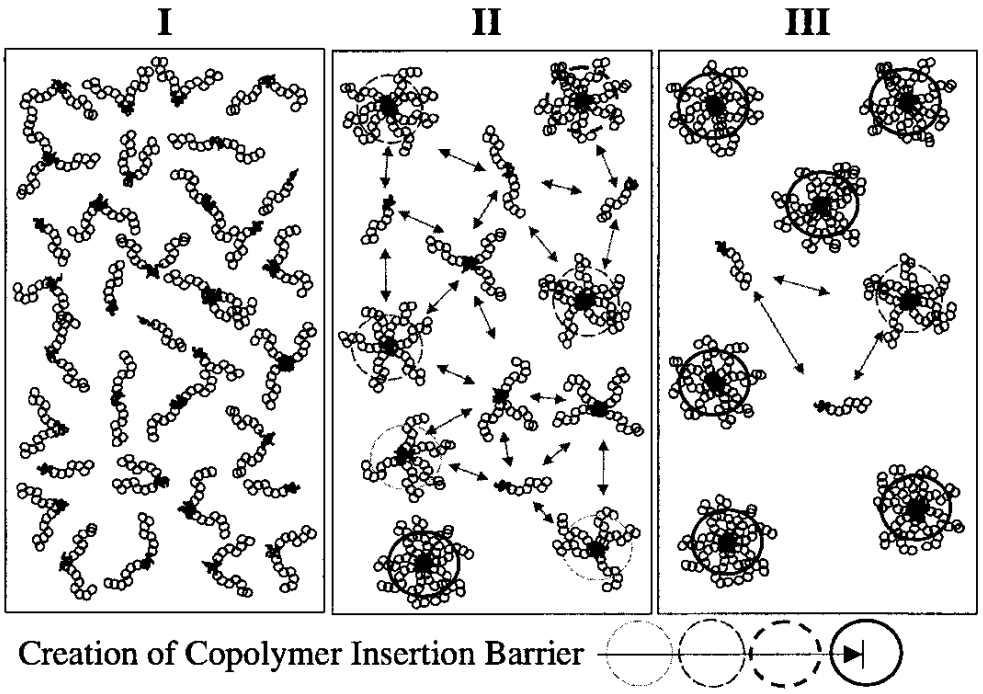

Figure 6.2. Schematic illustrating the formation of frozen polymer micelles in solution from quenching the solution with a selective solvent. As the copolymer insertion barrier is increased from quenching, I-III nucleation events increase and the concentration of free polymer chains is reduced until extremely low (III) and no rearrangements can further occur.[10]

This out of equilibrium behaviour often restricts block copolymer developments for an array of applications and prevents the full understanding of diblock copolymers in solution as the ability to control and form reproducible stable structures is difficult.[11] Nevertheless, with the discovery of reversible deactivation radical polymerisations (RDRP) techniques a range of new amphiphilic block copolymers have been produced, with a variety of additional functionalities.[12-16] The development of new amphiphilic block copolymers has opened up a range of new structures in solutions, with some structures reaching equilibrium similar to surfactant molecules.[17-20] Nevertheless the sometimes laborious synthesis of these diblock copolymers often negatively impacts the large scale implementation of these functional diblock copolymers. An alternative is the copolymer blending method, which is to blend together two polymers that vary in functionality or response to stimuli to obtain a blend structure, which has a composition and/or response which is an intermediate between the two parent polymers.[21-24] As shown previously in Chapter 5 this strategy is an exciting new method for block copolymer assembly as these blend structures have the ability to structurally match a pure system (a system formed by a single polymer) in solution.

The ability to successfully mimic the structure of pure spherical micelles through a blending strategy crucially depends on the system's ability to follow through its relaxation pathway and equilibrate.[21] This equilibration of relaxation pathway is often a misunderstood topic of polymer self-assemblies as it is difficult to deduce how far from equilibrium a system truly is or if a system has even reached true equilibrium. Furthermore, the fact that stable equilibrium micelles form rarely means that only a few reports on true thermodynamic equilibrium of polymer micelles in solution exist.[6,7,25-31]

Therefore to understand the ability of the copolymer blending method to produce stable equilibrium micelles a series of polymer systems and a range of assembly conditions were studied and the parameters needed for successful blending, to produce stable, reproducible structures, were sought. In this chapter the fundamental understanding of this copolymer blending method is explored and the limitations and mechanisms are elucidated further to

understand micelle equilibration and expand the copolymer blending protocol to an array of polymer systems.

6.3. Results and Discussion

6.3.1. Synthesis and molecular characterisation of the diblock copolymers

6.3.1.1. Synthesis of P(EHA-co-DMA)-b-PDMA and P(IBA-co-DMA)-b-PDMA diblock copolymers

For this study a series of diblock copolymers were synthesised (Scheme 6.1). As explored in Chapter 5 the block lengths within the P(DMAEMA-*co*-DEAEMA)-*b*-P(DMAEMA) diblock series were identical throughout but the solvophobic block composition was varied by copolymerisation. To explore the copolymer blending method further this polymer structure i.e. a copolymer solvophobic block which can be varied by copolymerisation linked to a homopolymer solvophilic block was maintained. First two hydrophilic poly(dimethyl acrylamide), P(DMA), macro chain transfer agents (macro-CTAs) were synthesised by RAFT polymerisation. For each series a degree of polymerisation 120 or 350 was targeted, allowing a change in the solvophilicity of each polymer system to be achieved. These macro-CTAs were then chain extended with dimethyl acrylamide (DMA) and varying amounts of hydrophobic monomer, either isobornyl acrylate (IBA) or 2-ethylhexyl acrylate (EHA) respectively, to afford diblock copolymers with a copolymer associating block. Moreover, by using the van Herk nonlinear least-squares fitting method with F_1 (mol fraction of DMA in the copolymer) and f_1 (mol fraction of DMA in the monomer feed) values, these associating blocks are shown to be purely statistical (the values for r_1 and r_2 were as follows; DMA/EHA r_1= 1.021, r_2=0.849 and DMA/IBA r_1 = 1.120, r_2 = 0.780).[32] All

diblock copolymers formed had low dispersity, known hydrophobic monomer incorporation and controlled molecular weight; the results are summarised in Table 6.1.

Scheme 6.1 General schematic of the polymerisation of DMA and chain extension with DMA and a hydrophobic monomer *via* RAFT polymerisation.

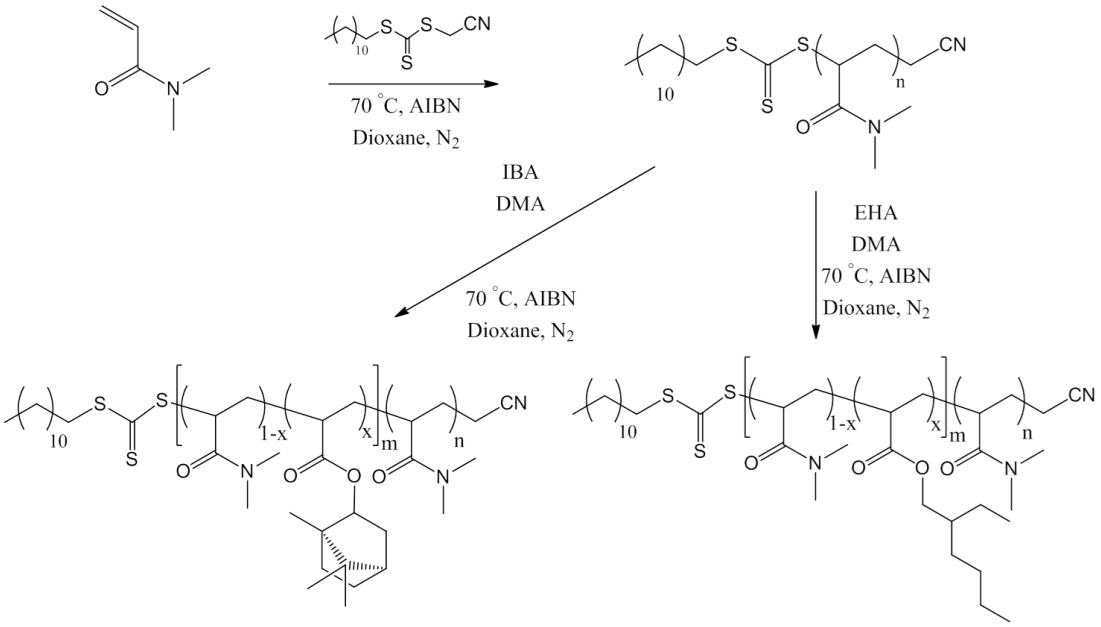

6.7-6.9 **6.1-6.6**

Table 6.1 Characteristics of diblock copolymers.

Monomer	Polymer	x[a]	n[a]	m[a]	M_n NMR[b]	M_n SEC[c]	$Đ$ SEC[c]
EHA	**6.1**	0.60	120	70	22.9	25.0	1.11
	6.2	0.50	120	69	22.2	24.9	1.20
	6.3	0.40	120	71	21.3	23.2	1.20
	6.4	0.90	350	250	77.3	77.9	1.11
	6.5	0.80	350	228	70.5	79.1	1.18
	6.6	0.70	350	260	71.3	74.6	1.14
IBA	**6.7**	0.60	120	68	23.1	23.6	1.30
	6.8	0.50	120	71	23.3	22.7	1.27
	6.9	0.40	120	66	22.0	25.8	1.24

[a] Determined by ^{1}H NMR spectroscopy. [b] Determined by end-group analysis from ^{1}H NMR spectroscopy. [c] From SEC based on poly(styrene) standards in $CHCl_3$.

6.3.2. Blending of diblock copolymers

Herein the self-assembly of diblock copolymer blends in aqueous solutions are investigated. Based on previous reports it is hypothesised that equilibrium must be reached and that the system must have the highest entropy possible ensuring the spontaneous formation of blend micelles which can also structurally match pure ones with the same composition (Figure 6.3). To understand this hypothesis further a range of different polymers and assembly conditions were explored. In Chapter 5 a range of compositions could be targeted by varying the blend ratios, but in this Chapter only one composition was explored for each of the three systems because a different set of variables were investigated, specifically polymer structure, *e.g.* chain length and monomer, in addition to the assembly route, to further understand the limitations and mechanisms of the blending method and the hypothesis that equilibrium must

be reached. In this Chapter three polymer systems were investigated; their blending ratios, assembly pathway and notation are listed below.

6.3.2.1. P(EHA-co-DMA)-b-PDMA diblock copolymer blends

For the P(EHA-*co*-DMA)-*b*-PDMA diblock copolymer blends the polymers **6.1** (60% EHA in the core) and **6.3** (40% EHA in the core) were blended together as dry polymer powders to match the composition of **6.2** (50% EHA in the core), where in the second system **6.4** (90% EHA in the core) and **6.6** (70% EHA in the core) were blended together as dry polymer powders to match the composition of **6.5** (80% EHA in the core). For each blend systems only one composition was targeted but the assembly pathway was varied. To distinguish between polymer systems the notation is as follows; *N-M-6.2*, *N* signifies if the polymer samples are blend (*B*) or pure (*P*), *M* represents the pathway, for example *TF* is thin film rehydration, *DD* is direct dissolution and *SS* is solvent switch. *6.2* represents the polymer which is to be targeted in the blend; the specific polymer and composition of which can be found in Table 6.1. Tables 6.2 and 6.3 represent the molar blending ratios and assembly routes for the P(EHA-*co*-DMA)-*b*-PDMA diblock copolymer sets.

Table 6.2. Molar mixing ratios and assembly pathway for the blended block copolymer systems **6.1**-**6.3**.

Blended diblock copolymer	Pathway	Mole fraction **6.1**	Mole fraction **6.3**	Theoretical EHA in core block
B-TF-**6.2**	TF	0.50	0.50	50%
B-DD-**6.2**	DD	0.50	0.50	50%
B-SS-**6.2**	SS	0.50	0.50	50%

Table 6.3. Molar mixing ratios and assembly pathway for the blended block copolymer systems **6.4**-**6.6**.

Blended diblock copolymer	Pathway	Mole fraction **6.4**	Mole fraction **6.6**	Theoretical EHA in core block
B-TF-**6.5**	TF	0.50	0.50	80%
B-DD-**6.5**	DD	0.50	0.50	80%
B-SS-**6.5**	SS	0.50	0.50	80%

6.3.2.2. P(IBA-co-DMA)-b-PDMA diblock copolymer blends

For the P(IBA-*co*-DMA)-*b*-PDMA diblock copolymer blends the polymers **6.7**(60% IBA in the core) and **6.9** (40% IBA in the core) were blended together as dry polymer powders to match the composition of **6.8** (50% IBA in the core). Blend systems were all blended to obtain the same composition but the pathway was varied. For that reason the composition of the core is not noted but the pathway is; molar mixing ratios and assembly routes are listed in Table 6.4. The notation for P(IBA-*co*-DMA)-*b*-PDMA diblock copolymer blends is the same for the polymer systems discussed in section 6.2.2.2.

Table 6.4. Molar mixing ratios and assembly pathway for the blended block copolymer systems **6.7**-**6.9**.

Blended diblock copolymer	Pathway	Mole fraction **6.7**	Mole fraction **6.9**	Theoretical IBA in core block
B-TF-**6.8**	TF	0.50	0.50	50%
B-DD-**6.8**	DD	0.50	0.50	50%
B-SS-**6.8**	SS	0.50	0.50	50%

6.3.3. Formation of blend micelles

6.3.3.1. Influence of pathway dependence on blending

As mentioned in the Chapter 1 it is well known that for amphiphilic diblock copolymers different pathways for assembly can produce a range of structures.[6,8,11] In this Chapter different assembly pathways were employed for a range of neutral polymers and the ability to form stable equilibrium blend micelles for each pathway was investigated to help understand the copolymer blending method further, Figure 6.4. The three pathways explored were: solvent switch method (SS), where polymers are blended as polymer powders and dispersed into a good solvent for both blocks producing a solution of mixed unimer chains, and once dispersed poor solvent for the associating block is slowly added and the original good solvent removed. For this method of assembly it is anticipated that as structures begin to form upon the addition of the selective solvent the equilibration will be very quick, yet as the solvent quality for one of the blocks decreases (by further addition of selective solvent) this equilibration time greatly will increase and possibly true equilibrium may not occur (Figure 6.4a – solvent switch). However, in some cases equilibrium may be reached before the solvent quality for one block is greatly reduced (Figure 6.4b – Solvent switch). The second pathway is direct dissolution (DD) where the bulk polymer powders are blended and subsequently added to the selective solvent (water). Upon initial dispersion it is anticipated that the structures formed will be representative of the bulk phase separated morphologies (Figure 6.4a – direct dissolution). Nevertheless these initial structures can under certain condition equilibrate (Figure 6.4b – direct dissolution). The final pathway is the thin film rehydration (TF), where the polymers are blended together and dispersed in a good solvent for both blocks, then the solvent is slowly removed at high temperature under vacuum producing a thin film of the polymers on the vial to which selective solvent is subsequently added. Similar to direct dissolution it is expected that these structures will initially represent

phase separated structures, typically bilayers, which may equilibrate under certain conditions (Figure 6.4b – thin film rehydration).

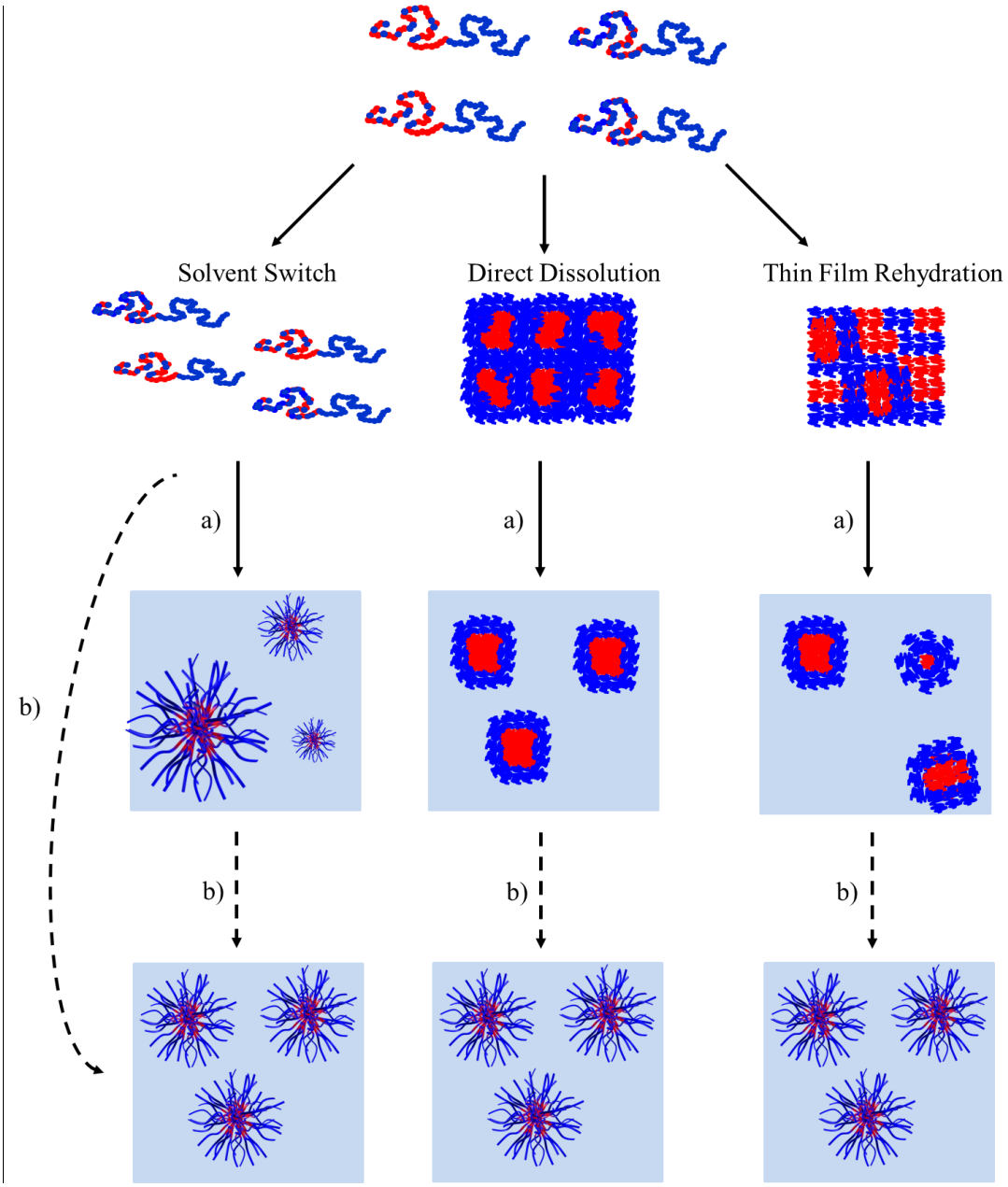

Figure 6.4. Diagram representing the various preparation pathways for amphiphilic diblock copolymer blends. First the dry polymer powders are mixed to the desired ratio and subsequently a preparation pathway is used for assembly. Solvent switch; the polymers are molecularly solubilised as unimers before being assembled cooperatively. Direct dissolution; selective solvent is added to the dry blended polymer powder. Thin film rehydration; the polymers are solubilised in a good solvent and annealed under vacuum to produce a thin film to which selective solvent is added. a) Representation of predicted structures upon initial dispersion into selective solvent for the coronal block. b) Structures formed in solution if the polymers can reach equilibrium. Note that regardless of pathway all equilibrated structures are identical.

The first sets of studies are focused on the P(EHA-*co*-DMA)-*b*-PDMA polymer series **6.1**-**6.3** with blends B-TF-**6.2**, B-DD-**6.2** and B-SS-**6.2**. Here the hydrophobic monomer is 2-ethylhexyl acrylate, this monomer was selected as the polymers produced are of low T_g and therefore the influence of glassy cores can be neglected in these set of studies (T_g values for the core block as explored by differential scanning calorimetry, DSC, **6.1** = -18 °C, **6.2** = -5 °C, **6.3** = 8 °C). Static and dynamic light scattering experiments were conducted at 20 °C and were used to analyse the formation and structure of blend micelles in water from a range of assembly pathways at a concentration of 2 g/L (Figures 6.5a and 6.5b). In the laser light scattering data shown in Figure 6.5a and 6.5b it can be observed from the variation in R_h and N_{agg} that the different pathways for assembly give different structures in solution. Specifically, for the thin film rehydration and direct dissolution routes Figures 6.5a and 6.5b both clearly show that the pure and blend micelles do not structurally match in both R_h and N_{agg}. On the other hand the pure and blend micelles formed using the solvent switch route form structurally identical micelles as observed by R_h and N_{agg} values from laser light scattering. These results indicate that for the solvent switch method these micelles, either blend or pure, probably reach equilibrium during assembly at each addition of selective solvent, therefore the structures formed are very similar to one another under these range of conditions.

A simple way to transform structures in solution is to increase in energy of the system from heat, and therefore all polymer solutions were subsequently heated to 75 ºC for 5 hrs before being cooled to room temperature under ambient conditions and then reanalysed by static light scattering (SLS) and dynamic light scattering (DLS). Interestingly once the solutions were heated to 75 °C for 5 hours the N_{agg} and R_h values are identical between the blended and pure systems of **6.2** for all routes of assembly (Figure 6.5b). There is an observed change in the structures upon heating which indicates the polymer chains must be able to reorganise within the system. This reorganisation (for direct dissolution and thin film rehydration) shows these systems, both blend and pure, are capable of reorganising in solution when

additional energy is introduced. Moreover, when the structures after heating are compared to those formed from the solvent switch pathway the structures are the same. It could then be assumed that because identical structures are observed regardless of assembly pathway the structures are at equilibrium. Furthermore, as the solvent switch structures do not change with heating it suggests that they were close to equilibrium in pure water before heating.

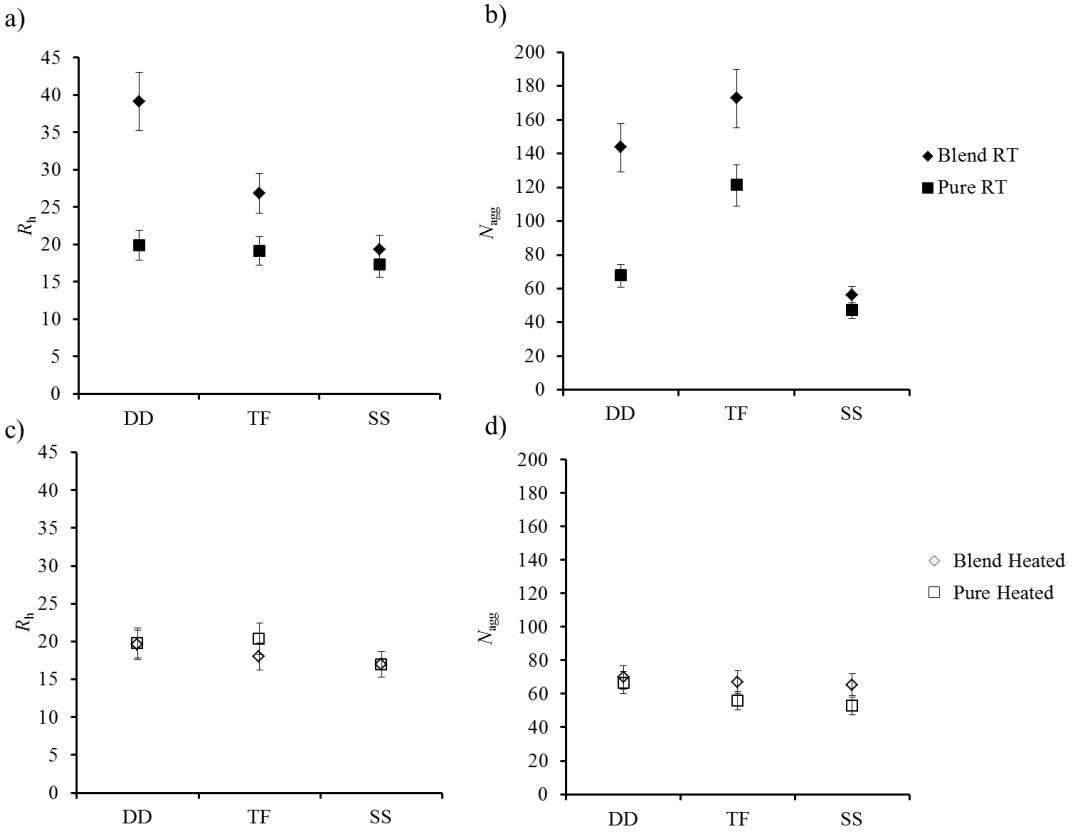

Figure 6.5 Relationship of Nagg and Rh with preparation pathway for the blended and pure solutions for the P(EHA-co-DMA)-b-PDMA diblock copolymers 6.2. a) Relationship of R_h with preparation pathway for the blended and pure left at room temperature. b) Relationship of N_{agg} with preparation pathway for the blended and pure left at room temperature. c) Relationship of R_h with preparation pathway for the blended and pure after being heated for 5 h at 75 °C. d) Relationship of N_{agg} with preparation pathway for the blended and pure after being heated for 5 h at 75 °C. DD = Direct dissolution, TF = Thin film rehydration, SS = Solvent switch. Error bars indicate 10% error on N_{agg} and R_h.

Further analysis of the distributions of relaxation times from DLS shows the dispersity of the samples is notably broad and clearly differs between the two systems before heating (Figure 6.6).

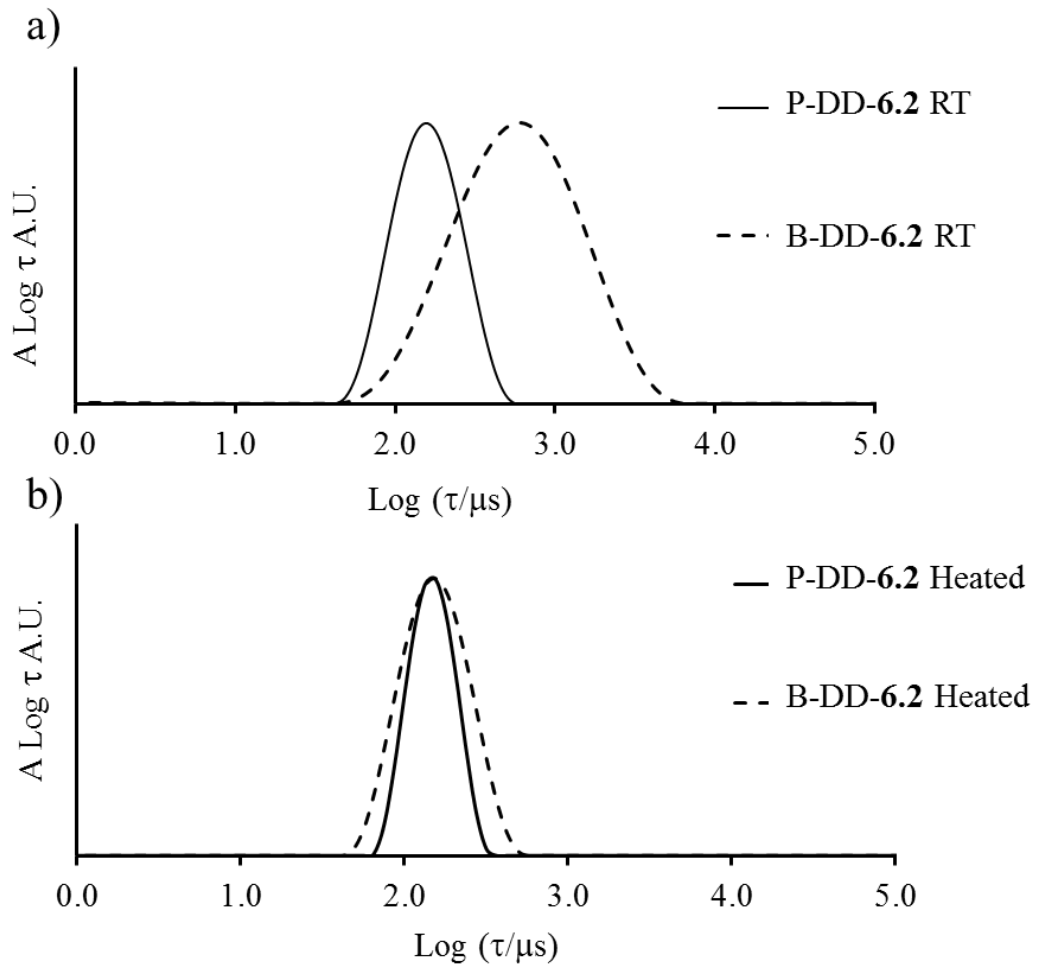

Figure 6.6 a) Relaxation distribution from DLS of P-DD-**6.2** and B-DD-**6.2** at room temperature. b) Relaxation distribution from DLS of P-DD-**6.2** and B-DD-**6.2** at room temperature after being heated for 5 hrs at 75 °C.

However, both pure and blend samples become notably smaller in dispersity upon heating and the morphologies are very similar despite different assembly routes, as observed by both DLS and cryogenic transmission electron microscopy, cryo-TEM (Figure 6.6 and 6.7). As all routes lead to the same structure and both pure and blend micelles are identical it is reasonable to conclude that equilibrium has been reached and an energy barrier has been

overcome by the addition of thermal energy, with stable equilibrium blend micelles being formed which structurally match pure micelles regardless of assembly pathway.

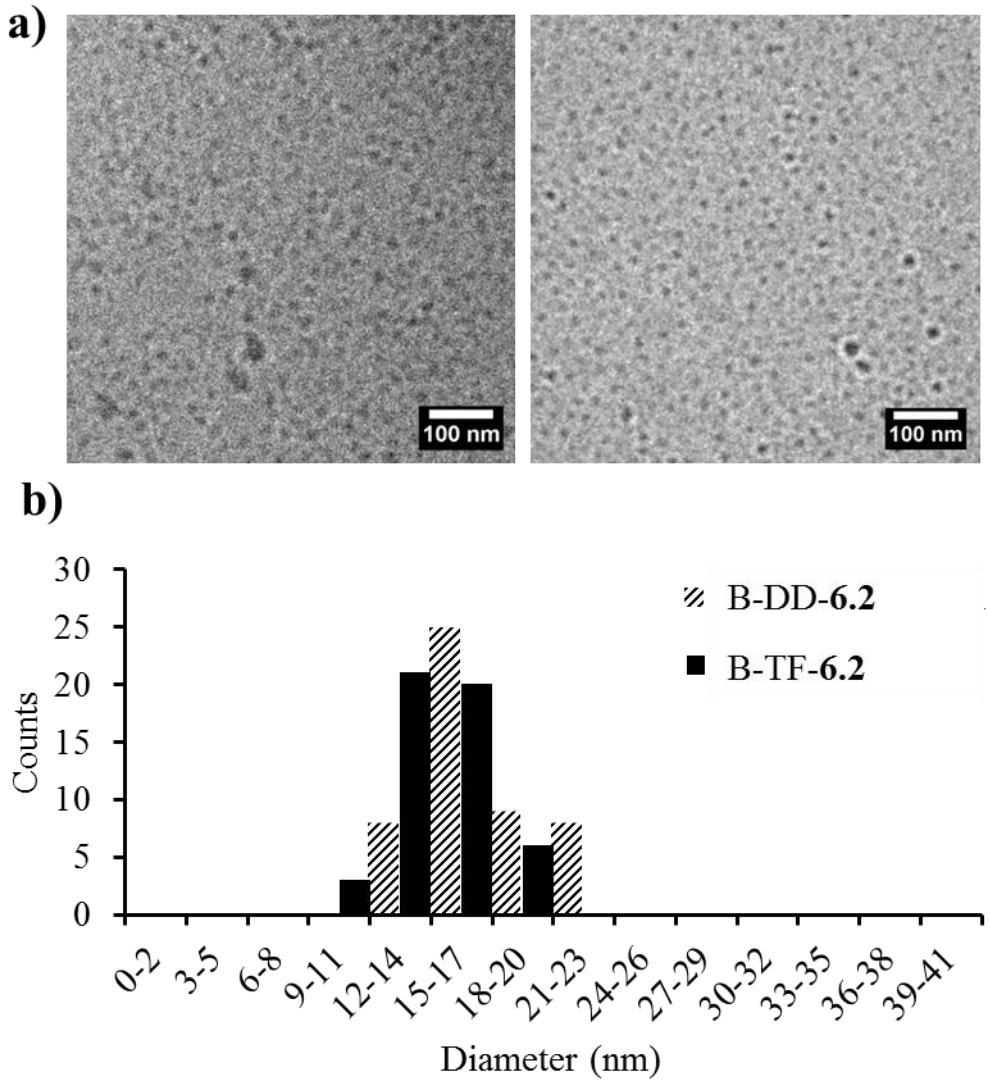

Figure 6.7 a) left, cryo-TEM micrograph for blend micelles from the TF protocol after heating, B-TF-**6.2**. right, cryo-TEM micrograph for blend micelles from the DD protocol after heating, B-DD-**6.2**. b) Histogram of core diameter for blended micelles from B-TF-**6.2** and B-DD-**6.2** after heating (averaged over 50 particles).

Although a change was noted for the thin film rehydration and direct dissolution routes the solvent switch method showed no observed change upon heating for both the pure or blend system. Therefore two possible scenarios may be present; the first is that perfect blended

micelles have already formed by the solvent switch pathway and regardless of heating there is no reorganisation to form new micelles although unimer exchange between micelles does occur. The second is that the system is kinetically trapped and no exchange occurs with heating.

Therefore to understand these kinetic limitations further a solution blending route was explored. Here, **6.1** and **6.3** are assembled using a specific pathway and heated individually to form what are believed to be equilibrium micelles. Once at equilibrium the solutions are cooled to room temperature under ambient conditions and then mixed as solutions and analysed by DLS and SLS after initial mixing, 10 days and then after being heated as a mixed solution.

From Table 6.5 the kinetics of reorganisation can be examined. In contrast to the P(DMAEMA-*co*-DEAEMA)-*b*-PDMAEMA diblock copolymers (see Chapter 5) no exchange can be observed at room temperature for the P(EHA-*co*-DMA)-*b*-PDMA blend systems, even after 10 days, regardless of the precursor solutions. This result strongly indicates these micelles are frozen, possibly as a consequence of a kinetic energy barrier. Additionally, using equation 6.1 and 6.2 it can be observed that the N_{agg} and R_h values after 10 days match to weight average values for non-blended micelles, thus suggesting that these blend solutions are a binary mixture of pure micelles which have not reorganised cooperatively.

$$N_{agg\ mix} = \frac{(C_{6.1}N_{agg\ 6.1}) + (C_{6.3}N_{agg\ 6.3})}{(C_{6.1} + C_{6.3})} \quad (6.1)$$

$$R_{h\ mix} = \frac{(C_{6.1}R_{h\ 6.1}) + (C_{6.3}R_{h\ 6.3})}{(C_{6.1} + C_{6.3})} \quad (6.2)$$

These blended solutions were subsequently heated to 75 °C for 5 hours and then reanalysed by laser light scattering. Once the micelle solutions have been heated a reorganisation of the system occurs and equilibrium blend micelles can then form. Specifically it can be observed that for the micelles formed by blending two solutions where solvent switch was the assembly pathway the structures do reorganise once heated. It can be inferred that for the previous experiments the micelles formed by the solvent switch route do indeed exchange unimer chains between micelles when heated, yet the structures are already at equilibrium and thus no reorganisation is observed. It is important to emphasise that regardless of pathway all routes lead to the same micelle structures once heated, as indicated by laser light scattering studies (Table 6.5).

Table 6.5 Characteristics of micelles formed from blending stock solutions of **6.1** and **6.3** from laser light scattering at 2.5 g/L in 18.2 MΩ water. For reference **6.2** is also shown at equilibrium.

Mixed solution	N_{agg} Initial	N_{agg} 10 days	N_{agg} Weight average	N_{agg} Heated	R_h Initial (nm)	R_h 10 days (nm)	R_h Weight average	R_h Heated (nm)
B-DD-**6.2**	81	83	95	55	34	34	34	15
B-TF-**6.2**	126	120	149	54	27	24	23	16
B-SS-**6.2**	66	66	72	53	14	13	15	15
6.2	52	52	N/A	55	15	17	N/A	16

As pointed out by Halperin and Alexander, the free energy associated with fusion/fission mechanisms is too high and thus the predominant mechanism for reorganisation towards

blend micelles is the dynamic exchange of unimers between micelles.[1,33-35] To understand this mechanism of blended micelle formation in solution further, simple variable temperature ^{1}H NMR spectroscopy was used to understand the mobility of the core block.

^{1}H NMR spectroscopy data shown in Figure 6.8 demonstrates the associating core block mobility. For these studies increases in the intensity of the resonances that correspond to the associating core block demonstrate that either the core has become more mobile, i.e. tumbles faster in solution, or that the core blocks solubilise in the solvent and have been released by the micelle. For this variable temperature ^{1}H NMR spectroscopy experiments B-DD-**6.2** were explored, although other systems showed identical behaviour. Here it can be observed that as the temperature increased the relative area of the peak at 0.8 ppm (representative of the EHA monomer CH_3 protons) also increased. This result indicates that the polymer chain may have been released by the micelle into the solvent and that perhaps the unimers do dynamically exchange. Furthermore, when the relative area of the peak at 0.8 ppm compared to the solvent peak was plotted against temperature a distinct trend can be observed (Figure 6.8b). Here a slow increase in area is initially observed as temperature is increased but then a significantly larger increase in peak area is observed which subsequently plateaus at approximately 50-60 °C. It is understood that the interaction of polymer chains with solvent is inversely proportional to the magnetic relaxation in ^{1}H NMR spectroscopy, specifically the relaxation is less for interacting polymer chains confined to the micelle core.[36] Therefore it is hypothesised that a linear trend could be anticipated if polymer chains were not released by the micelle, as an increase in temperature could yield increased micelle solvent interactions in solution or possibly increased swelling of the micelle core with solvent resulting in faster magnetic relaxation,[37] which possibly will show an increase in peak area linearly with temperature from ^{1}H NMR spectroscopy. Therefore, expulsion of a unimer chain from a micelle core will probably result in an increase in mobility in comparison to confined polymer chains in the core and consequently increased solvent polymer interactions resulting in faster relaxation compared to confined chains within the micelle core.[38] Where it is

predicted that at a specific temperature an increase in relative peak area greater than the confined chains may be observed as unimers escape form the micelle, and subsequently these "free" polymer chains have greater solvent interactions.[36,39] Hence a deviation from a hypothesised linear trend could possibly be expected which was observed by this system in this variable temperature ^{1}H NMR experiments. As such it is believed that the P(EHA-*co*-DMA)-*b*-PDMA diblock copolymer chains can possibly dynamically exchange unimers between micelles if the energy barrier for exchange is low enough. As the cores are assumed to have minimal thermodynamic incompatibility with one another and the P(EHA-*co*-DMA)-*b*-PDMA diblock copolymers **6.1** and **6.3** can exchange, blend micelles which structurally match pure micelles at the same composition of **6.2** can form.

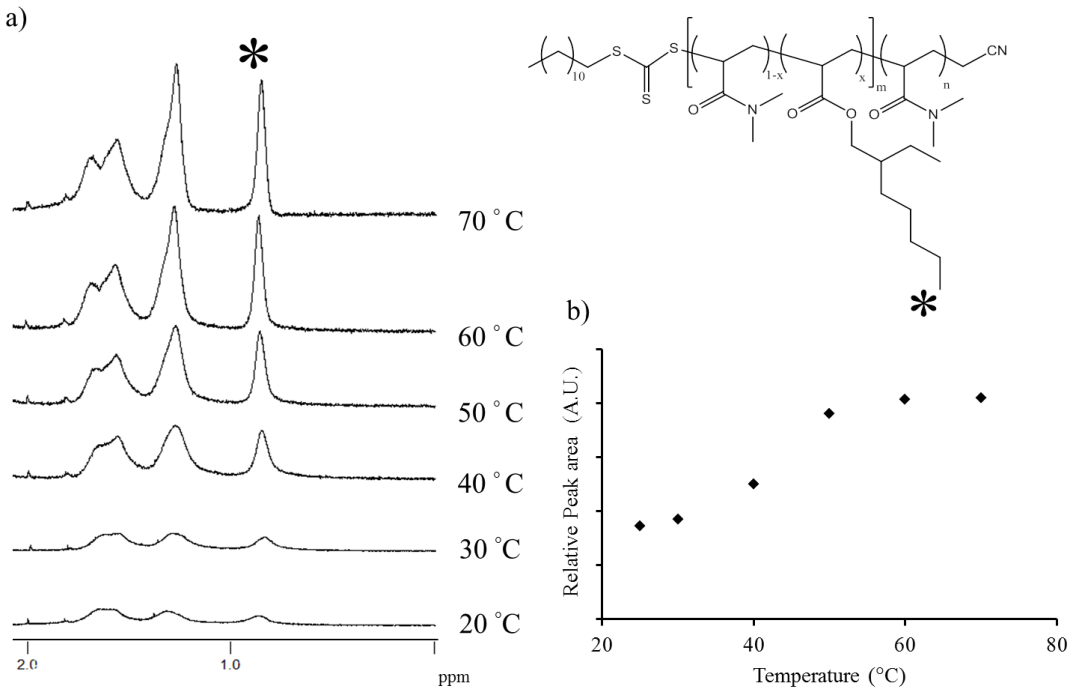

Figure 6.8 a) Partial ^{1}H NMR spectra for B-DD-**6.2** upon gradual heating from 20 °C to 70 °C in D_2O. Data normalised to solvent peak. b) Relationship between relative peak area at 0.8 ppm and temperature.

6.3.3.2. Effect of energy barrier

In the previous section the T_g of the core block for the P(EHA-*co*-DMA)-*b*-PDMA diblock copolymers was below that of all temperatures used. Although this means the core blocks are mobile, it does not conclude that low T_g polymers can rearrange to form equilibrium blend micelles. In section 6.2.3.1. it was concluded that for the equilibrium blend micelles to form the polymer must overcome a kinetic energy barrier for molecular exchange of the unimer chains. As stated in the introduction the energy barrier for molecular exchange may still be too high even for low T_g systems.[33,40-42] Therefore a second P(EHA-*co*-DMA)-*b*-PDMA diblock copolymer series was synthesised to examine the hypothesis that a kinetic energy barrier must be overcome. It is known that the energy barrier is proportional to the associating block length and interfacial tension between the associating block and the solvent. Consequently a P(EHA-*co*-DMA) associating block with a much larger degree of polymerisation *ca* 250 was synthesised and the EHA incorporation was kept much higher, all EHA incorporation was greater than 70%. This provides a blend system with a low T_g to ensure mobile cores, yet with a theoretically higher energy barrier for molecular exchange and consequently the influence of the energy barrier for molecular exchange to form equilibrium blended micelles from the copolymer blending method can be examined. It was hypothesised that either reorganisation would be slower or that it would never occur.

Here **6.4** (90% EHA in the core) and **6.6** (70% EHA in the core) were blended together to give an average composition of 80% EHA in the core matching **6.5**, Table 6.1. In contrast to the previous P(EHA-*co*-DMA)-PDMA diblock copolymers results obtained from laser light scattering analysis showed that for the direct dissolution and thin film rehydration protocols multiple irreproducible modes were present (Figure 6.9a) which meant that quantitative Zimm analysis was not possible. In spite of these irreproducible modes cryo-TEM analysis was undertaken to explore the copolymer blending method further for these diblock copolymers. The images in Figures 6.9b and 6.9c point towards one possible reason behind the problems observed with laser light scattering for thin film rehydration and direct

dissolution protocols. In contrast to the previous system with a short P(DMA-co-EHA) associating block for this system the thin film rehydration and direct dissolution routes exhibit multiple morphologies and much larger cylinder undulations, similar to those observed by Bates and co-workers by cryo-TEM.[8] The presence of multiple morphologies is a result that offers clear proof that these structures are frozen at room temperature, as dynamic micelles would have a uniform structure due to the strong amphiphilicity between the micelle core and solvent. This thus prevents molecular exchange and the formation of equilibrium blend structures, and accordingly although these micelles have mobile cores, equilibrium cannot be reached.[8]

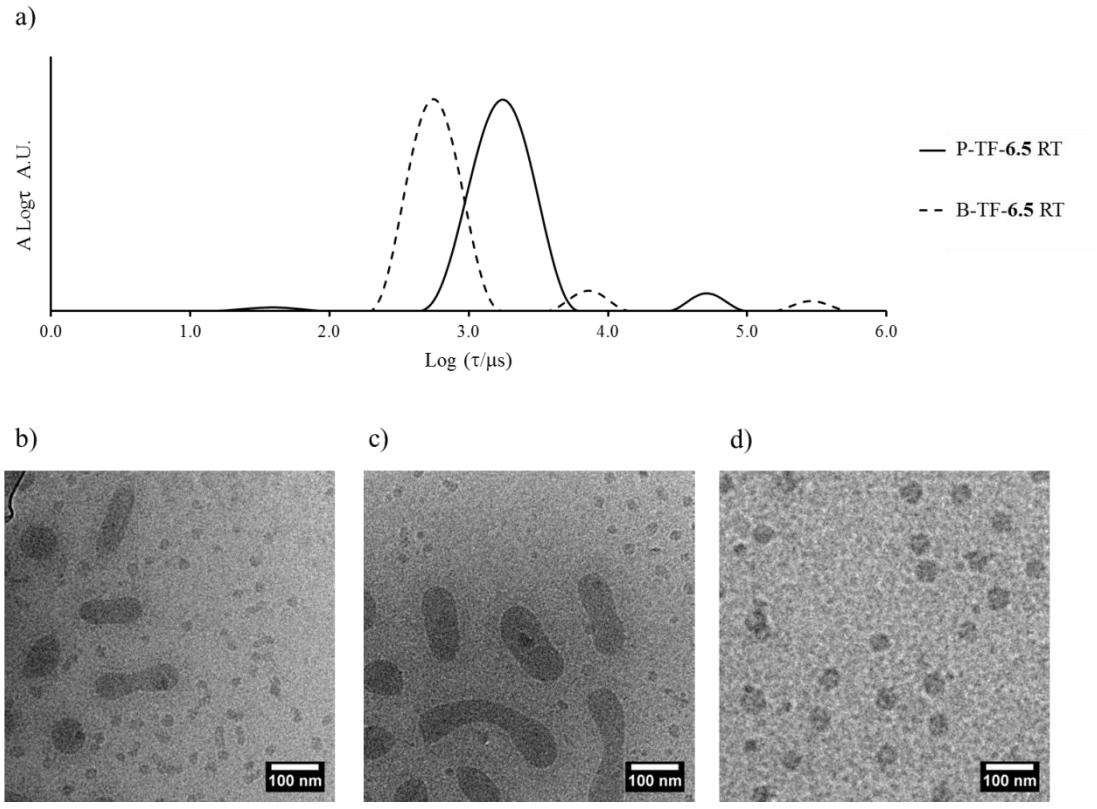

Figure 6.9 a) Relaxation distributions of P(EHA-*co*-DMA)-*b*-PDMA blended and pure by thin film rehydration. Cryo-TEM micrograph of P(EHA-*co*-DMA)-*b*-PDMA blend b) Prepared by direct dissolution, B-DD-**6.5**. c) Prepared by thin film rehydration, B-TF-**6.5**. d) Prepared by solvent switch, B-SS-**6.5**.

For the previous P(EHA-*co*-DMA)-*b*-PDMA series (with a shorter core and corona block) the polymers were indeed frozen upon initial dispersion, however, upon heating the system could rearrange and as hypothesised the polymers overcome a kinetic energy barrier. Nevertheless with this second P(EHA-*co*-DMA)-*b*-PDMA polymer series with increased EHA content and a longer core block a different behaviour is observed. For this system the same heating protocol was undertaken, each solution was heated to 75 °C for 5 hrs and subsequently cooled to room temperature under ambient conditions and reanalysed. For all the systems, B-DD-**6.5,** B-TF-**6.5** and B-SS-**6.5** no change in the relaxation distributions and the cryo-TEM structures was observed. It can therefore be concluded that there was no rearrangement for this system and that no exchange of polymer chains occurred between nanostructures despite a mobile core and a reduction in the interfacial tension with heating. However, from the mobile core the polymers within a structure may move and thus these larger disperse structures may rearrange locally and the structure may alter in morphology. Nonetheless the structures observed here for these polymers **6.4**-**6.6** have not overcome the kinetic barrier allowing unimer exchange and therefore a stable equilibrium blend structure is not formed and the structures formed do not structurally match the pure system.

Conversely, the solvent switch protocol cryo-TEM images show only one population in solution (Figure 6.9d). Laser light scattering analysis was undertaken and as previously observed the blend and pure micelles are identical both before and after heating to 75 °C for 5 hours. It can be deduced that for the solvent switch protocol equilibrium structures could form as the solvent quality is slowly reduced and consequently chain exchange is slowly reduced, causing equilibrium to be reached before the chain exchange slows down to the point where the chain exchange is slower than the equilibration time. These equilibrium structures (B-SS-**6.5**) are therefore locked in once the good solvent is removed and cannot exchange with heat but are indicative of structures formed at equilibrium. Here no change in the system was observed after heating, thus the hypothesis that the kinetic energy barrier for molecular exchange must be overcome to form equilibrium blend micelles was confirmed.

Here for this targeted system the energy barrier is too high which prevents reorganisation of the entire system and the formation of equilibrium blend micelles. Consequently the structural similarities between the pure and blend systems are not present.

From a combination of light scattering analysis and cryo-TEM it appears that the structures formed by **6.4**-**6.6** are frozen in solution. to investigate this further, variable temperature ^{1}H NMR spectroscopy analysis was used to probe the mobility of the core on the molecular level (Figure 6.10), in a similar manner to the previous system with a short P(EHA-*co*-DMA) core forming block. Here the B-DD-**6.5** system was explored and in contrast to the B-DD-**6.2** system a distinct linear relationship between relative peak area of the EHA methyl protons compared to the solvent peak and temperature is observed.

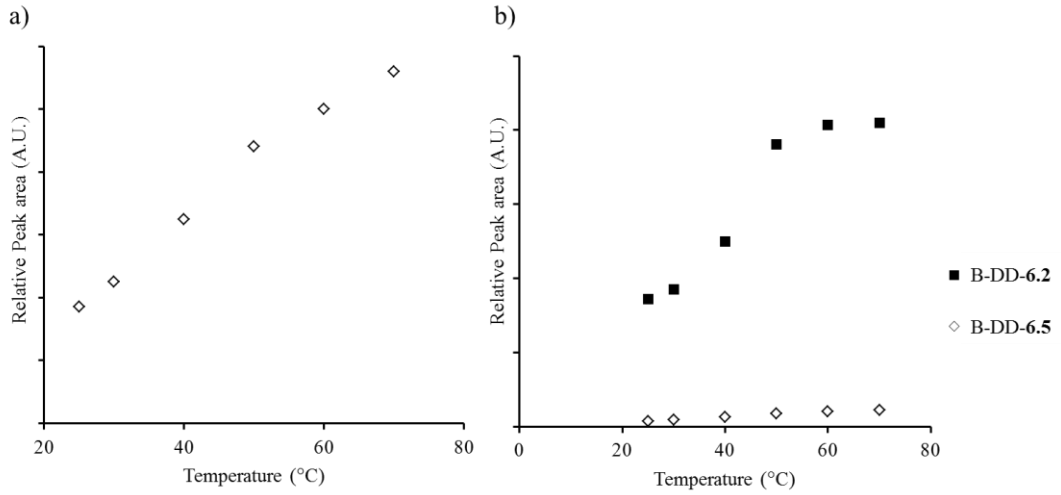

Figure 6.10 a) Relationship between relative peak area at 0.8 ppm from ^{1}H NMR spectroscopy and temperature for B-DD-**6.5** upon gradual heating from 20 °C to 70 °C in D_2O. b) Relationship between relative peak area at 0.8 ppm from ^{1}H NMR spectroscopy and temperature for B-DD-**6.5** and B-DD-**6.2** upon gradual heating from 20 °C to 70 °C in D_2O. Data normalised to solvent D_2O peak.

This linear trend as mentioned previously could be predicted for limited chain mobility or solvent interactions with temperature, such as a frozen micelle. This increase in solvent interactions through core swelling or faster relaxation in 1H NMR spectroscopy will thus have a larger relative peak area for the CH_3 protons on the hexyl chain associated with the

EHA monomer in the solvophobic block. Where the B-DD-**6.2** system shows a nonlinear trend this B-DD-**6.5** has a linear relation possibly indicating that limited core mobility from either unimer expulsions of solvent swelling in the core. Furthermore, when the relative peak area of B-DD-**6.5** is compared to B-DD-**6.2** a large difference in the intensities is observed (Figure 6.10b), specifically at low temperatures when both micelles are believed to be frozen. This larger decrease in intensity could be related to the decrease in mobility of the core from hydration; as the core is not completely solvophobic some solvent (water) could enter the micelles' cores. For the B-DD-**6.5** system, the relative peak area is much smaller than those for B-DD-**6.2** studies which feasibly indicates that less solvent penetrates into the micelle core as the solvophobicity is much greater in the B-DD-**6.5** system and subsequently the interfacial tension between the micelle core and solvent is also much larger. This larger interfacial tension may lead to a larger energy barrier for molecular exchange which was expected for this system.

6.3.3.3. Effect of T_g

In this section the influence of glass transition temperature (T_g) on the copolymer blending method is explored. Previously 2-ethylhexyl acrylate was chosen as it produces a low T_g polymer core, whereas in this section the hydrophobic monomer is isobornyl acrylate, by using IBA as the hydrophobic monomer core blocks with a high T_g are formed (T_g values for the core block as explored by differential scanning calorimetry, DSC, **6.7** = 88°C, **6.8** = 90°C, **6.9** = 87°C). For these studies the P(IBA-*co*-DMA)-*b*-PDMA diblock copolymer **6.7** (60% IBA in the core) and **6.9** (40% IBA in the core) were blended together to match the composition of **6.8** (50% IBA in the core), see Table 6.1 for specific polymer and composition data. Moreover these polymers **6.7**-**6.9** studied are at the same block lengths as the first PDMA-*b*- P(EHA-*co*-DMA), **6.1**-**6.3**, system and are thus used as a direct comparison to this system to understand the influence of T_g on the formation of equilibrium blend micelles. In the following section it should be highlighted that all the experimental

temperatures (room temperature to 75 °C) used are lower than the T_g values of the associating block for the PDMA-*b*-P(IBA-*co*-DMA) diblock copolymers, and as a consequence the core block remains glassy throughout.

Here in this section the studies are focused on the P(IBA-*co*-DMA)-*b*-PDMA polymer series **6.7**-**6.9** with blends B-TF-**6.8**, B-DD-**6.8** and B-SS-**6.8**. Therefore the same assembly pathways for the previous systems were also investigated for this polymer series. Although the solvent switch assembly route and the direct dissolution route lead to solubilised polymers in solution the thin film rehydration pathway did not solubilise the polymer in solution even after extended periods of time or heat. This insoluble behaviour was attributed to extended organised films being produced which cannot solubilise in solution.

Static and dynamic light scattering experiments were conducted on polymer solutions in water at a concentration of 2 g/L at 20 °C and in a similar manner to the pervious P(EHA-*co*-DMA)-*b*-PDMA polymer series light scattering was used to explore the formation and structure of blend micelles in solution. Here for this high T_g system it was observed that for the solutions left at room temperature the blend and pure systems only structurally match when the solvent switch pathway for assembly is used see Figure 6.11a. However, in contrast to the **6.1**-**6.3** P(EHA-*co*-DMA)-*b*-PDMA polymer analogues after heating to 75 °C for 5 hrs no change in the structures of the micelles were observed by both laser light scattering and cryo-TEM for both the solvent switch and direct dissolution protocols. Initially this could be interpreted as the polymer micelles already being at equilibrium before the solutions were heated. However in this situation identical structures would be observed irrespective of pathway and whether the micelles were blend or pure, which was not the case for these experiments. Therefore it strongly signifies that no rearrangement of the micelles occurred in solution and that the system is indeed frozen regardless of external energy from heating. In spite of this frozen behaviour the blend micelles formed by the solvent switch method still structurally match the pure system at the same composition. The structural similarities

between the blend and pure systems indicate that structures formed from the solvent switch protocol are frozen, but were potentially formed under equilibrium conditions (Figure 6.12).

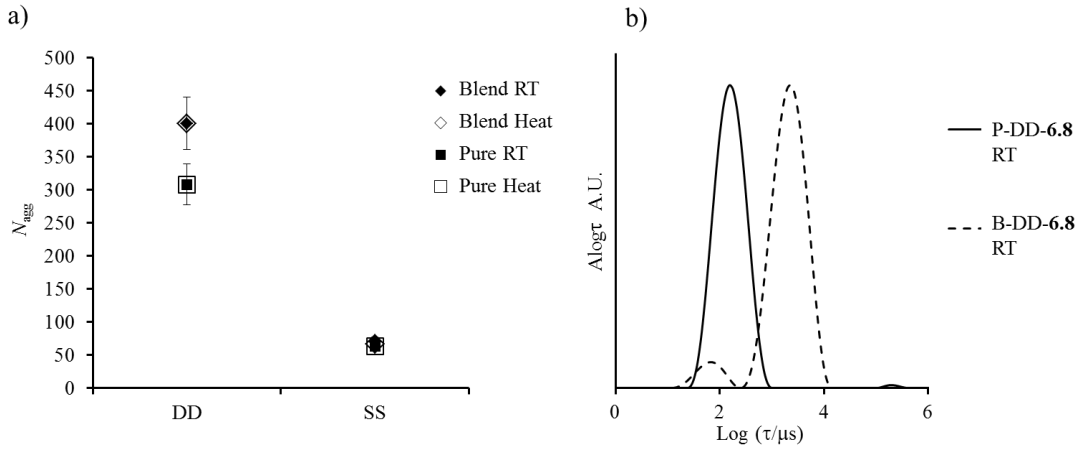

Figure 6.11 a) Relationship of N_{agg} with preparation pathway for the mixed and pure samples for the P(IBA-*co*-DMA)-*b*-PDMA systems. b) Relaxation distribution from DLS of P-DD-**6.8** and B-DD-**6.8** at room temperature.

As shown in Figure 6.11a (laser light scattering experiments of P(IBA-*co*-DMA)-*b*-PDMA diblock copolymers using the solvent switch protocol) both blend (B-SS-**6.8**) and pure micelles (P-SS-**6.8**) are observed to be structural analogues of each other. From cryo-TEM images (Figure 6.12) this structural similarity is further confirmed, indicating that equilibrium is reached before the structures are frozen in and chain exchange is inhibited and blend micelles can match pure micelles.

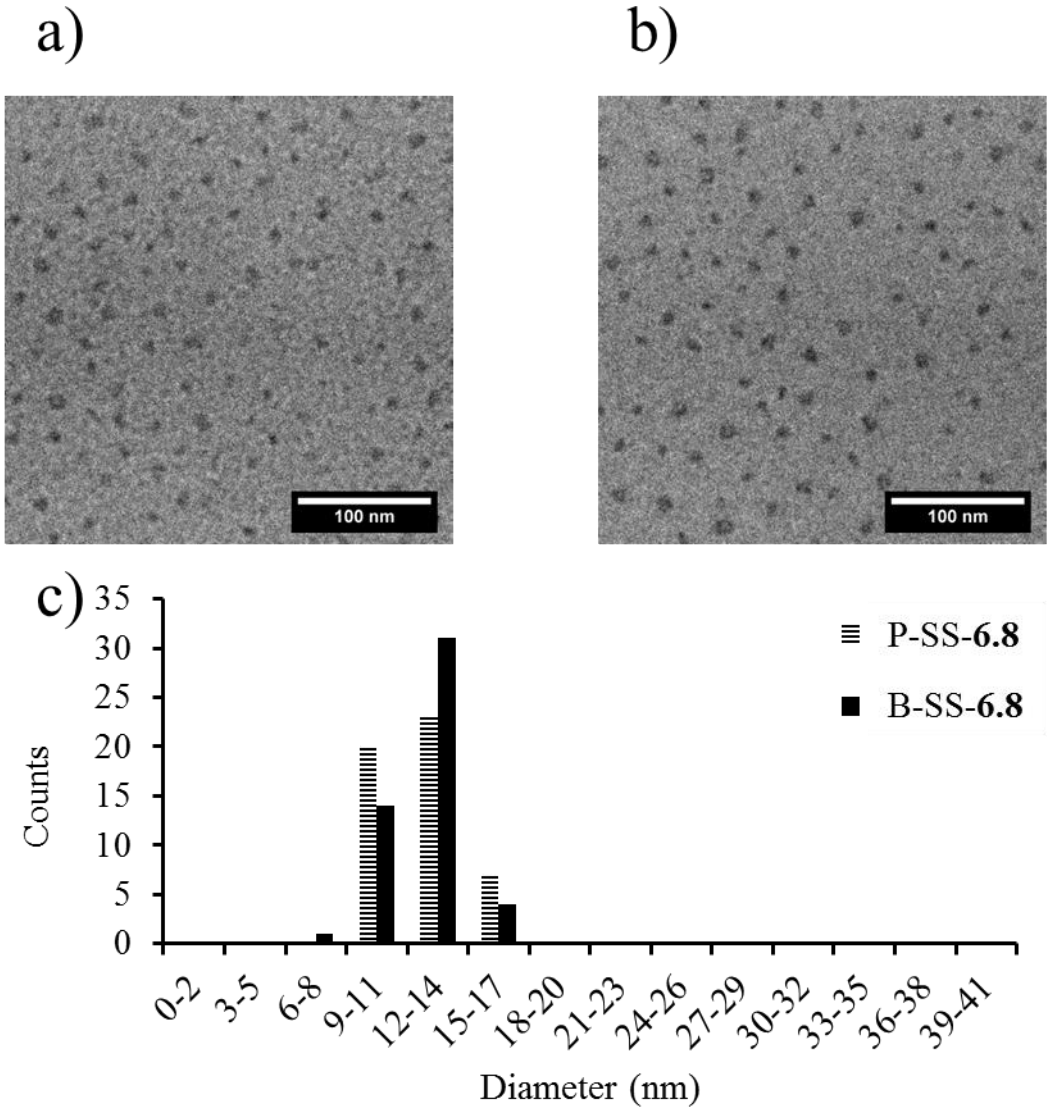

Figure 6.12 a) cryo-TEM micrograph for the P-SS-**6.8** after heating. b) cryo-TEM micrograph for B-SS-**6.8** after heating.c) Histogram of core diameter for blended micelles from P-SS-**6.8** and B-SS-**6.8** (averaged over 50 particles).

Although the solvent switch pathways are believed to be formed under equilibrium conditions and hence the blend and pure micelle systems are identical, the direct dissolution assembly route conversely produced very different structures in solution (Figure 6.11a). The dissolution of amphiphilic block copolymers upon adding selective solvent to dry polymer powder depends largely on how the polymer disperses molecularly and upon its structure in the bulk. It is known that direct dissolution protocols are often poor routes to produce

micelles as often frozen nanoparticles are produced resembling the structures formed in the bulk which do not molecularly disperse and reorganise in the solvent.[6] This frozen behaviour of the P(IBA-*co*-DMA)-*b*-PDMA diblock copolymer micelles in water is also highlighted by the distributions of relaxation times observed by DLS (Figure 6.11b); for the pure system a very broad distribution indicative of disperse out-of-equilibrium structures was observed for the B-DD-**6.8** and P-DD-**6.8**. Moreover, for the blend system we can clearly observe a distinct second mode of relaxation; as observed in Chapter 4 these slow modes are negligible in solution but are difficult to remove via filtration, the origin of this slow mode can be attributed to the presence of larger insoluble frozen bulk structures. These results indicate that for the P(IBA-*co*-DMA)-*b*-PDMA diblock copolymers using the direct dissolution pathway although the temperature was increased the experimental temperature was still lower than the T_g of the core forming block and the cores still remain glassy. It is hypothesised that these glassy micelle cores kinetically trap the structures formed in the bulk in solution and unimer exchange is consequently inhibited preventing equilibrium. Consequently the blended and pure systems do not structurally match using the direct dissolution route of assembly.[43]

Further experiments using variable temperature ^{1}H NMR spectroscopy were also used to assess information on core mobility, as it is considered that the lack of core mobility from a high glass transition temperature of the polymer core prevents equilibration and reorganisation of the structures. As observed from ^{1}H NMR spectroscopy the signals attributed to the core block methyl protons cannot be observed at room temperature or at 70 °C studied herein (Figure 6.13). This phenomenon leads to the conclusion that there is restricted mobility of the core and that the core block never resides in the solvent. Additionally, similarly to the B-DD-**6.2** system some solvent may still enter the core but in contrast to the B-DD-**6.2** this does not increase the core mobility despite the core hydration. This does not mean to say that water does not enter the core, only that the core block has very limited mobility regardless. The lack of mobility of the polymer chain is a consequence

of the high T_g of the core block which leads to frozen nanostructures. Thus blended and pure micelles in general will not structurally match for high T_g systems unless blend micelles are formed before the glassy core locks in the structures.

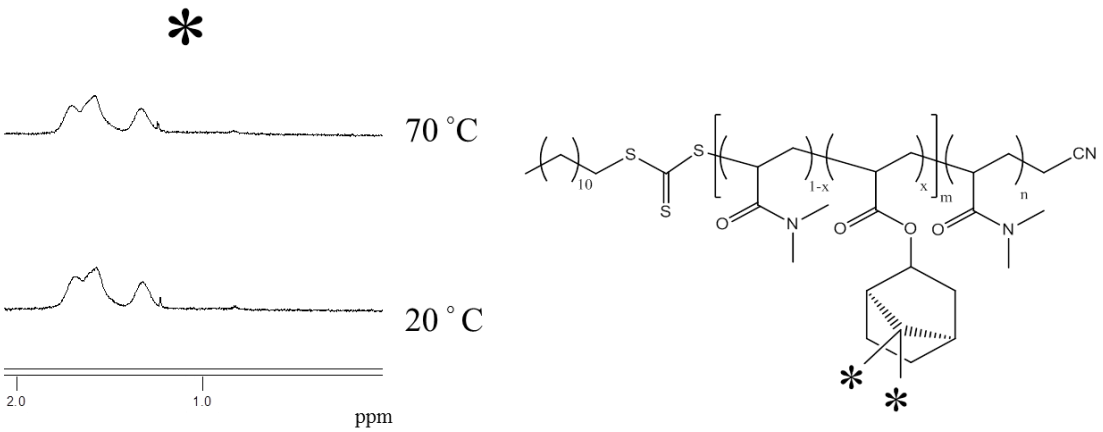

Figure 6.13 Partial ^{1}H NMR spectra for P(IBA-*co*-DMA)-*b*-PDMA diblock copolymers, B-SS-**6.8**, at 20 °C and 70 °C inD_2O. Expected ppm for asterix protons is 0.9-1.0. Data normalised to D_2O solvent peak.

6.3.4. Mechanism and thermodynamic limitations

The results presented herein demonstrate that both kinetic and thermodynamic considerations must be addressed for the blending protocol to be successful. From a kinetic aspect the structures must be able to overcome kinetic obstacles, of either a glassy micelle core or of the energy barrier for molecular exchange either during or after assembly to form blended micelles. From the thermodynamic aspect the polymer cores must be able to mix so that spontaneous mixing will be thermodynamically favourable. If both these factors are considered then a perfectly mixed system will provide the lowest Gibbs free energy as this is the most entropically favoured structure. The systems within this Chapter were designed to potentially overcome the kinetic and thermodynamic barriers by copolymerising solvophilic units within the core forming block.

Despite this, some systems did not produce perfectly blended systems. Specifically this was shown for the P(EHA-*co*-DMA)-*b*-PDMA, and P(IBA-*co*-DMA)-*b*-PDMA diblock copolymers using the thin film rehydration and direct dissolution routes for assembly. It is believed that the initial structures from the direct dissolution and thin film rehydration protocols before heating represent large metastable structures which have not perfectly mixed, but do have the capability to equilibrate if these structures can overcome the kinetic obstacles in place.[27] Consequently blended micelles can form and structurally match those of pure systems in solution if the moderately hydrophobic blocks can globally rearrange, that is rearrange between other structures in solution, reaching equilibrium.

Explicitly the direct dissolution and thin film rehydration protocols represent poor routes towards structures in the solution.[7] For these two protocols when the bulk powders or thin films are initially dispersed into the water the bulk structures will dictate the resulting morphologies. It can be predicted that the core block and coronal blocks will phase separate in the bulk. Hence, when the powders are dispersed in water if the $\chi_{CoreSolvent}$ is large enough the exchange of chains can be severely restricted are large ill-defined structures are produced

which do not form blend micelles but rather acts as precursor to structures in solution (Figure 6.14). After heating the solutions it was observed that reorganisation had occurred, specifically for the P(EHA-*co*-DMA)-*b*-PDMA polymers with small core blocks, as observed by laser light scattering and cryo-TEM. This reorganisation is believed to be a consequence of a decrease in the interfacial tension between the core forming block and the surrounding solvent upon heating (Figure 6.14).[6]

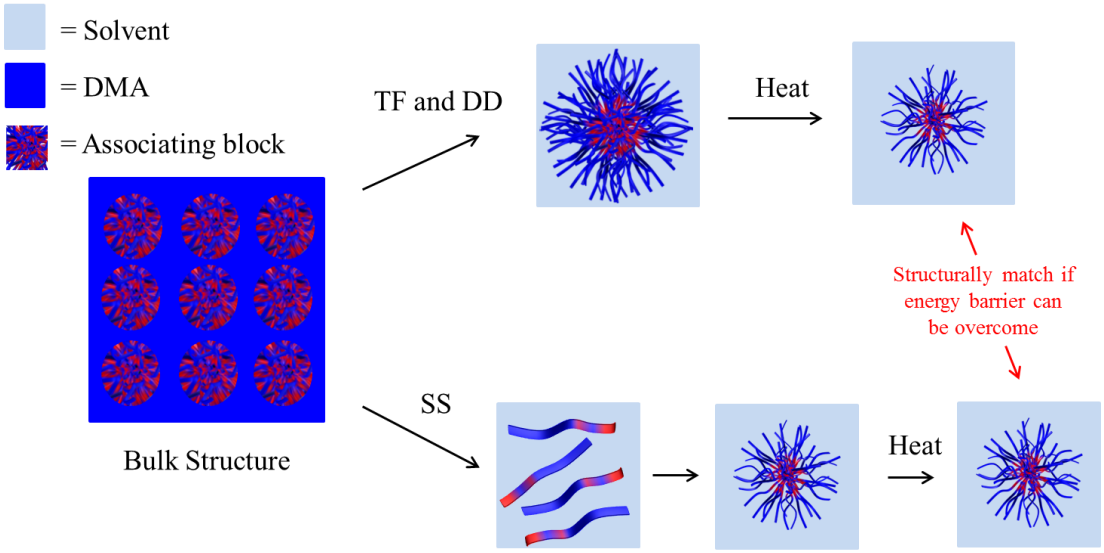

Figure 6.14 Schematic representation of the transformation of bulk metastable structures into blended equilibrated micelles.

In contrast, the P(DMAEMA-*co*-DEAEMA)-*b*-PDMAEMA diblock copolymers explored in Chapters 4 and 5 are dispersed using the direct dissolution protocol but the solutions are first adjusted by addition of acid and the bulk structure is completely destroyed. Therefore this is the same mechanism of dispersion and assembly for the solvent switch method. The addition of good solvent destroys the bulk structure to provide a solution of molecularly dissolved unimers which can then cooperatively assemble forming a perfectly blended system under equilibrium conditions during assembly.

As mentioned in the introduction Halperin and Alexander documented that the energy barrier for unimer exchange for polymeric micelles is proportional to the length of the collapsed

core block, $N_b^{2/3}$, and its interfacial tension between the associating block and the solvent, γ, in the form $E = \gamma N_b^{2/3}$.[34] As the solutions were heated the interfacial tension between the core and solvent is reduced, and once lowered enough molecular exchange can occur. Once this molecular exchange can occur unimers can reorganise within the system and over time the thermodynamically preferred structure is then reached, which will structurally match the micelles formed by a pure polymer system that has also reached equilibrium. At room temperature however, it was observed that no appreciable chain exchange had occurred over 10 days (Table 6.5), indicating that the energy barrier is too high for molecular exchange. Although after heating the micelles are representative of micelles formed under equilibrium conditions, once cooled to room temperature they do not exchange unimers and rearrange.

Kinetically it is now understood how blend structure can form; however, the thermodynamic factors must also be considered if a stable blend micelle is to form. Thermodynamically the blending must be favoured thus allowing structures to reach the Gibbs free energy minima, therefore both enthalpic and entropic considerations must be considered. The enthalpic change in core block stretching should not be relevant for these polymers as all core forming blocks were targeted to have the same block length. Therefore no difference in chain stretching between micelle cores in the blends should be present and any enthalpic differences within the blend systems are not large enough to prevent equilibration. From an entropic consideration there are more factors to address. The re-entry of polymer chains back into the parent micelle will disorder the micelle core and be entropically favoured. However, the largest amount of entropy is gained from a completely blended micelle core and the exchange of polymer chains to form blend micelles is the most favourable thermodynamic process, leading to the formation of blend micelles in each system if the kinetic constraints are overcome.

By understanding the free energy balance of micelles it can be understood why blend micelles can form identical structures to pure micelle systems. The free energy of polymer micelles is calculated from equation 6.3.[44]

$$f_{micelle} = f_{Interface} + f_{corona} + f_{core} \quad \textbf{(6.3)}$$

Consequently it can be understood that when a poorly hydrophobic polymer, one with low hydrophobic incorporation in the core forming block, is introduced the $f_{interface}$ and f_{core} values both reduce as the coronal blocks are identical for both polymers. This similarly matches the addition of polymer to reduce the interfacial tension in bulk blends.[45] By reducing the free energy by the addition of poorly hydrophobic polymer a decrease in aggregation can be observed for all diblock copolymer micelles as observed by SLS. When a specific core composition is targeted for the polymer micelles and they can overcome thermodynamic and kinetic obstacles then the same free energy as the pure system must be reached. In addition, for all series of diblock copolymers used the block lengths within each copolymer are quasi-identical, and as a consequence it is plausible that the packing of the polymer chains is not vastly changed in the blend micelle. Consequently when the energy terms are balanced and equilibrium is reached structures with similar core and coronal sizes to the pure systems are formed.

6.4. Conclusions

The considerations and mechanisms for the copolymer blending method have been investigated further in this Chapter. By exploring a range of diblock copolymers and assembly conditions the copolymer blending method can be easily extended using a range of assembly routes to produce blend structures that structurally match those of a pure sample at the same composition. Experimentally it was shown that the ability for this new blending route to be successful depends on the capability of the polymeric micelles reaching equilibrium whilst having compatible core blocks. From both light scattering analysis and cryo-TEM analysis it was understood that the governing factors influencing this are the core mobility with respect to the system globally, which is broken down specifically into two factors a) a glass transition temperature below that of the experimental temperatures used and b) an energy barrier low enough for molecular exchange. These two factors allow for a global equilibrium and the lowest free energy blend structure to form, which is the structural mirror of the pure system. This Chapter introduced and explored the limitations of the blending method and highlighted the kinetic concerns which must be taken into consideration to produce stable equilibrium micelles. Being able to understand these limitations allows for application advances over conventional polymeric nanostructure assemblies.

6.5. Acknowledgements

Dr. Joseph Patterson conducted the cryo-TEM experiments and assisted with data analysis.

6.6. Experimental

6.6.1. Materials

Monomers were filtered through a plug of silica prior to use and stored at 4 °C. AIBN (2,2'-azo-bis(isobutyronitrile)) was recrystallised from methanol and stored in the dark at 4 °C. All other materials were used as received from Aldrich, Fluka, or Acros.

6.6.2. Synthesis

6.6.2.1. General procedure for polymerisation of DMA

A solution of dimethyl acrylamide (DMA), 120 or 350 equivalents, 0.1 equivalents of AIBN and 1 equivalent of cyanomethyl dodecyl trithiocarbonate (CMDT) in 1,4-dioxane (1:1 volume compared to monomer) was added to a dry ampoule containing a stirrer bar. The solution was degassed using at least 3 freeze-pump-thaw cycles, back filled with nitrogen, sealed and placed in a pre-heated oil bath at 70 °C. After 2 hours the polymerisation was quenched by liquid nitrogen and opened to air, the crude reaction was diluted with the minimum amount of dichloromethane (CH_2Cl_2) and the solution was precipitated into cold diethyl ether and the polymer isolated by filtered. Precipitation was repeated a further two times to afford a yellow macroCTA polymer powder (See Table 6.1 for molecular weight data).

6.6.2.2. General procedure for chain extension of the MacroCTAs with DMA and IBA

MacroCTA (1.0 eq.), AIBN (0.1 eq.) and a combination of DMA with isobornyl acrylate (IBA), (70 eq.) were dissolved in 1,4-dioxane (1:1 volume compared to the monomer) and were added to a dry ampoule containing a stirrer bar. The solution was degassed using at least 3 freeze-pump-thaw cycles, back filled with nitrogen, sealed and placed in a pre-heated oil bath at 70 °C. After 5 hours the polymerisation was quenched by liquid nitrogen, the

crude reaction was diluted with the minimum amount of dichloromethane (CH_2Cl_2) and the solution was precipitated into diethyl ether and the polymer was isolated by filtered. Precipitation was repeated a further two times to afford a yellow powder (See Table 6.1 for molecular weight data).

6.6.2.3. General procedure for chain extension of the polymers with DMA and EHA

MacroCTA (1.0 eq.), AIBN (0.1 eq.) and a combination of DMA with 2-ethylhexyl acrylate (EHA), (70 eq. or 250 eq.) were dissolved in 1,4-dioxane (1:1 volume compared to the monomer) and were added to a dry ampoule containing a stirrer bar. The solution was degassed using at least 3 freeze-pump-thaw cycles, back filled with nitrogen, sealed and placed in a pre-heated oil bath at 70 °C. After 5 hours the polymerisation was quenched by liquid nitrogen, the crude reaction was diluted with the minimum amount of dichloromethane (CH_2Cl_2) and the polymer was precipitated into diethyl ether and isolated by filtered. Precipitation was repeated a further two times to afford a yellow powder (See Table 6.1 for molecular weight data).

6.6.2.4. Reactivity ratios of DMA and hydrophobic monomer

DMA and hydrophobic monomer (IBA or EHA) at different ratios, CMDT and AIBN were dissolved in 1,4-dioxane. The ratio of [monomers]: [CTA]: [AIBN] was 70: 1: 0.1, the solution was degassed using at least 3 freeze-pump-thaw cycles, back filled with nitrogen, sealed and placed in a pre-heated oil bath at 70 °C. The conversion was kept below 10% and the reaction was quenched by liquid nitrogen and opened to air. Aliquots were taken and characterised by ^{1}H NMR spectroscopy in $CDCl_3$.

Table 6.6. f_1 and F_1 values for the copolymerisation of DMA (f_1) and EHA (f_2).

Experiment	Mol fraction in initial feed (f_1)	Mol fraction in copolymer (F_1)
1	84	81
2	60	63
3	45	48
4	40	41
5	30	27

Table 6.7. f_1 and F_1 values for the copolymerisation of DMA (f_1) and IBA (f_2).

Experiment	Mol fraction in initial feed (f_1)	Mol fraction in copolymer (F_1)
1	80	75
2	63	58
3	51	45
4	39	34
5	30	28

6.6.3. Preparation of the aqueous solutions

6.6.3.1. Preparation of P(EHA-co-DMA)-b-PDMA diblock copolymer and P(IBA-co-DMA)-b-PDMA diblock copolymer micelles

Three preparation methods for the solutions were used. The first method involved mixing polymer powders together and solubilising in water, this is termed the direct dissolution (DD) protocol. Here the polymer powders were weighed out mixed as powders, then 18.2 MΩ water was added to give a polymer solution at 2.5 g/L which was stirred at room temperature overnight before analysis. Secondly a thin film rehydration approach was used (TF), this consisted of mixing dry polymer powders together in a vial and adding dichloromethane (CH_2Cl_2) at a concentration of 2 g/L, then stirred for 1 hour. Subsequently the dichloromethane was removed at 70 °C under vacuum for 24 h leaving a thin film of polymer on the vial. After 24 h, 18.2 MΩ water was successively added to give a polymer solution at 2.5 g/L which was left to stir at room temperature. The final protocol was the solvent switch (SS) method, the polymers were first solubilised in acetone at a concentration of 2 g/L for 1 hour, afterwards 18.2 MΩ water was slowly added to the solution to give a concentration of 0.67 g/L, and the excess acetone was subsequently removed under a slow purge of nitrogen for 24 h at room temperature and then removed under vacuum at 0 °C to give a polymer solution at 2.5 g/L. Once the polymer solutions were prepared the solutions from each protocol were split in two, one half of the solution was kept at room temperature whilst the second half was sealed and subjected to heating at 75 °C for 5 h and then left to cool to room temperature before analysis.

6.6.4. Polymer Characterisation

6.6.4.1. ^{1}H NMR spectroscopy

^{1}H NMR spectra were recorded on a Bruker DPX-400 spectrometer in $CDCl_3$ or D_2O. Chemical shifts are given in ppm downfield from tetramethylsilane (TMS).

6.6.4.2. Size exclusion chromatography

Size exclusion chromatography (SEC) measurements were performed with HPLC grade solvents (Fisher), dimethylformamide (DMF) with 1.06 g/L of LiCl at 40 ^{o}C as an eluent at a flow rate of 1 mL/min or chloroform ($CHCl_3$) with 2.5% volume of NEt_3 at 40 ^{o}C as an eluent at a flow rate of 1 mL/min, both on a set of two PLgel 5 μm Mixed-D columns. The molecular weights of the synthesised polymers were calculated relative to poly(methyl methacrylate) (PMMA) and poly(styrene) (PS) standards from refractive index chromatagrams.

6.6.4.3. Differential scanning calorimetry

Differential scanning calorimetry (DSC) was carried out in an aluminium sample holder with an empty aluminium pan as the reference. Changes in heat flow were recorded between -50 °C and 50 °C over two cycles with a scan rate of 5 °C /min under a nitrogen atmosphere. Calibrated was achieved using indium metal standards supplied by Mettler Toledo.

6.6.4.4. Refractive index increment

The specific refractive index increments (dn/dC) of the polymers in water were measured on a refractometer (Bischoff RI detector and a Shodex RI−101 RI detector) operating at a wavelength of 632 nm.

6.6.5. Micelle Characterisation

6.6.5.1. Laser light scattering

Measurements were performed at angles of observation ranging from 20° up to 150° with an ALV CGS3 setup operating at λ_0 = 632 nm and at 20 ± 1 °C. Data were collected in duplicate with 240 s run times. Calibration was achieved with filtered toluene and the background was measured with filtered solvent (NaCl 0.1 M).

6.6.5.2. Dynamic light scattering (DLS)

The intensity autocorrelation functions $g_2(t)$ obtained from dynamic light scattering were related to $g_1(t)$ (the normalised electric field autocorrelation functions) *via* the so-called Siegert relation. Then $g_1(t)$ was analysed in terms of a continuous distribution of relaxation times (eqn. 1.18 using the REPES routine[46] without assuming a specific mathematical shape for the distribution of the relaxation times ($A(\tau)$). The apparent diffusion coefficient D was calculated from eqn. 1.16 given that the average relaxation rates Γ of the scatterers were q^2 dependent, where q is the scattering vector given by $q=(4\pi n/\lambda_0).\sin(\theta/2)$ with θ the angle of observation and n = 1.333 the refractive index of the solvent (water). Its concentration dependence is given by $D = D_0(1+k_DC)$ where k_D is the dynamic second virial coefficient and D_0 the diffusion coefficient used for computing the hydrodynamic radius (R_h) of the scatterers according to the Stokes-Einstein eqn. 1.19. With η the solvent viscosity, k the Boltzmann's constant and T the absolute temperature. Values of R_h given in the following are then obtained after extrapolation to zero concentration.

6.6.5.3. Static light scattering (SLS)

The Rayleigh ratio of the solutions have been measured using toluene as a reference according to eqn. 1.12 where I_i represents the intensity scattered by species i and $R_{toluene}$ is the Rayleigh ratio of the reference. In dilute solutions if $R_g.q < 1$ where R_g is the radius of gyration, the q and concentration dependence of R_θ is given by eqn 1.10, where A_2 is the

second virial coefficient and M_w the weight average molecular weight. K is an optical constant given by eqn 1.11. Where $n_o = 1.496$ is the refractive index of the reference liquid (toluene), dn/dC is the specific refractive index increment determined by differential refractometry (see Table 4.1) and N_A is Avogadro's number. Values of M_w are then obtained after extrapolation to zero concentration and zero angle and used to derive the aggregation number of the micellar aggregates $N_{agg} = M_w/M_{w,unimers}$. For spherical morphologies, it is possible to deduce the core radius, R_c, from the aggregation number, using equation (2.1) assuming the core block is dehydrated and the density matches that of the bulk value, ρ.[9] When in some cases two modes of relaxation were observed by DLS measurements, R_θ was described as the sum of two contributions according to eqn. 1.25, where f and s stand respectively for fast and slow modes and using 1.26. Where A_f and A_s are the relative amplitudes of the fast and slow modes obtained by DLS. The slow mode of relaxation observed can be attributed to spurious aggregates with a negligible weight fraction but larger scattering intensity.[47,48]

6.6.5.4. Cryogenic transmission electron microscopy samples (cryo-TEM)

Cryo-TEM was conducted on a FEI Sphera microscope operated at 200 keV. 3.5 μL of sample were added to freshly glow discharged Quantifoil R2/2 TEM grids. The grids were blotted with filter paper under high humidity to create thin films and rapidly plunged into liquid ethane. The grids were transferred to the microscope under liquid nitrogen and kept at < -175 ^oC while imaging.

6.7. References

(1) Nyrkova, I. A.; Semenov, A. N. *Macromol. Theory Simul.* **2005**, *14*, 569.
(2) Bendejacq, D. D.; Ponsinet, V. *J. Phys. Chem. B* **2008**, *112*, 7996.
(3) Hadgiivanova, R.; Diamant, H.; Andelman, D. *J. Phys. Chem. B* **2011**, *115*, 7268.
(4) von Gottberg, F. K.; Smith, K. A.; Hatton, T. A. *J. Chem. Phys.* **1998**, *108*, 2232.
(5) Nyrkova, I. A.; Semenov, A. N. *Eur. Phys. J. E* **2005**, *17*, 327.
(6) Nicolai, T.; Colombani, O.; Chassenieux, C. *Soft Matter* **2010**, *6*, 3111.
(7) Stejskal, J.; Hlavatá, D.; Sikora, A.; Konňák, Č.; Pleštil, J.; Kratochvíl, P. *Polymer* **1992**, *33*, 3675.
(8) Jain, S.; Bates, F. S. *Macromolecules* **2004**, *37*, 1511.
(9) Patterson, J. P.; Robin, M. P.; Chassenieux, C.; Colombani, O.; O'Reilly, R. K. *Chem. Soc. Rev.* **2014**, *43*, 2412.
(10) Johnson, B. K.; Prud'homme, R. K. *Phys. Rev. Lett.* **2003**, *91*, 118302.
(11) Hayward, R. C.; Pochan, D. J. *Macromolecules* **2010**, *43*, 3577.
(12) Matyjaszewski, K.; Spanswick, J. *Materials Today* **2005**, *8*, 26.
(13) G. Moad, E. R., S. Thang, *Macromolecules* **1998**, *31*, 5559.
(14) Keddie, D. J. *Chem. Soc. Rev.* **2014**, *43*, 496.
(15) Lu, A.; Cotanda, P.; Patterson, J. P.; Longbottom, D. A.; O'Reilly, R. K. *Chem. Comm.* **2012**, *48*, 9699.
(16) Schilli, C. M.; Zhang, M.; Rizzardo, E.; Thang, S. H.; Chong, Y. K.; Edwards, K.; Karlsson, G.; Müller, A. H. E. *Macromolecules* **2004**, *37*, 7861.
(17) Wright, D. B.; Patterson, J. P.; Pitto-Barry, A.; Cotanda, P.; Chassenieux, C.; Colombani, O.; O'Reilly, R. K. *Polym.Chem.* **2015**, *6*, 2761
(18) Shedge, A.; Colombani, O.; Nicolai, T.; Chassenieux, C. *Macromolecules* **2014**, *47*, 2439.
(19) Dutertre, F.; Boyron, O.; Charleux, B.; Chassenieux, C.; Colombani, O. *Macromol. Rapid Commun.* **2012**, *33*, 753.
(20) Lejeune, E.; Drechsler, M.; Jestin, J.; Muller, A. H. E.; Chassenieux, C.; Colombani, O. *Macromolecules* **2010**, *43*, 2667.
(21) Tian, M. M.; Qin, A. W.; Ramireddy, C.; Webber, S. E.; Munk, P.; Tuzar, Z.; Prochazka, K. *Langmuir* **1993**, *9*, 1741.
(22) Sens, P.; Marques, C. M.; Joanny, J. F. *Macromolecules* **1996**, *29*, 4880.
(23) Renou, F.; Nicolai, T.; Nicol, E.; Benyahia, L. *Langmuir* **2008**, *25*, 515.
(24) Palyulin, V. V.; Potemkin, I. I. *Macromolecules* **2008**, *41*, 4459.
(25) Lu, J.; Bates, F. S.; Lodge, T. P. *ACS Macro Lett.* **2013**, *2*, 451.
(26) Li, Z.; Dormidontova, E. E. *Soft Matter* **2011**, *7*, 4179.
(27) Meli, L.; Lodge, T. P. *Macromolecules* **2009**, *42*, 580.
(28) Lund, R.; Willner, L.; Richter, D.; Dormidontova, E. E. *Macromolecules* **2006**, *39*, 4566.
(29) Lu, J.; Choi, S.; Bates, F. S.; Lodge, T. P. *ACS Macro Lett.* **2012**, *1*, 982.
(30) Choi, S.-H.; Lodge, T. P.; Bates, F. S. *Phys. Rev. Lett.* **2010**, *104*, 047802.
(31) Rager, T.; Meyer, W. H.; Wegner, G.; Winnik, M. A. *Macromolecules* **1997**, *30*, 4911.
(32) Van Herk, A. M.; Dröge, T. *Macromol. Theory Simul.* **1997**, *6*, 1263.
(33) Halperin, A. *Macromolecules* **2011**, *44*, 5072.
(34) Halperin, A.; Alexander, S. *Macromolecules* **1989**, *22*, 2403.
(35) Kelley, E. G.; Murphy, R. P.; Seppala, J. E.; Smart, T. P.; Hann, S. D.; Sullivan, M. O.; Epps, T. H. III *Nat. Commun.* **2014**, *5*, 3599.
(36) Cheng, G.; Hammouda, B.; Perahia, D. *Macromol. Chem. Phys.* **2014**, *215*, 341.
(37) Growney, D. J.; Mykhaylyk, O. O.; Armes, S. P. *Langmuir* **2014**, *30*, 6047.
(38) Hiller, W.; Engelhardt, N.; Kampmann, A.-L.; Degen, P.; Weberskirch, R. *Macromolecules* **2015**.

(39) Vamvakaki, M.; Palioura, D.; Spyros, A.; Armes, S. P.; Anastasiadis, S. H. *Macromolecules* **2006**, *39*, 5106.
(40) Colombani, O.; Ruppel, M.; Burkhardt, M.; Drechsler, M.; Schumacher, M.; Gradzielski, M.; Schweins, R.; Muller, A. H. E. *Macromolecules* **2007**, *40*, 4351.
(41) Won, Y. Y.; Davis, H. T.; Bates, F. S. *Macromolecules* **2003**, *36*, 953.
(42) Nose, T.; Iyama, K. *Comput. Theor.Polym. Sci.* **2000**, *10*, 249.
(43) Choi, S. Y.; Bates, F. S.; Lodge, T. P. *J. Phys. Chem. B* **2009**, *113*, 13840.
(44) Forster, S.; Abetz, V.; Muller, A. H. E. *Polyelectrolytes with Defined Molecular Architecture II* **2004**, *166*, 173.
(45) Gaillard, P.; Ossenbach-Sauter, M.; Riess, G. *Die Makromol. Chem. Rapid Commun.* **1980**, *1*, 771.
(46) Jakes, J. *Collect. Czech. Chem. Commun.* **1995**, *60*, 1781.
(47) Sedlak, M. *J. Chem. Phys.* **1996**, *105*, 10123.
(48) Chassenieux, C.; Nicolai, T.; Durand, D. *Macromolecules* **1997**, *30*, 4952.

7. Conclusions and future outlook

This thesis has dealt with the solution self-assembly of amphiphilic polymers in both polar and non-polar media. In Chapters 2 and 3 it was demonstrated that hydrophobically end group modified amine polymers self-assemble into discrete spherical micelles in non-polar media. When self-assembled in non-polar media the amines in the micelle core create unique nanoenvironments with a high local concentration of amine functionality. Consequently an increased basicity in solution was observed by potentiometric titrations in organic media. These self-assembled nanostructures were explored as an alternative to metal salt detergents which are currently used in lubricant formulations to neutralise acid compounds formed during the combustion process. This was achieved using both potentiometric titrations and total base number (TBN) analysis (as described in Chapter 3). The combination of these two analytical methods provided complementary analysis of the polymers and highlighted the need for both techniques to ensure a full understanding of their neutralisation ability and hence their potential application as a lubricant additive. Specifically, the potentiometric titrations provide information on the strength of the base and the TBN analysis method examined the amount of base present in the system, both of which determine the efficacy of the material in acid neutralisation.

Chapter 4 explored the assembly and dynamics of pH responsive amphiphilic diblock copolymers, in solution, where the associating block was a tuneable copolymer block. By using a host of analytical techniques it was observed that a range of micelles were formed in aqueous media and that their behaviour, both aggregation and dynamics, was dependant on the solution pH and the composition of the associating block. Moreover, a key conclusion from this Chapter was the importance of using complementary analysis and characterisation methods to obtain in depth structural analysis of self-assembled materials. For example, although large changes in aggregation number were observed between the polymer micelles of differing core composition, the hydrodynamic radius of the micelles in solution, as

measured by DLS, did not significantly change between systems. Thus, DLS alone does not provide adequate information on the system and complementary SLS studies should be undertaken when examining such a series of polymer micelles. Nevertheless, despite the large range of nanostructures, the limitation of this system is that to change the nanostructure found at a defined pH value a new polymer must be synthesised. Hence Chapters 5 and 6 explored a new assembly protocol for these diblock copolymers with the aim to negate the need for exhaustive synthetic of precursor block copolymers. Specifically, the new assembly protocol was to blend two diblock copolymers together to form a blended structure with a targeted intermediate composition of the two parent diblock copolymers. These blended assembles were then compared to assemblies prepared from the compositionally pure diblock copolymer systems. The blending protocol demonstrated that if the diblock copolymers can reach equilibrium then the blend structure formed is structurally identical to a structure formed by a single polymer system at the same composition. Thus it was concluded that the blending protocol provided significant benefits over the synthesis of a range of polymers and their subsequent assembly in solution.

Future work and outlooks to extend this research on amphiphilic block copolymers would initially focus on further testing of the amine polymer in non-polar media (such as mineral oil) as lubricant additives. Specifically, to analyse these polymers in a formulation with other additives present e.g. rust inhibitors, viscosity modifiers and, within an engine environment. These experiments would better mimic the different environments that the amine polymers would be subjected to once formulated into a commercial product.

In the second part of this thesis, the blending protocol was shown to be a very effective alternative to the traditional approaches of solution self-assembly from a block copolymer of single composition. Our work to date has used this blending protocol used in this thesis was used to alter the structure of spherical micelles in solution, therefore, an extension of this protocol would be two fold; First would be to understand the core behaviours further of the

blend and pure micelles, although structurally the micelles are identical between blend and pure micelles at equilibrium, the next outlook would be to understand if the domains within the nanostructures behaviour identical i.e. catalytically active micelles or fluorescent probes within the micelle core. The second is to apply this technique to different morphologies e.g. forming blended cylinders. This would be an important target as the assembly of diblock copolymers to form cylindrical micelles occurs in a small compositional window, which can require extensive synthesis of a specific composition to access. Instead, our new method allows for the blending of just two diblock copolymers to access a range of compositions and hence allow for straightforward targeted self-assembly. In addition to forming a new blend structure an extension of the protocol is to explore the changes that arise from blending different morphologies e.g. blending a vesicle and a spherical micelle.

As a final suggested area to advance this research an option would be to combine both the research topics of this thesis. The amphiphilic amine polymers explored in the early chapters offer great potential as a new lubricant additive and have been widely accepted by our industrial sponsor with a patent application. Therefore, it is possible to streamline the large scale synthesis and for applications of these new diblock copolymers an alternative would be to use the copolymer blending protocol. The blending protocol would allow for a range of amine nanostructures to be formed but would be synthetically less demanding and more time efficient for large scale applications.